TRACKING FACILITIES FOR LOW NOISE HIGH GAIN ANTENNAE PROVIDING FOR POLARIZATION DIVERSITY

BY

DENNIS N. COOPER, B.E. (Hons.)

Thesis submitted for
the Degree of Doctor of Philosophy
Department of Electrical Engineering,
The University of Adelaide.

June 1968

CSIRO

DIVISION OF RADIOPHYSICS

P.O. BOX 76, EPPING, N.S.W., 2121 (CNR. VIMIERA AND PEMBROKE ROADS) TELEPHONE 869 1111. TELEGRAMS CORESEARCH SYDNEY

The Registrar,
University of Adelaide,
North Tce.,
ADELAIDE, S.A. 5000.

3rd January, 1969.

Dear Sir,

I hereby authorize the Barr Smith Library, University of Adelaide, to make copies of my Ph.D thesis, entitled:

"Tracking Facilities for Low Noise High Gain Antennae, Providing for Polarization Diversity",

available for loan and photocopying.

Yours sincerely,

(Dennis N. Cooper.)

TABLE OF CONTENTS

Table of Contents (continued) Page

Table of Contents (continued) Page

SUMMARY

Deep space research by means of satellites has placed considerable demands on the antenna installations used for receiving telemetered data from the orbiting vehicle. The reception of information from very distant satellites requires that the antenna have a very high gain and a low noise figure so that a minimum of extraneous noise enters the system. However, to receive this data, the antenna must always be pointed toward the vehicle and must be steerable. This requires either an antenna system which is able to track the target automatically or an antenna control system linked to a path predictor. In the limiting situation where the target is far from earth, the weak signals received preclude the use of automatic tracking systems and complete reliance must be placed on the predicted orbit. However, to establish the actual path of the vehicle, it must be tracked as long as possible to allow any divergence from the desired orbit to be determined and to allow any flight path corrections to be performed.

This thesis discusses the provision of tracking facilities in large low noise reflector antennae. This is desirable since it allows greater tracking accuracy and range than is possible with a

subsiduary tracking installation. It also allows more efficient use of the costly main antenna reflector. A new method of obtaining tracking information using the circularly symmetric modes in circular waveguide is presented. This technique has the advantages of complete polarization diversity and compatibility with high efficiency low noise feed systems. In fact, the modifications to waveguide feeds to improve their feed efficiency also satisfy the requirements for improved tracking capabilities by equalizing the performance of the error modes and increasing the relative size of the difference mode aperture. The price paid for these advantages in the antenna design is the complex receiver necessary to process the output signals from the antenna, since the direction information is derived from the relative phases of the reference and error modes.

The multimode tracking system can be considered to be oriented towards circular polarization as the right and left hand components may be processed separately to give tracking information. In the situation where the received signal has predominantly one rotation component, the other can be ignored without introducing tracking error, and a simpler receiver configuration can be used.

As an extension to the problem of tracking with narrow beamwidth antennae, the possibility of improving the search and acquisition properties of such systems has been investigated. Improving acquisition time in a given system is best approached by beam broadening to increase the search element size. The increases in beamwidth obtained by defocussing large reflector antennae has been investigated with particular reference to the multimode tracking system. It has been found that, in both focally excited and cassegrain systems, search element increases of about one order can be obtained whilst maintaining adequate phase tolerances between the error and reference modes.

Practical tests on both plain and corrugated waveguide feeds show that the multimode tracking feed is feasible, although in its simplest form with no attempt to improve feed efficiency it gives a high edge illumination for the error modes with a resultant susceptibility to noise. The spread of the reference and error mode phase centres is insufficient to produce phase errors large enough to cause tracking instability.

STATEMENT

The author wishes to state that this thesis contains no material which has been accepted for the award of any other degree or diploma in any University, and that, to the best of the author's knowledge and belief, this thesis contains no material previously published or written by another person, except when due reference is made in the text of the thesis.

Dennis N. Cooper

ACKNOWLEDGEMENTS

The author wishes to thank Professor E. O. Willoughby of the Electrical Engineering Department for suggesting this project and to acknowledge his help and guidance throughout the course of the research.

He would also like to thank the technical staff of the Electrical Engineering Department for their assistance in constructing equipment and for assistance in performing measurements in the field. Thanks are also due to the Mechanical Engineering Department Workshop for the construction of the antenna model.

The author is indebted to the Radiophysics Branch of the Commonwealth Industrial and Scientific Research Organisation (C.S.I.R.O.), Sydney, Australia, for the use of their facilities and in particular to Mr. H. C. Minnet and Dr. B. Thomas for valuable discussions.

The author would also like to thank the Administration of the C.S.I.R.O. for making available a postgraduate scholarship which enabled him to undertake this project. He is also grateful to the University of Adelaide for financial support during the last nine months of the project.

CHAPTER I

INTRODUCTION

1.1 Large Steerable Antennae

1.1.1 Introduction

The advent of deep space exploration by satellite has placed considerable demands upon antenna installations used for receiving telemetered data. Broadly, the problems associated with systems designed to collect data from vehicles in large solar orbits can be split into two groups:

(a) those concerned with ensuring that the antenna is pointing toward the target,

and (b) the problem of sensibly receiving the information required.

As in any system design, there will be considerable overlap between these two categories.

The former group of problems, which necessitate the design of a steerable system, includes all the problems associated with placing an object in a particular orbit. The interest for an antenna engineer is the design of an aerial system which enables the actual path of the vehicle to be tracked as long as possible, independent of any predictions, thus making possible comparison between the desired or predicted path and the

actual orbit, and the calculation of necessary corrections. In the limiting situation with the vehicle at very large distances from earth and consequently low received signal strengths, tracking may be no longer feasible and reliance must be placed on computed predicted paths.

The second group involves production of a receiving system with a noise figure adequate for the task in hand. With the capital expenditure and difficulties involved in experiments of this kind, together with the nature of the signals to be detected, this invariably means producing a system with the lowest noise figure possible. From the antenna point of view this means designing a system of maximum signal to noise at the output, for any working position of the antenna.

Perhaps the most important single parameter to be determined in the design is the frequency of operation. This choice involves a delicate balance between several factors, the most important being noise considerations, atmospheric absorption, ionospheric reflection, the power and equipment handling capabilities of the satellite and the cost requirements of the project. Of these noise is the most important factor since the signals to be detected are extremely weak owing to the

large space attenuation over the transmission distance. With the introduction of parametric and especially maser low noise amplifiers, the noise introduced in the first stage of the receiver is no longer the limiting factor; consequently the frequency must be chosen to minimize atmospheric noise contributions, both man made and natural. This usually places the operating frequency in the range 1000 to 6000 MHz. (i.e. wavelengths from 30 to 5 cms). This range is well above any man made interference and not yet in the range where atmospheric absorption[1] may limit performance. It is also approaching the upper limit of frequency for which transmitters with reasonable power output can be built and lies comfortably in the range of discrete frequencies at which 'masers' operate.

It is worth noting that maximum signal to noise ratio from an antenna does not necessarily mean maximizing the forward gain, for noise contributions from the sidelobe structure may be significant and need control. In other words, a minimum effective antenna noise temperature is required, the effective antenna temperature being conveniently described[2] by

$$T_a = \frac{1}{4\pi} \int_s G(\theta,\phi).T(\theta,\phi)\, d\Omega \qquad (1.1)$$

where T_a = effective antenna noise temperature

$G(\theta, \phi)$ = antenna gain function

$T(\theta, \phi)$ = effective spatial noise temperature distribution

$d\Omega$ = elementary solid angle.

For antennae intended for deep space research, however, maximum gain is normally sought since the overall systems are designed to avoid the necessity of tracking at low angles of elevation (hence reducing ground noise contributions through sidelobes) or too near hot (radiating) bodies. The antennae are also sited in remote areas to minimize man made interference.

The physical size of the receiving antenna will be a function of the frequency chosen. The antenna dimensions can also be shown[3] to be directly proportional to the distance involved (all other factors given)

$$\text{range} = D \sqrt{\frac{P_T G_T \eta_R}{16\, kT_a F \Delta f (\frac{S}{N})}} \qquad (1.2)$$

where D = diameter of assumed circular aperture

P_T = transmitted power

G_T = gain of transmitting antenna

η_R = overall efficiency of receiving system

k = Boltzman's constant

T_a = effective antenna noise temperature

F = receiver noise figure

Δf = system frequency bandwidth

S/N = desired signal to noise ratio.

In this formula the only parameters affected by receiving antenna design are the antenna noise temperature, T_a, the receiving efficiency η_R and the diameter D. Of the other factors P_T transmitted power and G_T transmitting antenna gain would have maxima set by economical payload and life of the satellite whilst the bandwidth Δf is mainly controlled by the information to be transmitted.

This discussion is intended to show some of the factors influencing the design of antennae for deep space research and to show the need for large steerable antennae with low noise temperature. It is worth noting at this stage that the branch of radio astronomy dealing with the reception of signals from remote stars (as opposed to the intensive study of our own sun) also requires antennae with similar requirements to the above, although they are derived in a different manner. The frequencies of interest in radio astronomy are no longer under the control of the system designer but are determined solely by the structure of the star or object of interest. However, the important hydrogen line does occur within the above range, being at 21 cm wavelength (i.e. approximately 1400 Mc/s). The demands

of the scientists in this field are mainly for high resolution and high sensitivity. From the Rayleigh λ/D criterion, high resolution necessitates a large antenna size (since wavelength fixed) which in turn provides high antenna gain. The high sensitivity requirement to detect very weak signals means that extraneous noise in the receiving system must be reduced to a minimum, i.e. need minimum antenna noise temperature. And, of course, radio astronomy antennae must be steerable to accommodate rotation of the earth although tracking facilities are not required.

1.1.2 Large Aperture Antennae

There are two approaches to achieving antennae with large effective diameters and which may be made steerable. These are the array of a number of discrete coherent radiators, and the reflector antenna consisting of a primary radiator (or radiators) and a passive reflector (or reflectors). At first the antenna array seems to be the best proposition for producing a narrow scanning beam since the elements may be fixed and beam steering may be achieved electronically, offering high scan rates. Electronic scanning may be achieved by altering the frequency of operation, a system with very restricted application, or by altering the phase or amplitude or both of individual elements. The array

also offers great flexibility in synthesis of an optimum secondary radiation pattern since each individual element may be varied in amplitude, phase and position, at least at the design stage.

However, for very large antennas under the present terms of reference, the array has some severe limitations. The array has an inherent property of gain reduction as the scan angle away from the normal to the array increases. This is caused by a reduction in the projected area of the aperture so reducing its energy collecting potential. As the array consists of a large number of almost identical antenna elements which must be manufactured to close tolerances, the interconnection and control circuits become very complex, although the random failure of one or two elements will not degrade performance severely. In practice the scan angle of an array is limited by mutual coupling effects between elements. This mutual coupling increases with scan angle causing degradation of the radiation pattern and probable secondary effects within the array due to the change in impedances of the elements. Finally, arrays, in general, have a high noise temperature.(4) Consequently, arrays are best suited to moderate gain, limited scan applications, especially where high scan rates are necessary.

Large reflector antennae can be designed to have wide scanning angles with virtually no change in the electrical performance, since the system as a whole moves. This, however, places high demands on the mechanical design, owing to the large weight of the structure and the necessity of maintaining the reflector shape within close tolerances. Due to the large mass (and hence inertia) of such an antenna the scanning rates must be slow, and the accelerations required must also be quite low to keep the power requirements of the drive systems low. On the other hand, since maser and other low noise amplifiers can be conveniently used with reflector antennae they are capable of very low noise temperatures. Scanning with reflector antennae can also be achieved using a fixed reflector and moving only the primary radiation (or feed) system. This allows higher scan rates to be achieved, but involves somewhat limited scanning angle and some inefficiency in the use of the reflector since only a portion of it is illuminated at any one time.

It is these arguments that justify the current demand for large fully steerable reflector antennae. A recent review of satellite ground station antennae has been given by Reed.(5) At present the maximum diameter antennae built to operate in the above-mentioned

frequency range (1000 MHz - 6000 MHz) form the Jet Propulsion Laboratory, Pasadena, California, deep space exploration tracking network and are 210 ft. in diameter.

In this thesis it is intended to discuss the provision of tracking facilities in systems such as those discussed above. The main aim has been to develop a tracking system which will perform with the same order of accuracy as current techniques, whilst allowing an ultimate antenna performance in a purely receiving role of the best possible quality. Consequently, under these terms of reference, the tracking facility must only be considered of secondary importance to the low noise, high gain receiving capabilities of the antenna.

Before considering the tracking system developed, it is necessary to survey briefly the current techniques for achieving high efficiency feed systems and tracking feeds for large reflector antennae.

1.2 High Efficiency Feed Design

From equation (1.2) above, it can be seen that, in a given application, the size of the antenna required is dependent upon the receiver efficiency. The overall efficiency of the receiving system will be given by the product of the efficiencies of the various units making up the system; consequently any improvement which can

be made in antenna efficiency will be significant. Because the cost of large reflector antennae increases with approximately the cube of the diameter, there is much to be said, for economic reasons alone, for achieving the highest possible antenna efficiency in a given system design as the feed system tends to be a relatively minor part of the overall installation cost. Moreover, in the case of existing antennae installations, improvement of feed system efficiency will extend the usefulness of the antenna and also allow maximum use of the initial capital outlay. It is for these reasons that considerable efforts have been made to improve feed system design and hence antenna efficiency.

Initially there was considerable scope for improvement in efficiencies which, in the case of the simple focally excited paraboloid reflector (Fig. 1.1(a)) with an unsophisticated feed horn, were only in the vicinity of 50%. The introduction of the optical Cassegrain telescope principle to microwave reflector antennae (Fig. 1.1(b))[6,7,8,9,10] allowed greater flexibility in the illumination of the main reflector and the possibility, in theory at least, of very high efficiencies.[9] However, the need for greater control of the primary radiation pattern characteristics still existed. It is this side of feed design which is of

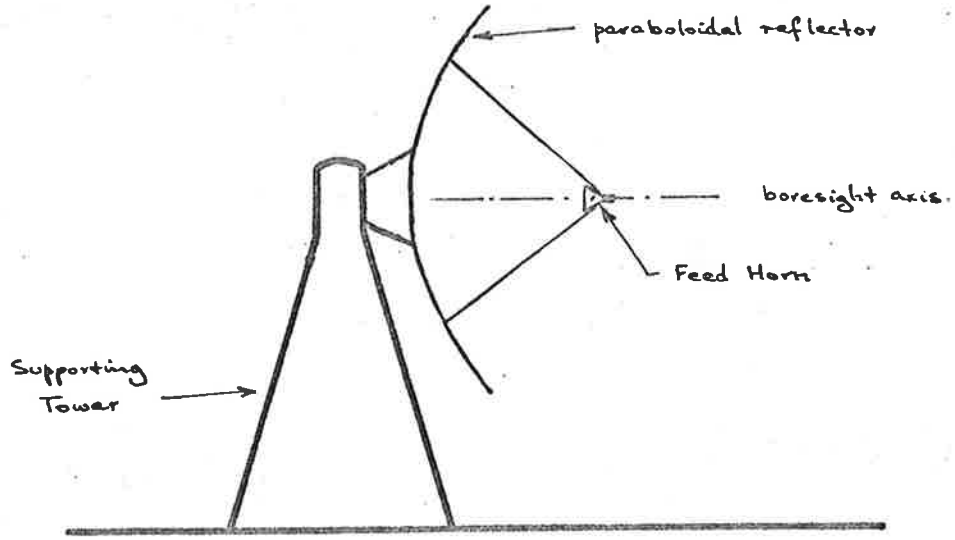

(a) Focally Excited Paraboloidal Antenna

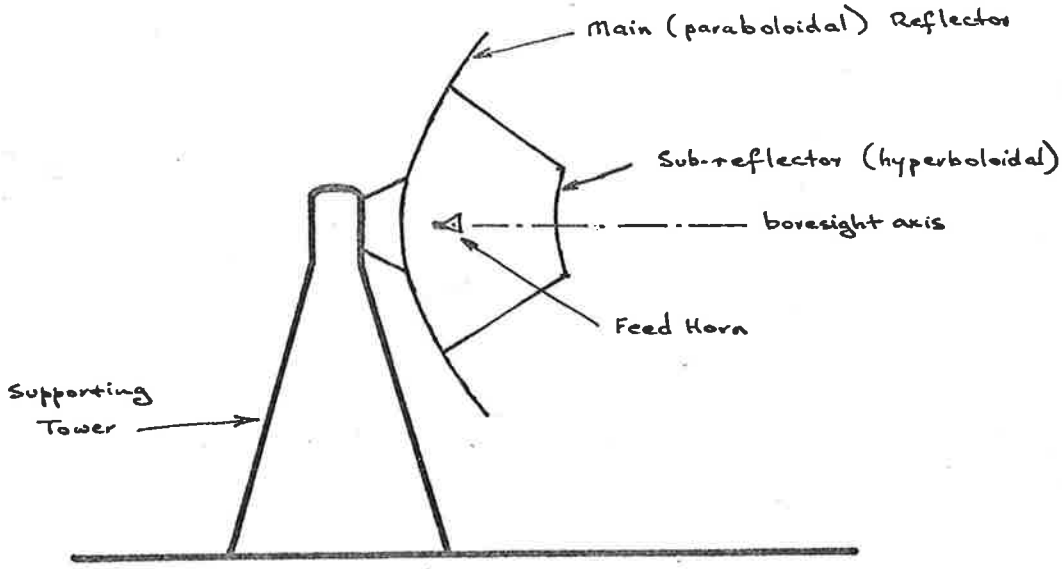

(b) Cassegrain Antenna System

Fig. 1.1 Paraboloidal Reflector Antenna Systems.

concern when provision of tracking facilities is considered.

Feed systems in low noise situations are exclusively waveguide and horn combinations feeding directly to a low noise amplifier. Arrays are not used at present owing to the inherent losses associated with the transmission and interconnection system. The possibility of active array elements, or amplifiers directly behind the radiating element, must not be dismissed, with the increasing application of semiconductors and integrated circuit techniques at high frequencies. However, the cooling of such an array would be extremely difficult.

Because of the unknown and shifting attitudes of satellites in their orbits and the possibility of changes in signal polarization by the earth atmosphere, the receiving systems are always circularly polarized. This immediately restricts the feed systems to either square or circular waveguide systems, due to symmetry conditions. Of these two possibilities, circular waveguides produce more symmetrical radiation patterns,[11,12] which also have a better sidelobe structure;[11] consequently most of the recent research has concentrated on this type of waveguide.

A more detailed discussion of research into high

efficiency feed systems will be given in Chapter IV and with particular reference to the multimode tracking system developed. For the moment it suffices to know that any tracking system must be compatible with circular waveguide feed systems. Furthermore, another important aspect emerges from the above discussion: this is the need for polarization diversity in the system. It is essential that the system be independent of the return signal polarization both in purely receiving applications and where tracking is required. Even if a satellite has attitude control, changes in signal polarization may occur over the signal path and in particular near earth and the possibility of failure in the attitude control system must also be accommodated.

1.3 Tracking Feeds for Large Reflector Antennae

1.3.1 Introduction

The idea of tracking antennae stemmed from the military problem of detecting and tracking airborne targets in situations where conventional two dimensional radar did not give complete information on target position. Tracking radar also allowed automatic gun aim control. Consequently conventional tracking radar relied on a passive target and the antenna system

performed a two way transmit-receive function, i.e. to illuminate the area and detect the presence of any return echo, indicating a target. With the introduction of artificial satellites, the problem of keeping the ground station receiving antenna pointed at the satellite was relatively easily overcome by adapting the conventional tracking radar techniques. There were some differences, of course. The satellite contained its own transmitter and thus the antenna system became a continuous receive-only installation, with relatively strong signals at least from earth orbiting vehicles. Secondly, the satellite path was predictable and if necessary could be followed by predetermining the path and feeding the information to the antenna drive system. However, in order to check the actual orbit at least one tracking station would be necessary.

In the deep space probe situation, where it is expected that the vehicle will eventually go out of tracking range due to the low signal to noise ratio achievable, it is important that an accurate measure of the actual orbit be determined and that it be determined sufficiently early to allow corrections to the path to be made and rechecked. The accuracy of the path determined can be improved by tracking with widely separated antennas (as in the usual system of three antennas

approximately equally spread about the earth when overlap exists) and using a "triangulation" technique to compute the path. This demand for long range tracking shows the need to provide tracking facilities on the main receiving reflector to extend the tracking distance to the maximum possible and with the best attainable accuracy. Up until now this facility has not been included on large antenna installations since the tracking methods available compromised the efficiency of the antenna in a purely receiving situation.

The author does not intend to give a detailed discussion of the development of tracking radar, which has been adequately covered in the literature, listed in the extensive, but by no means exhaustive, bibliography on tracking radar included with the thesis, but rather to comment on the basic types of system available and their developments.

1.3.2 Monopulse Tracking Methods

All tracking systems employed today use monopulse techniques for deriving directional error information. This name is derived from the true radar situation where all directional information can ideally be derived from a single transmitted pulse. Monopulse techniques for use in a three dimensional tracking

system may be divided into three types:

(a) amplitude comparison[13,14] (fig. 1.2)

(b) phase comparison[14] (fig. 1.3) and

(c) phase-amplitude comparison.[15]

The third type mentioned is a combination of the first two, using one technique in each of two orthogonal reference planes. It can be shown[16] that in the non-ideal situation where complex targets exist the performance of phase-amplitude monopulse circuits is inferior to either of the other systems. A complex target may be described as a collection of point sources with amplitudes, phases and polarizations differing; these parameters may or may not be correlated.

Phase comparison techniques have the disadvantage of requiring reasonable separation between the antennae in order to achieve good resolution; in fact the greater the distance between them the better the resolution, although the possibility of ambiguity also increases with separation. In the case where very weak signals must be handled and antennae must be physically large to provide the high gains needs, this requirement for separated antennae becomes economically impossible and the method is rarely used.

Amplitude comparison monopulse, on the other

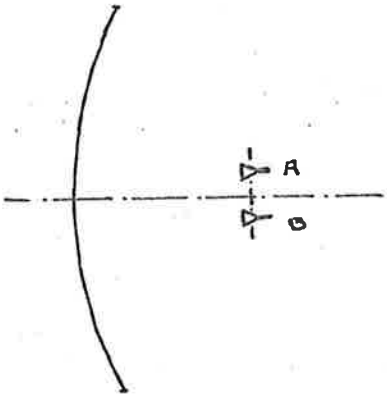

(a) Reflector and Separate Feed Horns

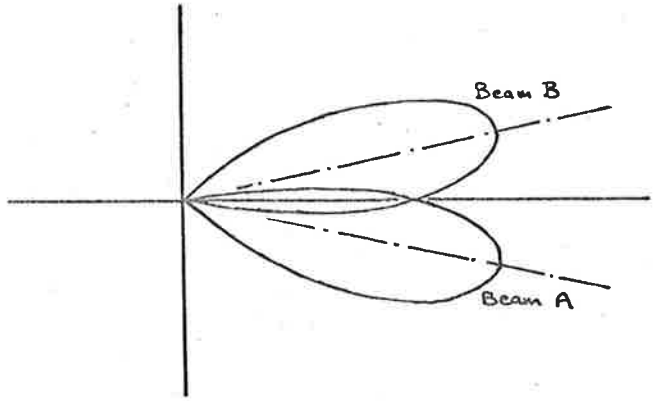

(b) Skewed beams produced by off-axis feed horns.

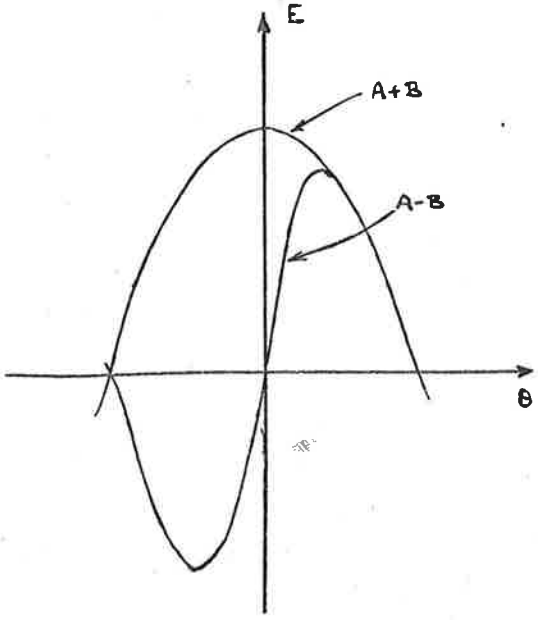

(c) Sum and Difference Voltage Characteristics

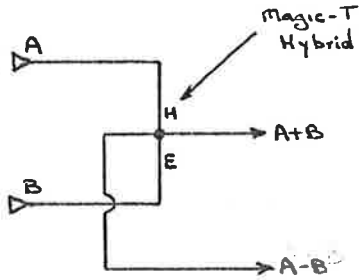

(d) Bridge circuit to derive sum and difference signals

Fig. 1.2 Basic Amplitude Comparison Monopulse System in two dimensions.

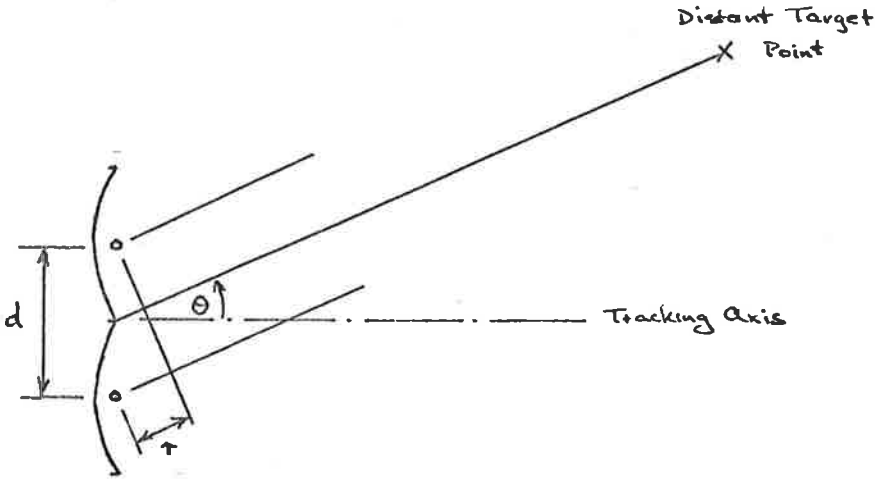

path diff^{ce} $\tau = d \sin\theta$

$\therefore$ phase diff^{ce} $\alpha = \frac{2\pi}{\lambda} . d . \sin\theta$ radians

error signal = difference signal

$= K \sin\alpha$

$\simeq K . \frac{2\pi d}{\lambda} . \theta$ for small θ

Fig 1.3 Phase Comparison Monopulse System.

hand, is achieved using a single reflector and slightly offset feed horns to produce skewed beams (fig. 1.2). The sum and difference modes shown in the diagram (fig. 1.2 (c)) may also be regarded as produced by primary illumination functions given even and odd aperture distributions; in many instances this approach is far more useful.

For three dimensional tracking information a minimum of three horns is necessary to provide error signals in orthogonal planes; however, it is usual to admit a certain amount of redundancy and use four horns (fig. 1.4(a)) because this allows a more symmetrical arrangement, giving simpler signal processing circuits and allowing better aperture distributions to be formed.

1.3.3 Limitations of Simple Four Horn Cluster and its Derivatives

In its basic form the four horn cluster monopulse feeds has several limitations. These stem from its inefficient illumination of the antenna reflector (At the moment the efficiency concerned is the overall efficiency of the antenna, not just aperture efficiency. In low noise applications it is particularly important to consider the sidelobe structure of the primary feed system). In both the sum and difference modes this

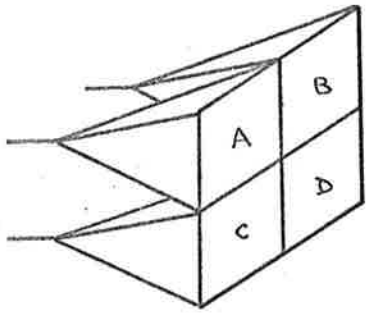

(a) Basic Four Horn Cluster.

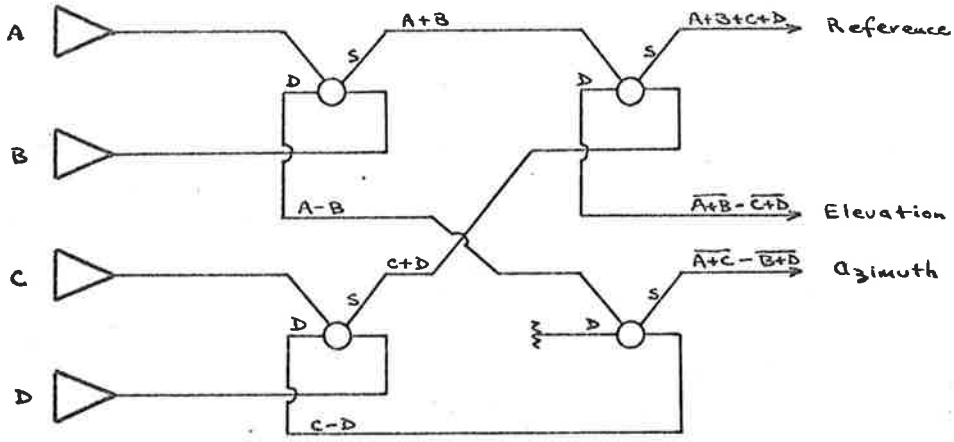

(b) Bridge Circuit for Processing Two Angle Monopulse.

Fig. 1.4 Four Horn Monopulse System.

basic feed leaves much to be desired[17,19].

The first of these inadequacies to receive much attention stemmed from the military necessity for high tracking accuracy. From fig. 1.2(c) it can be seen that the tracking accuracy requires a large difference slope. It has been shown[17] that to achieve optimum difference pattern illumination the effective feed aperture in the difference mode must be twice that of the sum mode; several methods have been proposed to overcome this problem.[18,20,21,22]

The investigations into improving on-axis or sum mode performance in tracking systems was stimulated by the introduction of communication satellites and, later, deep space probes. Keeping[19] appears to have been the first to stress the importance of the on-axis feed performance in low noise applications, when discussing the tracking feed design for the Haystack Microwave Research Facility.[23]

The first attempts to produce low noise monopulse feed systems have used a conventional four horn cluster to excite higher order modes in a pyramidal horn[24,25,26,19] (fig. 1.5). All these systems excite large numbers of modes in the square horn; this may be up to twelve modes.[25] The large number of waveguide modes means extremely difficult control of the phasing and

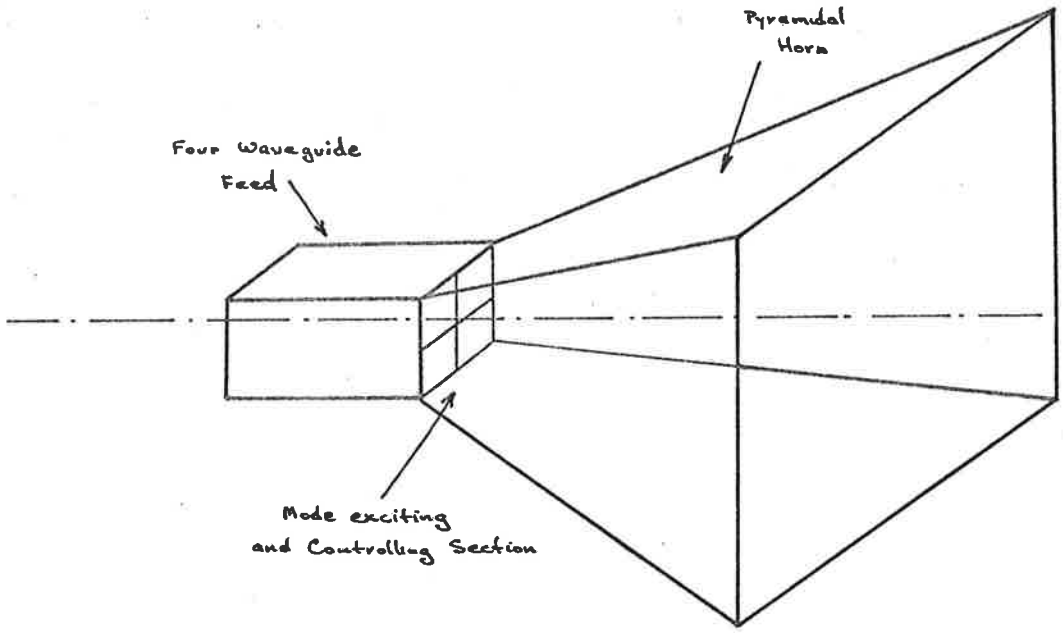

Fig. 1.5 Square Horn Monopulse Feed.

amplitude of the desired modes as well as suppression of any unwanted modes; the actual modes used varies with the design. The preservation of tight control on relative amplitudes and phases with these systems also tends to produce a very narrow bandwidth system. Although these systems represent a great improvement on the simple four horn cluster, they still suffer from some disadvantages when viewed in relation to tracking in deep space projects. Because the system still relies on a four waveguide feed to generate the waveguide modes, the sum and difference tracking patterns are not derived independently and the signal processing bridge circuit (fig. 1.4(b)) is still necessary. This introduces inevitable loss into the transmission system with a consequent increase in system noise temperature. Furthermore, none of the techniques for improving feed and aperture efficiency of large reflector antennae can be implemented since these are almost invariably based upon circular waveguide modes and in order to achieve the maximum receiving efficiency with very low noise these techniques must be employed.

In the next chapter the author describes[27] a tracking system suitable for use in circular waveguide. The initial proposal was briefly described in a communication to the Proceedings of Institute of

Electrical and Electronic Engineers, a copy of which is included with this thesis. The system to be described has three main features; these are complete polarization diversity if necessary, independent generation of the even and odd illuminations necessary for on-axis and tracking signals, and finally compatibility with all the techniques for achieving high efficiency feeds in circular waveguide.

CHAPTER II

A MULTIMODE TRACKING FEED

2.1 Introduction

In the previous Chapter the problems involved in the provision of tracking facilities on large low noise antenna installations have been discussed. These may be summarized by stating that any system devised must be compatible with current techniques for achieving low noise, high efficiency feeds, with no compromise of the receiving performance, and must have complete polarization diversity to accommodate changes in signal polarization characteristics due to signal path or satellite attitude. The first of these conditions makes it obligatory that the system be designed on circular waveguide. It is essential for the method to produce the reference and error signals simultaneously and continuously.

The reference or on-axis signal must have the form shown as the sum signal in fig. 1.2(c), and the error characteristic must be like that of the difference signal in the same diagram. The reference characteristic is seen to be basically the same shape as that required from an antenna in a normal receiving situation and so the main receiving modes may be used to provide a reference channel. This implies that the reference

and error signals are produced directly by the antenna, which is a desirable feature for low noise applications. In deference to the conventional four horn monopulse terminology, the reference and error signal characteristics may still be termed sum and difference patterns.

The difference patterns may be generated either by extra modes propagating within the circular waveguide sum feed or by some external radiating mechanism. With either of these methods there are stringent requirements for cross-coupling between the reference and error modes in order to preserve the illumination efficiency and noise performance of the sum channel. The use of external apertures to generate the error modes is not suitable for two main reasons. Firstly, the large paraboloids in use, with $^{f}/D$ ratios of approximately 0.4, require basic feed apertures in the region 1.3 - 1.5 wavelengths in diameter; consequently any external aperture, whether it be annular in form or two diametrically opposite guides to produce a difference, can have an inner dimension no less than this aperture size. Such radiating systems produce a multilobe pattern in which the first few lobes are of much the same size (cf. an interferometer).

Fig. 2.1 illustrates the shape of such patterns by giving the radiation pattern of a coaxial waveguide

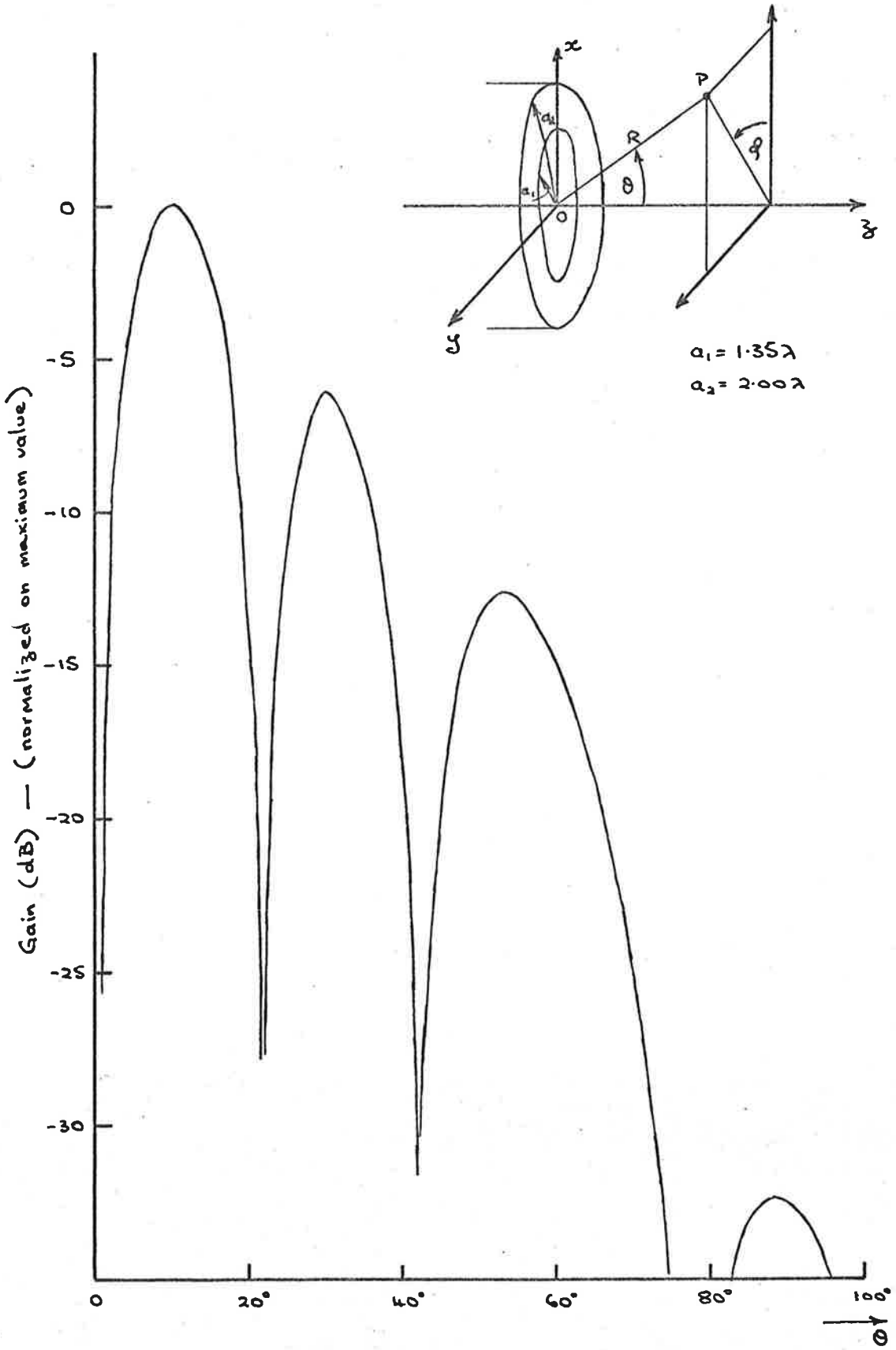

Fig. 2.1 Radiation from Coaxial Waveguide.

with dimensions compatible with a simple waveguide feed. The mode used is the TEM mode, which gives a central null as required for difference modes, and is assumed to be matched at the aperture. The field in the waveguide is assumed to be of the form[28]

$$E_\rho = K_1 \frac{1}{\rho} = \sqrt{\frac{\mu}{\epsilon}} \cdot H_\theta$$

where (ρ, θ, z) are the coordinates for fields within the waveguide and K_1 is a constant. The radiation pattern for a field of this type can be shown, from Appendix I, to be

$$E = K_2 \cdot \frac{1+\cos\theta}{\sin\theta} \cdot [J_o(k a_2 \sin\theta) - J_o(k a_1 \sin\theta)] \cdot \frac{e^{-jkR}}{R}$$

where K_2 = constant

and a_1, a_2 = inner and outer radii of the co-axial guide.

A plot of this function and the coordinates are given in fig. 2.1. It will be noted in this case that some two and a half lobes are within a nominal 60° paraboloid edge. This is certainly not suitable for use with a large reflector antenna. There is also the possibility of a "false zero" between the second and third lobes in a tracking system.

The same problem applies to a cassegrain system since the basic aperture size increases in much the same ratio as the effective focal length when compared with the simple paraboloid. This multilobe pattern would lead to poor utilization of the aperture, the probability of ambiguities in tracking and poor noise performance due to spillover. The second difficulty in providing tracking feeds external to the main waveguide feed stems from some of the techniques used to improve the radiation characteristics of the basic feed. Many methods for improving feed efficiency modify the aperture plane[29,30,31,32,4,46] outside the waveguide by providing an anisotropic surface of some kind. This forces the minimum internal dimensions of any tracking error system to be greater. These limitations caused by the geometry of an antenna system make the provision of error patterns by extra modes propagating in the basic feed more attractive, especially in the low noise situations.

2.2 Modes in Circular Waveguide

2.2.1 Sum Mode

The dominant mode in circular waveguide is the TE_{11} mode. Its field within the waveguide is shown in fig. 2.2(a) and may be represented by the following

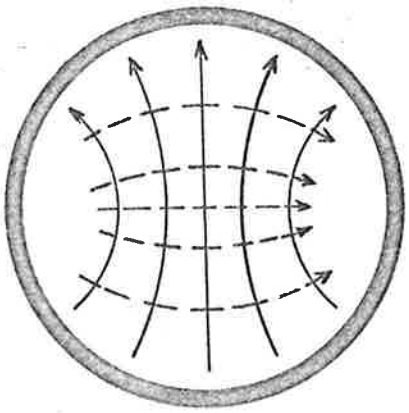

(a) TE11

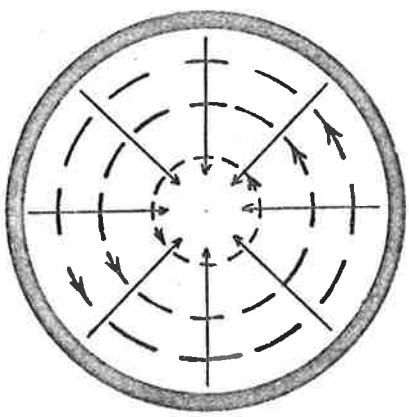

(b) TM01

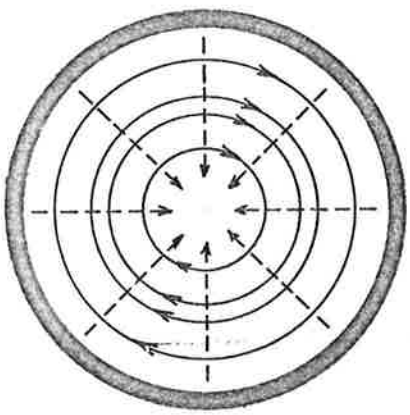

(c) TE01

Electric Field ——

Magnetic Field - - - -

Fig. 21 Circular Waveguide Field Patterns.

formulae(33)

$$E_z = 0 \qquad H_z = \kappa_{11}^2 \cos\theta \cdot J_{11}(\kappa_{11}\rho) \cdot e^{-\gamma_{11} z}$$

$$E_\theta = j\omega\mu \kappa_{11} \cos\theta J_1'(\kappa_{11}\rho) e^{-\gamma_{11} z} = -\frac{j\omega\mu}{\gamma_{11}} H_\rho \qquad (2.1)$$

$$E_\rho = j\omega\mu \sin\theta \frac{J_1(\kappa_{11}\rho)}{\rho} \cdot e^{-\gamma_{11} z} = \frac{j\omega\mu}{\gamma_{11}} H_\theta$$

where (ρ, θ, z) are cylindrical coordinates with the z-axis coincident with the axis of the waveguide

γ_{11} = propagation constant = $\alpha_{11} + j\beta_{11}$

$= (\kappa_{11}^2 - k^2)^{\frac{1}{2}}$

and α_{11} = attenuation constant

β_{11} = phase constant

$k = 2\pi/\lambda$ = free space phase constant

and $J_1'(\kappa_{11} a) = 0$, a = waveguide radius

$\therefore \kappa_{11} a = 1.84118$ for TE_{11} mode.

The radiation by this mode from an open waveguide end may be calculated(34) and is given by

$$E_\theta = -\frac{\omega\mu}{2R}\left[1+\frac{\beta_{11}}{k}\cos\theta\right]J_1(\kappa_{11}a)\,\frac{J_1(ka\sin\theta)}{\sin\theta}.\sin\phi.e^{-jkR}$$

$$= f_\theta(R,\theta)\sin\phi.\ e^{-jkR}$$

$$E_\phi = -\frac{ka\omega\mu}{2R}.\left[\frac{\beta_{11}}{k}+\cos\theta\right].J_1(\kappa_{11}a).\frac{J_1'(ka\sin\theta)}{1-(\frac{k\sin\theta}{\kappa_{11}})^2}.\cos\phi.e^{-jkR}$$

$$= f_\phi(R,\theta).\cos\phi\,.e^{-jkR} \qquad (2.2)$$

assuming no fringing and a perfect match at the open end of the waveguide. (The coordinate system is given in fig. 2.3).

The nature of this radiation pattern is shown diagrammatically in fig. 2.3(a). The gain function for this mode may be calculated from[35]

$$G(\theta,\phi) = 4\pi.\frac{P(\theta,\phi)}{P_t} \qquad (2.3)$$

where $P(\theta,\phi)$ = power radiated per unit solid angle

$$= \frac{R^2}{2\eta}|E|^2$$ where η = intrinsic impedance of medium

$$= \sqrt{\frac{\mu_o}{\epsilon_o}}$$ for air

and P_t = total power radiated

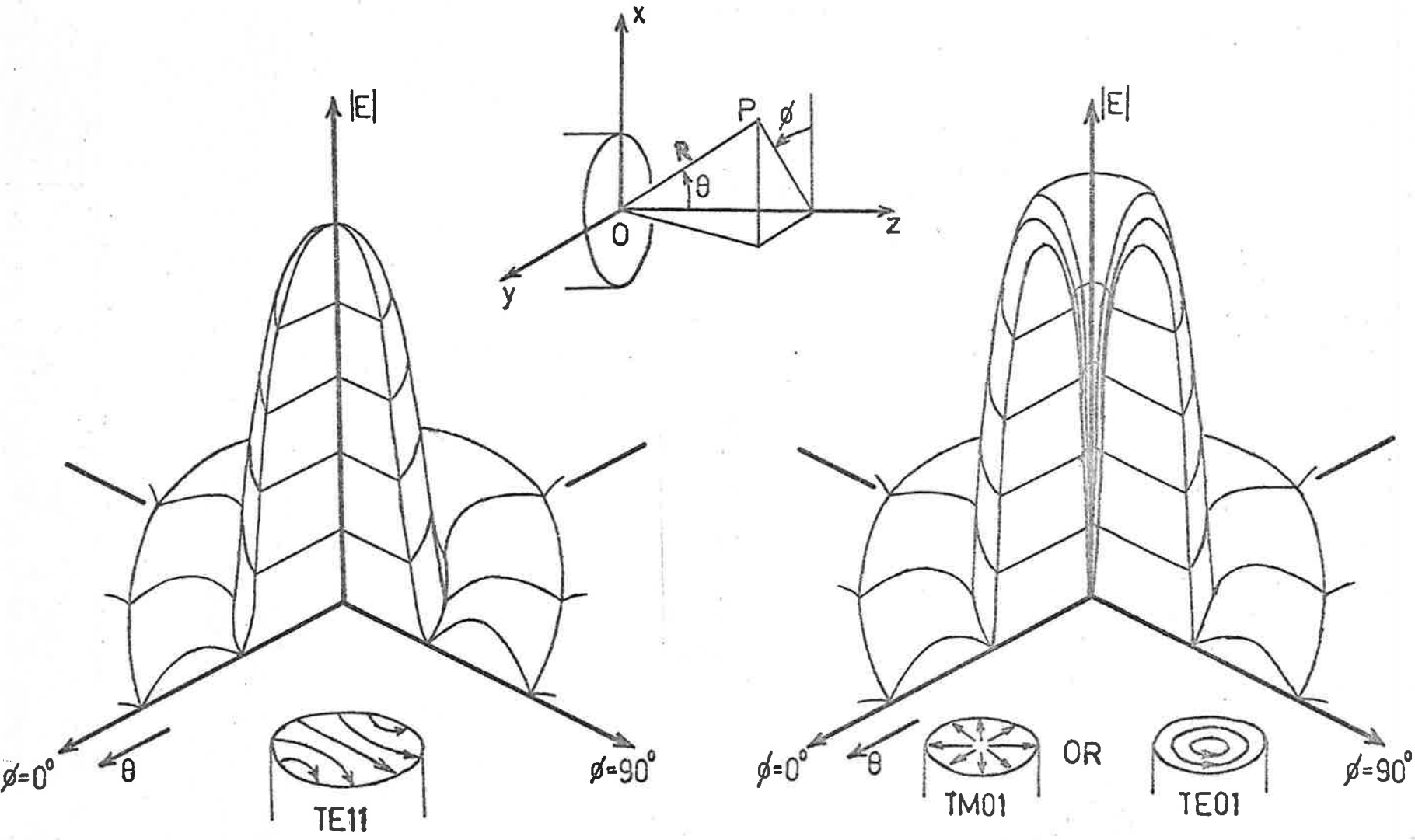

Fig. 2.3 Radiation Patterns

= total power propagating in waveguide for matched conditions[36,37]

$$= \frac{\pi}{4}\omega\mu\beta_{11} \quad [(\kappa_{11}a)^2 - 1] \cdot J_1^2(\kappa_{11}a)$$

This gain function is plotted in fig. 2.4 and from this it can be seen that the TE_{11} mode has a radiation characteristic suitable for the reference or sum channel in the tracking system. It is upon this mode that all circular waveguide feeds for paraboloidal antennae are based.

The radiation pattern of a paraboloid, fed by such a waveguide radiator, can also be approximated and computed (see Appendix I for notes on calculation of radiation patterns). In this case the expressions are

$$\left.\begin{matrix} E_\theta \\ E_\phi \end{matrix}\right\} = -\frac{j\omega\mu}{2\pi} \cdot \frac{e^{-jkR}}{R} \cdot \sqrt{\frac{\epsilon}{\mu}} \quad \left\{\begin{matrix} I_\theta \\ I_\phi \end{matrix}\right. \qquad (2.4)$$

where

$$I_\theta = \pi \sin\phi \int_0^E \{\cos\theta.\cos\xi/2\ [J_0(u).\overline{f_\theta + f_\phi} - J_2(u).\overline{f_\theta - f_\phi}$$

$$- 2j\ \sin\theta.\sin\xi/2.J_1(u)\}\ \exp\{-jk\rho[1 + \cos\theta.\cos\xi]\}$$

$$\rho^2.\sin\xi\ \sin\xi/2\ d\xi$$

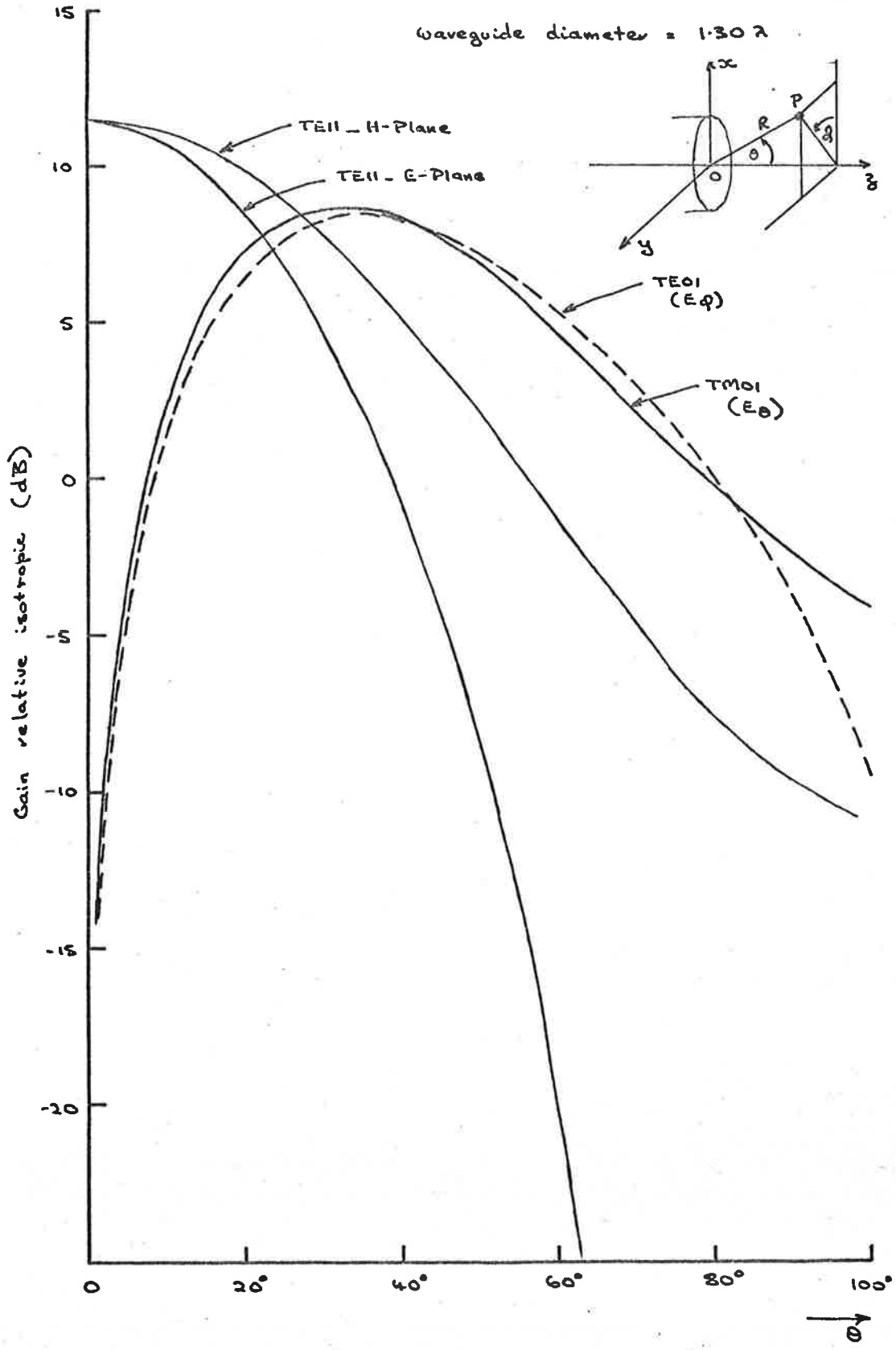

Fig. 2.4 Radiation from Circular Waveguide

$$I_\phi = \pi\cos\phi\int_0^E \{J_0(u).\overline{f_\theta + f_\phi} + J_2(u).\overline{f_\theta - f_\phi}\}$$

$$\exp\{-jk\rho[1 + \cos\theta\cos\xi]\}\rho^2.\sin\xi.d\xi$$

and $u = k\rho.\sin\theta.\sin\xi$

$f_\theta = f_\theta(\rho,\xi)$ and $f_\phi = f_\phi(\rho,\xi)$ are defined above in equations (2.2)

The gain function may be calculated as before (equation (2.3)) and this is given in fig. 2.5 together with the coordinate system. An important feature of this pattern is that the gain near boresight is almost constant.

2.2.2 The Difference Modes

Tracking error information can be obtained in circular waveguide if another mode is excited which has a voltage radiation characteristic, and hence by reciprocity the same receiving characteristic, like that shown as the difference pattern in fig. 1.2(c) for any plane ϕ = constant and whose phase relative to a dominant mode excited in the same guide by the same source is given by the azimuth angle, ϕ. With this information, the distance of the source off the boresight axis is given by the amplitude of the difference mode and the direction, from some set of reference axes, by the phase.

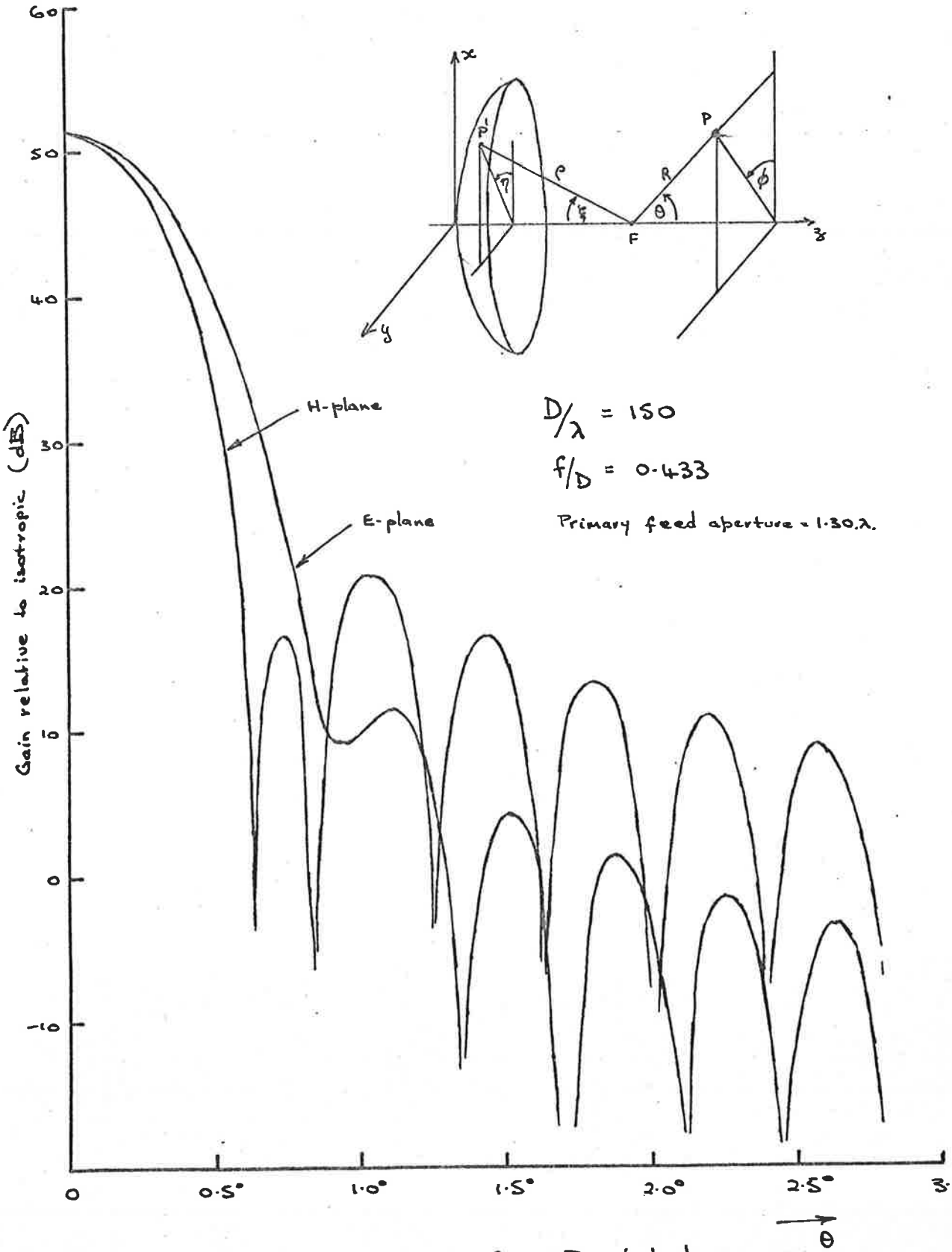

Fig. 2.5 TE11 Radiation from Paraboloid

Both these conditions are satisfied by the circularly symmetric modes in circular waveguide; these are the magnetic mode, TM_{01}, and the electric mode, TE_{01}. Their fields within the waveguide are given by[33]

TM_{01}:

$$E_z = \kappa'^2_{01} \cdot J_o(\kappa'_{01}\rho) \cdot e^{-\gamma'_{01} z} \qquad H_z = 0$$

$$E_\rho = -\gamma'_{01}\, \kappa'_{01}\, J'_o(\kappa'_{01}\rho) \cdot e^{-\gamma'_{01} z} = \frac{\gamma'_{01}}{j\omega\epsilon} \cdot H_\theta \qquad (2.5)$$

$$E_\theta = H_\rho = 0$$

where the symbols are as defined under equation (2.1) with the prime denoting a transverse magnetic mode. In this case the boundary condition is satisfied by $J_o(\kappa'_{01} a) = 0$ or $\kappa'_{01} a = 2.4048$.

and for TE_{01}:

$$E_z = 0 \qquad H_z = \kappa^2_{01}\, J_o(\kappa_{01}\rho) \cdot e^{-\gamma_{01} z}$$

$$E_\theta = j\omega\mu\, \kappa_{01}\, J'_o(\kappa_{01}\rho)\, e^{-\gamma_{01} z} = \frac{j\omega\mu}{\gamma_{01}} \cdot H_\rho \qquad (2.6)$$

$$E_\rho = H_\theta = 0$$

and $J'_o(\kappa_{01} a) = 0$, i.e. $\kappa_{01} a = 3.83171$.

These fields are shown in figs.2.2(b) and (c). From symmetry considerations the radiation patterns for these modes must be of the form shown in fig. 2.3(b), with the TM_{01} mode responding only to E_θ components of an incident signal and the TE_{01} mode only to E_ϕ. By inspection it can also be seen that a reversing voltage characteristic will be obtained as a source of constant polarization passes through boresight for either mode. It can be easily demonstrated that the phase criterion is also satisfied for each of these modes by considering a circularly polarized source at the point P shown in fig. 2.3. A signal polarization diagram can be drawn and is shown in fig. 2.6. The source signal may be written as

$$E_S = E_o . e^{j(\omega t + \alpha)}$$

and

$$E_\theta = \mathrm{Re}\ (E_S)$$

$$= E_o \cos\ (\omega t + \alpha)$$

$$E_\phi = \mathrm{Im}(E_S)$$

$$= E_o . \sin(\omega t + \alpha)$$

Since the circularly symmetric modes respond only to E_θ in the TM_{01} case and E_ϕ in the TE_{01} case the received

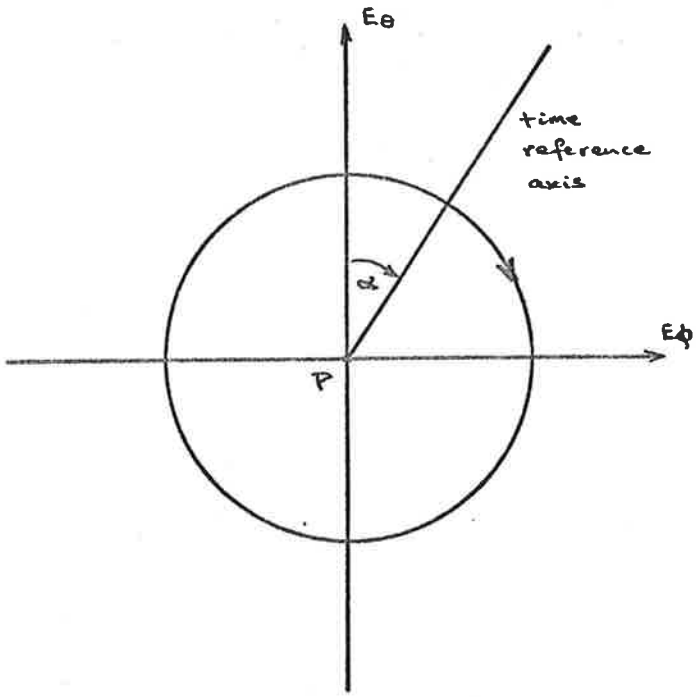

Fig. 2.6 Signal polarization at point P and in plane normal to OP (fig. 2.3)

signals may be written:

for TM_{01} mode: $E_m = C_1 E_o \cos(\omega t + \alpha)$ where $C_1 = C_1(R, \theta)$

for TE_{01} mode: $E_e = C_2 E_o \sin(\omega t + \alpha)$ $C_2 = C_2(R, \theta)$

For the reference (or in practice TE_{11}) mode, provided the point P is close to the boresight axis (i.e. θ small), the radiation pattern may be considered symmetrical and written as

$$E_\theta = C_3 . \sin\phi$$
$$E_\phi = C_3 . \cos\phi \qquad \text{(from equation 2.2)}$$

where $C_3 = C_3(R,\theta)$.

By reciprocity, the received reference signal will be of the form

$$E = C_4 E_o \left(\cos(\omega t + \alpha)\sin\phi + \sin(\omega t + \alpha)\cos\phi\right)$$

$$= C_4 E_o . \sin(\omega t + \alpha + \phi)$$

$$[= C_4 \ \mathrm{Im}\ (E_s . e^{j\phi})]$$

The results for a signal with the opposite hand polarization are essentially the same and may be obtained by replacing ω with $(-\omega)$ in the above analysis.

From these results, it can be seen that the relative phase between a circularly polarized signal received using a circularly symmetric mode and sum mode

with a symmetric pattern is a measure of the azimuth angle of the source relative to the system axes. As indicated above, this is true in the vicinity of boresight in the practical case of a TE_{11} reference mode. Since the system would normally be used in conjunction with a servodrive system, moderate phase error (15^{o}-20^{o}) can be tolerated and so non-ideal off-axis performance can be admitted.

These results show that only one circularly symmetric mode need be detected for tracking error information when the signal is circularly polarized. The sum mode would normally be designed to extract maximum power from the circularly polarized signal (i.e. detect in time and space quadrature and add the signals). However, such a system has severe limitations in a polarization diverse situation. These are caused by the phase shift between the two modes no longer being dependent solely upon the azinuth of the source but also on the ellipticity of source polarization. This may be demonstrated by considering, say, the signal received by the TM_{01} mode.

The general elliptically polarized source signal can be written

$$E_s = E_o \left(e^{j\omega t} + e^{-j\omega t}\right)e^{j\alpha}$$

thus

$$E_\theta = \mathrm{Re}(E_s)$$

$$= E_o \left[\cos(\omega t + \alpha) + b \cos(\omega t - \alpha) \right]$$

$$= E_o . A . \cos(\omega t + \beta)$$

$$\text{where } A^2 = (1+b)^2 \cos^2\alpha + (1-b)^2 \sin^2\alpha$$

$$\text{and } \beta = \arctan\left[\frac{1-b}{1+b} \tan\alpha\right]$$

Assuming the sum mode detects the desired circularly polarized component it will have the same form as before and the phase difference can be seen to depend upon the ellipticity, measured by b. This phase error has the effect of causing cross-coupling between the servodrive systems. Provided it is only moderate, say 15°-20°, it can be tolerated, but in the general polarization diverse situation, greater errors are probable.

Apart from phase error considerations, the simple two mode tracking system is not practicable for linearly polarized signals since the difference mode will be inoperative when the mode and signal polarizations are orthogonal. These difficulties can be overcome by detecting both the circularly symmetric modes and then processing the signals received in such a way that right and left circularly polarized components (or vertical and horizontal components) are treated separately. In this

way complete polarization diversity can be obtained for the tracking system.

Before proceeding with the analysis of the received signals in the three mode case, some properties of the radiation patterns of the circularly symmetric modes of interest in the tracking system will be considered. The approximate patterns for the modes radiating from the open end of a waveguide can be calculated and, assuming matched conditions, the expressions are[34]

TM_{01}:

$$E_\theta = -j \frac{k a \kappa'_{01}}{2R \sin\theta} \cdot \left[\frac{\beta'_{01}}{k} + \cos\theta \right] \cdot \frac{J_o(k a \sin\theta) . J'_o(\kappa'_{01} a)}{1 - (\frac{\kappa'_{01}}{k \sin\theta})^2} . e^{-jkR}$$

$$= f_3(R,\theta) . e^{-jkR}$$

and TE_{01}:

$$E_\phi = j \frac{k a \omega \mu}{2R} \left[\frac{\beta_{01}}{k} + \cos\theta \right] \cdot \frac{J_o(\kappa_{01} a) . J'_o(k a \sin\theta)}{1 - (\frac{k \sin\theta}{\kappa_{01}})^2} . e^{-jkR}$$

$$= f_4(R,\theta) . e^{-jkR}$$

where the symbols are as previously defined. The gain functions may be calculated using equation (2.3) and the

following power expressions(37)

$$TM_{01}: \quad P_t = \frac{\pi}{4} \cdot \omega\varepsilon \cdot \beta'_{01} (\kappa'_{01} a)^2 \cdot J_1^2(\kappa'_{01} a)$$

and $$TE_{01}: \quad P_t = \frac{\pi}{4} \cdot \omega\mu \cdot \beta_{01} \left[(\kappa_{01} a)^2 - 1\right] \cdot J_o^2(\kappa_{01} a)$$

These gain functions are plotted, together with the TE_{11} pattern for comparison,† in fig. 2.4 for the case of a 1.3λ diameter waveguide. This is a suitable size for illuminating a paraboloid with an $^f/_D$ roughly 0.4. It is also near the minimum waveguide size for propagation of the TE_{01} mode, which needs a diameter above 1.22λ. In this case the radiation patterns of the TE_{01} and TM_{01} modes are seen to be very similar. In fig. 2.7 the radiation patterns for the same modes from a waveguide of diameter 4.3λ are given; this is the approximate aperture necessary to feed a cassegrain system with a subreflector half angle of 15^o. Here the radiation patterns of the two circular modes are no longer very similar although the maximum difference over the range of interest is less than 2 dB.

These gain functions for radiation from circular waveguide do show one drawback for use with reflector systems: the high edge gain. The very moderate edge

† The question occasionally arises of the validity of comparing gain functions directly, especially in the receiving case, in a multimode waveguide radiator. Provided the modes within the guide are uncoupled, it is easy to prove that this is legitimate by the reciprocity theorem (see Appendix II).

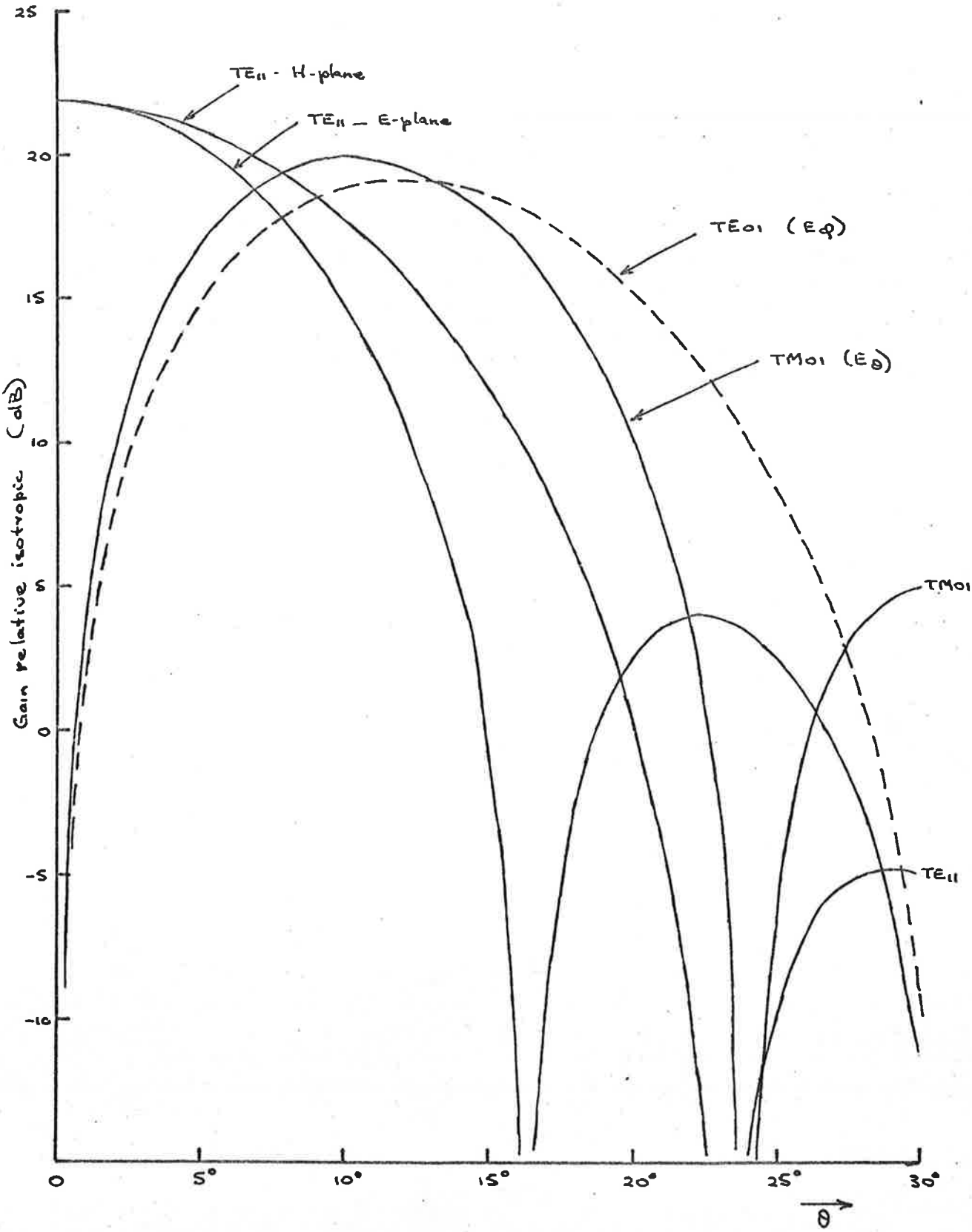

Fig. 2.7 Gain functions for waveguide, diam. = 4·3λ

taper means that there is considerable loss of efficiency due to spillover. The large spillover also means susceptibility to noise. This is particularly important in the case of a front fed paraboloid where spillover illuminates the hot ground with its high noise contribution. The cassegrain system is less effected by ground noise but spillover past the subreflector will introduce additional unwanted sky-noise and will limit tracking close to hot radiating bodies. The problem of spillover can be considered inherent in any simple system including the simple four horn monopulse. Hannan[17] has shown that to overcome it the effective aperture for the difference modes must be twice that for the sum modes. Because of the single aperture restriction, imposed earlier, the possibility of achieving optimum tracking performance is limited to altering the feed aperture distributions to this end; in the normal usage the ultimate receiving performance would not be sacrificed for tracking performance.

The expressions for radiation from a paraboloidal reflector may be written as follows:

TM_{01}:

$$E_\theta = -\frac{j\omega\mu}{R}.e^{-jkR}.\sqrt{\frac{\epsilon}{\mu}}\int_0^E f_3\,[\cos\theta.\cos\xi/2.J_1(u) + j\sin\theta.\sin\xi/2.J_0(u)]\exp\{-jk\rho[1+\cos\theta\cos\xi]\}\,\rho^2\sin\xi\sec\xi/2\,d\xi \qquad (2.9)$$

where $u = k\rho \sin\theta.\sin\xi$ and $f_3 = f_3(\rho,\xi)$

and TE_{01}:

$$E_\phi = j\omega\mu . \frac{e^{-jkR}}{R} . \sqrt{\frac{\epsilon}{\mu}} \int_0^E f_4 . J_1(u) . \exp\{-jk\rho[1 + \cos\theta.\cos\xi]\}$$

$$\rho^2 . \sin\xi . d\xi \qquad (2.10)$$

where $u = k\rho \sin\theta.\sin\xi$ and $f_4 = f_4(\rho,\xi)$.

The corresponding gain function is plotted in fig. 2.8. (The equivalent case for a cassegrain system has not been calculated but will give results very similar to those given. For various methods of treating a cassegrain system see Appendix I). Once again the two patterns are almost identical over the first lobe, the difference being a maximum near the first off-axis null, but over the range of $0-0.6^\circ$ remaining less than 1 dB.

The need for the gain functions of the two tracking modes to be similar arises from the same reasons as the desirability of a symmetric sum mode pattern. This is to avoid the introduction of ellipticity into the system by the mode characteristics and corresponding errors in determining the azimuth direction. If the ellipticity of both the reference mode and the error mode combination were identical for angles (θ,ϕ) of interest, it could be accommodated by modifying,for

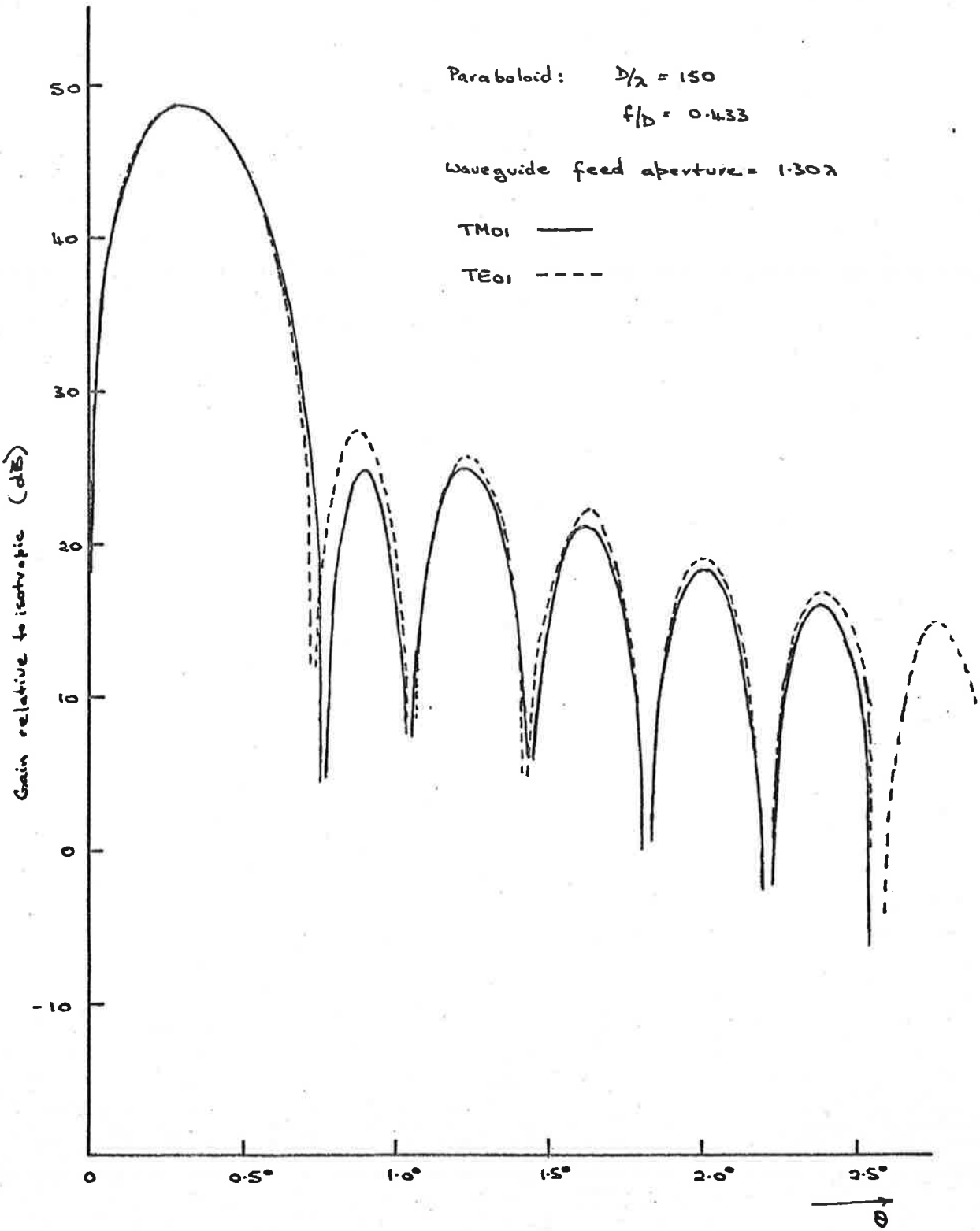

Fig. 2.8 Difference Mode Radiation from Paraboloid.

calculation purposes, the input signal accordingly and treating the system as perfect. However, it is unlikely that this situation would occur in practice and more benefit derives from designing for symmetric beams, especially in the reference case where efficiency will also be enhanced.

These radiation expressions also exhibit another desirable feature when considered in terms of a servo-controlled tracking antenna. This is a voltage error characteristic linear about boresight. This is easily seen in the above expressions by assuming θ is small such that

$$\cos\theta \simeq 1$$

$$\text{and} \quad \sin\theta \simeq \theta$$

Substituting these values and using

$$J_0'(x) = -J_1(x)$$

$$\text{and} \quad J_0(x) \simeq 1 \qquad \text{for } x \ll 1$$

$$J_1(x) \simeq \frac{x}{2}$$

equations (2.7-10) can be reduced to the form

$$E = K(R).\theta \text{ for small } \theta.$$

A comparison of the slopes near boresight for the two modes gives a good indication of system symmetry in this cricical region. For the examples plotted, the

slope differences are calculated as:

1.3λ w.g.	TM_{01}	:	TE_{01}	slope difference	= 1 dB
4.3λ w.g.	"	"	"	"	= 1.4 dB
150λ paraboloid	"	"	"	"	0.1 dB

These figures may be interpreted as the additional power gain needed in the TE_{01} receiver channel to equate the effective slopes. These figures are representative of the ideal system and are probably well within the gain tolerance of amplifiers used in a practical system. Accordingly for practical purposes they can be ignored.

2.3 Comparison of Difference Slope with Amplitude Comparison Monopulse

The voltage difference pattern slope on boresight provides a measure of the pointing accuracy that can be expected from a tracking antenna, a larger slope giving better accuracy. In this case the performance of the multimode tracking system can be gauged by comparing the difference slope with that obtainable in the conventional four horn amplitude comparison case. This is most easily done by forming a pair of equivalent static split beams from the actual reference and error mode patterns.

Fig. 2.9 gives the reference and error mode gain functions for a multimode system in circular waveguide. As before the error mode is the TE_{01} radiation from a large paraboloid and similarly, the reference mode is the TE_{11} mode, but with the addition of TM_{11} mode[11] to produce a symmetric beam. This additional mode is included by straight superposition of the TE_{11} and TM_{11} fields in the waveguide. The waveguide field for TM_{11} mode is given by

$$E_z = B.\kappa'^2_{11} \cos\theta.\ J_1(\kappa'_{11}\rho).e^{-\gamma'_{11}z} \qquad H_z = 0$$

$$E_\rho = -B.\gamma'_{11}\kappa'_{11}\cos\theta.J'_1(\kappa'_{11}\rho).e^{-\gamma'_{11}z} = \frac{\gamma'_{11}}{j\omega\epsilon} H_\theta$$

$$E_\theta = B.\ \gamma'_{11} \sin\theta \frac{J_1(\kappa'_{11}\rho)}{\rho} . e^{-\gamma'_{11}z} = -\frac{\gamma'_{11}}{j\omega\epsilon} H_\rho$$

where the symbols are as previously defined with the boundary condition $J_1(\kappa'_{11}a) = 0$, hence $\kappa'_{11}a = 3.83171$ and where B is the amplitude factor relative to unity for the TE_{11} mode. The power associated with this mode is

$$P_t = B^2.\frac{\pi}{4}.\omega\epsilon.\ \beta'_{11}\ (\kappa'_{11}a)^2.\ J_2^2(\kappa'_{11}a)$$

The equivalent voltage characteristics are given in fig. 2.10.

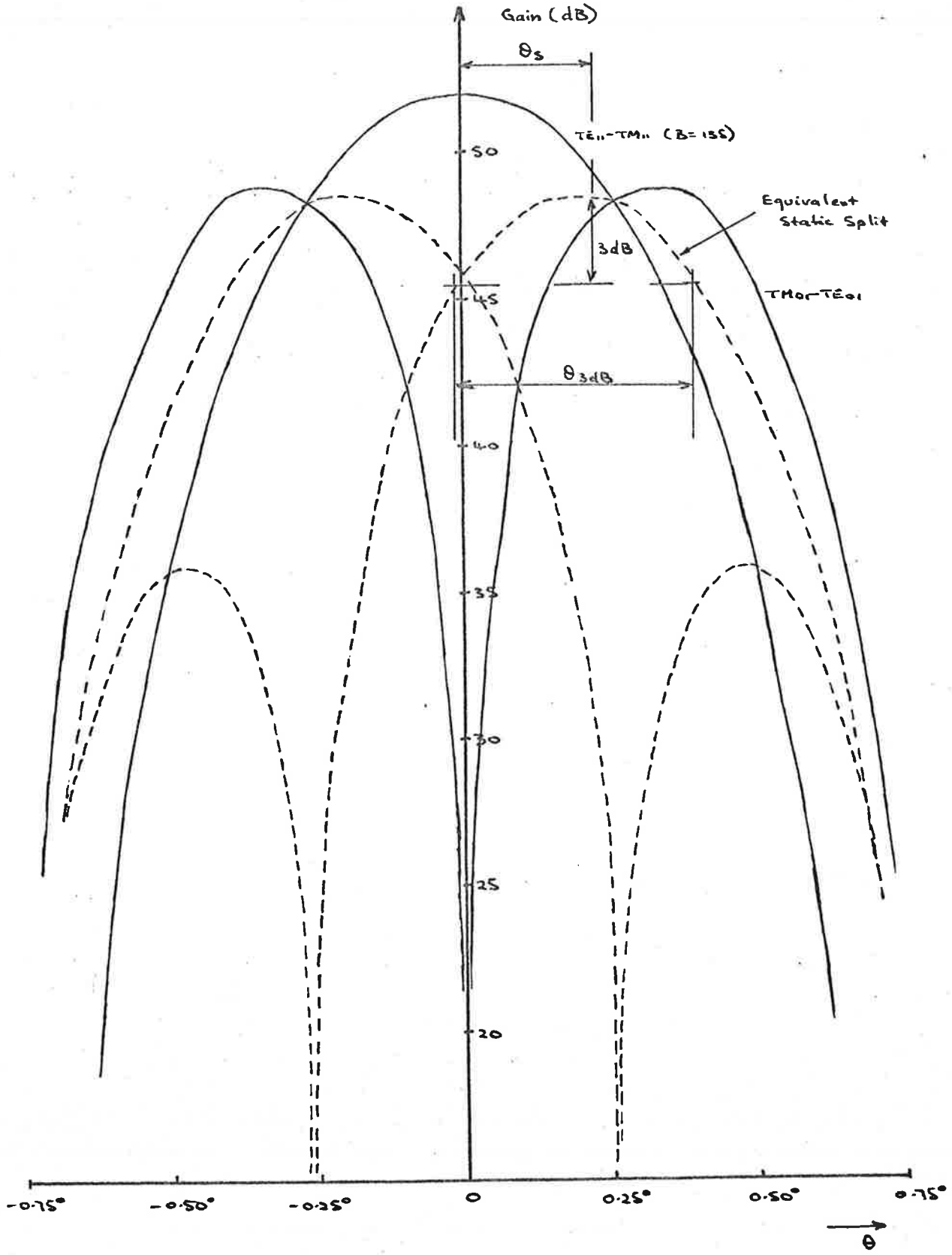

Fig. 2.9 Gain functions for multimode antenna.

$D/\lambda = 150$ $f/D = 0.433$

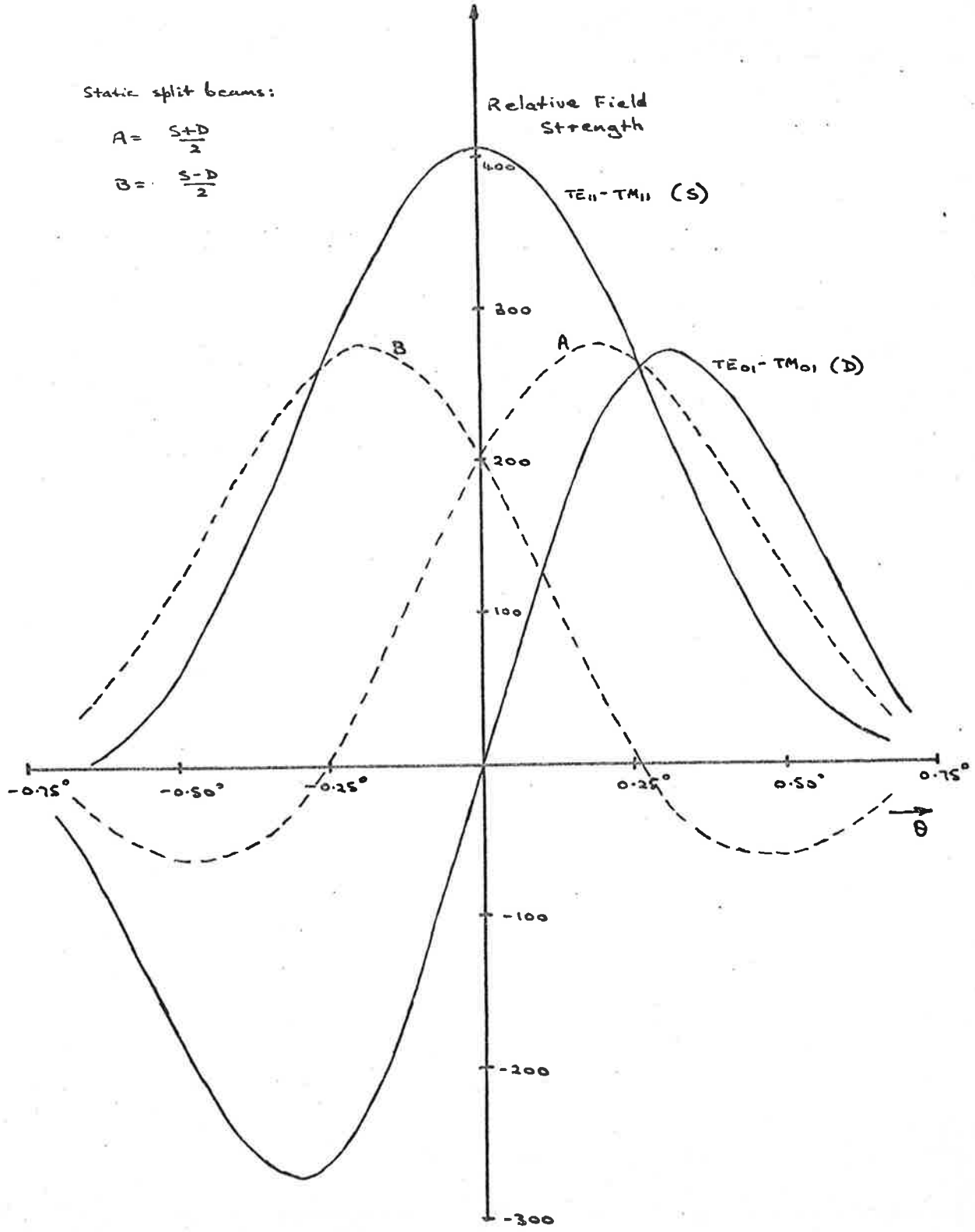

Fig. 2.10 Voltage characteristics for multimode antenna

$D/\lambda = 150$ $f/D = 0.433$

The equivalent pair of static split beams are formed from the voltage characteristic by

$$A = \frac{S + D}{2}$$

and $$B = \frac{S - D}{2}$$

These characteristics are shown in figs. 2.9 and 2.10. This pair of beams is an ideal uncoupled pair and would not be attainable in practice.(38) Following Pelchat(38) the squint angle may be defined as half the angle between the two beams.

$\therefore$ From fig. 2.9 $\theta_s = 0.2^\circ$

3 dB beamwidth $= \theta_{3dB} = 0.41^\circ$ for $D/\lambda = 150$

and thus $$\frac{\theta_s}{\theta_{3dB}} = 0.49$$

This ratio is characteristic of any large antenna with a similar illumination function for the shape of the beam is essentially independent of λ/D and only the angular spread alters.(39) Accordingly that class of large reflector antennae ($D/\lambda > 20$) with $f/D = 0.43$ and excited by this same combination of modes will always produce an equivalent static split with a squint ratio = 0.49.

Fig. 2.11 gives curves reproduced from Pelchat which show that the difference slope obtainable from the

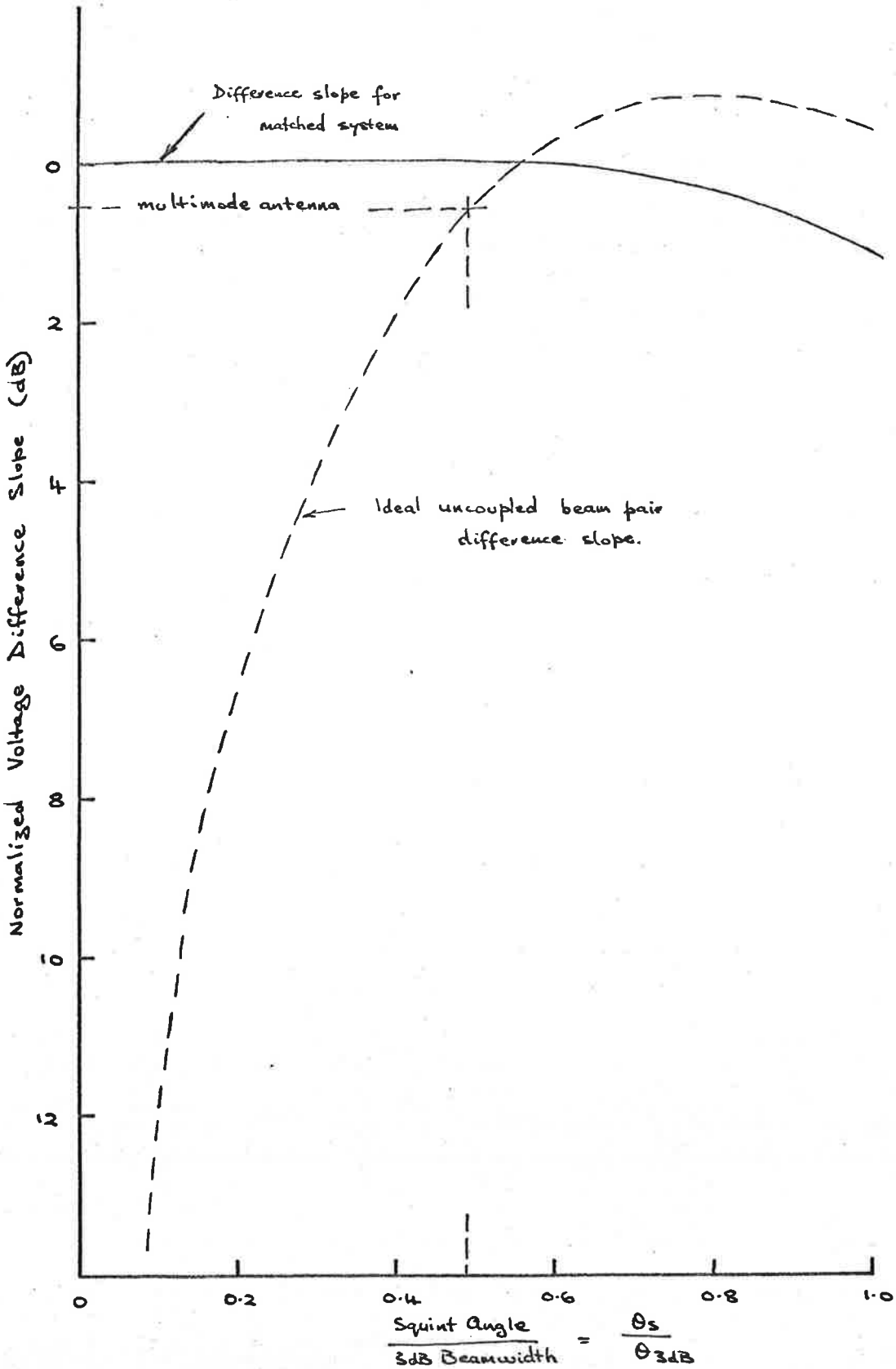

Fig. 2.11 Difference Voltage Pattern Slope (from Pelchat)

multimode system is approximately 0.5 dB less than that obtainable from an optimally matched two beam antenna. (This curve assumes the beam has the form $\frac{\sin \mu}{\mu}$ which is a good approximation for antennae with large D/λ). This indicates that the tracking performance of the multimode system is at least comparable with that obtainable from more conventional systems and can be considered competitive in low noise systems.

2.4 Signal Processing in Multimode Tracking Systems

The actual processing method used in a tracking system will depend upon antenna design for the reference or sum mode channel. In general the antenna may produce either of two output forms. The first is simply the output of horizontally and vertically polarized components of the received signal. The second form of design is one which produces outputs from the right- and left-hand circularly polarized components of the received signal. In a practical low noise system the second is the preferred system, for the phase shifting mechanism becomes an integral part of the antenna design and avoids the necessity of external hybrid circuits to form circularly polarized signals. In some systems a separate tracking frequency may be available, in which case the tracking signal would be sampled as horizontal

and vertical components; however, in the deep space probe satellite the weight and power requirement would preclude a second transmitter solely for tracking purposes.

Both forms of antenna produce the same error signals, but by different processing networks. For convenience these will be termed "Linear polarization processor" and "Circular polarization processor". For the remainder of this section it will be assumed that the reference mode has a symmetric radiation pattern and no ellipticity will be introduced into the signal polarization by this mode. Similarly the radiation patterns of the two circularly symmetric modes will be assumed identical to eliminate polarization ellipse modifications by the error channels. In practice these ideals can be achieved at least when the target is close to the boresight axis. The target or signal source will be assumed to appear at the antenna as a single point, P, in space (see fig. 2.3).

The signal emanating from the source will in general be elliptically polarized and may be written as:

$$E_s = E_o(k_1 e^{j\omega t} + k_2 e^{-j\omega t}).e^{j\delta} \qquad (2.11)$$

referred to the E_θ, E_ϕ radiation coordinates at point P,

and where k_1, k_2 are the amplitudes of the right and left hand circularly polarized components respectively. The phase term, δ, is as shown in fig. 2.12. Other relations describing the signal are

$$k_1 = \frac{a + b}{2}$$

$$k_2 = \frac{a - b}{2}$$

where a, b are semi-major and semi-minor axes of the ellipse.

r.h. comp. l.h. comp.

$$E_\theta = \mathrm{Re}(E_s) = E_o [k_1 \cos(\omega t + \delta) + k_2 \cos(\omega t - \delta)]$$
$$E_\phi = \mathrm{Im}(E_s) = E_o [k_1 \sin(\omega t + \delta) - k_2 \sin(\omega t - \delta)] \quad (2.12)$$

2.4.1 Linear Polarization Processor

From fig. 2.4 and equation 2.2, and assuming a symmetric pattern, the vertical and horizontal components derived from the reference channel may be written as

$$E_x = \alpha(R,\theta) [E_\theta \cos\phi - E_\phi \sin\phi]$$
$$\text{and} \quad E_y = \alpha(R,\theta) [E_\theta \sin\phi + E_\phi \cos\phi] \quad (2.13)$$

where $\alpha(R,\theta)$ is a pattern factor and for angles near boresight may be written as

$$\alpha = \frac{K_r}{R} \quad (2.14)$$

where K_r is a constant.

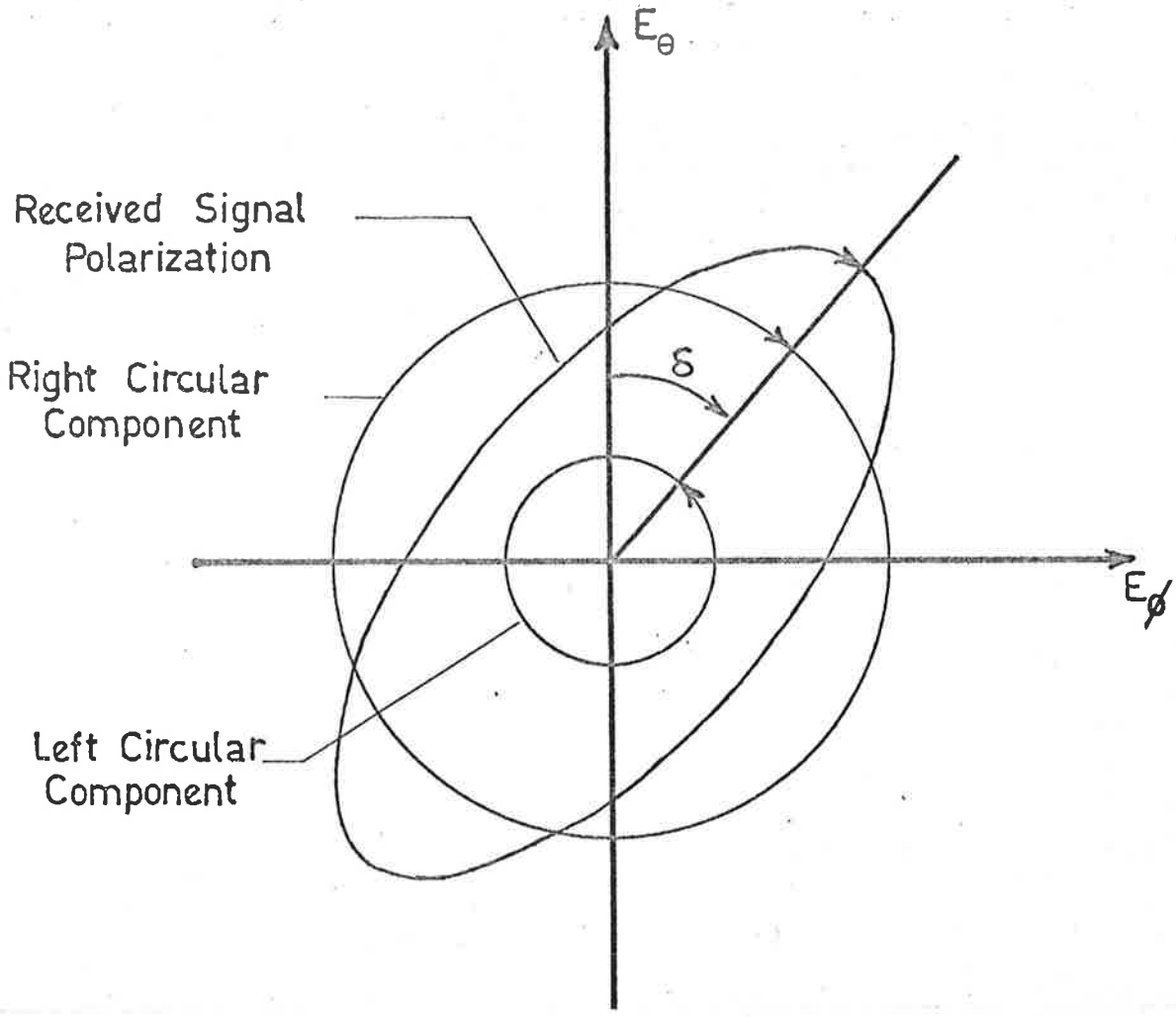

Fig. 2.12 Signal Polarization Diagram

The corresponding signals received by the difference modes are given by

$$E_t = \beta(R,\theta).E_\theta$$
$$E_p = \beta(R,\theta).E_\phi \qquad (2.15)$$

where $\beta(R,\theta)$ is a pattern factor and for targets near boresight may be approximated by

$$\beta = \frac{K_e}{R}. \qquad (2.16)$$

where K_e is a constant.

The error voltages to be derived will be applied to orthogonal drive axes of the antenna system. These axes may be chosen as the vertical and horizontal, or x- and y-, axes. The form of the error signals desired is

$$\text{vertical error voltage } e_x = k.\frac{\beta}{\alpha}.\cos\phi$$
and (2.17)
$$\text{horizontal error voltage } e_y = k.\frac{\beta}{\alpha}.\sin\phi$$

where k = constant gain factor and β/α is a normalized gain factor dependent on the off-axis distance of the source. These signals may be derived as follows:

Equations (2.13) may be rewritten as

$$E_\theta = \frac{1}{\alpha}(E_y \sin\phi + E_x \cos\phi)$$
$$E_\phi = \frac{1}{\alpha}(E_y \cos\phi - E_x \sin\phi)$$

and substituting in equation (2.15) gives

$$E_t = \frac{\beta}{\alpha}(E_y \sin\phi + E_x \cos\phi)$$

$$E_p = \frac{\beta}{\alpha}(E_y \cos\phi - E_x \sin\phi)$$

These equations, together with equation (2.17), give

$$k\,E_t = E_y \cdot e_y + E_x \cdot e_x$$

$$k\,E_p = E_y \cdot e_x - E_x \cdot e_y$$

or

$$e_x = k \cdot \frac{E_t E_x + E_p E_y}{E_x^2 + E_y^2}$$

$$e_y = k \cdot \frac{E_t E_y - E_p E_x}{E_x^2 + E_y^2} \qquad (2.18)$$

These equations show that by a suitable multiplication and addition operations on the received signals, error voltages may be derived, suitable for use in a servodrive system. The division by $E_x^2 + E_y^2$ is a normalization process and is normally achieved by automatic gain control in the i.f. amplifiers. However, it is difficult in practice to represent these equations exactly, since in the ideal case both the numerator and denominator contain second harmonic components. This is easily verified using the following relations.

From equations(2.12) and (2.13)

$$E_x = \alpha.\mathrm{Re}(E_s.e^{j\phi})$$

$$= \alpha.E_o.\ [k_1\ \cos(\omega t+\delta+\phi) + k_2\ \cos(\omega t-\delta-\phi)] \qquad (2.19)$$

and $E_y = \alpha.\mathrm{Im}(E_s.e^{j\phi})$

$$= \alpha.E_o\ [k_1\ \sin(\omega t+\delta+\phi) - k_2\ \sin(\omega t-\delta-\phi)]$$

and hence

$$E_x^2 + E_y^2 = \alpha^2\ |E_s|^2$$

$$= \alpha^2\ E_o^2\ [k_1^2 + k_2^2 + 2k_1k_2\ \cos 2\omega t] \qquad (2.20)$$

Also from equations (2.12), (2.15) and (2.19)

$$E_tE_x + E_pE_y = \alpha.\beta.E_o^2\ [k_1^2 + k_2^2 + 2k_1k_2\ \cos 2\ \omega t].\cos\phi$$

and $$E_tE_y - E_pE_x = \alpha.\beta.E_o^2\ [k_1^2 + k_2^2 + 2k_1k_2\ \cos 2\ \omega t].\sin\phi$$

(2.21)

Practical multipliers are designed to give only the low frequency or "d.c." output from the product, i.e. the average value of the output. In practice then, we have

$$\overline{E_tE_x + E_pE_y} = \overline{E_tE_x} + \overline{E_pE_y}$$

$$= \alpha.\beta.E_o^2\ (k_1^2 + k_2^2).\cos\phi \qquad (2.22)$$

and $\overline{E_t E_y - E_p E_x} = \overline{E_t E_y} - \overline{E_p E_x}$

$$= \alpha.\beta.E_o^2\ (k_1^2 + k_2^2).\sin\ \phi$$

where the bar denotes an averaging process. This averaging process can also be applied to the denominator $E_x^2 + E_y^2$, but it is possible to eliminate the need for two multipliers to form these squares (or two squaring circuits) and incorporate the normalization in an a.g.c. system, using square law detectors. This can be shown from equations (2.19) and (2.20), which, after suitable manipulation, give

$$E_x^{\ 2} + E_y^{\ 2} = 2.\ \overline{E_x^2 + E_y^2}$$

$$= 2.\alpha^2.E_o^2\ (k_1^2 + k_2^2) \qquad (2.23)$$

Rewriting equation (2.18) in the practical form gives

$$e_x = \frac{k}{2} \cdot \frac{\overline{E_t E_x} + \overline{E_p E_y}}{|E_x|^2 + |E_y|^2} = k.\frac{\beta}{4\alpha}.\cos\ \phi \qquad (2.24)$$

$$e_y = \frac{k}{2}\ \frac{\overline{E_t E_y} - \overline{E_p E_x}}{|E_x|^2 + |E_y|^2} = k.\frac{\beta}{4\alpha}.\sin\phi$$

where the gain factor k can be adjusted to accommodate the additional two factors in the denominator introduced by the power dividers. Fig. 2.13 gives the block

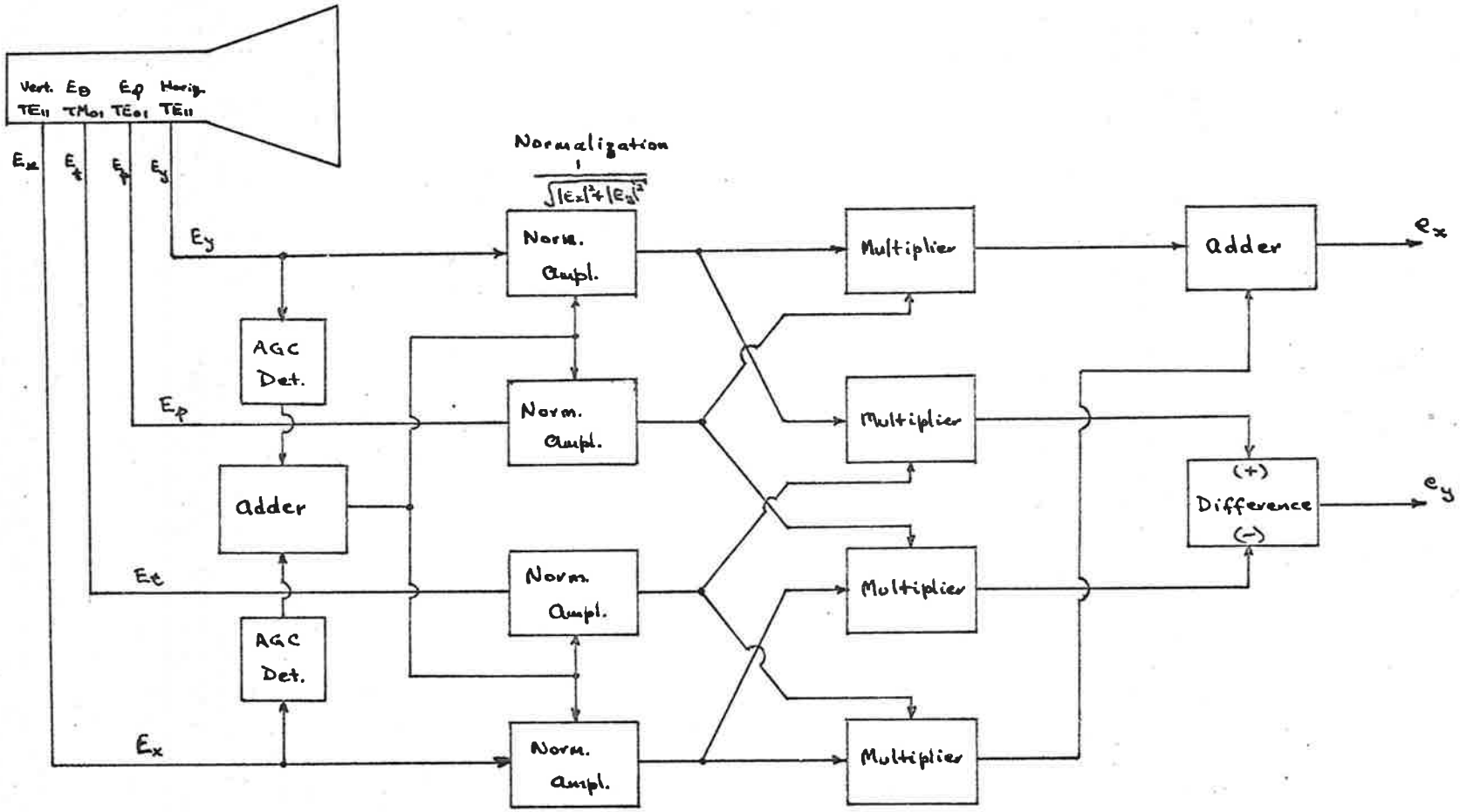

Fig. 2.13 Linear Polarization Processor

diagram of a system capable of processing the received signals in this manner. Fig. 2.14 shows how equivalent vertical and horizontal signals for use in such a processor can be obtained from right and left hand circularly polarized signals.

The block diagram of the system in fig. 2.13 shows that the price paid for a system with complete polarization diversity and independent optimization of the reference feed is a very complex processor containing four separate channels and requiring four multipliers. In an essentially linearly polarized situation, either the vertical or horizontal signal channel, depending on polarization of source, could be omitted to reduce the system to a three channel one. This, however, will introduce an error into the determination of the azimuth angle for non ideal linear polarization, i.e. cross-coupling is introduced between the drive axes. This can be illustrated by the form of the error signals, if the horizontal channel is removed.

$$e_x = \frac{\alpha.\beta.E_o^2}{2\sqrt{2}\ |E_x|^2} \cdot [(k_1^2 + k_2^2)\cos\phi + 2k_1k_2\ \cos(2\delta + \phi)]$$

and $$e_y = \frac{\alpha.\beta.E_o^2}{2\sqrt{2}\ |E_x|^2} \cdot [(k_1^2 + k_2^2)\sin\phi - 2k_1k_2\ \sin(2\delta + \phi)]$$

Coupling between e_x and e_y is only eliminated if $\phi = -\delta$

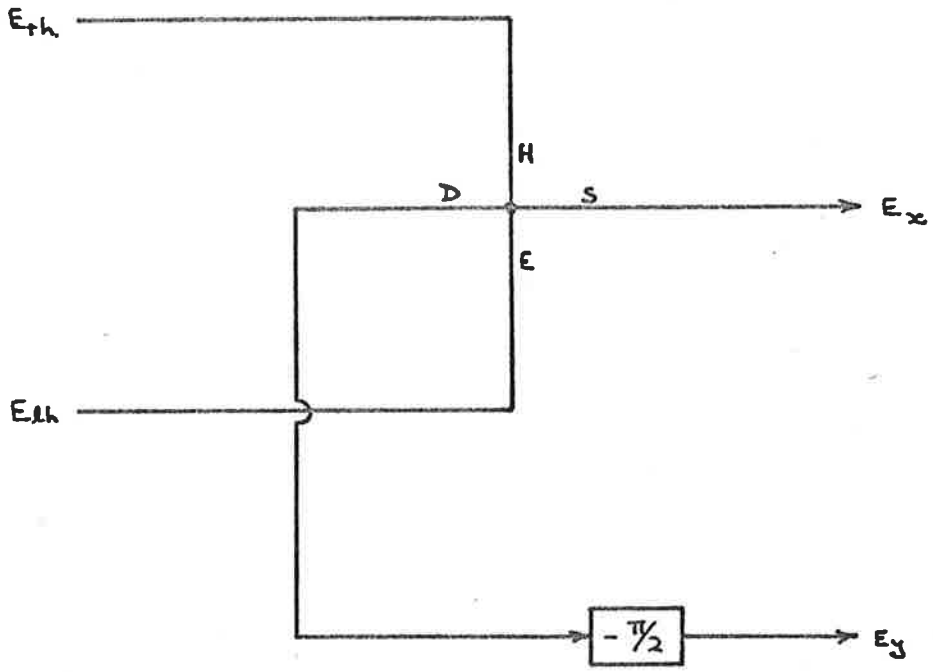

Fig. 2.14 Production of Vertical and Horizontal Signals from Circular Components.

which corresponds to the major axis of the polarization ellipse lying in the direction of the detected linearly polarized signal, or if the signal is circularly polarized, i.e. k_1 or k_2 zero.

2.4.2 Circular Polarization Processor

Reference channel outputs proportional to the right and left hand circularly polarized components of an input signal are formed by the process illustrated in fig. 2.15. This is true independent of whether the equivalent delay and hybrid network forms an integral part of the antenna or whether it is achieved outside of the antenna.

From fig. 2.15 and equation 2.19 the received circularly polarized components are

$$\begin{aligned} E_{rh} &= \sqrt{2}.\ a(R,\theta).\ E_o\ k_1 \cos(\omega t + \delta + \phi) \\ E_{lh} &= \sqrt{2}.\ a(R,\theta).\ E_o\ k_2 \cos(\omega t - \delta - \phi) \end{aligned} \qquad (2.25)$$

Similarly, signals proportional to the circularly polarized components of the incident energy can be produced from the two difference modes by using a circuit as in fig. 2.15 but substituting E_t and E_p for the vertical and horizontal polarization signals, E_V and E_H. From equations(2.12)and (2.15) the output from the hybrid will be

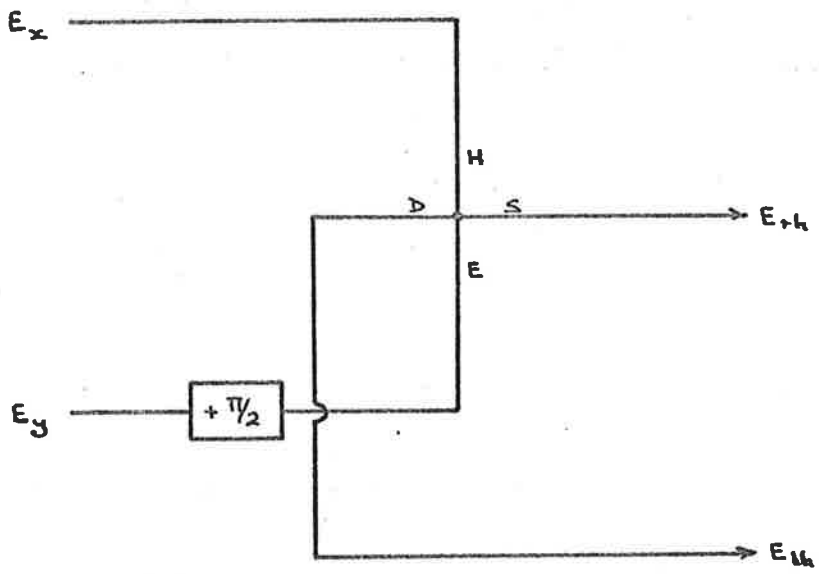

Fig. 2.15 Circular Components from Linear Polarization Signals.

$$E'_{rh} = \sqrt{2}\ \beta\ E_o\ k_1\ \cos(\omega t + \delta)$$

and $$E'_{lh} = \sqrt{2}\ \beta\ E_o\ k_2\ \cos(\omega t - \delta) \qquad (2.26)$$

Equations (2.25) and (2.26) show that the outputs from the right and left circular components detected by the sum and difference modes differ in phase by the azimuth angle, ϕ. By multiplying the signals, both in phase and time quadrature, suitable error voltage signals can be derived in both the left hand and right hand polarization cases. To maintain sensible outputs the signals must be normalized against the reference channel output. The error voltages may be calculated as

right hand channel:

$$e_x = k.\ \frac{\frac{1}{2}.\overline{E_{rh}\ E'_{rh}}}{|E_{rh}|^2}$$

$$= k.\frac{\beta}{4a}.\cos\phi \qquad (2.27)$$

and $$e_y = k.\ \frac{\frac{1}{2}.\overline{E_{rh}\ E'_{rh}(+\pi/2)}}{|E_{rh}|^2}$$

$$= k.\frac{\beta}{4a}.\sin\phi$$

where k is a gain constant and $E'_{rh}(+\pi/2)$ denotes E'_{rh} delayed by 90°.

left hand channel:

$$e_x = k. \frac{\overline{\frac{1}{2}.E_{lh}\ E'_{lh}}}{|E_{lh}|^2}$$

$$= k.\frac{\beta}{4\alpha}.\cos\phi \qquad (2.28)$$

and $$e_y = k. \frac{\overline{\frac{1}{2}.E_{lh}\ E'_{lh}(-\pi/2)}}{|E_{lh}|^2}$$

$$= k.\frac{\beta}{4\alpha}.\sin\phi$$

where $E'_{lh}(-\pi/2)$ denotes E'_{lh} advanced 90° with respect to E_{lh}.

These relations show that tracking without error may be obtained by selecting either the right and left hand circularly polarized component of the input signal. In situations where the source signal is predominantly circularly polarized this allows a receiver with only two basic signal channels to be used, with no error introduced by the polarization loss. Such a system, with a simple switching arrangement to select the right or left hand component, is shown in fig. 2.16.

To obtain complete polarization diversity it is necessary to combine the outputs of the left and right hand channels. However, it would be unwise simply to add the error voltage outputs, for, in the event of one or other of the input components becoming zero, this

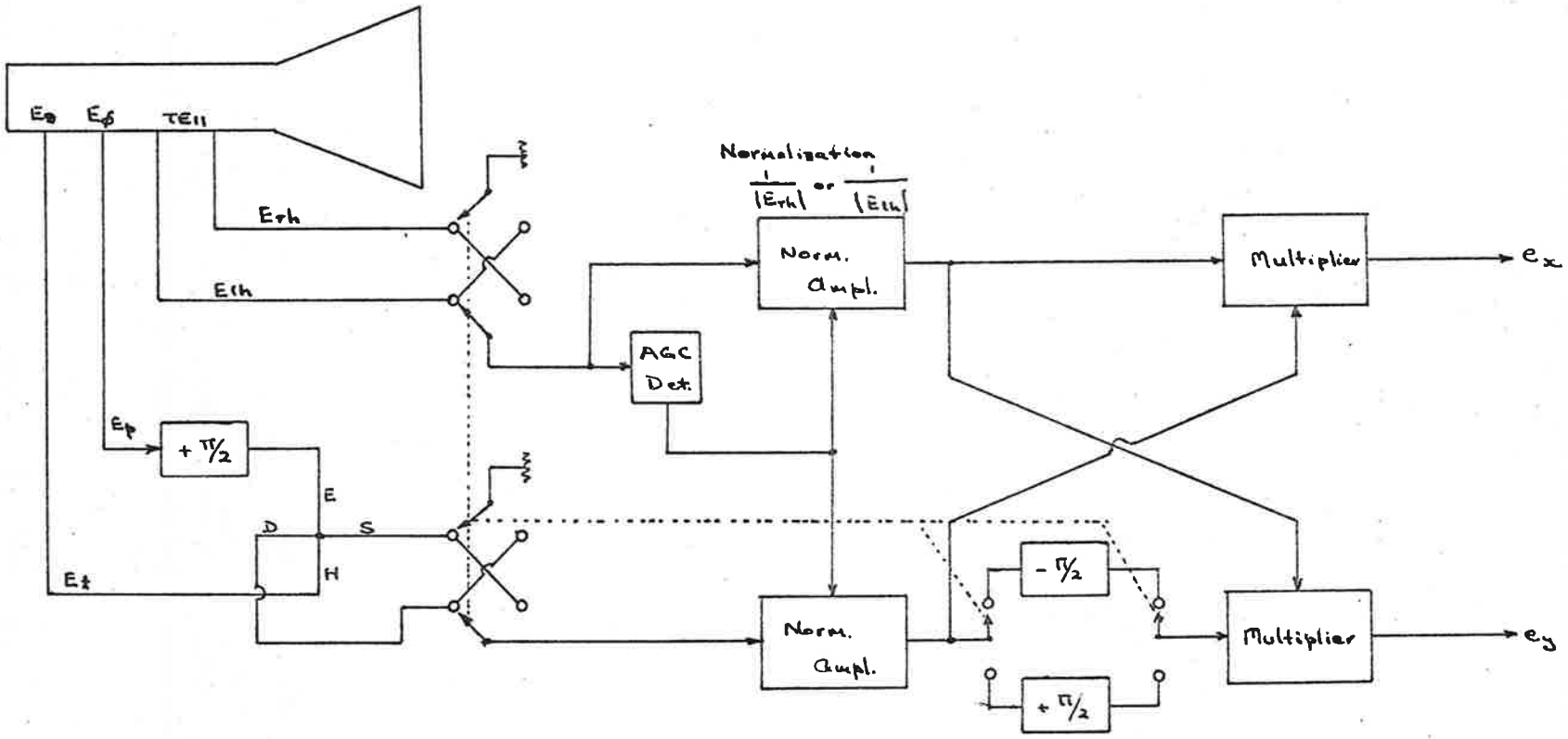

Fig. 2.16 Simplified Circular Polarization Processor

channel will be operating at maximum gain and thus will introduce large noise voltages to the drive system, causing excessive tracking jitter. This problem can be overcome by normalizing each signal against a combined amplitude factor from the two reference channels. In this case the error voltage relations become

$$e_x = k. \frac{\frac{1}{2}. [\overline{E_{rh}\, E'_{rh}} + \overline{E_{lh}\, E'_{lh}}]}{|E_{rh}|^2 + |E_{lh}|^2}$$

$$= k.\frac{\beta}{4\alpha}.\cos\phi \qquad (2.29)$$

and $$e_y = k. \frac{\frac{1}{2}. [\overline{E_{ry}\, E'_{rh}(+\pi/2)} + \overline{E_{lh}\, E'_{lh}(-\pi/2)}]}{|E_{rh}|^2 + |E_{lh}|^2}$$

$$= k.\frac{\beta}{4\alpha}.\sin\phi$$

These relations are seen to be identical with those found in the complete Linear Polarization Processor. A block diagram of the complete circular polarization processor is given in fig. 2.17. As in the previous case, the price paid for complete polarization diversity in the tracking system is a rather complex four channel receiving system.

Consideration of the circular polarization processor relations indicates that a tracking system using

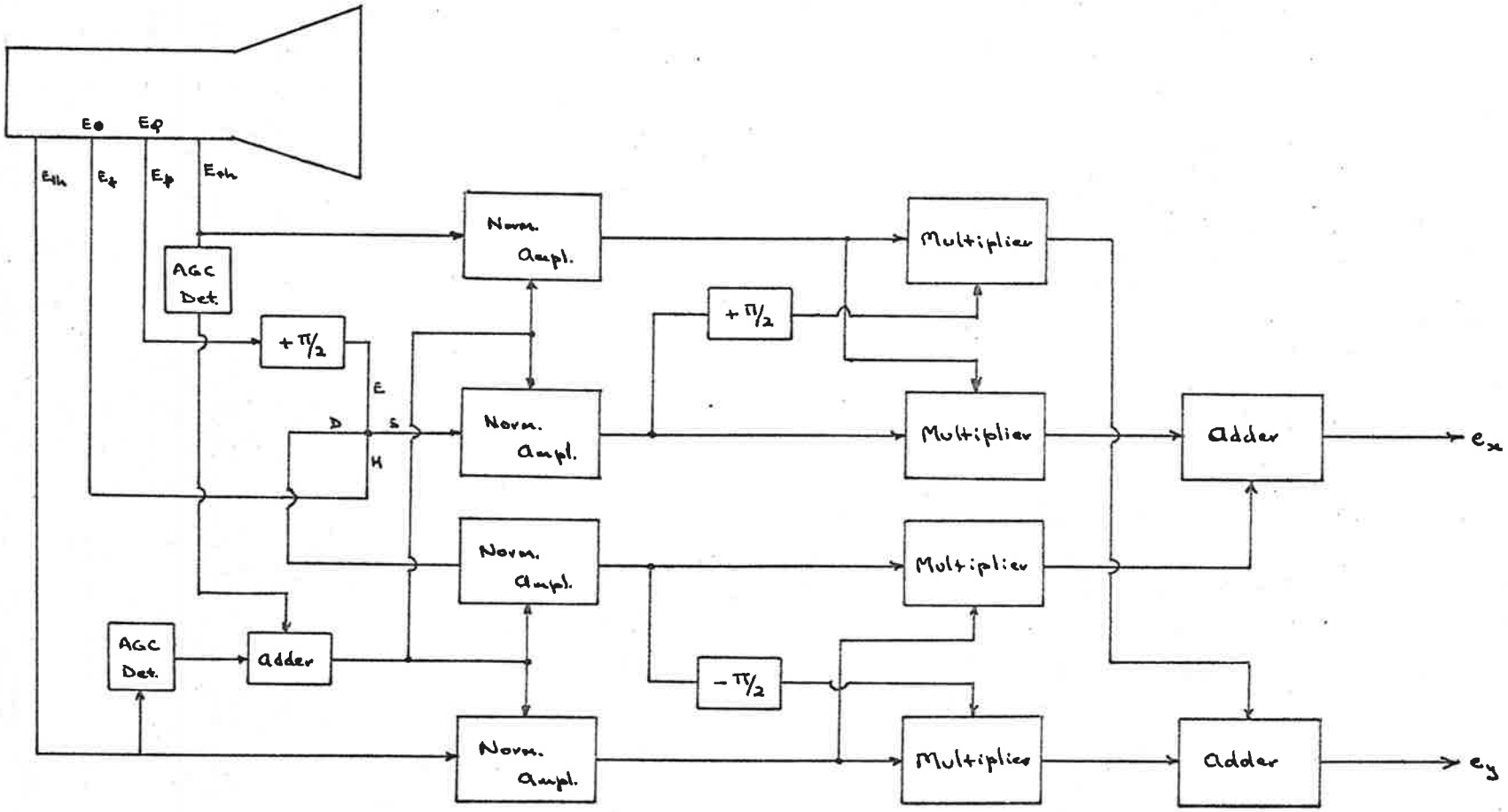

Fig. 2.17 Circular Polarization Processor

the TE_{11} reference mode and the TE_{01}-TM_{01} difference mode combination is circular polarization oriented. This means that one of the circularly polarized components can be neglected without introducing tracking error, so allowing a simpler tracking receiver. This may well be an advantage when the signals are expected to be predominantly circularly polarized.

2.4.3 Complex Signal Analysis

In the derivation of error signal relations in sections 2.4.2 and 2.4.3, the received signal was assumed to appear as emanating from a single point source at a point (θ, ϕ) relative to the antenna axes. In practice, however, this may not be so and the actual signal may appear as a combination of several signals, incident at various elevation and azimuth angles. Naturally the range of variation in the elevation angle, θ, is limited by the beamwidth of the antenna. Such signals may arise due to multipath propagation in the atmosphere or in the conventional radar situation, the reflection properties of the target may be approximated as a collection of point sources with differing reflection coefficients.

By assuming that all apparent sources are near boresight (i.e. angles of elevation, θ, are small), the sum mode gain can be considered constant over the source

region and the error modes will have voltage gains proportional to the angular distance off boresight. The target is considered to be sufficiently distant for lines from the antenna to the source points to be nearly parallel. A reference plane is constructed near the target, normal to the line of sight from the antenna. The reference axes in this plane correspond to the drive axes of the antenna mount and, since θ is small, the two coordinates may be assumed to remain coincident for small changes in the antenna attitude. Variations in distance of source points from the reference plane may be accommodated by the phase of the signals. The reference plane is shown in fig. 2.18, where

(x_b, y_b) = coordinates of point of intersection of boresight axis

and (x_i, y_i) = coordinates of source point, i.

Other parameters to be defined are

δ_i = polarization angle (see fig. 2.12)

k_{1i}, k_{2i} = right and left hand circular polarization components which include an amplitude factor

and p_i = phase angle accounting for different effective distances of source points from the antenna.

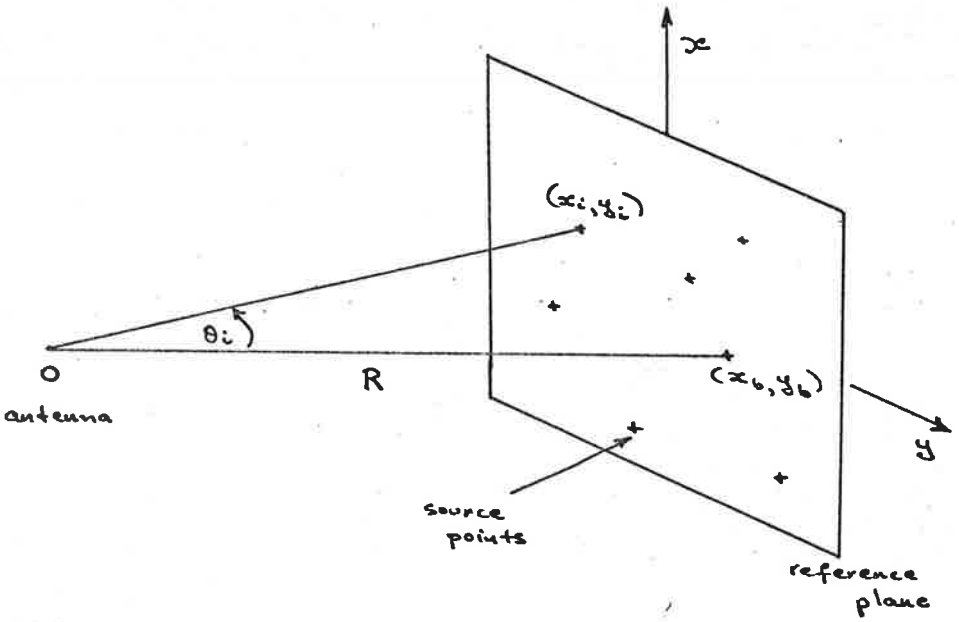

(a) Relation between antenna and reference plane.

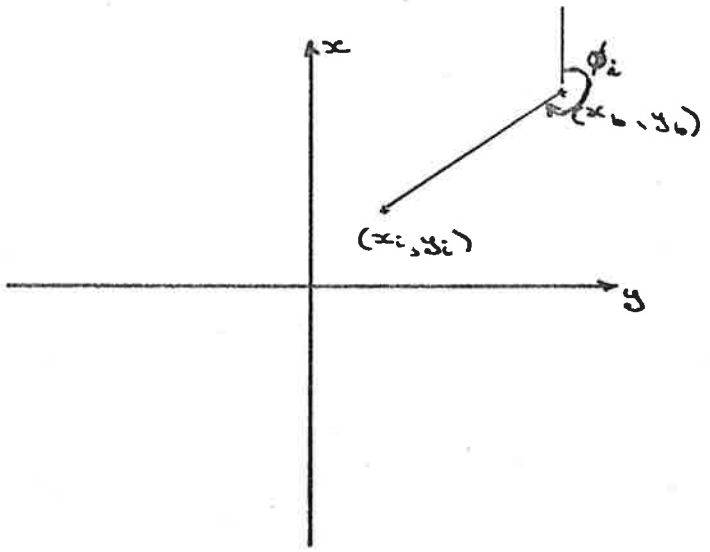

(b) Reference plane.

Fig. 2.18 Co-ordinates for Multi-source Signals.

Any source point has an angle of boresight given by

$$\theta_i = \frac{1}{R} \cdot \left[(x_b - x_i)^2 + (y_b - y_i)^2 \right]^{\frac{1}{2}} \qquad (2.30)$$

and an azimuth angle

$$\phi_i = \arctan\left[\frac{y_i - y_b}{x_i - x_b} \right] \qquad (2.31)$$

The reference mode gain

$$\alpha = \frac{K_r}{R} \qquad \text{(equation 2.14)}$$

and the difference mode gain

$$\beta = \frac{K_e}{R}. \qquad \text{(equation 2.16)}$$

Using the relations of section 2.4.1, the received signals may be written, (assuming n source points)

$$E_x = \frac{K_r}{R} \cdot E_o \sum_{i=1}^{n} [k_{1i} \cos(\omega t + p_i + \delta_i + \phi_i) + k_{2i} \cos(\omega t + p_i - \delta_i - \phi_i)]$$

$$E_y = \frac{K_r}{R} \cdot E_o \sum_{i=1}^{n} [k_{1i} \sin(\omega t + p_i + \delta_i + \phi_i) - k_{2i} \sin(\omega t + p_i - \delta_i - \phi_i)] \qquad (2.32)$$

$$E_t = \frac{K_e . E_o}{R} \sum_{i=1}^{n} [k_{1i} \cos(\omega t + p_i + \delta_i) + k_{2i} \cos(\omega t + p_i - \delta_i)] . \theta_i$$

and

$$E_p = \frac{K_e . E_o}{R} \sum_{i=1}^{n} [k_{1i} \sin(\omega t + p_i + \delta_i) - k_{2i} \sin(\omega t + p_i - \delta_i)] . \theta_i$$

The signal processing relations are

$$e_x = \tfrac{1}{2} . k . \frac{\overline{E_t E_x} + \overline{E_p E_y}}{|E_x|^2 + |E_y|^2}$$

and

$$e_y = \tfrac{1}{2} . k . \frac{\overline{E_t E_y} - \overline{E_p E_x}}{|E_x|^2 + |E_y|^2}$$

From equation (2.32) and after simplification

$$|E_x|^2 + |E_y|^2 = 2 . \frac{K_r E_o}{R}^2 \left\{ [\sum_i k_{1i} \cos(p_i + \delta_i + \phi_i)^2 + [\sum_i k_{2i} \cos(p_i - \delta_i - \phi_i)]^2 + [\sum_i k_{1i} \sin(p_i + \delta_i + \phi_i)]^2 + [\sum_i k_{2i} \sin(p_i - \delta_i - \phi_i)]^2 \right\} \qquad (2.33)$$

$$\overline{E_t E_x} + \overline{E_p E_y} = \frac{K_r K_e E_o^2}{R^2} \sum_i \sum_j \theta_j \{k_{1i}k_{1j} \cos(\delta_i-\delta_j+\phi_i+p_i-p_j) + k_{2i}k_{2j} \cos(\delta_i-\delta_j+\phi_i-p_i+p_j)\} \quad (2.34)$$

and

$$\overline{E_t E_y} - \overline{E_p E_x} = \frac{K_r K_e E_o^2}{R^2} \sum_i \sum_j \theta_j \{k_{1i}k_{1j} \sin(\delta_i-\delta_j+\phi_i+p_i-p_j) + k_{2i}k_{2j} \sin(\delta_i-\delta_j+\phi_i-p_i+p_j)\} \quad (2.35)$$

For small angles θ, the polarization angle will be independent of θ when measured from the reference axes. Defining a new variable

$$\gamma_i = \delta_i + \phi_i$$

which measures the polarization angle from the vertical (x) axis and is independent of (x_b, y_b), equations (2.33-35) may be rewritten as

$$|E_x|^2 + |E_y|^2 = 2 \frac{K_r E_o}{R}^2 \left\{ [\sum_i k_{1i} \cos(p_i+\gamma_i)]^2 + [\sum_i k_{2i} \cos(p_i-\gamma_i)]^2 + [\sum_i k_{1i} \sin(p_i+\gamma_i)]^2 + [\sum_i k_{2i} \sin(p_i-\gamma_i)]^2 \right\}$$

$$= 2 \frac{K_r E_o}{R}^2 \left\{ \sum_i \sum_j k_{1i}k_{1j} \cos(\gamma_i-\gamma_j+p_i-p_j) + \sum_i \sum_j k_{2i}k_{2j} \cos(\gamma_i-\gamma_j-p_i+p_j) \right\} \quad (2.36)$$

$$\overline{E_t E_x} + \overline{E_p E_y} = \frac{K_r K_e E_o^2}{R^2} \sum_i \sum_j \theta_j \left\{ k_{1i} k_{1j} \cos(\gamma_i - \gamma_j + \phi_j + p_i - p_j) + k_{2i} k_{2j} \cos(\gamma_i - \gamma_j + \phi_j - p_i + p_j) \right\}$$

(2.37)

and

$$\overline{E_t E_y} - \overline{E_p E_x} = \frac{K_r K_e E_o^2}{R^2} \sum_i \sum_j \theta_j \left\{ k_{1i} k_{1j} \sin(\gamma_i - \gamma_j + \phi_j + p_i - p_j) + k_{2i} k_{2j} \sin(\gamma_i - \gamma_j + \phi_j - p_i + p_j) \right\}$$

(2.38)

Equation (2.36) shows that the normalizing term $|E_x|^2 + |E_y|^2$ is independent of (x_b, y_b) as is expected for small θ.

From equations (2.37) and (2.38) and using equations (2.30) and (2.31), the error voltages may be expressed as

$$e_x = K \sum_{i=1}^{n} \sum_{j=1}^{n} \left\{ (x_j - x_b) \left[k_{1i} k_{1j} \cos(\gamma_i - \gamma_j + p_i - p_j) + k_{2i} k_{2j} \cos(\gamma_i - \gamma_j - p_i + p_j) \right] - (y_j - y_b) \left[k_{1i} k_{1j} \sin(\gamma_i - \gamma_j + p_i - p_j) + k_{2i} k_{2j} \sin(\gamma_i - \gamma_j - p_i + p_j) \right] \right\}$$

(2.39)

and

$$e_y = K \sum_{i=1}^{n} \sum_{j=1}^{n} \Big\{ (x_j - x_b) \left[k_{1i} k_{1j} \sin(\gamma_i - \gamma_j + p_i - p_j) \right.$$

$$\left. + k_{2i} k_{2j} \sin(\gamma_i - \gamma_j - p_i + p_j) \right]$$

$$+ (y_j - y_b) \left[k_{1i} k_{1j} \cos(\gamma_i - \gamma_j + p_i - p_j) + k_{2i} k_{2j} \cos(\gamma_i - \gamma_j - p_i + p_j) \right] \Big\}$$

(2.40)

where K is a constant.

These expressions for the error voltages, equations (2.39) and (2.40), allow the computation of the tracking system response to any given set of parameters, γ_i, p_i, k_{1i}, k_{2i}, x_i and y_i. The antenna movement, given by the locus of (x_b, y_b) in the reference plane, will be in the direction

$$\tau = \arctan \left({}^{e_y}/_{e_x} \right)$$

and with a rate dependent on the magnitudes of the error signals, i.e. $(e_x^2 + e_y^2)^{\frac{1}{2}}$. Realizing that

$$\sum_{i=1}^{n} \sum_{j=1}^{n} a_i \, a_j \sin(\alpha_i - \alpha_j) = 0$$

the apparently cross-coupled voltage relations, equations (2.39) and (2.40) can be rewritten as

$$\frac{e_x}{K} = \sum_{i=1}^{n}\sum_{j=1}^{n}\Big\{k_{1i}k_{1j}[x_j\cos(\gamma_i-\gamma_j+p_i-p_j)-y_j\sin(\gamma_i-\gamma_j+p_i-p_j)]$$

$$+ k_{2i}k_{2j}[x_j\cos(\gamma_i-\gamma_j-p_i+p_j)-y_j\sin(\gamma_i-\gamma_j-p_i+p_j)]\Big\}$$

$$- x_b \sum_{i=1}^{n}\sum_{j=1}^{n}[k_{1i}k_{1j}\cos(\gamma_i-\gamma_j+p_i-p_j)$$

$$+ k_{2i}k_{2j}\cos(\gamma_i-\gamma_j-p_i+p_j)]$$

$$= A - x_b.C \qquad (2.41)$$

and

$$\frac{e_y}{K} = \sum_{i=1}^{n}\sum_{j=1}^{n}\Big\{k_{1i}k_{1j}[x_j\sin(\gamma_i-\gamma_j+p_i-p_j)+y_j\cos(\gamma_i-\gamma_j+p_i-p_j)]$$

$$+ k_{2i}k_{2j}[x_j\sin(\gamma_i-\gamma_j-p_i+p_j)+y_j\cos(\gamma_i-\gamma_j-p_i+p_j)]\Big\}$$

$$- y_b \sum_{i=1}^{n}\sum_{j=1}^{n}[k_{1i}k_{1j}\cos(\gamma_i-\gamma_j+p_i-p_j)$$

$$+ k_{2i}k_{2j}\cos(\gamma_i-\gamma_j-p_i+p_j)]$$

$$= B - y_b.C \qquad (2.42)$$

Equations (2.41) and (2.42) show that, for a given set of system parameters, the vertical error voltage e_x depends

only on the vertical antenna position x_b and similarly e_y depends only on y_b. Thus there is no cross-coupling between the drive channels, even in this complex signal case. A balance point where both the error voltages, e_x and e_y, are zero will always exist and can be obtained by placing the left hand sides of equations (2.41) and (2.42) equal to zero. Hence the balance point (x_b', y_b') is given by

$$x_b' = A/C$$

$$\text{and } y_b' = B/C$$

where the sums B and C are defined in equations (2.41) and (2.42).

This balance, or equilibrium, point of the antenna is of interest in a tracking system since it allows the final pointing direction of the antenna to be related to the spread of the individual source points. It is desirable that the antenna point within the area defined by the source for this allows the reference mode to operate at its maximum gain position, and in the military situation, when the system is used to aim a passive projectile, this is particularly important. Fig. 2.19 shows a table giving some indication of the frequency a particular relative miss distance might be expected. This table was generated by randomly selecting the

		$d \leq 0.01$	$0.01 < d \leq 0.1$	$0.1 < d \leq 1$	$1 < d \leq 100$	$10 < d \leq 100$	$100 < d$	Total
$n = 2$	x	0.819	5.658	17.707	8.780	1.258	0.176	34.50
$s = 10250$	y	0.644	5.385	17.873	8.849	1.298	0.098	34.15
$n = 3$	x	0.776	4.906	15.217	3.264	0.070	0.00	24.23
$s = 10048$	y	0.627	5.474	14.928	3.712	0.159	0.00	24.90
$n = 5$	x	0.677	4.359	10.271	0.577	0.00	0.00	15.88
$s = 5024$	y	0.697	4.598	10.370	0.896	0.00	0.00	16.56
$n = 10$	x	0.464	3.050	7.077	0.512	0.00	0.00	11.10
$s = 4098$	y	0.537	3.587	6.857	0.464	0.00	0.00	11.45

d = relative miss distance = $\dfrac{x_b' - x_{max}}{x_{max} - x_{min}}$

n = number of source points

s = size of sample

Fig. 2.19 Miss distance distributions (as percentages of sample)

system parameters, k_{1i}, k_{2i}, γ_i and p_i, and calculating the balance point (x_b', y_b'). From the balance point a relative distance outside the target was calculated and the results grouped as shown in the table. As is expected with a random process, the results for vertical and horizontal miss distances and almost identical and this affords some check on the size of the samples and the randomness of the parameter choice.

In the above discussion, the system parameters were assumed constant, i.e. the signals were assumed to have constant amplitudes, polarizations and phases with time. In practice, the signals from the individual sources may well have approximately constant amplitudes and polarizations, but it is unlikely that phases of the r.f. signals will be correlated. In this case, by averaging the error voltage signals over a sufficient length of time, the cross-product terms in equations (2.41) and (2.42) disappear, leaving

$$e_x = K \sum_{i=1}^{n} (x_i - x_b)(k_{1i}^2 + k_{2i}^2) \qquad (2.43)$$

and

$$e_y = K \sum_{i=1}^{n} (y_i - y_b)(k_{1i}^2 + k_{2i}^2) \qquad (2.44)$$

with a corresponding balance point

$$x_b' = \frac{\sum_i x_i (k_{1i}^2 + k_{2i}^2)}{\sum_i (k_{1i}^2 + k_{2i}^2)} \qquad (2.45)$$

and

$$y_b' = \frac{\sum_i y_i \, (k_{1i}^2 + k_{2i}^2)}{\sum_i (k_{1i}^2 + k_{2i}^2)} \qquad (2.46)$$

Accordingly, when the phases may be considered uncorrelated, the balance point is given by the centroid of the source points, weighted according to their powers, and this point is always within the limits of the source points.

CHAPTER III

BEAM BROADENING IN REFLECTOR ANTENNAE

3.1 Introduction

With large steerable antennae, which have very narrow beamwidths, the problem of locating a target may be difficult and time consuming unless the direction of the source is known precisely. The acquisition time for such an antenna is dependent on two main factors. These are the beamwidth of the antenna and its maximum drive rate. Together these properties determine the time taken for the antenna to search a given area, and an increase in either reduces the time necessary.

Large steerable antennae are very heavy installations with comparatively low maximum drive rates, which are limited by drive power considerations and acceleration rates. In space probe usage the drive rates need only be approximately the sidereal rate (15° per hour), although earth satellites may require tracking rates up to 1° per second. Systems are usually designed only to meet the tracking rate specified by the application, because of the cost of providing additional drive speed, and increases in order to improve acquisition time on unknown targets are not considered. (In the normal usage of satellite tracking this does not impose a

severe limitation since the orbits are predictable.) Naturally, in an existing installation the drive rates are fixed and cannot be altered to improve search time.

The other factor influencing acquisition time - the beamwidth - is of more interest, since this can be controlled by the antenna feed system and does not require large mechanical alterations to be adjusted. The size of search element of the antenna is conveniently described by the solid angle contained by the antenna beam. The significant angle may be defined as

$$\Omega = 2\pi\left[1 - \cos\left(\frac{\theta_{10dB}}{2}\right)\right] \qquad (3.1)$$

where θ_{10dB} is the 10 dB beamwidth of the antenna. For small beamwidths equation (3.1) may be approximated as

$$\Omega = \frac{\pi}{4}\cdot\theta_{10dB}^{2} \qquad (3.2)$$

This indicates that the size of a search element, and accordingly the acquisition time, is dependent upon the square of the beamwidth, and that even moderate changes in beamwidth can have a significant effect.

In large reflector, or aperture, antennae with a constant phase distribution, the beamwidth is dependent upon the size of the aperture (D/λ) and the

feed illumination function,[40] a more severe taper producing a larger beamwidth. With a given antenna the actual physical size of the aperture is fixed but the variations in feed taper may be considered as causing changes in the effective aperture of the antenna. When there is no longer a constant phase distribution in the aperture, the radiation pattern may be severely modified. With odd phase distributions skewness occurs together with coma and loss of symmetry in the main beam. In the previous chapter symmetry in the main beam was shown to be desirable for receiving efficiency and especially desirable in the case of tracking systems. Any skewness in the radiation pattern is also undesirable since the physical and electrical axes of the antenna no longer align. Even distributions, on the other hand, produce symmetric patterns with no beam tilt. Silver[41] shows the effect of small quadratic errors to be an increase in sidelobe level, a filling of the nulls and a reduction in absolute gain. The beamwidth is slightly increased. In any case an increase in the beamwidth is accompanied by a reduction in gain or in other words beamwidth is traded for gain.

In a focally excited paraboloidal reflector, increases in beamwidth are restricted to increasing the taper or providing a curved phase front in the aperture.

An increase in taper - or decrease in effective aperture - can be achieved by using a primary feed horn with a larger aperture and a consequent narrower beam. However, this is generally not practicable, since the antenna only requires increased beamwidth while it is in the search mode and, on target acquisition, it must be able to revert to its maximum receiving efficiency configuration. As beam broadening must only be considered as an aid to target acquisition and has a secondary role in the case of large low noise antennae, the feed system will be designed to give maximum efficiency and must be regarded as fixed. This restricts beam broadening to phase effects in the aperture. Even distributions can be obtained by defocussing the antenna by moving the feed horn axially away from the paraboloid focus.

In a cassegrain antenna system the same restrictions apply to the feed horn. In this case, however, there are three possibilities for defocussing the antenna, since the sub-reflector, or the feed horn, or both, may be displaced axially. The cassegrain sub-reflector also allows the possibility of modification of the basic hyperboloid shape to produce a different amplitude or phase distribution in the main aperture. As the sub-reflector is a passive device, many schemes could be proposed to effect this modification. However, it

must be remembered that any method must allow a quick and automatic return to the original configuration. The author considers that one of the few feasible approaches involves a split reflector consisting of an outer annular section and an inner circular section which is movable independent of the outer part. The effect of this provision, which is in fact a step change in the aperture phase distribution, is discussed later.

Although the provision of defocussing equipment may appear to add complexity to a system, the modern trend toward computer linked antenna installations[23] which compute the best-fit paraboloid and adjust the feed system accordingly, requires a feed position control system in any case. These techniques are probably most suited to cassegrain installations where all corrections and changes can be controlled by the sub-reflector, which is a passive element and eliminates any need for flexible electrical connections.

3.2 Defocussing Focally-fed Paraboloidal Reflectors

3.2.1 Derivation of Radiation Formula

The formula for the radiation from a defocussed paraboloid antenna is derived by using the current integration technique.[42] This method is used in preference to an aperture integration technique since

defocussing causes large phase variations across the aperture and the usual approximations made in aperture methods assumes an almost constant phase.(43) The current distribution method, which develops the radiation pattern from the approximate surface current distribution over the reflector, is general in its application and has no restrictions on the amplitude or phase distributions.

The development of the radiation integral follows closely that given in Appendix I for the focussed case.

Silver(44) gives the scattered field intensity in the far zone as

$$\underset{\sim}{E}_S = \frac{-j\omega\mu}{2\pi R}.e^{-jkR} \int_S \{\hat{\underset{\sim}{n}} \times \underset{\sim}{H}_i - [(\hat{\underset{\sim}{n}} \times \underset{\sim}{H}_i).\hat{\underset{\sim}{R}}]\hat{\underset{\sim}{R}}\} e^{+jk\underset{\sim}{\sigma}.\hat{\underset{\sim}{R}}} dS \qquad (3.1)$$

and $$\underset{\sim}{H}_S = (\frac{\epsilon}{\mu})^{\frac{1}{2}}.(\hat{\underset{\sim}{R}} \times \underset{\sim}{E}_S) \qquad (3.2)$$

where the coordinates have been altered to correspond to fig. 3.1, the primary feed being centred at point G

μ = magnetic inductive capacity

ϵ = electric inductive capacity

$\hat{\underset{\sim}{n}}$ = normal to the surface, S,

and $\underset{\sim}{H}_i$ = magnetic field component of the primary radiation at the reflector surface.

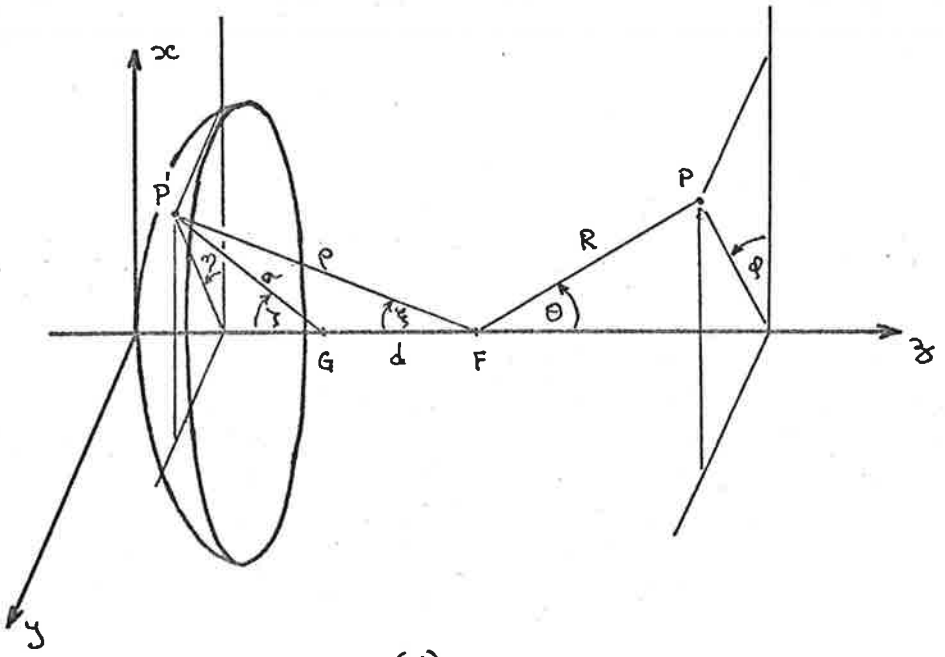

(a)

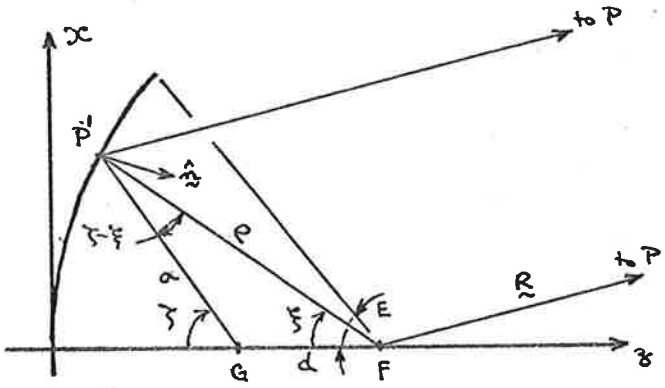

(b)

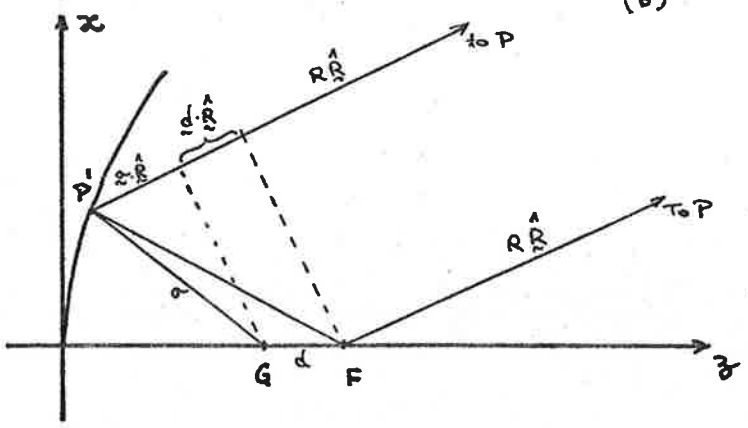

(c)

Fig. 3.1 Single Reflector Geometry

As the reflector is assumed in the far field of the primary radiator

$$\underset{\sim}{H}_i = \left(\frac{\epsilon}{\mu}\right)^{\frac{1}{2}} \hat{\underset{\sim}{\sigma}} \times \underset{\sim}{E}_i \tag{3.3}$$

and as equation (3.1) shows that there is no radial component in the far field, the scattered field becomes

$$\left.\begin{matrix} E_\theta \\ E_\phi \end{matrix}\right\} = -\frac{j\omega\mu}{2\pi R} \cdot e^{-jkR} \left(\frac{\epsilon}{\mu}\right)^{\frac{1}{2}} \left\{ \begin{matrix} \hat{\underset{\sim}{\theta}} \cdot \underset{\sim}{I} \\ \hat{\underset{\sim}{\phi}} \cdot \underset{\sim}{I} \end{matrix} \right. \tag{3.4}$$

where

$$I = \int_S \hat{\underset{\sim}{n}} \times (\hat{\underset{\sim}{\sigma}} \times \underset{\sim}{E}_i)\, e^{+jk\underset{\sim}{\sigma}\cdot\hat{\underset{\sim}{R}}}\, dS \tag{3.5}$$

For a paraboloidal surface, S,

$$dS = \rho^2 \sin\xi \sec \xi/2 \, d\xi \, d\eta \tag{3.6}$$

where

$$\rho = \frac{2f}{1 + \cos\xi} \tag{3.7}$$

with f = focal length of the antenna.

From fig. 3.1(b)

$$\sigma = [\rho^2 + d^2 - 2\rho d \cos\xi]^{\frac{1}{2}} \tag{3.8}$$

where d = displacement of the feed phase centre toward the vertex,

$$\hat{\sigma} = \hat{\rho} \cos(\zeta - \xi) + \hat{\xi} \sin(\zeta - \xi) \qquad (3.9)$$

and $$\hat{n} = -\hat{\rho} \cos \xi/2 + \hat{\xi} \sin \xi/2 \qquad (3.10)$$

The radiation from the feed at G may be represented by

$$E_i = (\hat{\zeta} E_\zeta + \hat{\eta} E_\eta) e^{-jk\sigma} \qquad (3.11)$$

in the far field. Thus, using

$$\hat{\zeta} = -\hat{\rho} \sin(\zeta - \xi) + \hat{\xi} \cos(\zeta - \xi) \qquad (3.12)$$

$$\hat{n} \times (\hat{\sigma} \times E_i) = \hat{\rho} E_\zeta \sin \xi/2 + \hat{\xi} E_\zeta \cos \xi/2 + \hat{\eta} E_\eta \cos(\zeta - \xi/2) \qquad (3.13)$$

Using the relations

$$\begin{aligned}
\hat{\rho} \cdot \hat{\theta} &= \cos\theta \cdot \sin\xi \cdot \cos(\phi - \eta) + \sin\theta \cdot \cos\xi \\
\hat{\rho} \cdot \hat{\phi} &= \sin\xi \cdot \sin(\phi - \eta) \\
\hat{\xi} \cdot \hat{\theta} &= \cos\theta \cdot \cos\xi \cdot \cos(\phi - \eta) - \sin\theta \cdot \sin\xi \\
\hat{\xi} \cdot \hat{\phi} &= -\cos\xi \cdot \sin(\phi - \eta) \\
\hat{\eta} \cdot \hat{\theta} &= \cos\theta \cdot \sin(\phi - \eta) \\
\hat{\eta} \cdot \hat{\phi} &= \cos(\phi - \eta)
\end{aligned} \qquad (3.14)$$

$$[\hat{n} \times (\hat{\sigma} \times E_i)]_\theta = E_\zeta [\cos\theta \cdot \cos(\phi - \eta) \cdot \cos\xi/2 - \sin\theta \cdot \sin\xi/2]$$

$$+ E_\eta \cos\theta \cdot \cos(\zeta - \xi/2) \cdot \sin(\phi - \eta) \qquad (3.15)$$

and

$$[\hat{\underset{\sim}{n}} \times (\hat{\underset{\sim}{\sigma}} \times \underset{\sim}{E}_i)]_\phi = E_\zeta \cos\xi/2 \sin(\eta-\phi) + E_\eta \cos(\zeta-\xi/2). \cos(\eta-\phi) \qquad (3.16)$$

In order that a fixed set of radiation coordinates (R,θ,ϕ) with the origin at F may be used, the phase term must be modified to include the effect of the feed displacement, d. From fig. 3.1(c) the new phase term must be

$$e^{-jk[R+\sigma - \underset{\sim}{\sigma}.\hat{\underset{\sim}{R}} - \underset{\sim}{d}.\hat{\underset{\sim}{R}}]}$$

$$= e^{-jk[R+d\cos\theta]} \cdot e^{-jk\sigma[1-\hat{\underset{\sim}{\sigma}}.\hat{\underset{\sim}{R}}]} \qquad (3.17)$$

since $\underset{\sim}{d} = -d.\hat{\underset{\sim}{z}}$ and $\hat{\underset{\sim}{R}}.\hat{\underset{\sim}{z}} = \cos\theta$.

Using equation (3.9) and

$$\hat{\underset{\sim}{R}} = \hat{\underset{\sim}{\zeta}}[\sin\xi.\sin\theta.\cos(\phi-\eta) - \cos\theta.\cos\xi]$$

$$+ \hat{\underset{\sim}{\xi}}[\sin\theta.\cos\xi.\cos(\phi-\eta) + \sin\xi.\cos\theta]$$

$$+ \hat{\underset{\sim}{\eta}} \sin\theta.\sin(\phi-\eta)$$

$$[1-\hat{\underset{\sim}{\sigma}}.\hat{\underset{\sim}{R}}] = 1 + \cos\zeta\cos\theta - \sin\zeta.\sin\theta.\cos(\phi-\eta)$$

The expanded expression for the scattered electric field may now be written as

$$\left.\begin{matrix} E_\theta \\ E_\phi \end{matrix}\right\} = -\frac{j\omega\mu}{2\pi R} \cdot e^{-jk\,[R + d\cos\theta]} \cdot \left(\frac{\varepsilon}{\mu}\right)^{\frac{1}{2}} \cdot \left\{ \begin{matrix} I_\theta \\ I_\phi \end{matrix}\right. \qquad (3.18)$$

where

$$I_\theta = \int_0^{2\pi} \int_0^{E} \{ E_\zeta [\cos\theta.\cos\tfrac{\xi}{2}/2.\cos(\phi-\eta) - \sin\theta.\sin\tfrac{\xi}{2}/2]$$

$$+ E_\eta \cos\theta.\cos(\zeta - \tfrac{\xi}{2}/2).\sin(\phi-\eta) \}.\exp\{-jk\sigma[1 +$$

$$\cos\zeta.\cos\theta - \sin\zeta.\sin\theta.\cos(\phi-\eta)]\} \rho^2 \sin\xi \sec\tfrac{\xi}{2}/2 \, d\xi d\eta$$

and (3.19)

$$I_\phi = \int_0^{2\pi} \int_0^{E} \{ E_\zeta \cos\tfrac{\xi}{2}/2.\sin(\eta-\phi) + E_\eta \cos(\zeta - \tfrac{\xi}{2}/2)\cos(\eta-\phi)$$

$$\exp\{....\} \cdot \rho^2 \sin\xi \sec\tfrac{\xi}{2}/2 \, d\xi \, d\eta \qquad (3.20)$$

and E = edge angle of the reflector.

In most cases of practical interest, and especially in the case of waveguide feed horn radiation, the primary field for a linearly polarized antenna may be expressed as

$$E_\zeta = f_1(\zeta).\sin\eta$$

and $$E_\eta = f_2(\zeta).\cos\eta$$

Then, by performing the substitution

$$\exp\{jk\sigma \sin\zeta \sin\theta \cos(\phi-\eta)\} = J_o(k\sigma \sin\zeta \sin\theta)$$

$$+ 2 \sum_{n=1}^{\infty} j^n J_n(k\sigma \sin\zeta .\sin\theta)\cos n(\phi-\eta)$$

and integrating over the feed azimuth angle, η,

$$I_\theta = \pi.\sin\phi \int_0^E \{f_1 [\cos\theta.\cos\xi/2(J_o(u)-J_2(u)) - 2j \sin\theta .$$

$$\sin\xi/2\, J_1(u)] + f_2 \cos\theta.\cos(\zeta-\xi/2)[J_o(u)+J_2(u)]\}$$

$$\exp\{-jk\sigma[1+\cos\zeta\cos\theta]\}\rho^2 \sin\xi \sec\xi/2\, d\xi$$

(3.21)

and

$$I_\phi = \pi.\cos\phi \int_0^E \{f_1 \cos\xi/2\,[J_o(u)+J_2(u)] + f_2 \cos(\zeta-\xi/2)$$

$$[J_o(u)-J_2(u)]\} \exp\{-jk\sigma[1+\cos\zeta\cos\theta]\}$$

$$\rho^2 \sin\xi \sec\xi/2\, d\xi \qquad (3.22)$$

where $u = k\sigma \sin\zeta \sin\theta$

$= k\rho \sin\xi \sin\theta$

This form for the scattered field intensity is used to calculate the radiation pattern when the dominant TE_{11} mode radiation from waveguide provides the primary field. The functions, f_1 and f_2, in this case are defined by equation (2.2) in the previous chapter.

For the circularly symmetric modes, TE_{01} and TM_{01}, the primary radiation pattern has no azimuthal variation and only one field component is present in each case. Thus for the TM_{01} mode

$$\underset{\sim}{E}_i = E_\zeta \hat{\underset{\sim}{\zeta}} . e^{-jk\sigma}$$

$$= f(\zeta) . \hat{\underset{\sim}{\zeta}} . e^{-jk\sigma}$$

and the radiation from a paraboloid reflector, in a similar manner, may be reduced to

$$E_\theta = - \frac{j\omega\mu}{2\pi R} . e^{-jk[R + d\cos\theta]} (\frac{\epsilon}{\mu})^{\frac{1}{2}} . I_\theta \qquad (3.23)$$

where

$$I_\theta = 2\pi \int_0^E f \left[j \cos\theta . \cos \xi/2 \; J_1(u) - \sin\theta \sin\xi/2 \; J_0(u) \right]$$

$$\exp \{ -jk\sigma [1 + \cos\zeta \cos\theta] \} \rho^2 \sin\xi \sec\xi/2 \; d\xi$$

(3.23)

and $u = k\sigma \sin\xi \sin\theta$.

For the TE_{01} mode, the corresponding expressions are

$$\underset{\sim}{E}_i = E_\eta \, \hat{\underset{\sim}{\eta}} \, . e^{-jk\sigma}$$

$$= f(\eta) \, \hat{\underset{\sim}{\eta}} \, . e^{-jk\sigma}$$

and

$$E_\phi = - \frac{j\omega\mu}{2\pi R} . e^{-jk\,[R + d\,\cos\theta]} \left(\frac{\epsilon}{\mu}\right)^{\frac{1}{2}} I_\theta \qquad (3.25)$$

where

$$I_\phi = 2\pi j \int_0^E f \cos(\zeta - \xi/2) J_1(k\sigma \sin\zeta \sin\theta)$$

$$\exp\{-jk\sigma[1 + \cos\zeta\cos\theta]\}\rho^2 \sin\xi \sec \xi/2 \, d\xi \qquad (3.26)$$

The gain functions for these scattered fields may be derived using the usual formula

$$G(\theta,\phi) = \frac{2\pi}{\lambda_t} \left(\frac{\epsilon}{\mu}\right)^{\frac{1}{2}} |RE|^2 \qquad (3.27)$$

3.2.2 Influence of Antenna Diameter and Focal Length on Defocussed Radiation Patterns

The size of a reflector antenna is quite obviously given by its diameter, which it is usual to measure in wavelength or to express as the ratio D/λ. It can be shown that, for a focussed antenna with an essentially plane wavefront in the aperture, the beamwidth of the secondary radiation pattern is proportional to the size of the antenna[40] and the gain is dependent upon the

square of the size.(35) However, the actual shape of the secondary pattern is almost independent of the size factor, D/λ.(39)

The shape of a paraboloidal reflector is most conveniently described by its focal length to diameter ratio. In a first order approximation this parameter has no influence on the radiation pattern of an antenna, but as the factor becomes small and the reflector becomes deeper, the approximation that the radii of curvature of the reflector surface are very large compared with wavelength is no longer valid. Another concern with low f/D antennae is the increased cross-polarization energy in the radiated field caused by high curvature. In practice an antenna design is a compromise between a relatively shallow, high f/D structure with the necessity of supporting a feed system a long way from the reflector surface and imposing mechanical design problems, and a deep, low f/D dish with its high attendant cross-polarization. The antennae used have, in general, an f/D in the region 0.4 - 0.43, allowing reasonable surface tolerances to be maintained for all working positions, while keeping low cross-polarization.

In order that typical results for defocussed antennae may be obtained, it is desirable to investigate the influence of the two parameters, f/D and D/λ, which

describe the paraboloid reflector, on the defocussed system radiation patterns. From purely geometrical considerations, the effect of defocussing has little influence on the amplitude distribution over the reflector aperture, but causes large phase variations. From fig. 3.1(b) the phase difference between the centre and edge of the reflector, by ray optics, is approximately

$$\alpha = \frac{2\pi}{\lambda}. \; d(\cos E - 1) \text{ radians} \qquad (3.23)$$

where E = edge angle of the reflector

$$= 2. \arctan \left\{ \frac{1}{4(f/D)} \right\}$$

and d = feed displacement.

So the focal length-diameter ratio is a significant factor, requiring smaller displacements for the same phase taper as the f/D ratio is decreased. This simple approach indicates that the size of the antenna has no influence on the final radiation pattern. A more complete appraisal of the influence of these factors can be made by investigating more closely the radiation integrals equations (3.21) and (3.22). Only the θ-component of the scattered field need be considered since the ϕ-component has a similar form and the results from one can be applied to the other.

Assuming that the antenna is large, over the range of interest

$$\cos\theta \simeq 1$$

$$\text{and } \sin\theta \simeq 0$$

and, making the substitution

$$r = \frac{\rho \sin\xi}{a}$$

where a = radius of the antenna aperture, equation (3.21) becomes

$$I_\theta \simeq \pi . \sin\phi \int_0^1 \{ f_1 [J_o(u) - J_2(u)] + f_2 \cos(\zeta - \xi/2) \sec\xi/2$$

$$[J_o(u) + J_2(u)]\} \exp\{-jk\sigma[1 + \cos\zeta]\} r \, dr \qquad (3.24)$$

and $$u = k a r \sin\theta$$

$$\simeq k a r \theta \qquad (3.25)$$

Assuming that the feed displacement, d, is small compared with the radius of the antenna and also that the focal length is of the same order as the radius, the terms involving the displacement may be expanded to give the following approximate forms

$$\cos(\zeta - \xi/2) . \sec \xi/2 = \cos\zeta + \sin\zeta . \tan \xi/2$$

$$\simeq 1 - \frac{d}{a} \cdot \frac{r^2}{2\, f/a} \cdot \left[\frac{1}{\frac{f}{a} + \frac{r^2}{4\, f/a}}\right]^2 \qquad (3.26)$$

and

$$k\sigma[1+\cos\zeta] = 2.k.\frac{f}{a}.\left[a - \frac{d}{\frac{f}{a}+\frac{r^2}{4\,f/a}}\right] \qquad (3.27)$$

Hence

$$\exp\{-jk\sigma[1+\cos\zeta]\} = \exp\{-j\,2\,k\,f\}.$$

$$\exp\left\{ j\,2\,k\,\frac{f}{a}\,\frac{d}{\frac{f}{a}+\frac{r^2}{4\,f/a}}\right\} \qquad (3.28)$$

Equation (3.26) represents an amplitude term in the integrand, and for large reflector antennae, where the feed displacement is only a few percent of the diameter, may be assumed to be unity with little error. Equation (3.28), however, is a phase term consisting of a constant and variable part. The variable phase term is seen to be dependent upon both the feed displacement and the focal length to radius, or focal length-diameter, ratio. Consequently, the radiation pattern from a defocussed antenna is shown to be insensitive to variations in the size of the aperture but quite dependent upon the focal length-diameter ratio for a given feed displacement.

The influence of focal length on the modification of an antenna radiation pattern by defocussing is illustrated in fig. 3.2. These patterns are calculated

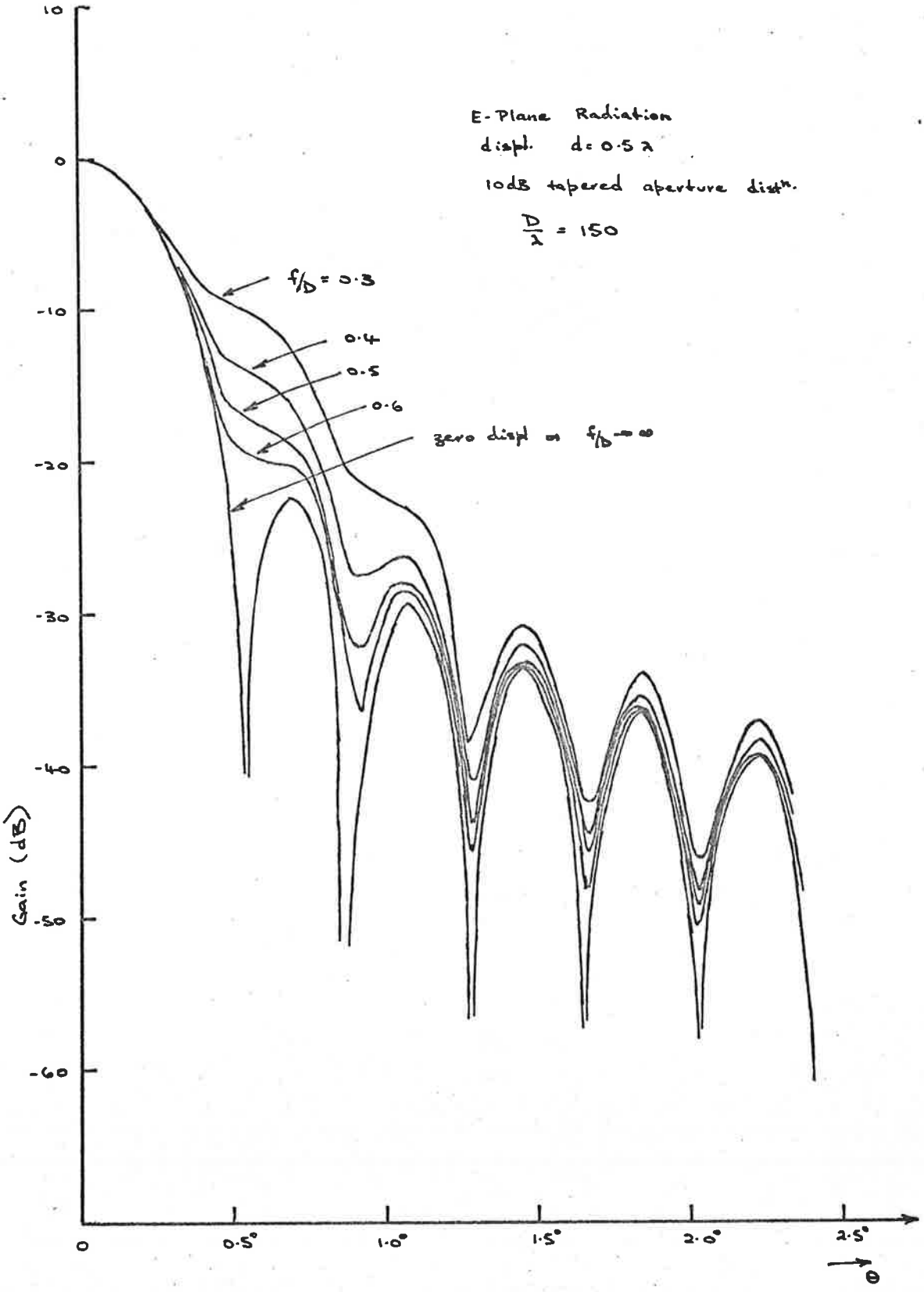

Fig. 3.2 (a) Effect of f/D on Defocussed Radiation Pattern.

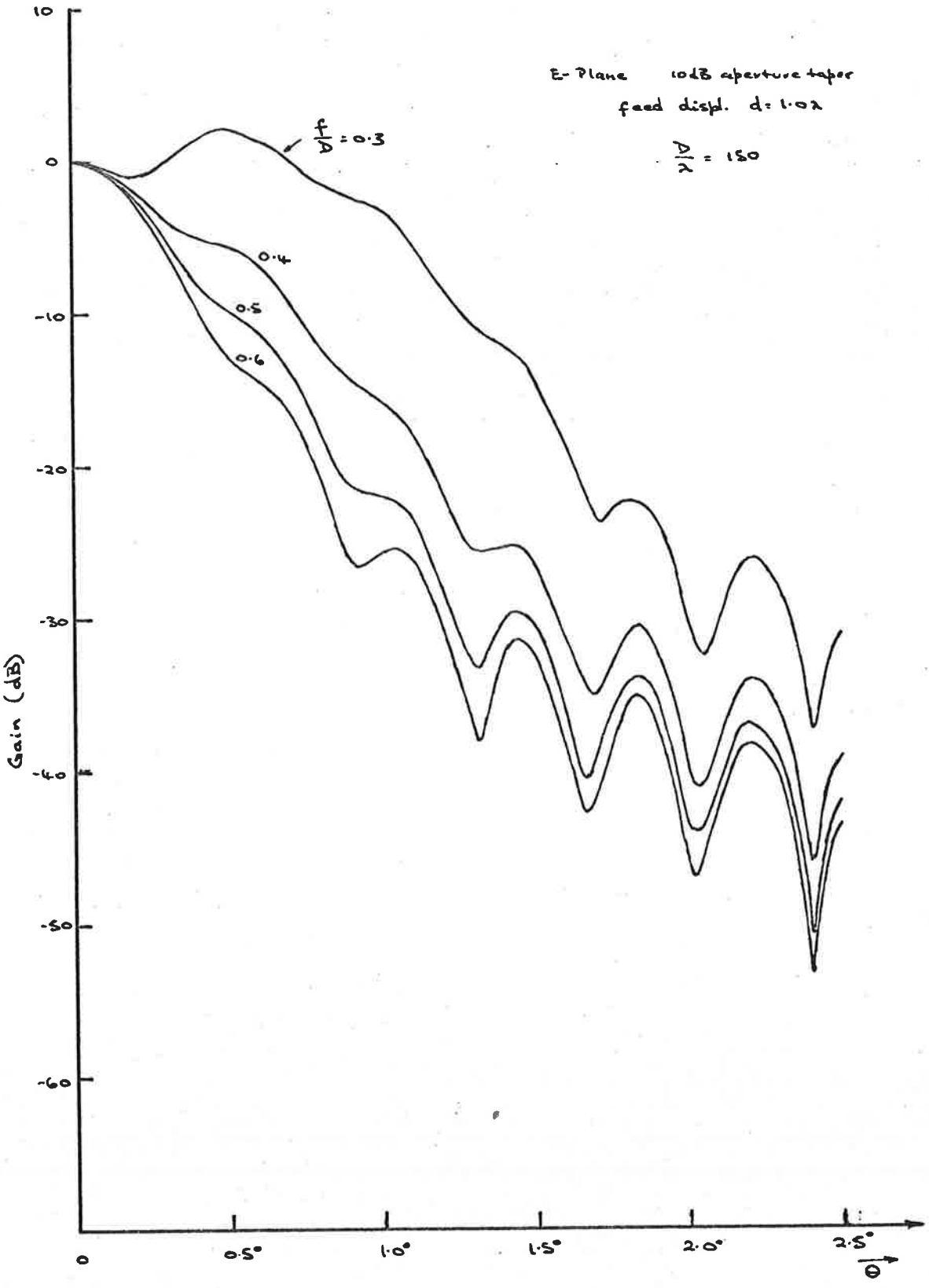

Fig. 3.2 (b) Effect of f/D on Defocussed Radation Pattern

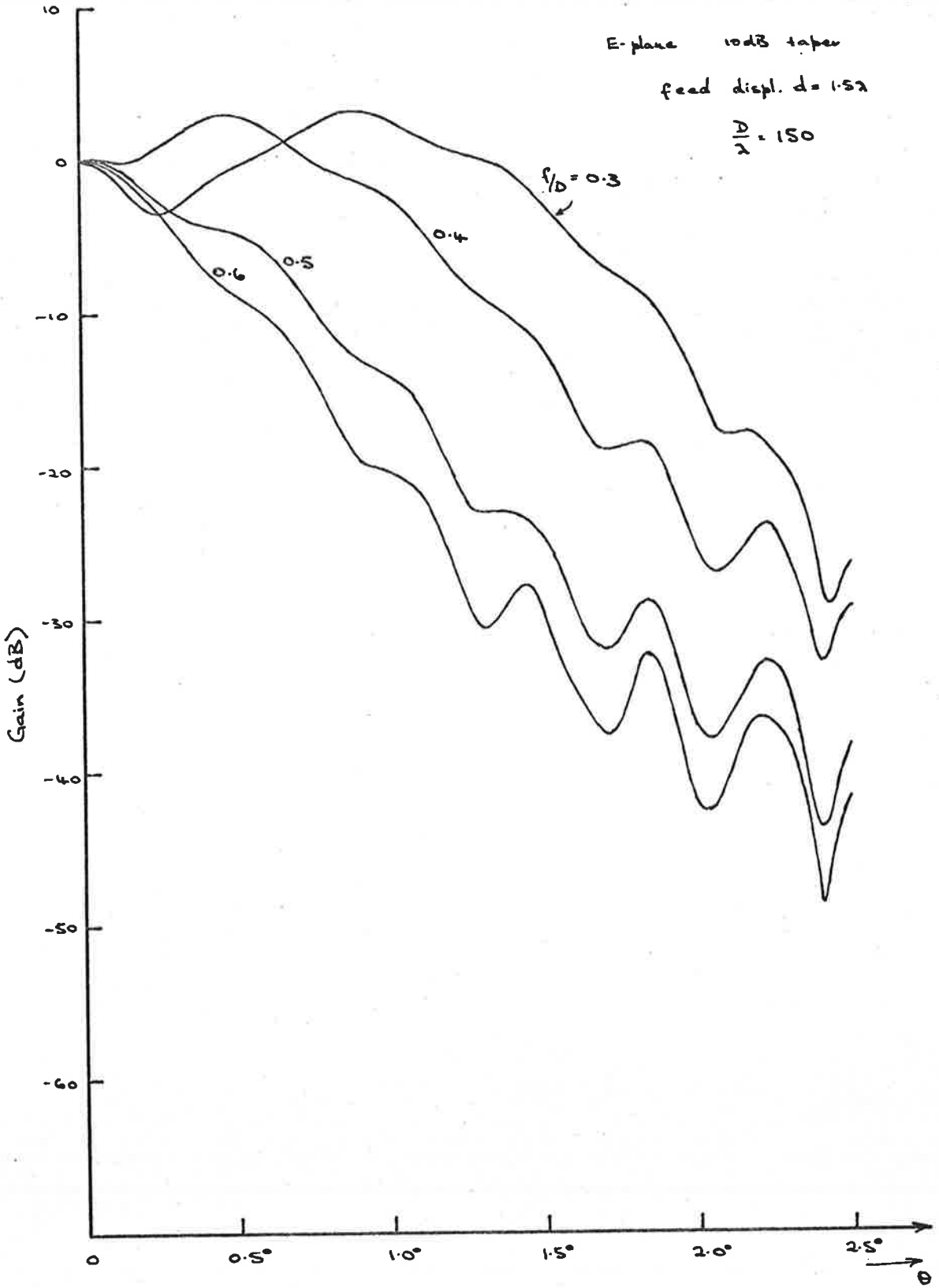

Fig. 3.2 (c) Effect of f/D on Defocussed Radiation Patterns

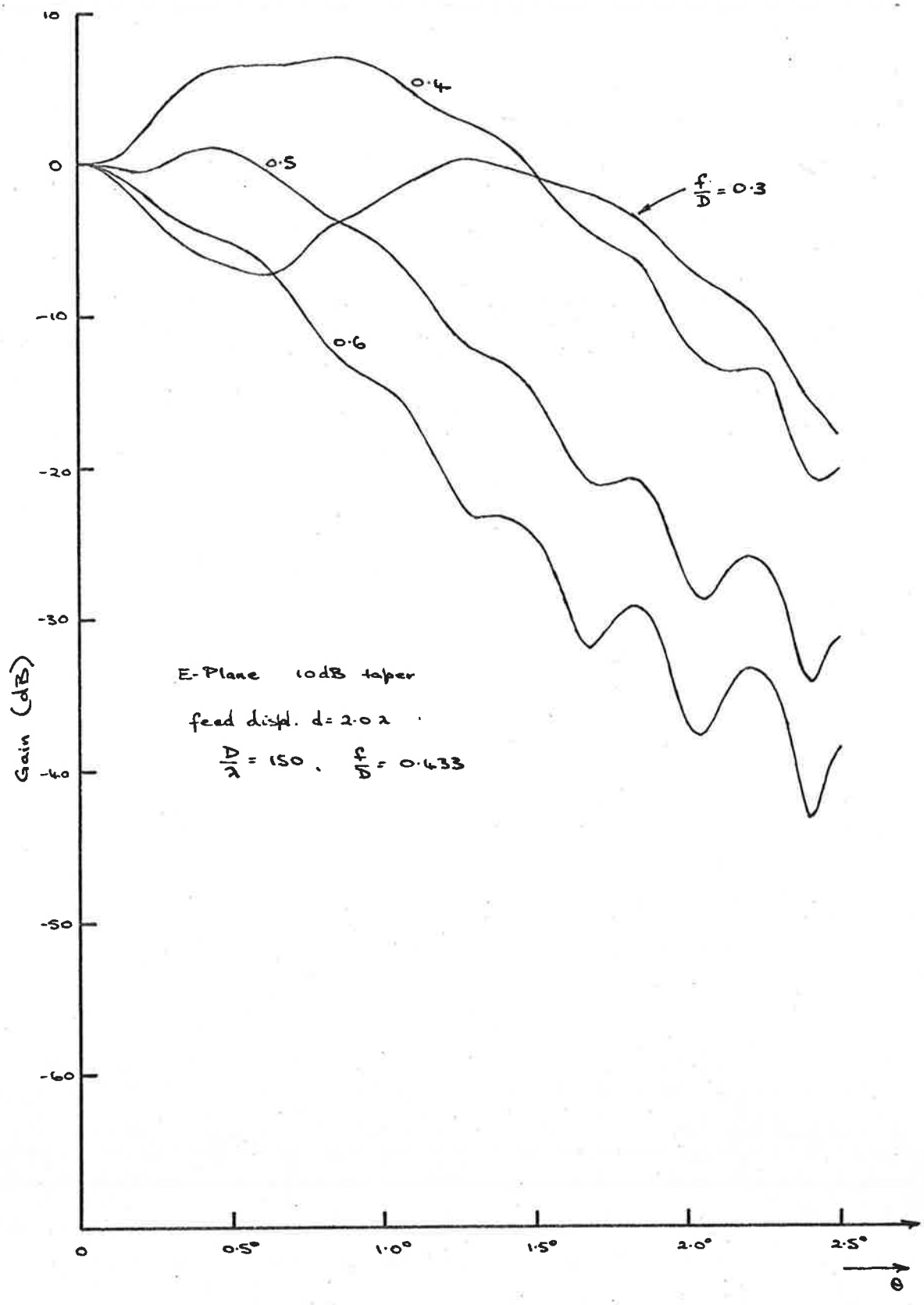

Fig. 3.2 (d) Effect of f/D on Defocussed Paraboloid Radiation

using equations (3.21) and (3.22) with

$$f_1 = f_2 = 1 - 0.6838\ r^2$$

to produce a 10 dB tapered aperture distribution.

Although the phase term, equation (3.28), in the radiation integral does not allow a simple connection between feed displacement and focal length-diameter ratio, the patterns in fig. 3.2 show that the distortion of the focussed pattern, caused by defocussing, is similar for all the $^f/_D$ ratios considered. Since the values considered more than span the range of values used in practice, patterns from an antenna with a fixed focal length-diameter ratio may be taken as typical. The value chosen for convenience in calculation is $^f/_D = 0.433$, corresponding to an edge angle of 60°.

3.2.3 Paraboloid with Defocussed Multimode Tracking Feed

From the discussion of the multimode tracking feed in Chapter II, the radiation patterns for the sum and difference must have the following properties in an ideal system:

(a) the sum mode pattern must be symmetrical i.e. independent of azimuth angle, ϕ.

(b) the radiation patterns of the TE_{01} and TM_{01} difference modes must be identical,

(c) the phase difference between the two difference modes must remain constant for all angles, θ and ϕ,

and (d) the phase difference between the sum and difference modes must be independent of the angles θ and ϕ.

Although these conditions are the ideal, in practice some variations in phase and amplitude characteristics can be tolerated, and in specifying limits the whole of the receiver amplifier and servo drive system characteristics and tolerances must be considered. In the defocussed antenna it is necessary that these conditions be met for each feed displacement, d, although relative shifts between the modes as the displacement is varied can be compensated by variable phase shifters mechanically or electrically linked to the defocussing mechanism.

Figs. 3.3, 3.4 and 3.5 give the amplitude characteristics of radiation by TE_{11}-TM_{11}, TE_{01} and TM_{01} fed paraboloid reflectors for feed displacements up to 2.5 wavelengths. As previously mentioned, the two mode combination used for the sum mode allows a symmetrical beam to be formed. Only the E-plane characteristics are plotted for the sum mode because the feed combination used gives calculated values of gain with less than 0.2 dB difference between the E- and H-plane

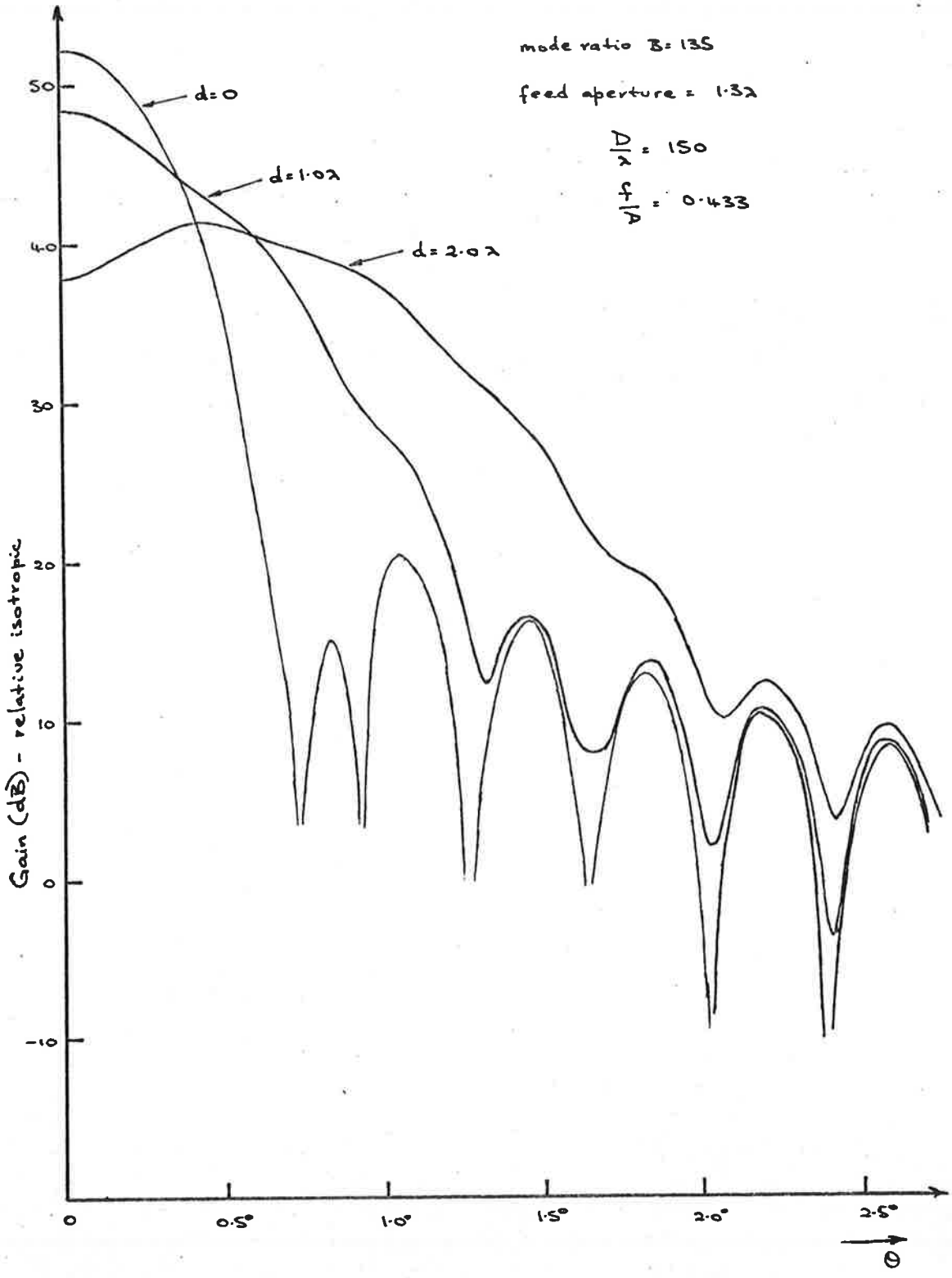

Fig. 3.3 (a) Mixed Mode Radiation from Defocussed Paraboloid.

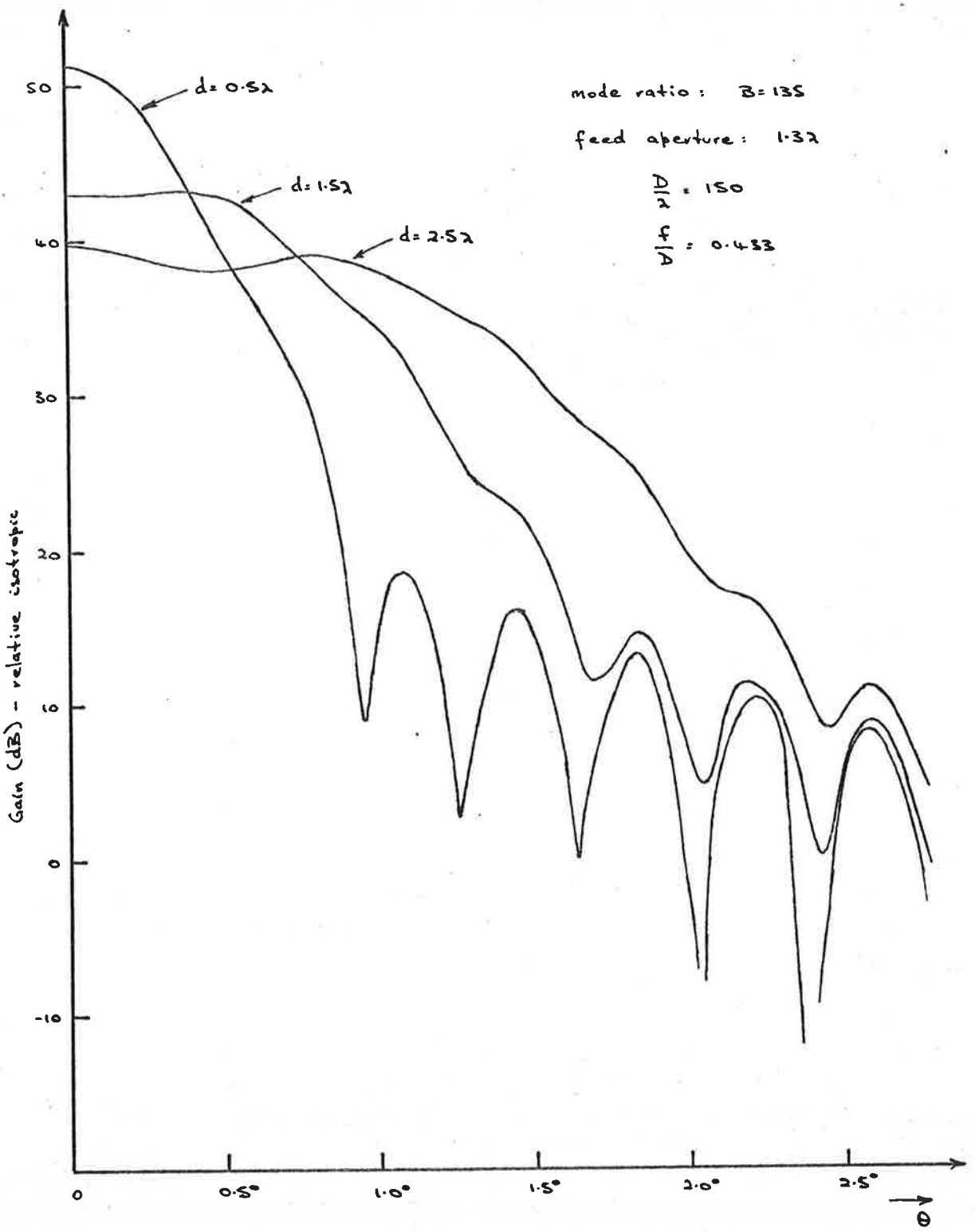

Fig. 3.3 (b) Mixed Mode Radiation from Defocussed Paraboloid.

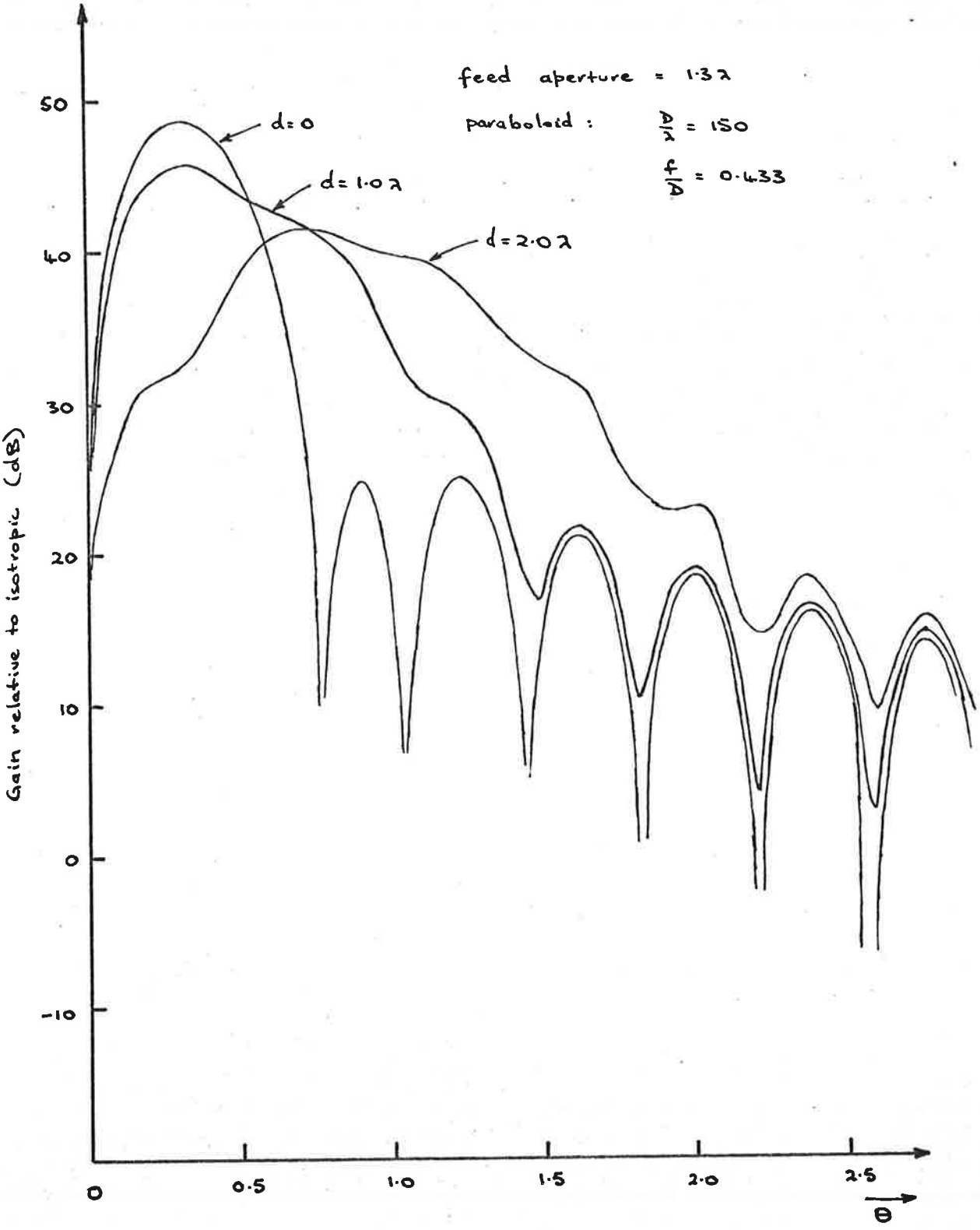

Fig. 3.4 (a) TM01 Radiation from Defocussed Paraboloid

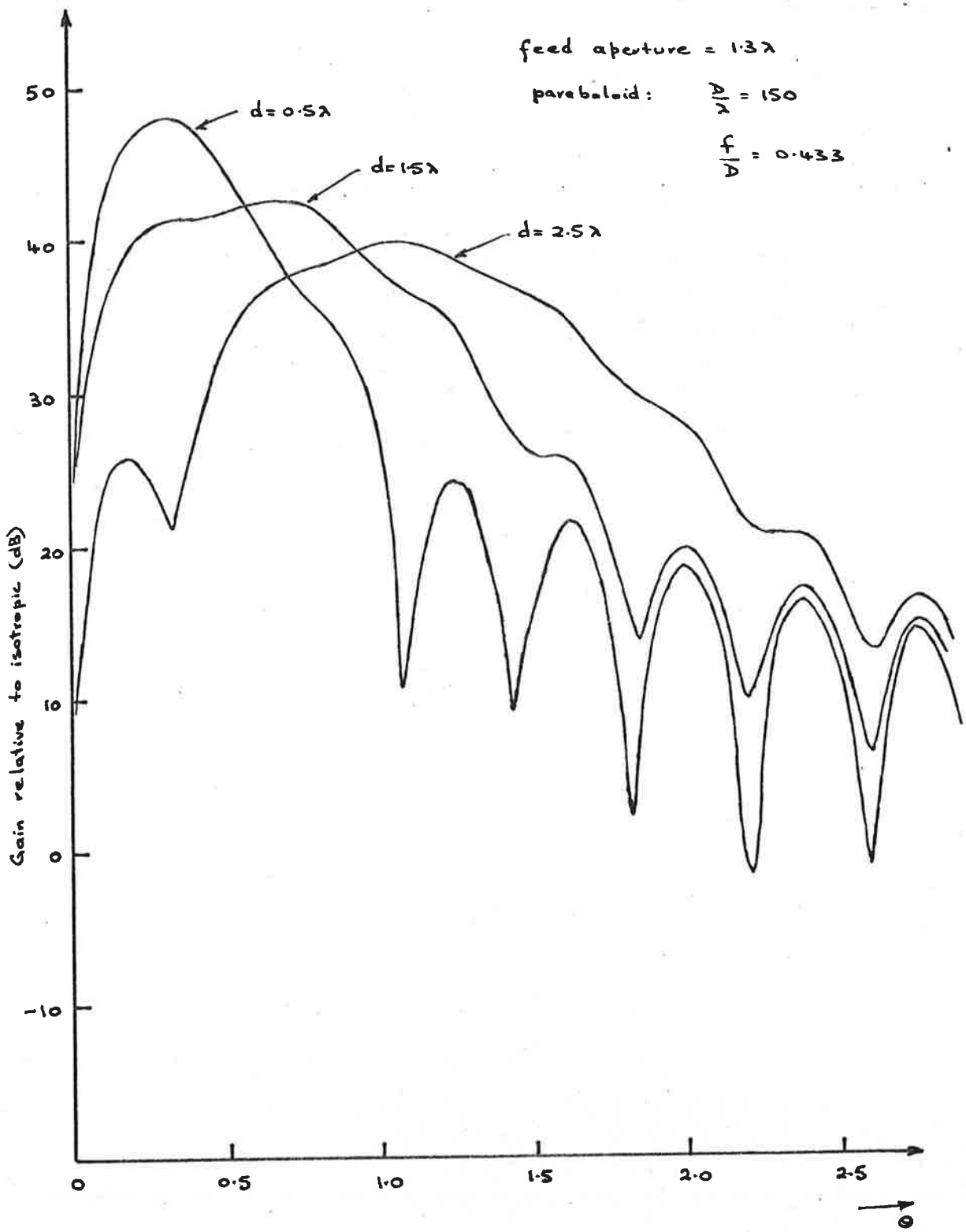

Fig. 3.4(b) TM_{01} Radiation from Defocussed Paraboloid

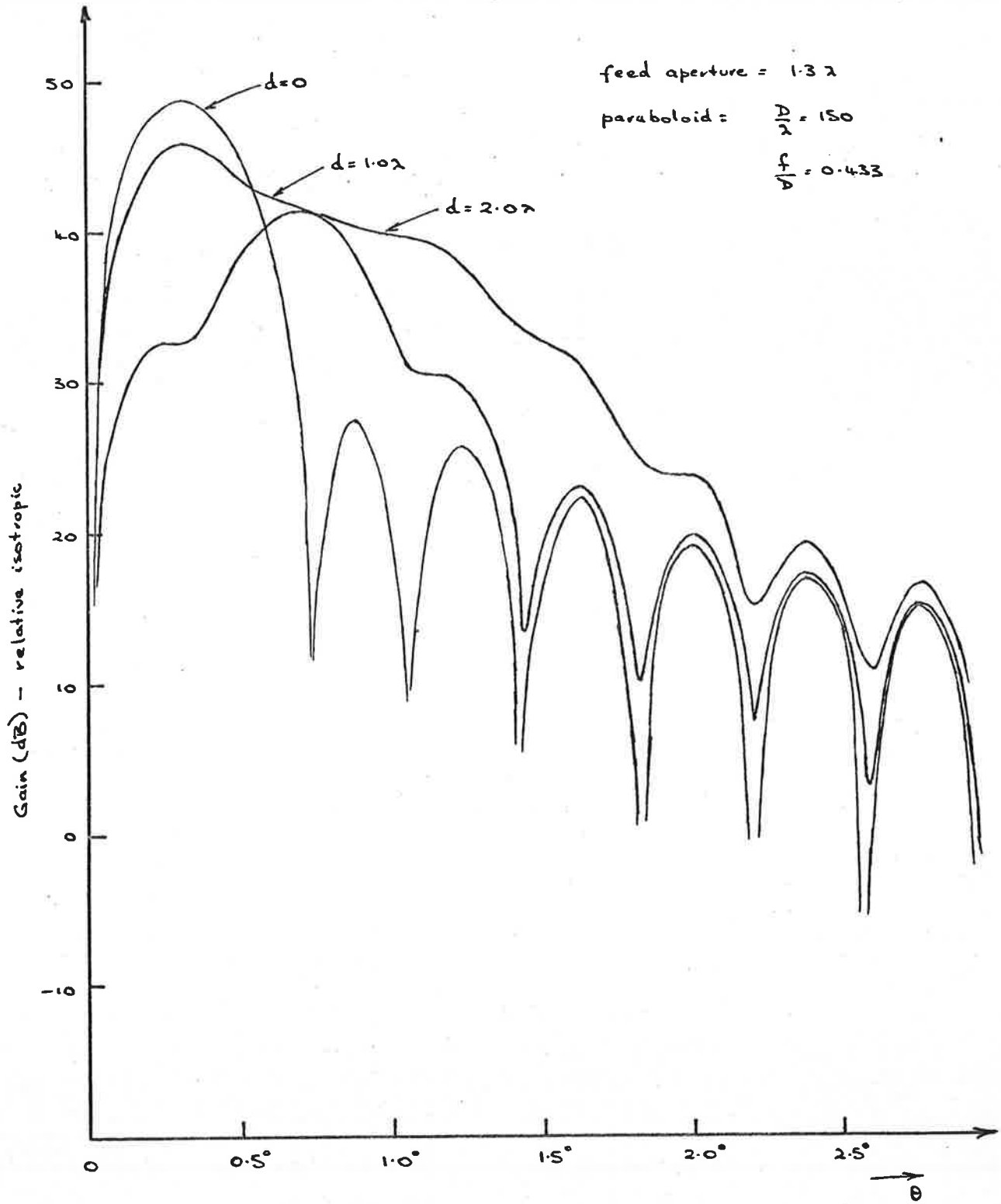

Fig. 3.5 (a) TE01 Radiation from Defocussed Paraboloid

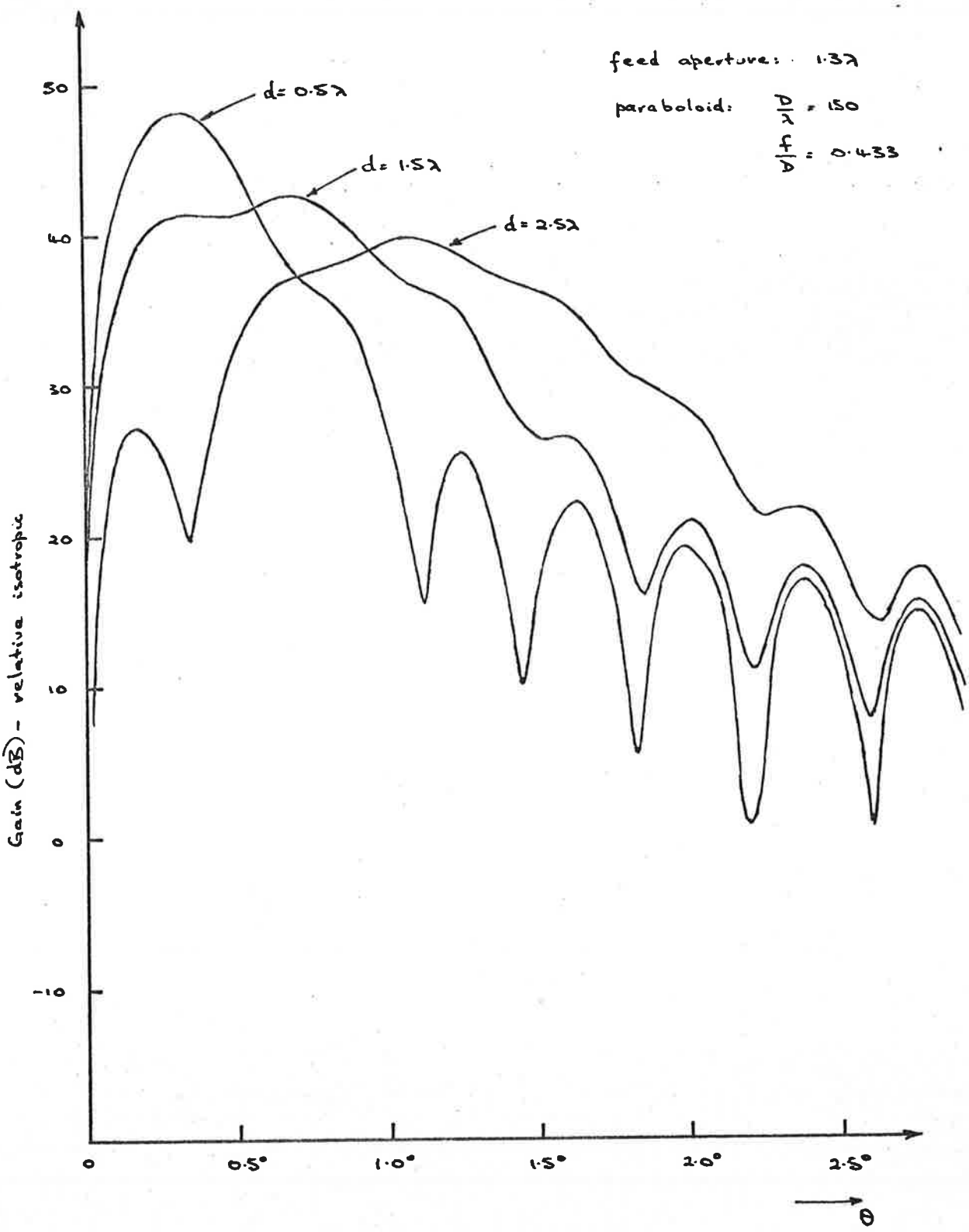

Fig. 3.5(b) TE01 Radiation from Defocussed Paraboloid.

characteristics at least up to 20 dB beamwidth. Similarly the phase characteristics are within one degree over the same range. For comparison of the increase in beamwidths attainable, the 3 dB, 10 dB and 20 dB beamwidths of the sum mode are tabulated against feed displacement in fig. 3.6.

Taking the 20 dB beamwidth of the sum mode as a typical working range in each case, the difference mode patterns for TE_{01} and TM_{01} modes have gain differences less than a 1.5 dB maximum and typically less than 1.0 dB. These figures exclude the curves for $d = 2.5\lambda$, where a new lobe has definitely appeared in the centre of the radiation pattern causing large differences between the two patterns at the first minimum off boresight, although at other points within the range the above tolerances apply.

In fig. 3.7 the range of phase differences between the TE_{01} and TM_{01} modes and the TM_{01} and TE_{11}-TM_{11} modes are tabulated for each feed displacement. The large phase difference range for the TM_{01} - TE_{11}-TM_{11} case with $d = 2.0\lambda$ and 2.5λ is caused by the development of the small inner lobe in the difference patterns. Fig. 3.8 graphically illustrates how the centres of these phase ranges, relative to the focussed case, vary with feed displacement. These curves give the phase compensation characteristic for a workable tracking system.

$d\ (\lambda)$	0	0.5	1.0	1.5	2.0	2.5
θ_{3dB}	0.46	0.50	0.60	1.38	2.20	2.22
θ_{10dB}	0.82	0.88	1.36	2.10	2.58	3.14
θ_{20dB}	1.08	1.46	1.96	2.84	3.34	4.00

$\frac{D}{\lambda} = 150$ $\frac{f}{D} = 0.433$

Fig. 3.6 Sum mode beamwidths for Paraboloid Reflector.

d (λ)	0·0	0·5	1·0	1·5	2·0	2·5
$TM_{01}-TE_{01}$	0·3°	6·8°	7·5°	10°	14°	26°
TM_{01} - Ref.	0·4°	26°	31°	32°	110°	132°

$\frac{D}{\lambda} = 150$ $\frac{f}{D} = 0.433$

Fig. 3.7 Phase difference ranges over θ_{20dB}

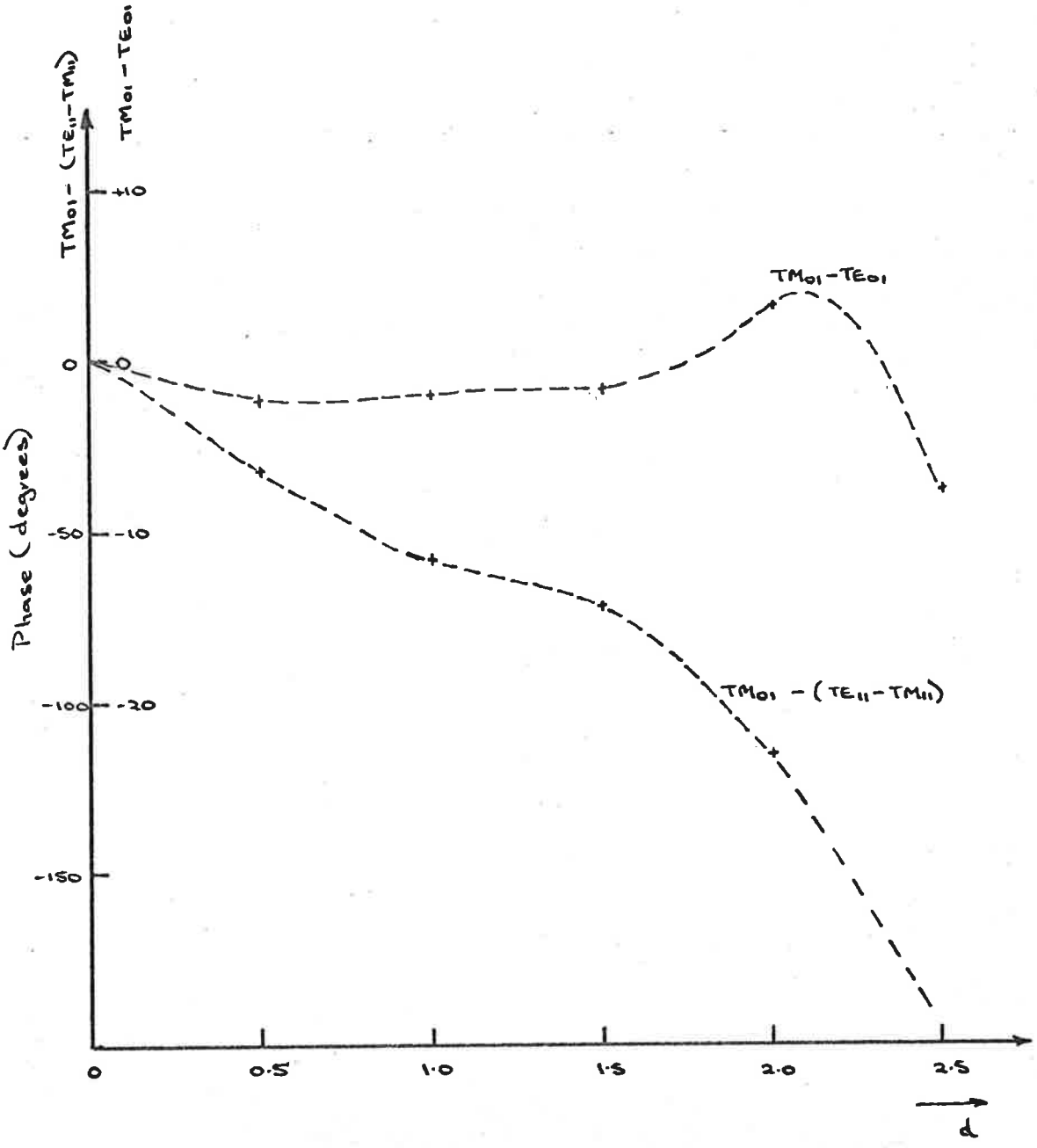

Fig. 3.8 Phase Compensation Curves for Defocussed Paraboloid.

For the two large feed displacements considered there is a considerable range of phase differences as the elevation angle, θ, is varied. As it is unlikely that a practical servo system could tolerate much more than $\pm$ 30° phase difference about the design centre, defocussing to this degree is not feasible and a maximum feed displacement of between 1.5λ and 2.0λ only is allowable. Over this range of displacements the phase difference between the circularly symmetric modes can be neglected.

A feed displacement of 1.5λ gives an approximate three times increase in the 3 dB beamwidth and about a two and a half times increase in the 10 dB beamwidth. This corresponds to an increase in the search element size of between six and nine times, which can be considered a significant increase in search element size and would produce a much lower acquisition time. However, the increase is probably not great enough to warrant the special inclusion of defocussing apparatus, although in cases where the feed system is designed to compensate automatically for the paraboloidal reflector deflections, basic equipment for defocussing is available and could be readily modified to make use of beam broadening properties.

3.3 Defocussed Cassegrain Antennae

The use of the cassegrain geometry for large low noise reflector antennae has several advantages over the simple focally excited paraboloid. These advantages nearly all stem from noise considerations. The contribution of ground noise due to spillover is greatly reduced and ultra-low noise amplifiers, such as the maser, with their heavy ancillary equipment, can be placed at the base of the antenna, so avoiding the mechanical problem of designing an antenna to retain reasonable tolerances while carrying a heavy load at the focus, or the electrical problem of long transmission lines introducing additional noise. Against these advantages must be weighed the provision of a second precision reflector, although this is much smaller than the main surface. The use of a two reflector system also gives greater flexibility to the system design, particularly with relation to the illumination of the main reflector.

In designing a cassegrain system, the same conditions as before apply to the choice of the main paraboloid with regard to cross-polarization and focal length-diameter ratio, with the exception that, with the reduced problem of weight at the focus and no active elements requiring long transmission lines, slightly

shallower dishes may be used. The choice of the sub-reflector involves the consideration of many factors.

If the feed phase centre is to remain in front of the main reflector, the focal length of the hyperboloid sub-reflector must be less than the focal length of the main reflector. The diameter of the sub-reflector must be chosen in relation to its focal length so that illumination can be achieved sensibly from a waveguide derived feed system. The shape of the sub-reflector, dictated by the eccentricity, is a compromise between the increase in the effective focal length of the entire system and the curvature of sub-reflector. The eccentricity of the hyperboloid decreases from infinity to one as the hyperboloid changes from a flat plate to a surface of infinite curvature i.e. a line folded back on itself. The effective focal length of a cassegrain system is given by

$$f_e = f_p . m$$

where f_e = effective focal length

f_p = focal length of the paraboloid

and m = magnification $\frac{e+1}{e-1}$ with e = eccentricity.

In general, the magnification is chosen to be about 4-5, corresponding to eccentricities of 1.6 to 1.5. The magnification is roughly approximated by the ratio of

the paraboloid edge angle to the hyperboloid edge angle, so that a paraboloid with an edge angle of 60°, in a cassegrain system, would require a primary feed angle of 12°–15°.

The one remaining factor to be considered in the choice of a sub-reflector is its diameter in relation to the main reflector, or, in other words, the extent of aperture blocking in the focal plane. For a plane circular aperture with a symmetric illumination function, the shape of the radiation pattern is given by[45]

$$g(u) = \int_{r_i}^{1} f(r)\, J_o(ur)\, r\, dr \qquad (3.29)$$

where $g(u)$ = voltage radiation characteristic

$f(r)$ = feed distribution

and r_i = inner radius of the aperture.

For a uniform feed function, $f(r)$, and for a feed with a 10 dB taper, the effect of aperture blocking on gain and sidelobe level is summarized in the following table.

Aperture blocking		0	10% rad. (1% area)	20% rad. (4% area)
uniform	gain (dB)	0	-0.09	-0.35
	sidelobe level (dB)	-17.6	-16.9	-15.2
10 dB taper	gain (dB)	0	-0.14	-0.57
	sidelobe level (dB)	-23.9	-21.9	-18.0

These figures indicate that aperture blocking reduces the gain and increases the sidelobe level of the secondary radiation pattern. The diameter of a sub-reflector is generally chosen in the range 10-15% of the main reflector.

3.3.1 Derivation of Radiation Formula

The derivation of a formula for the radiation from a cassegrain antenna system may be considered in two parts. The first is the calculation of the field illuminating the main reflector from the primary radiator and sub-reflector properties and, having performed this calculation, the derivation of the secondary radiation pattern from the main reflector. As the derivation of the radiation pattern from a paraboloidal reflector is considered elsewhere (Appendix I and section 3.2.1), this section will be primarily concerned with the former problem.

The illumination for the main reflector may be calculated either as the field incident at the reflector surface or directly as a surface current distribution. At this stage it is more convenient to derive the incident field at the reflector surface, which allows the already established formulae for radiation from a paraboloid to be used.

The two methods available for establishing the diffracted field of the hyperboloid are the geometric optics approach and the surface current integration technique (see Appendix I). The former method is only accurate in the limit of zero wavelength and has the disadvantage of giving a high edge illumination with a sudden cut-off on the main reflector, which does not occur in practice, resulting in apparently high sidelobe levels. The current integration technique, although still only an approximate method, gives a much better indication of the diffracted field. Although a cassegrain system, with parameters in the ranges discussed above, strictly speaking produces a sub-reflector for which the main reflector lies in the Fresnel field, it will be assumed here that the Fraunhofer or far field approximations can be applied. The implications of this further approximation are considered in Appendix III.

Using the coordinate system shown in fig. 3.9, from equations (3.4) and (3.5), the scattered electric field may be approximated by

$$\left.\begin{matrix} E_\xi \\ E_\eta \end{matrix}\right\} = -\frac{j\omega\mu}{2\pi\rho}\,.e^{-jk\rho}\,\left(\frac{\epsilon}{\mu}\right)^{\frac{1}{2}}\left\{\begin{matrix} \hat{\xi}\,.\,\underset{\sim}{I} \\ \hat{\eta}\,.\,\underset{\sim}{I} \end{matrix}\right. \qquad (3.30)$$

where

$$\underset{\sim}{I} = \int_S \underset{\sim}{\hat{E}}_h \times (\hat{\chi} \times \underset{\sim}{E}_i).e^{jk\chi.\hat{\rho}}\,dS \qquad (3.31)$$

for the origin at H.

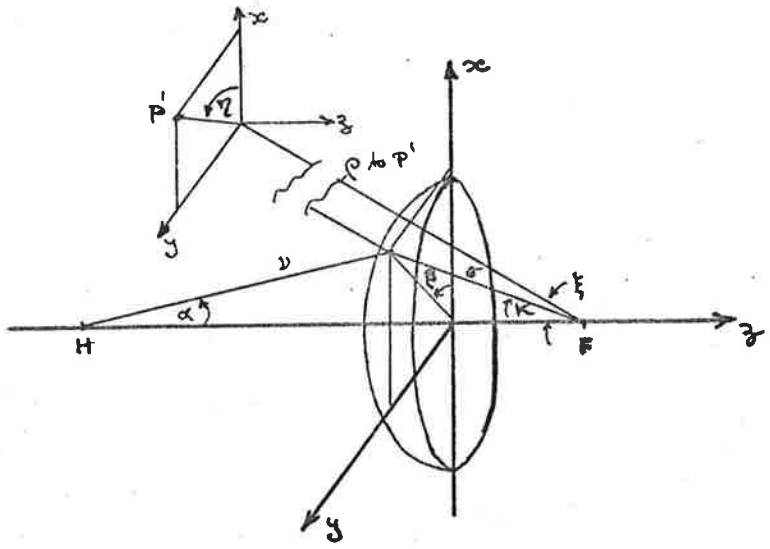

(a)

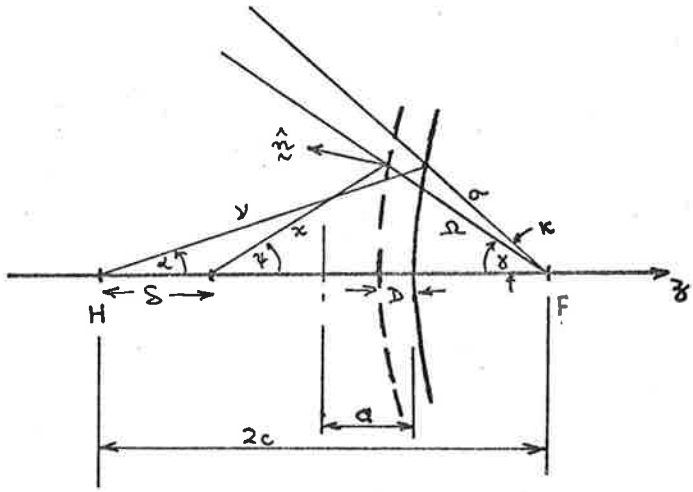

(b)

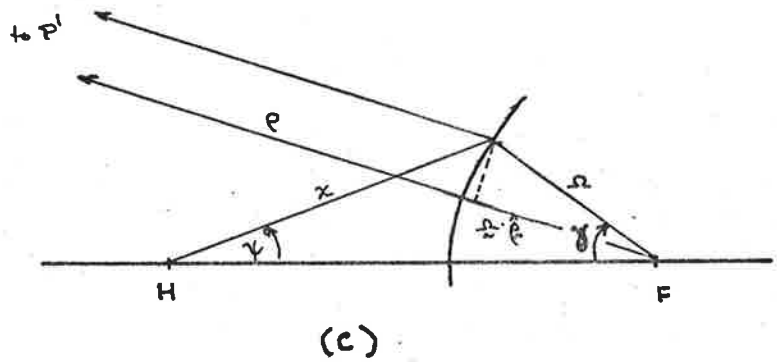

(c)

Fig. 3.9 Cassegrain System Geometry

For the hyperboloid surface, S,

$$dS = -\frac{\nu^2 \sin\alpha\, m(\alpha)}{1 - e\cos\alpha} \cdot d\alpha\, d\beta \qquad (3.32)$$

where $$\nu = \frac{-e\,c\,(1-\frac{1}{e^2})}{1 - e\cos\alpha} \qquad (3.33)$$

and $$m(\alpha) = [(1 - e\cos\alpha)^2 + (e\sin\alpha)^2]^{\frac{1}{2}} \qquad (3.34)$$

with $e = c/a$.

From fig. 3.9(b)

$$\chi = [\nu^2 + (\delta + D)^2 - 2\nu(\delta + D)\cos\alpha]^{\frac{1}{2}} \qquad (3.35)$$

where D = sub-reflector displacement away from paraboloid focus

and δ = feed displacement toward the sub-reflector,

$$\hat{n}_h = \frac{1}{m(\alpha)}[(1 - e\cos\alpha)\hat{\nu} + e\sin\alpha\,\hat{a}] \qquad (3.36)$$

and $$\hat{\chi} = \cos(\psi - \alpha)\hat{\nu} + \sin(\psi - \alpha)\hat{a} \qquad (3.37)$$

The primary radiation from the feed at H may be written

$$E_i = (E_\psi \hat{\psi} + E_\beta \hat{\ell}) \cdot e^{-jk\chi} \qquad (3.38)$$

in the far field. Thus, using

$$\hat{\underset{\sim}{\psi}} = -\sin(\psi-\alpha)\hat{\underset{\sim}{\nu}} + \cos(\psi-\alpha)\,\hat{\underset{\sim}{\alpha}} \qquad (3.39)$$

$$\hat{\underset{\sim}{n}}_h \times (\hat{\underset{\sim}{\chi}} \times \underset{\sim}{E}_i) = \frac{1}{m(\alpha)}\{\hat{\underset{\sim}{\nu}}\, E_\psi\, e \sin\alpha - \hat{\underset{\sim}{\alpha}}\, E_\psi (1 - e\cos\alpha)$$

$$- \hat{\underset{\sim}{\beta}}\, E_\beta\, [\cos(\psi-\alpha) - e\cos\psi]\} \qquad (3.40)$$

From the relations

$$\begin{aligned}
\hat{\underset{\sim}{\xi}}\cdot\hat{\underset{\sim}{\nu}} &= \cos\xi \sin\alpha \cos(\eta-\beta) + \sin\xi\cos\alpha \\
\hat{\underset{\sim}{\xi}}\cdot\hat{\underset{\sim}{\alpha}} &= \cos\xi\cos\alpha\cos(\eta-\beta) - \sin\xi\sin\alpha \\
\hat{\underset{\sim}{\xi}}\cdot\hat{\underset{\sim}{\beta}} &= \cos\xi\sin(\eta-\beta) \qquad (3.41) \\
\hat{\underset{\sim}{\eta}}\cdot\hat{\underset{\sim}{\nu}} &= -\sin\alpha\sin(\eta-\beta) \\
\hat{\underset{\sim}{\eta}}\cdot\hat{\underset{\sim}{\alpha}} &= -\cos\alpha\sin(\eta-\beta) \\
\hat{\underset{\sim}{\eta}}\cdot\hat{\underset{\sim}{\beta}} &= \cos(\eta-\beta)
\end{aligned}$$

$$[\hat{\underset{\sim}{n}}_h \times (\hat{\underset{\sim}{\chi}} \times \underset{\sim}{E}_i)]_\xi = \frac{1}{m(\alpha)}\{E_\psi[\cos\xi(e-\cos\alpha)\cos(\eta-\beta)$$

$$+ \sin\xi\sin\alpha] - E_\beta\cos\xi[\cos(\psi-\alpha) - e\cos\psi]\sin(\eta-\beta)\} \qquad (3.42)$$

and

$$[\hat{\underset{\sim}{n}}_h \times (\hat{\underset{\sim}{\chi}} \times \underset{\sim}{E}_i)]_\eta = \frac{1}{m(\alpha)}\{E_\psi\,(\cos\alpha - e)\sin(\eta-\beta)$$

$$- E_\beta\,[\cos(\psi-\alpha) - e\cos\psi]\cos(\eta-\beta)\} \qquad (3.43)$$

From fig. 3.9(c), shifting the origin to F, produces a modified phase term

$$\exp\{-jk[\rho + \chi - \underset{\sim}{\Omega}\cdot\hat{\underset{\sim}{\rho}}]\}$$

where $\Omega = [(2c+D)^2 + \nu^2 - 2\nu(2c+D)\cos\alpha]^{\frac{1}{2}}$

From $\hat{\underset{\sim}{\rho}} = \hat{\underset{\sim}{\nu}}[\sin\xi\sin\alpha\cos(\eta-\beta) - \cos\xi\cos\alpha]$

$$+ \hat{\underset{\sim}{\alpha}}[\sin\xi\cos\alpha\cos(\eta-\beta) + \cos\xi\sin\alpha]$$

$$+ \hat{\underset{\sim}{\beta}}\sin\xi\sin(\eta-\beta)$$

and $\hat{\underset{\sim}{\Omega}} = -\hat{\underset{\sim}{\nu}}\cos(\alpha+\gamma) + \hat{\underset{\sim}{\alpha}}\sin(\gamma+\alpha)$

$$\hat{\underset{\sim}{\Omega}}\cdot\hat{\underset{\sim}{\rho}} = \cos\xi\cos\gamma + \sin\xi\sin\gamma\cos(\eta-\beta)$$

If feed or sub-reflector displacements are considered separately the following relations are useful

$$\Omega\cos\gamma = 2c + D - \nu\cos\alpha$$

$$= 2c - \delta - \chi\cos\psi$$

and $\Omega\sin\gamma = \chi\sin\psi$

$$= \nu\sin\alpha$$

The expanded expression for the far field radiation from a hyperboloid becomes

$$\left.\begin{matrix} E_\xi \\ E_\eta \end{matrix}\right\} = -\frac{j\omega\mu}{2\pi\rho} \cdot e^{-jk\rho} \left(\frac{\varepsilon}{\mu}\right)^{\frac{1}{2}} \left\{ \begin{matrix} I_\xi \\ I_\eta \end{matrix}\right. \qquad (3.44)$$

where

$$I_\xi = \int_0^{2\pi}\int_0^{A} \{E_\psi[\cos\xi(e-\cos\alpha)\cos(\eta-\beta)+\sin\xi\sin\alpha]$$

$$- E_\beta \cos\xi\,[\cos(\psi-\alpha)-e\cos\psi]\sin(\eta-\beta)\}$$

$$\exp\{-jk[\chi-\Omega(\cos\xi\cos\gamma+\sin\xi\sin\gamma\cos(\eta-\beta)]\}$$

$$dS(\alpha)\,d\alpha\,d\beta$$

and

$$I_\eta = \int_0^{2\pi}\int_0^{A} \{E_\psi(\cos\alpha-e)\sin(\eta-\beta)-E_\beta[\cos(\psi-\alpha)-e\cos\psi]$$

$$\cos(\eta-\beta)\}\exp\{....\}\,dS(\alpha)\,d\alpha\,d\beta$$

where

$$dS(\alpha) = -\frac{\nu^2\sin\alpha}{1-e\cos\alpha}$$

and A = edge angle of the sub-reflector.

For a circularly symmetric linearly polarized feed,

$$E_\psi = f(\psi) \sin\beta$$

and $$E_\beta = f(\psi) \cos\beta$$

and since Ω is independent of the azimuth angle β

$$\exp\{ jk\Omega \sin\xi\sin\gamma \cos(\eta-\beta)\} = J_o(u) + 2\sum_{n=1}^{\infty} j^n J_n(u).$$

$$\cos n(\eta-\beta)$$

where $u = k\Omega \sin\xi \sin\gamma$

and the integration over the azimuth angle can be performed. Hence

$$I_\xi = \pi \sin\eta \int_0^A f \{[(e-\cos\alpha)[J_o(u)-J_2(u)] - [\cos(\psi-\alpha)$$

$$- e\cos\psi][J_o(u)+J_2(u)]]\cos\xi + 2j\sin\xi\sin\alpha J_1(u)\}$$

$$\exp\{- jk[\chi-\Omega\cos\xi\cos\gamma]\} \, dS(\alpha)\, d\alpha \qquad (3.45)$$

and

$$I_\eta = \pi\cos\eta \int_0^A f\{(e-\cos\alpha)[J_o(u)+J_2(u)] - [\cos(\psi-\alpha)$$

$$- e\cos\psi][J_o(u)-J_2(u)]\} \cdot \exp\{-jk[\chi-\Omega\cos\xi\cos\gamma]\}$$

$$dS(\alpha)\, d\alpha \qquad (3.46)$$

Similarly, expressions for circularly symmetric waveguide feeds can be derived and together with equation (3.43) give the scattered field.

Magnetic mode (TM_{01}):

$$E_\psi = f(\psi)$$

$$\text{and } E_\beta = 0$$

giving

$$I_\xi = 2\pi \int_0^A f \{ \sin\xi \sin\alpha \, J_0(u) + j \cos\xi (e - \cos\alpha) \, J_1(u) \}$$

$$\exp\{ - jk[\chi - \Omega \cos\xi \cos\gamma] \} \, dS(\alpha) \, d\alpha \qquad (3.47)$$

and $I_\eta = 0$.

Electric mode (TE_{01}):

$$E_\psi = 0$$

$$\text{and } E_\beta = f(\psi)$$

giving

$$I_\eta = 2\pi j \int_0^A f \, [e \cos\psi - \cos(\psi - \alpha)] J_1(u)$$

$$\exp\{ -jk[\chi - \Omega \cos\xi \cos\gamma] \} dS(\alpha) \, d\alpha \qquad (3.48)$$

and $I_\xi = 0$.

As before the gain function may be derived as

$$G(\xi,\eta) = \frac{2\pi}{P_t}\left(\frac{\epsilon}{\mu}\right)^{\frac{1}{2}} |\rho E|^2$$

where P_t = total power

$$= \int \frac{(\rho E)^2}{2\eta} \, d\Omega$$

with $d\Omega$ = elemental solid angle

$$= \sin\psi \, d\psi \, d\beta$$

and = intrinsic impedance of air

$$= \left(\frac{\mu}{\epsilon}\right)^{\frac{1}{2}}$$

The corresponding expressions for radiation from the paraboloid, with the incident field given by equation (3.43), are easily found from expressions for radiation from a focussed paraboloid (see Appendix I).

For the sum or linearly polarized mode, the incident field can be written

$$E_\xi = f_1(\rho,\xi).\sin\eta \,.e^{-jk\rho}$$

and $$E_\eta = f_2(\rho,\xi).\cos\eta \,.e^{-jk\rho}$$

and the scattered field from the paraboloid

$$\left.\begin{matrix} E_\theta \\ E_\phi \end{matrix}\right\} = -\frac{j\omega\mu}{2\pi} \cdot \frac{e^{-jkR}}{R} \cdot \left(\frac{\epsilon}{\mu}\right)^{\frac{1}{2}} \left\{ \begin{matrix} I_\theta \\ I_\phi \end{matrix}\right. \qquad (3.49)$$

where

$$I_\theta = \pi \sin\phi \int_0^E \{\cos\theta \cdot \cos \xi/2 \; [f_1 \; (J_0(w) - J_2(w)) + f_2 \; (J_0(w) + J_2(w))] - 2j f_1 \sin\theta \sin \xi/2 \; J_1(w)\} \exp\{-jk\rho [1 + \cos\theta \cos\xi]\} \; \rho^2 \sin\xi \sec \xi/2 \; d\xi \quad (3.50)$$

and

$$I_\phi = \pi \cos\phi \int_0^E \{f_1 [J_0(w) + J_2(w)] + f_2 [J_0(w) - J_2(w)]\} \exp\{-jk\rho [1 + \cos\theta \cos\xi]\} \; \rho^2 \sin\xi \; d\xi \quad (3.51)$$

where $w = k\rho \sin\theta \sin\xi$.

If the incident field at the paraboloid reflector is circularly symmetric

$$f_1 \; (\rho, \xi) = f_2 \; (\rho, \xi) = f$$

and equations (3.49) and (3.50) become

$$I_\theta = 2\pi \sin\phi \int_0^E f \{\cos\theta \cos \xi/2 \; J_0(w) - j \sin\theta \sin \xi/2 \; J_1(w)\} \exp\{-jk\rho [1 + \cos\theta \cos\xi]\} \; \rho^2 \sin\xi \sec \xi/2 \; d\xi \quad (3.52)$$

and

$$I_\phi = 2\pi \cos\phi \int_0^E f\, J_o(w)\, \exp\{-jk\rho[1 + \cos\theta \cos\xi]\}$$

$$\rho^2 \sin\xi\, d\xi \qquad (3.53)$$

For the circularly symmetric magnetic mode (TM_{01}) the incident field at the main reflector is

$$E_\xi = f(\rho,\xi)\ e^{-jk}$$

and $\quad E_\eta = 0$

and the scattered field is obtained from equation (3.48) with

$$I_\phi = 0$$

and $$I_\theta = 2\pi \int_0^E f\ [j \cos\theta \cos^{\xi}/2\ J_1(w) - \sin\theta \sin^{\xi}/2\ J_o(w)]$$

$$\exp\{-jk\rho[1 + \cos\theta \cos\xi]\}\ \rho^2\ \sin\xi \sec\ ^{\xi}/2\ d\xi$$

(3.54)

The circularly symmetric electric mode (TE_{01}) gives the following relations

incident field:

$$E_\xi = 0$$

$$E_\eta = f(\rho\,\xi).\ e^{-jk\rho}$$

and

$$I_\theta = 0$$

$$I_\phi = 2\pi\, j \int_0^E f\, J_1(w)\, \exp\{-jk\rho[1 + \cos\theta \cos\xi]\}\rho^2 \sin\xi d\xi$$

(3.55)

3.3.2 Radiation from Cassegrain Feed System

As the nature of the secondary radiation from a reflector antenna system can be predicted from the feed function for the aperture, for the cassegrain system which involves a lengthy computation to determine the final radiation characteristic, it is convenient to first consider the effective illumination of the main reflector by the primary feed - sub-reflector combination. In this way the effect of both feed and sub-reflector displacements on the final radiation pattern can be predicted.

(a) Feed Displacement

Considering first the displacement of the primary feed alone, the gain and phase characteristics in the far field for diffraction by a hyperboloid are shown in fig. 3.10, where the primary feed is linearly polarized and has a 10 dB taper to the edge angle of the sub-reflector and is represented by

$$f(\chi,\psi) = \frac{1}{\chi} \cdot 0.095 \frac{J_1(10.5 \sin\psi)}{\sin\psi} (1 + \cos\psi) \qquad (3.56)$$

which gives a shape approximately that of a waveguide radiator. The curves are given for the E-plane only since the H-plane has very similar patterns. The characteristics shown indicate that the illumination of

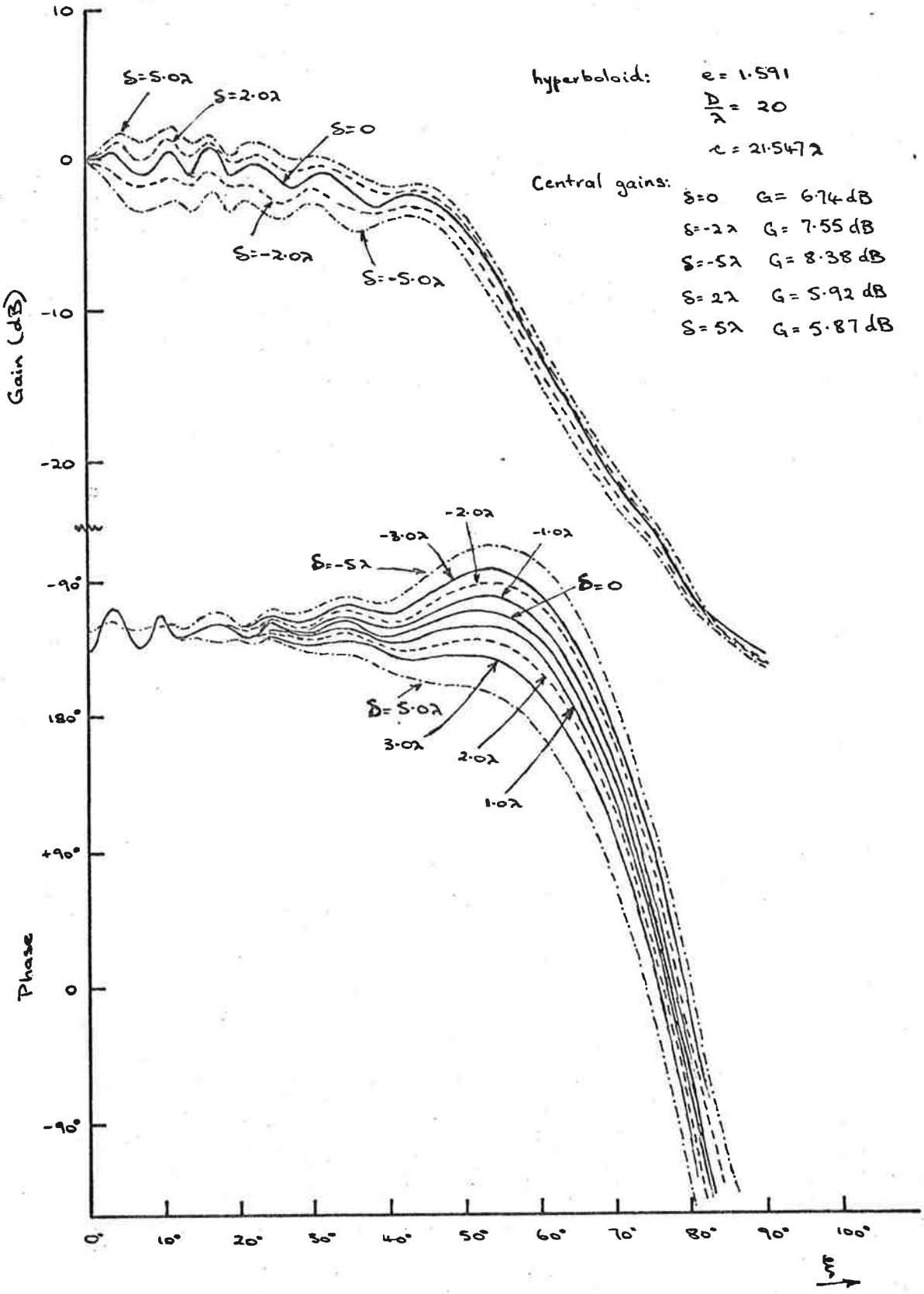

Fig. 3.10 Effect of Feed Displacement on Cassegrain Illumination.

the main reflector is only slightly dependent upon the feed displacement. For a maximum feed displacement of 5λ, which is close to a practical upper limit, the gain characteristics have very similar shapes and, together with the central absolute gains, indicate that the average amplitude distribution remains almost constant. The phase characteristics show a slowly increasing phase taper with feed displacement and for $\delta = 5\lambda$ the phase taper is approximately 50° or about $\lambda/8$. This corresponds to the maximum allowable phase taper[41] which does not significantly reduce the antenna gain or upset the sidelobe structure.

The property of insensitivity to feed position, at least on the axis, in the cassegrain system is as expected, since this type of antenna is geometrically equivalent to a single reflector antenna with the focal length increased by the magnification of the sub-reflector assembly. In this case the paraboloid has an $f/D=0.433$ while the complete system has effectively $f/D=1.90$. It is due to this insensitivity that inordinately large primary feed displacements would be required to produce significant phase tapers in the main aperture, making it an impracticable method of producing beam broadening.

(b) Sub-reflector Displacement

Fig. 3.11 shows an equivalent set of phase and gain characteristics for sub-reflector displacements along the axis. As before, the gain characteristics show that the amplitude distribution varies only slightly in shape and average level as the system is defocussed; however, the phase characteristics show large variations in phase taper with sub-reflector shift. Comparing these phase characteristics with those given by fig. 3.12, which shows the equivalent phase taper caused by a shift of the feed in a focally excited reflector antenna, a shift of the sub-reflector is seen to be equivalent to a shift of the primary feed in the single reflector case. Accordingly, the same increases in secondary beamwidth compared with the single reflector system can be expected in the cassegrain case for similar shifts of the sub-reflector. Similar results would be obtained by moving the cassegrain feed system, i.e. primary feed and sub-reflector, as a whole. However, the effect of moving the primary radiator as well will be insignificant and only serves to increase the practical difficulties.

In low noise cassegrain systems, the primary feed will be directly connected to a low noise amplifier mounted at the base of the paraboloid and so the avoidance of moving the primary feed is necessary to ensure

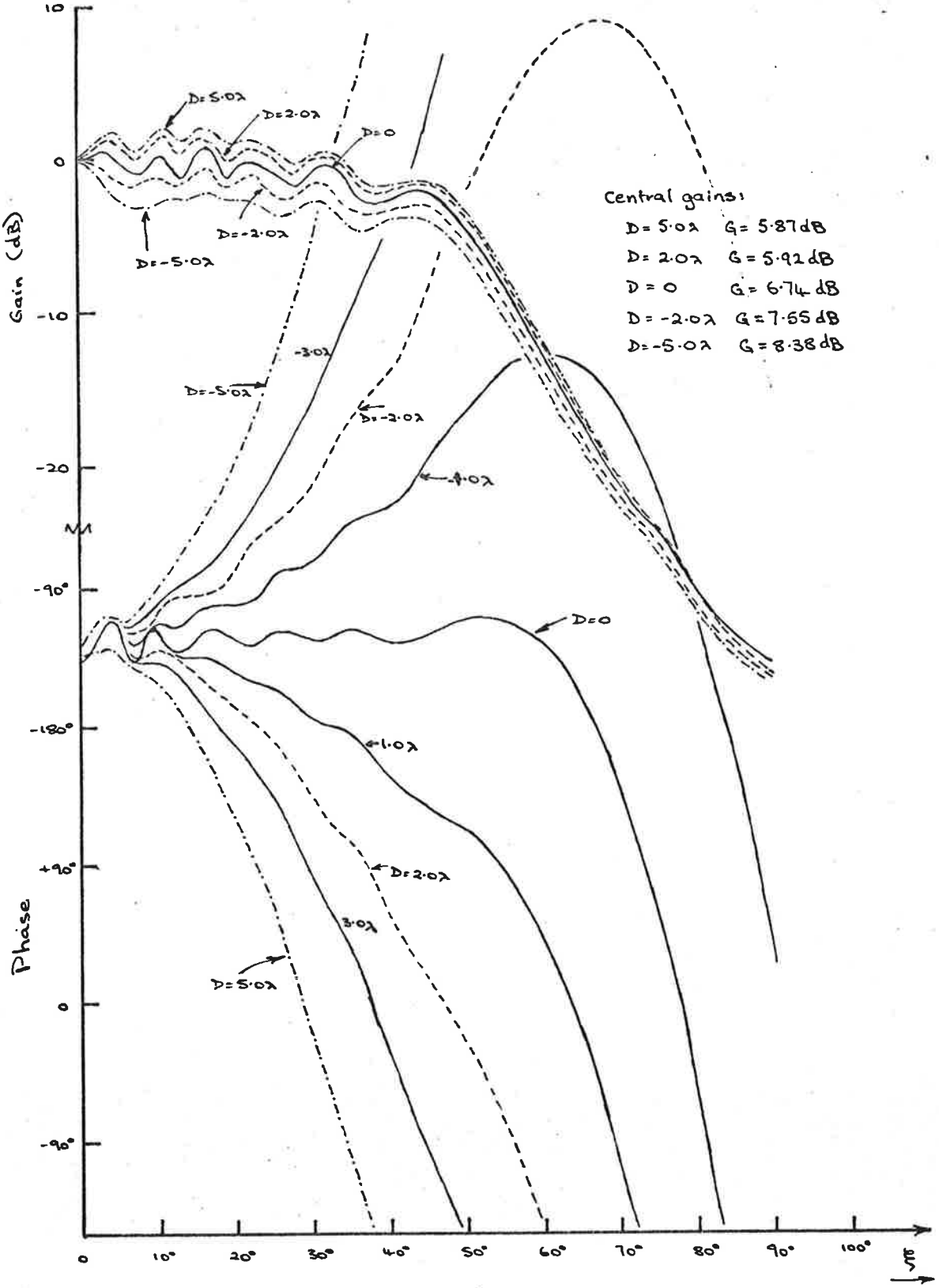

Fig. 3.11 Effect of Sub-reflector Displacement on Cassegrain Feed Function.

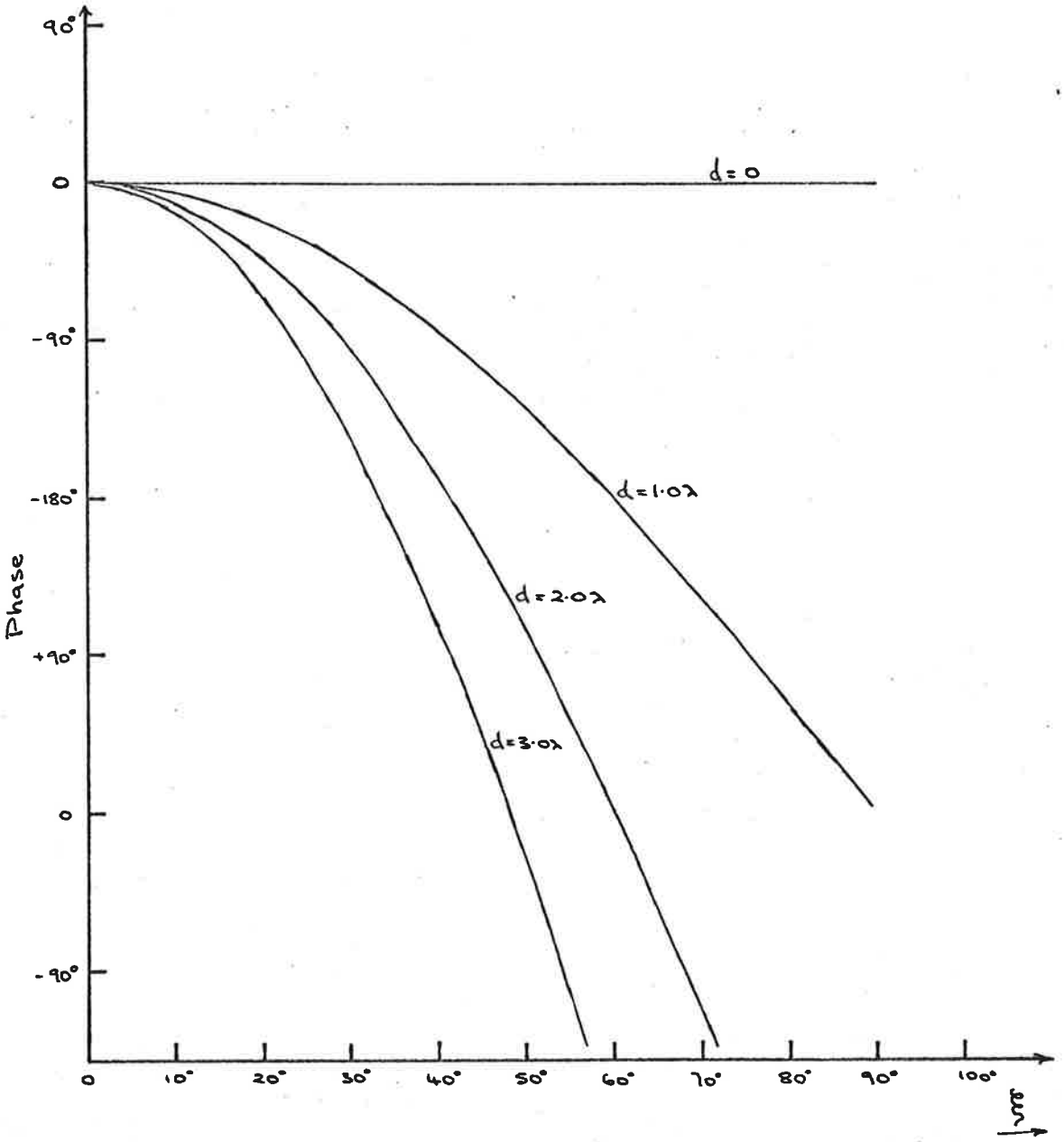

Fig. 3.12 Phase tapers due to feed displacement in focally excited antenna.

minimum noise in the transmission system. Consequently, modification of the antenna radiation pattern by movement of the passive sub-reflector only is a highly desirable feature. Defocussing system could easily be incorporated with a sub-reflector control designed to make use of the best-fit paraboloid at all times.

For completeness, fig. 3.13 gives a comparison of the geometric optics approximation to the hyperboloid diffraction with that calculated from the far field current integration formula. Apart from the phase and amplitude ripples near boresight, the main difference to note is the edge taper in the far field or more accurate case, which will give a more accurate picture of sidelobe structure than the sharp cut-off produced by the ray optics technique.

Figs. 3.14 and 3.15 give the phase and gain patterns for the circularly symmetric modes for the focussed case, together with a geometric optics approximation, and for a representative value of sub-reflector displacement. The large amplitude fluctuations near boresight for both phase and gain are caused by interference phenomena between current zones on the sub-reflector.

(c) Compensatory Displacements of Primary Feed and Sub-reflector

From the geometry of the cassegrain system (fig.

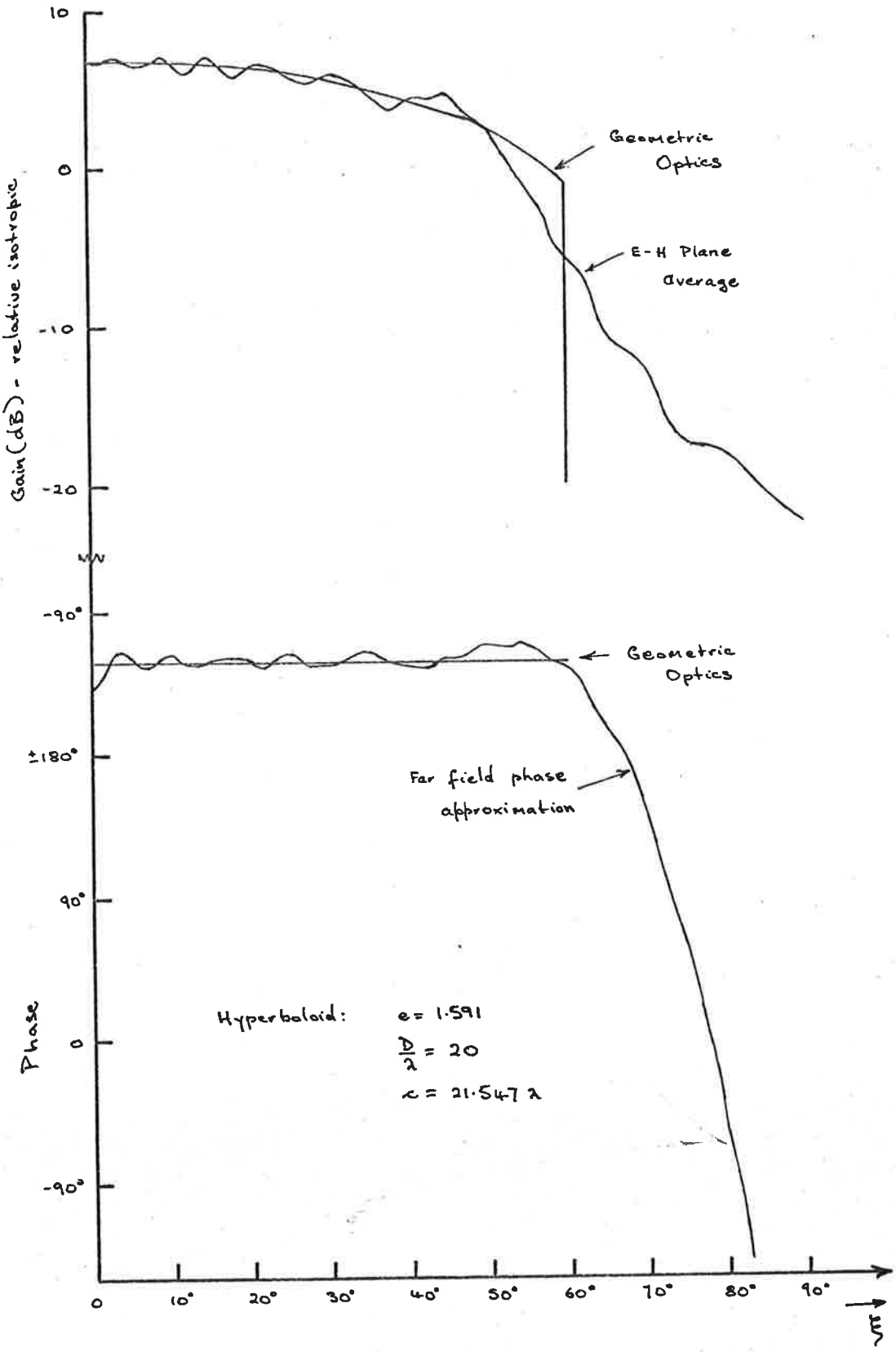

Fig. 3.13 Comparison of Average Radiation Pattern of Hyperboloid with Ray Optics Approximation.

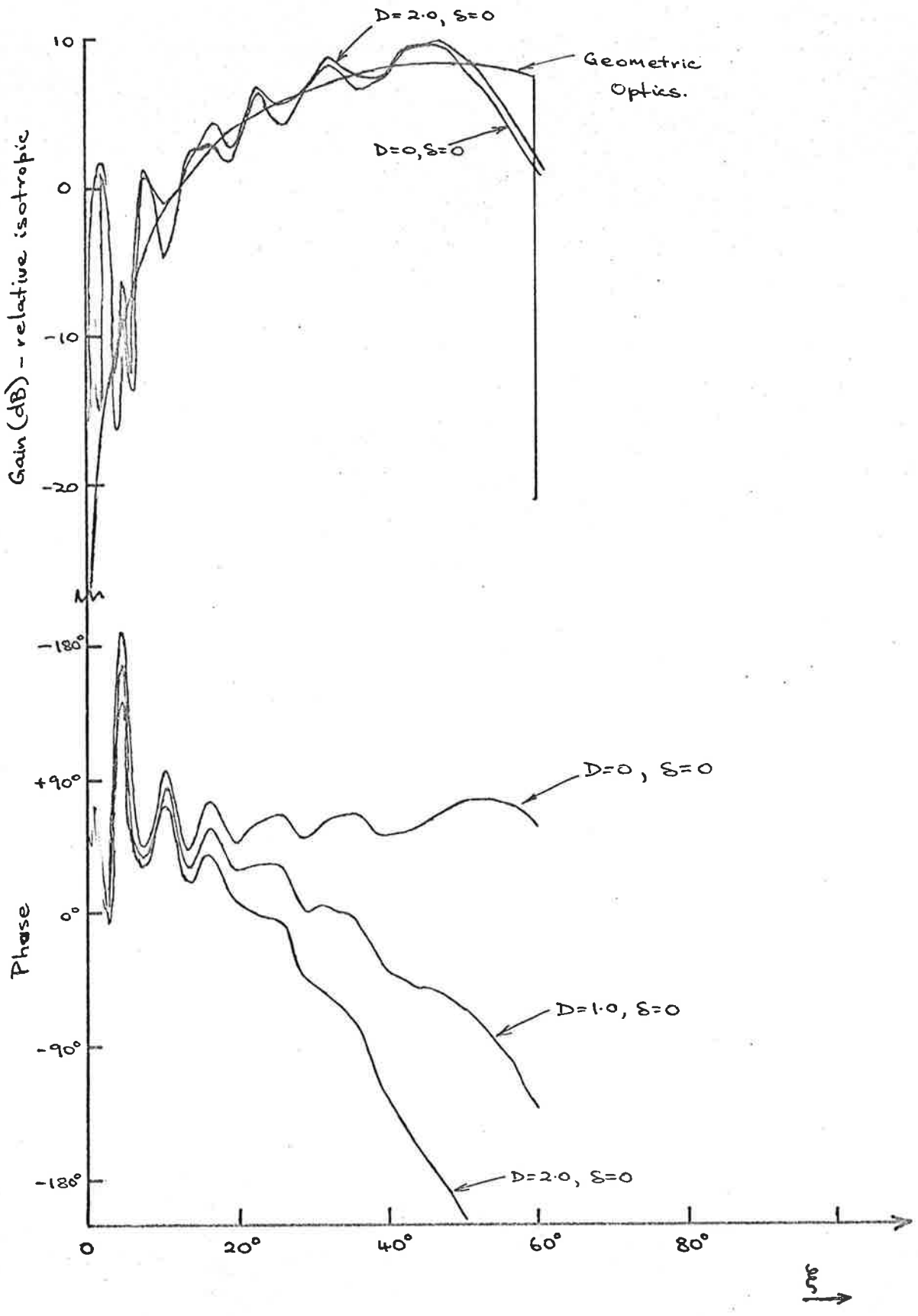

Fig. 3.14 Hyperboloid Diffraction of TM_{01} Waveguide Radiation.

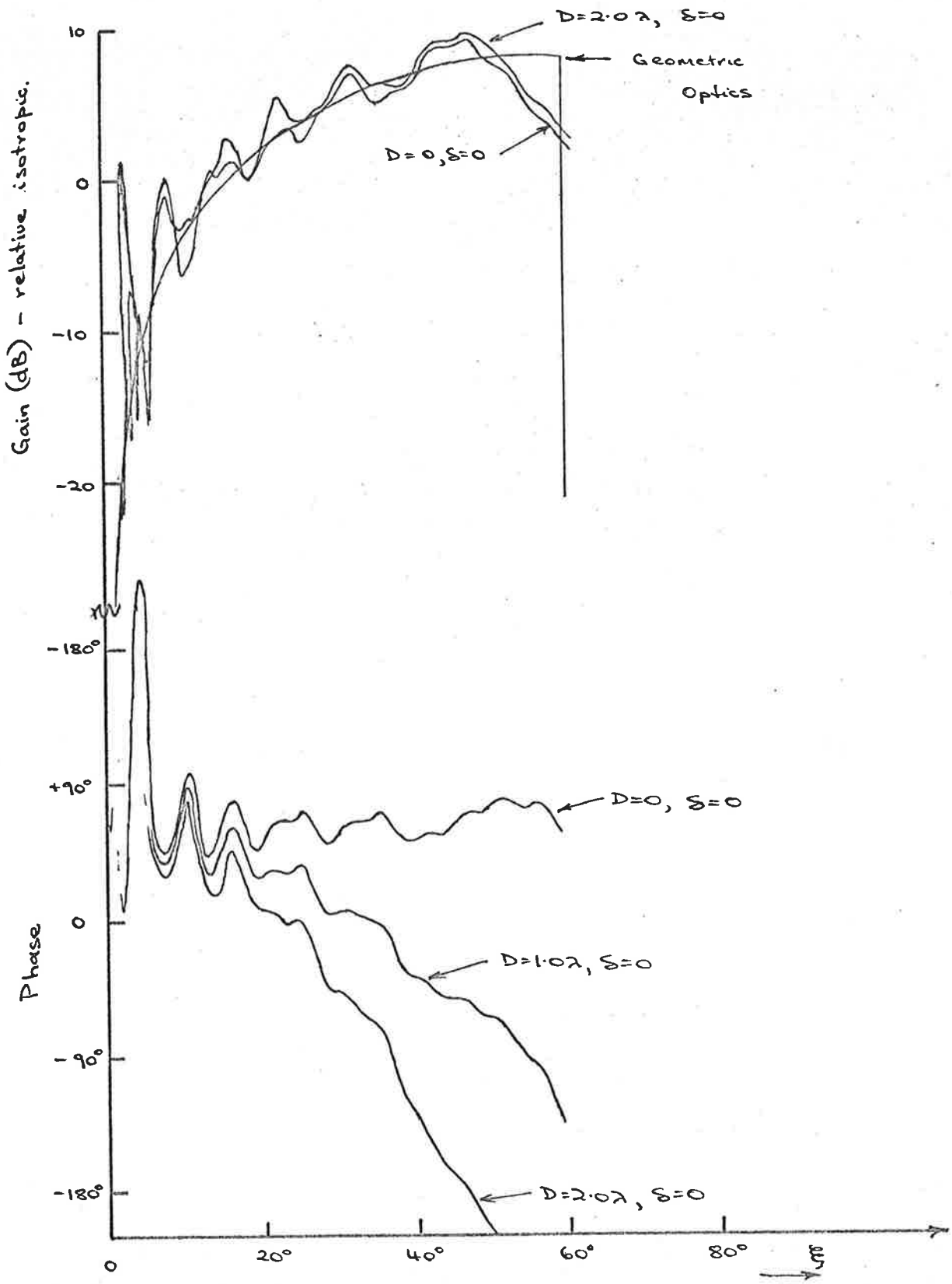

Fig. 3.15 Hyperboloid Diffraction of TE_{01} Waveguide Radiation.

3.9) it can be seen that large displacements of the feed toward the sub-reflector will produce a narrowing of the diffraction pattern from the hyperboloid. This in turn will produce a broadening of the main reflector radiation.

From geometric optics, for the standard system chosen in which e = 1.591, $\alpha = 15^{\circ}$ and sub-reflector diameter = 20 , a shift of feed ten wavelengths toward the sub-reflector will cause a reduction of 20% in the aperture measured to the edge ray (i.e. leaves primary feed at 15°) with a phase taper of $\lambda/4$ to this point, which would indicate a beamwidth increase of about the same amount (20%).

Figs. 3.11, 3.14 and 3.15 show that suitable movement of the sub-reflector could compensate for the phase taper across the aperture caused by the feed displacement, allowing the secondary radiation to maintain a characteristic with well-defined lobes and minima, which is necessary for constant phase differences between the modes.

Fig. 3.16 gives some examples of the sub-reflector radiation for compensatory displacements. Owing to the large feed displacements necessary to achieve only moderate increases in beamwidth, this technique has little practical use.

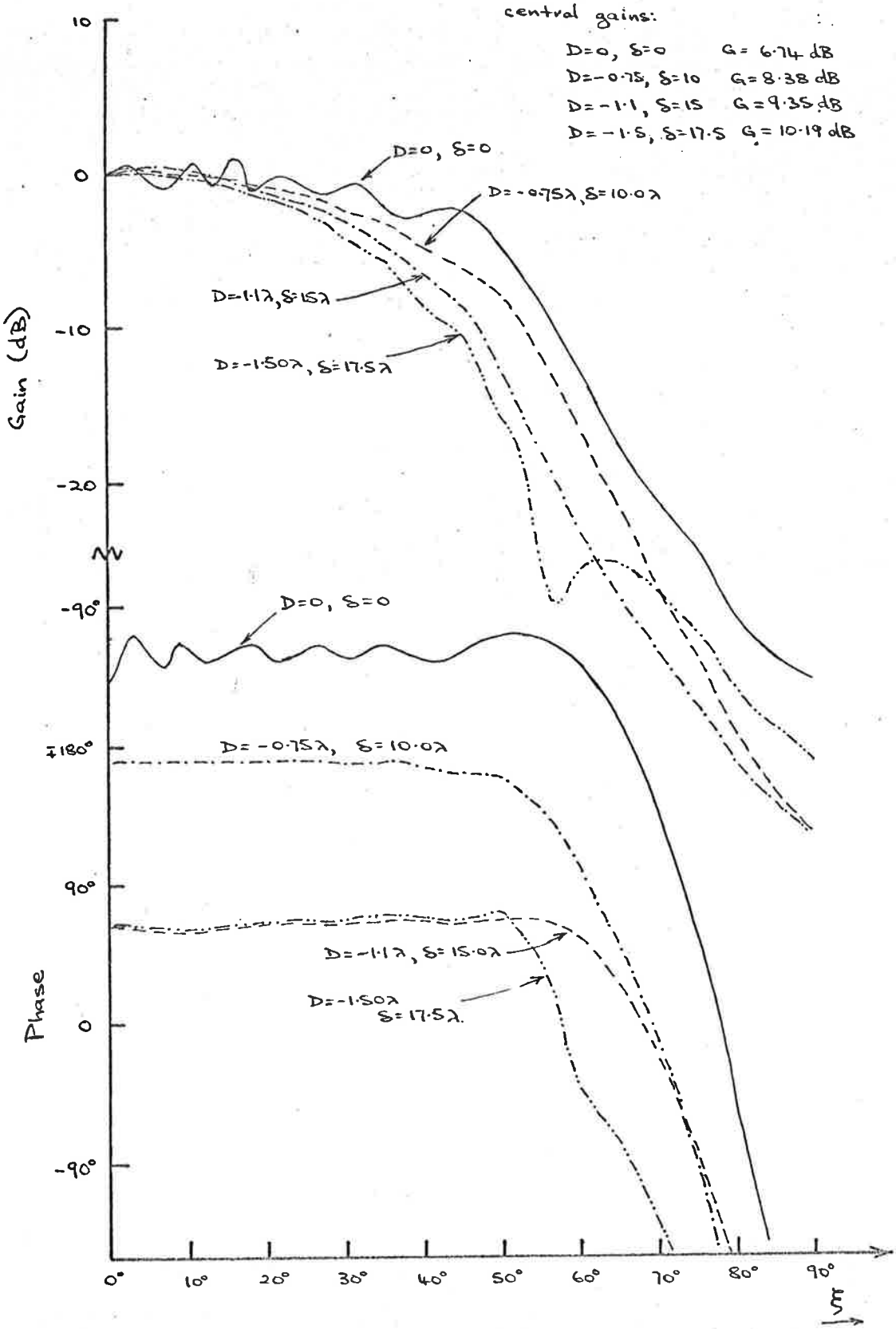

Fig. 3.16 Phase compensating defocussing of hyperboloid.

3.3.3 Radiation from Cassegrain System Defocussed by Sub-reflector Movement

From the discussion in the previous section, the only technique of interest for beam broadening in cassegrain antennae is the axial displacement of the hyperboloidal sub-reflector. For convenience and to reduce computation time the illumination function for the paraboloidal reflector is taken to be circularly symmetric and given by the average of the E- and H-plane distributions calculated from the hyperboloid diffraction formulae. In the case of the circularly symmetric waveguide mode feeds, the diffraction patterns are truly symmetric and this involves no error. However, in the linearly polarized radiation case, the diffraction pattern is ideally not symmetric, but the orthogonal patterns are sufficiently similar, within 0.5 dB in amplitude and a few degrees in phase for all examples given, that the error introduced is negligible for a practical comparison of patterns.

Figs. 3.17, 3.18 and 3.19 give radiation patterns for a linearly polarized primary feed with a 10 dB amplitude taper and for the circularly symmetric waveguide feeds, calculated from equations 3.48 and 3.51-54. The beamwidths for the reference mode are tabulated in fig. 3.20. The nature of the radiation patterns

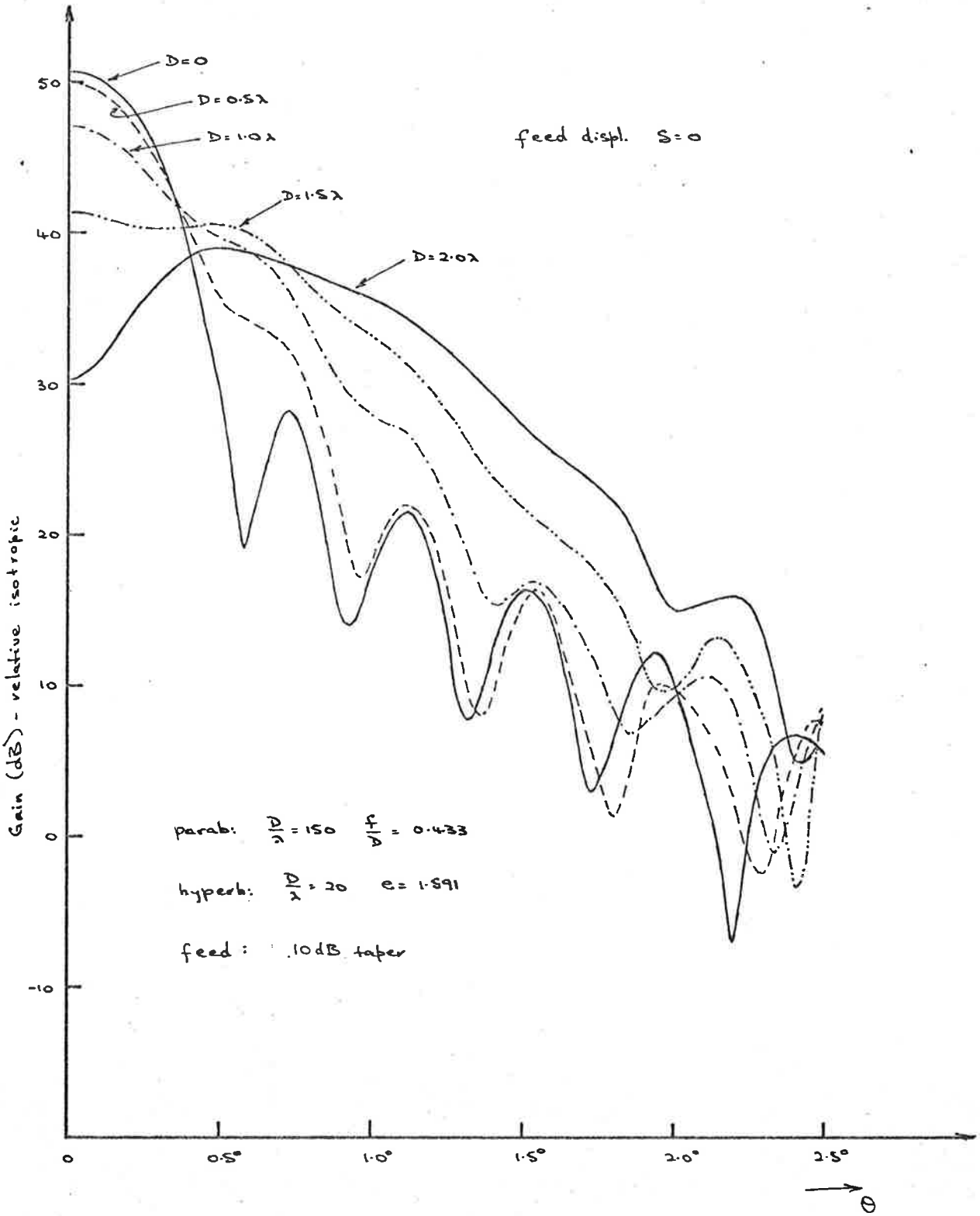

Fig. 3.17 Linearly Polarized Radiation from Defocussed Cassegrain Antenna

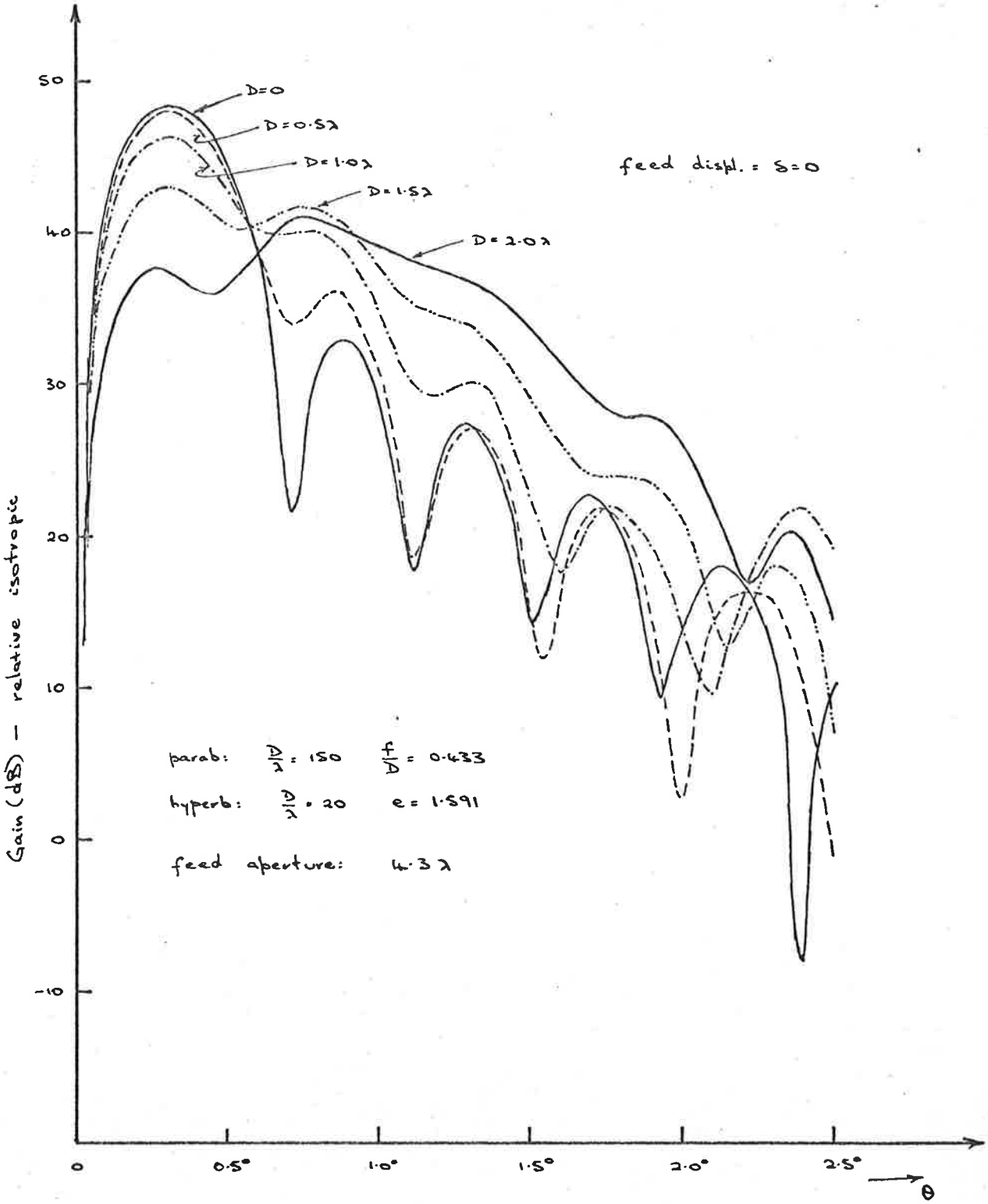

Fig. 3.18 TM01 Radiation from Defocussed Cassegrain Antenna.

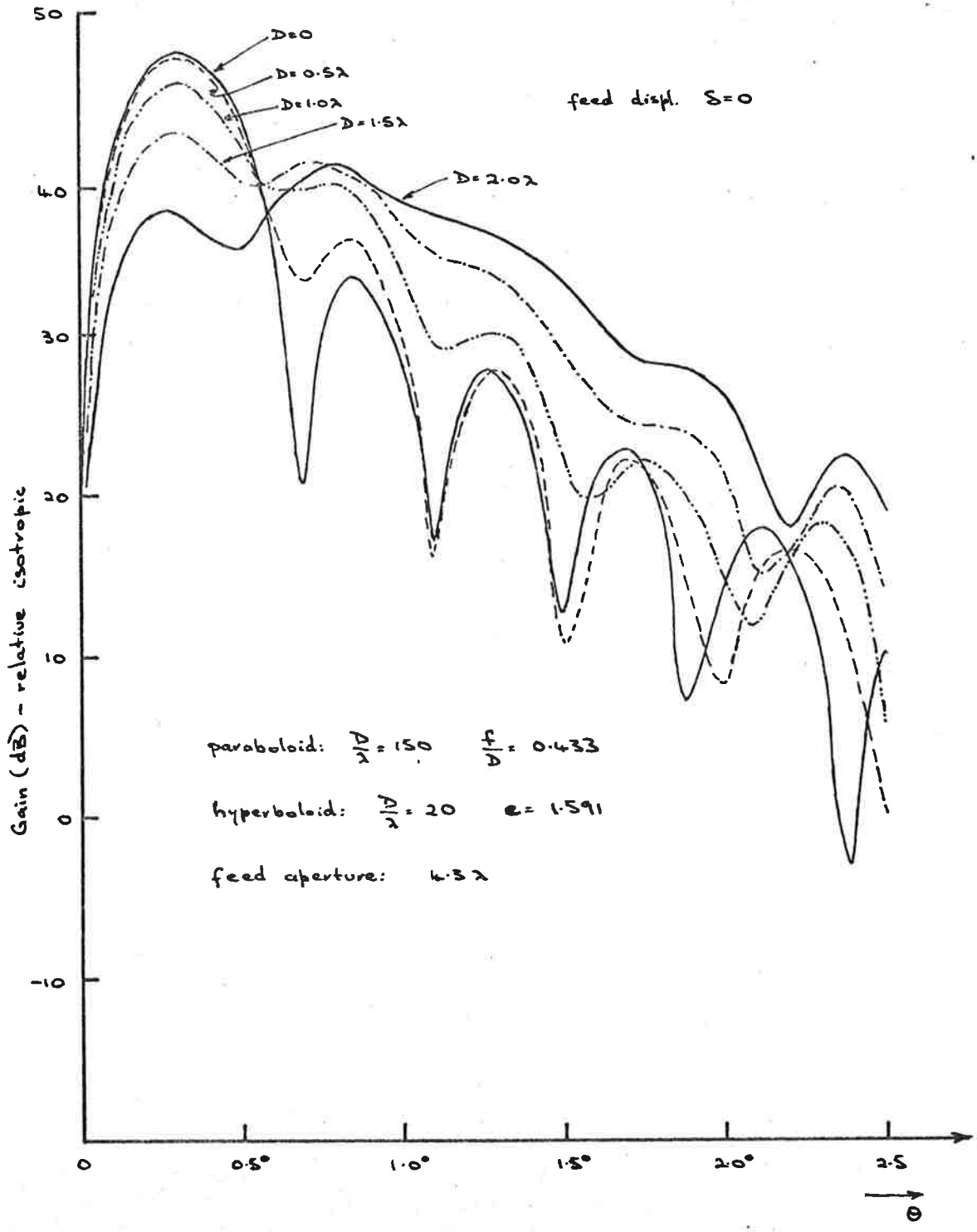

Fig. 3.19 TE_{01} Radiation from Defocussed Cassegrain System

$D =$	0λ	0.5λ	1.0λ	1.5λ	2.0λ
θ_{3dB}	0.46°	0.43°	0.50°	1.42°	——
θ_{10dB}	0.75°	0.82°	1.38°	2.25°	2.84°
θ_{20dB}	0.97°	1.58°	2.16°	3.08°	3.78°

Main reflector $\frac{D}{\lambda} = 150$ $\frac{f}{D} = 0.433$

Sub-reflector $\frac{D}{\lambda} = 20$ $e = 1.591$

Fig. 3.20 Beamwidths for Cassegrain Antenna Defocussed by Subreflector Displacement.

obtained is seen to be very similar to those found in the single reflector case (figs. 3.3, 3.4 and 3.5) at least with regard to the amplitude characteristics and beamwidths. This suggests that a similar degree of beam broadening may be obtained from the cassegrain system.

As in the previous case, the properties of the radiation patterns of interest are the similarity between the amplitude functions for the two difference modes, the phase differences between the modes for a given displacement, and how this phase difference varies with displacement. The differences in amplitude for the circularly symmetric modes are slightly greater than before. Taking the 20 dB beamwidth of the reference mode as maximum working angle, the maximum difference between the TM_{01} and TE_{01} patterns is 1.6 dB for all displacements up to 2.0 λ; however, the average value is much less than this, being approximately 0.5 dB. In most practical systems this is an allowable tolerance.

The range of variation of phase difference with the elevation angle, θ, is tabulated against sub-reflector displacement in fig. 3.21. The maximum usable sub-reflector displacement, with phase compensation with elevation angle, is seen to lie somewhere between 1.5λ and 2.0λ. The phase compensation curves for the

$D(\lambda)$ =	0	0.5	1.0	1.5	2.0
$TM_{01} - TE_{01}$	1°	15°	14°	14°	18°
TM_{01} - Ref.	3.2°	68°	47°	40°	97°

Main reflector $\frac{D}{\lambda} = 150$ $\frac{f}{D} = 0.433$

Sub reflector $\frac{D}{\lambda} = 20$ $e = 1.591$

Fig. 3.21 Phase difference ranges for elevation angle θ within θ_{20dB}

defocussed system are given in fig. 3.22. Once again, in practice the differences in phase between the two difference modes may be ignored.

As before, a displacement of 1.5λ gives a three times increase in beamwidth, resulting in a search element increase of nine times. This will allow the acquisition time to be reduced by approximately one order. As mentioned previously, this may not be large enough to warrant the expense of a special defocussing system to improve acquisition time, but where feed control is desired to maintain optimum efficiency in normal operation, it may be provided with little extra capital outlay.

For comparison purposes fig. 3.23 is included, showing the radiation patterns for the three modes with the sub-reflector moved 1.5λ away from the paraboloid and the feed moved toward the sub-reflector 17.5λ to produce an essentially constant phase in the aperture. As can be predicted from the feed functions given in the previous section, this results in an increase in beamwidth of about 25% whilst maintaining a definite sidelobe structure for the linearly polarized and TM_{01} type feeds. The same effect is not evident in the TE_{01} case, since by moving the feed closer to the sub-reflector, the angle subtended at the feed is increased and, together with the nature of the primary feed (fig.2.7), this results in

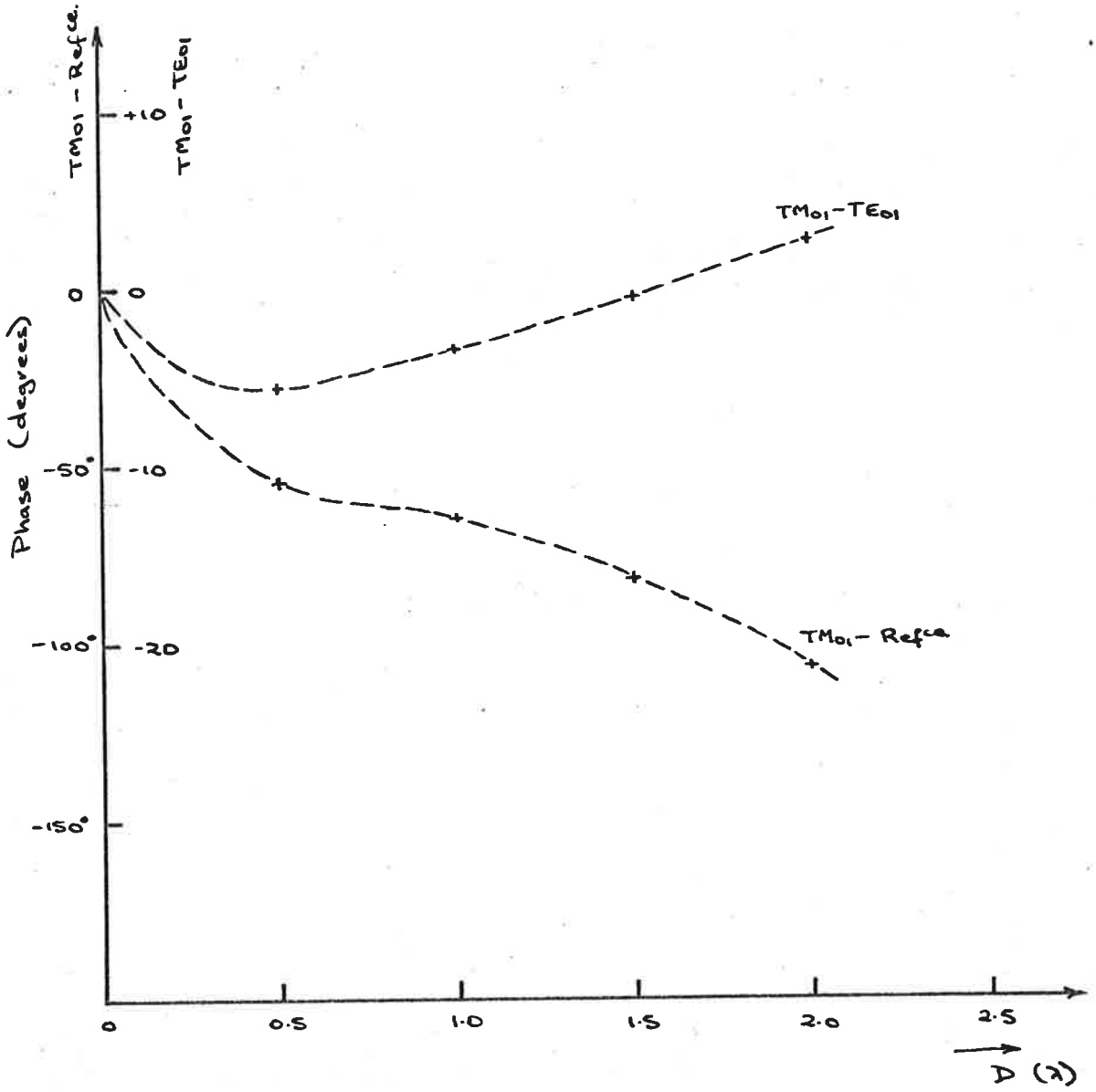

Fig. 3.22 Phase Compensation Curves for Defocussed Cassegrain Antenna

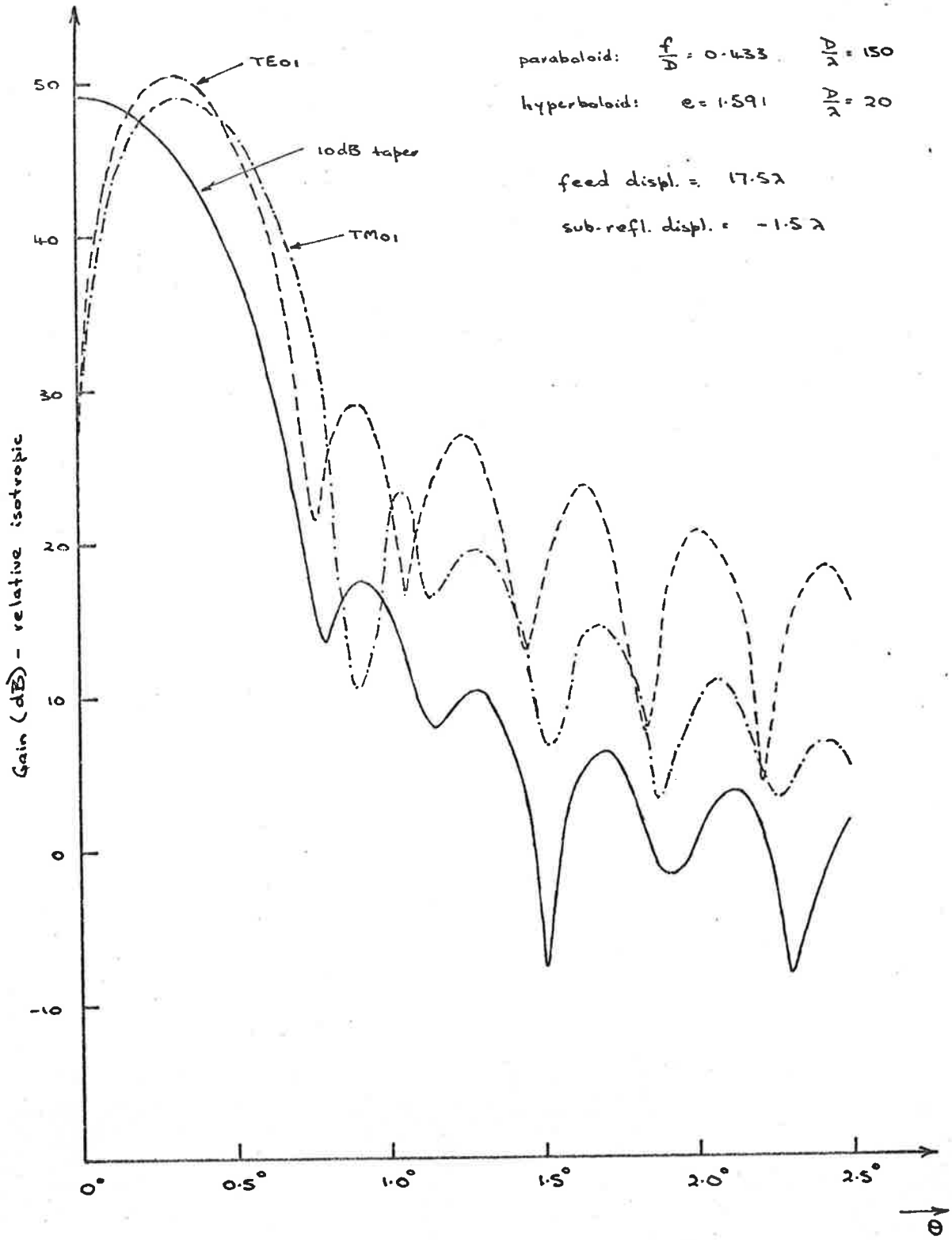

Fig. 3.23 Phase Compensating Defocussing of Cassegrain Antenna.

more efficient usage of the primary energy and a higher gain, with much the same beamwidth. Ignoring this effect, however, the gains in beamwidth achieved by such large displacements are too small to make the technique practicable, even though the relative phases between all three modes remain essentially independent of the elevation angle, θ .

3.4 Sub-reflector Modification in Cassegrain System

In the above discussion, only the defocussing effects of shifts in the primary feed and sub-reflector were considered. It is obvious from ray optics that very large defocussing displacements are required to achieve any significant change in the effective aperture of the complete system and that, because this change is always accompanied by large phase changes, the resulting curvature of the wavefront is a far more significant effect and causes degradation of the beam shape before significant changes in aperture usage occur. In the cassegrain dual reflector system, a change in the sub-reflector shape can achieve a significant change in aperture usage. The changes possible may be separated for convenience into two separate categories: the replacement of the existing sub-reflector by a completely new surface, and the modification of the existing surface.

As it is necessary to maintain symmetrical radiation patterns, the sub-reflector must remain a surface of revolution. In the general case, this may take any form and will produce an evenly distributed phase taper together with any amplitude effects. Because of the parabolic nature of the main reflector, retaining a plane wavefront in the main aperture requires that the sub-reflector remain a correctly placed hyperboloid (not admitting at this stage derivatives of the Gregorian telescope). Achieving reductions in the effective aperture in this way would require a hyperboloidal sub-reflector with increased eccentricity and placed nearer the primary feed. In the limiting case the sub-reflector would degenerate into flat plate placed midway between the hyperboloid foci. In this case, using the previous example of a cassegrain system, the new aperture diameter would be reduced to about $^{3}/_{8}$ the original value, based on a 15° primary feed edge ray and resulting in an approximate beamwidth increase of three times. Other shapes introducing phase tapers could extend this change, but add the problem of maintaining reasonable phase shifts between modes. In practice, this scheme is only suitable for situations where an increased beamwidth and reduced gain is required for a particular job and the sub-reflector can be manually changed. When beam broadening

is only required during the search mode of a tracking antenna, an automatic device for changing the sub-reflector is required and is practically impossible to implement, especially when it is realized that on large antennae the sub-reflector may be some 15-20 ft. in diameter.

The most obvious modification to an existing sub-reflector, which produces an increase in beamwidth of the overall system, is the complete removal of an outer annular section of the sub-reflector so that only a small centre portion of the main reflector is illuminated. A similar approach, electrically, is to cover the outer annulas by some flange which causes the contributions from this section to have rapidly varying phases and produce little contribution to the secondary pattern. Either of these techniques, however, would be difficult to achieve automatically. One of the few possibilities, which remains relatively simple mechanically, is the splitting of the sub-reflector into independently movable inner and outer sections. In this way a step change in the phase in the main aperture could be achieved. Ideally, this would require an inner section designed to give the required beamwidth, surrounded by a number of narrow sections producing annuli in the illumination function alternatively in and out of phase and thus

contributing nothing in the far field. This is analogous to the Fresnel zone technique of physical optics. A practical system would probably only allow two or three movable sections, which only permits moderate increases in beamwidth and produces very high sidelobe levels. Fig. 3.24 gives the example of a plane aperture, with a tapered distribution, split at $^{2}/_{3}$ radius such that the inner and outer regions are anti-phase. It can be seen that the 10 dB beamwidth increases only two times and the sidelobe level increases from -27.5 dB to -11.5 dB. This technique is not very amenable to the difference mode patterns where there are relatively high illumination levels at the split and in the outer region (fig. 3.24).

Overall, the modification of the sub-reflector in a cassegrain system to achieve an increase in beamwidth suitable for tracking purposes is not a very attractive proposition, especially when such changes must be achieved automatically.

3.5 Conclusion

The investigation into the defocussing of reflector antenna systems has shown that the simple focally excited antenna and the dual reflector cassegrain system can be considered almost equivalent, if movements of the primary feed in the former are treated as equiv-

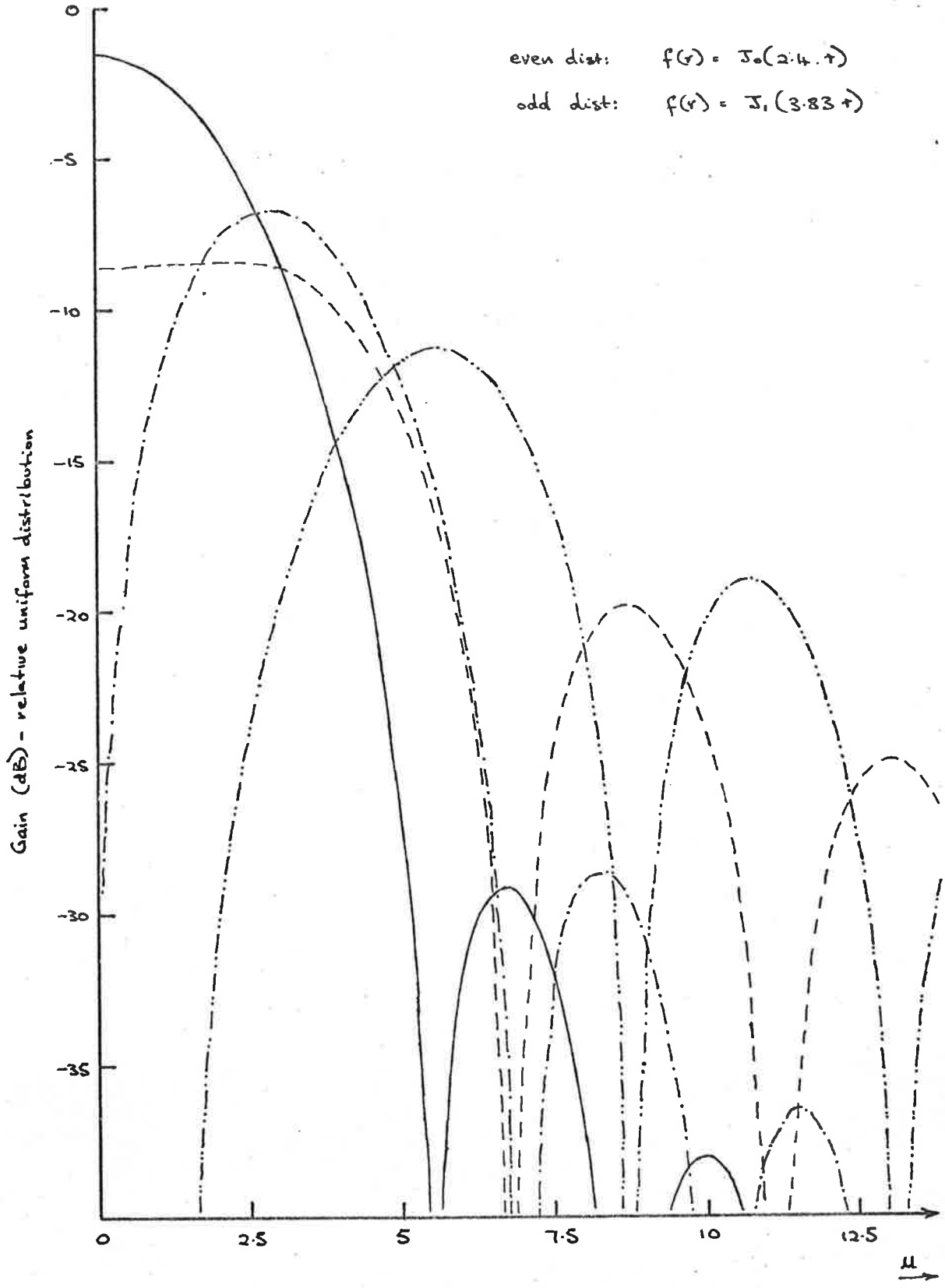

Fig. 3.24 Effect of Step Change of π rads. in Aperture Distribution at r = 0.66.

alent to sub-reflector movements in the latter. The range of increase in beamwidths by these techniques is up to three times whilst maintaining adequate phase tolerances for use with a multimode tracking system and servodrive control. Increases of this order allow reduction in acquisition time of about one order. The significance of this reduction will depend largely on the application and the capital cost of the defocussing equipment. One advantage of the defocussing technique proposed is that it can be treated as an extension of any servo controlled feed system designed to make use of the best-fit reflector surface under various loading conditions.

CHAPTER IV

TRACKING MODES AND HIGH EFFICIENCY FEEDS

4.1 Development of High Efficiency Feeds for Reflector Antennae

It was established in Chapter I that high efficiency feed research for large circular aperture reflector antennae has centred upon circular waveguide systems. This is due to the inherent circular symmetry of circular waveguide, which makes it suitable for use with circularly polarized systems, and due also to the more symmetrical radiation pattern compared with that produced by the alternative square waveguide.

The first step toward high efficiency feeds is the production of a feed horn with a symmetric radiation pattern, i.e. equal beamwidths in all planes. The second is to institute some means of beam shaping to produce the desired illumination function in the aperture, which controls aperture efficiency and sidelobe structure.

Research in the former case has developed from two main directions. The first has been the empirical modification of the physical aperture conditions of the radiator. The modifications have taken several forms. The provisions of radial metal pins or posts[31,46]

both within and without the waveguide, at the radiating aperture improves the symmetry of the dominant mode radiation from circular waveguide by reducing the effective aperture in the E-plane, where the conducting fins are parallel to the electric field vector, whilst having little effect on the H-plane conditions, for which the electric field is normal to the fins. The other main modification used is to provide a circular metallic flange or ground plane around the aperture and to place on this a series of concentric annular chokes.[30,32] The chokes are designed to trap near field energy on the ground plane surrounding the radiating aperture and re-radiate it with the correct phase and amplitude so that the feed aperture distribution approximates the $J_1(x)/x$ form and gives a radiation pattern with low sidelobe energy. In both cases, the modifications to the waveguide aperture structure have effectively produced anisotropic boundary conditions at the aperture.

The other approach to obtaining symmetric waveguide feed horns is the modification of the waveguide field reaching the aperture to produce a more desirable aperture distribution. This technique involves the mixing of transverse electric and transverse magnetic mode pairs in circular waveguide.[11,47,48,49] The first order solution consists of a combination of the

dominant TE_{11} mode with the TM_{11} mode to produce an essentially symmetric beam with the normal angular taper. This method has been extended[50] by the addition of higher modes as well as the basic TE_{11} and TM_{11} modes to allow beam shaping and consequent control of the aperture distribution. The higher order modes used are the TE_{1n} - TM_{1n} combinations. The difficulty with this technique is the excitation and control of the many modes present so as to give the right amplitude and phase relations at the aperture.

These two approaches to the problem of improving feed radiation properties have been placed on a theoretical basis by the consideration of the focal plane fields of large paraboloidal reflectors with an incident plane wave. Koch[51] has produced a structure of concentric chokes surrounding the waveguide aperture, essentially the same as Geyer's.[30] More notable is the approach of Minnet and Thomas,[29] who have developed waveguide feeds based on guides with anisotropic boundaries. The boundaries of the waveguide are made to approximate an infinite ratio of circumferential to longitudinal conductance by circumferential slots, approximately a quarter wavelength deep. Whereas these slots act as quarter wave chokes to longitudinal electric field components, the tangential components are shorted by the metal

surface between the slots. These waveguides are conveniently described as corrugated. Waveguides of this form propagate hybrid modes, neither transverse electric nor transverse magnetic, which exactly match the focal plane field of the reflector. This technique is conveniently compared with the mixed mode technique of Potter[11] described above, except that each TE - TM pair is now replaced by a single hybrid mode, thus reducing the number of modes to be controlled to half. It is also reported by Minnet and Thomas that to avoid an abrupt change in boundary conditions at the aperture, caused by the radial face of the last slot, an anistropic flange must also be provided around the aperture. This technique would then seem to combine both the empirical approaches mentioned above.

As the provision of any surface other than a pure conductor in a waveguide causes cross-coupling between the transverse electric and transverse magnetic modes, the author has investigated the hybrid modes associated with thin linings, particularly dielectrics, in normal waveguide. The formulae and pertinent results of this work are given in Appendix IV. It is necessary that the waveguide lining be thin because it is only possible to satisfy the conditions for a symmetric radiation pattern in the inner region and so contributions to the

radiated field from the field within the lining must be negligible, and also because a practical dielectric has loss and any loss associated with a waveguide lining would add to the system noise temperature. The assessment of the usefulness of such a lining would involve a comparison of the improvement in noise figure by the modified illumination functions with the degradation caused by a lining in the short length of guide near the aperture. The investigation shows that it is possible in theory to produce a mode in the inner (air filled) region, with symmetric radiation properties, by using a uniaxially anisotropic dielectric. To produce this with a thin lining requires that the dielectric either have a low dielectric constant and a high anisotropy (i.e. ratio of longitudinal to circumferential dielectric constant) or have a high circumferential dielectric constant and low anisotropy. In either case the practical provision of such a lining within a waveguide is very difficult.

4.2 Tracking Modes in High Efficiency Feed Systems

The effect of methods to improve the radiation pattern of the dominant mode in circular waveguide upon the circularly symmetric modes can be discussed by considering three types of feed: those with radial

posts or fins at the aperture, those with anisotropic flanges and, finally, corrugated waveguide feeds. The form of feed using mixed modes in normal waveguide need not be considered since the radiation characteristics of the circular modes are unchanged by the addition of extra modes, assuming no interaction between the modes is present.

The criterion for judging the effect of efficiency improving techniques on the tracking modes is the degree of improvement in radiation pattern equality between the two difference modes, if any.

4.2.1 Fin or Post Loaded Waveguides

The assessment of the effect of broadly spaced posts or fins, either inside or outside the waveguide, at the aperture of a feed horn is difficult to determine accurately because the overall effect is a complex function of their spacing and size. A qualitative idea of the effects can be obtained by considering the waveguide electric field intensity in the aperture.

For the TE_{01} or circularly symmetric electric mode, the electric field intensity in the waveguide is purely transverse and only a tangential component exists (see fig. 2.2(c)). The electric field is always

normal to any radial object and the electric field distribution should be unaffected. So the radiation pattern of the TE_{01} mode in waveguide, loaded by radial fins or posts at the aperture, should be the same as for normal waveguide.

If the radial fins are internal and their depth and spacing are such that they appear as a series of quarter wave slots around the boundary, the waveguide can be treated as one with a diameter measured to the inner ends of the fins and with an anisotropic boundary with infinite circumferential and zero longitudinal impedance. The resulting field distributions for the TE_{01} mode in this waveguide would then be identical with the TM_{01} in plain waveguide of the same size. This feature is discussed further under corrugated waveguides.

The TM_{01} mode may be considered an orthogonal mode to the TE_{01} mode and has only a radial component of electric field in the transverse plane (see fig. 2.2(b)). However, being a transverse mangetic mode, a longitudinal component of electric field also exists. Any radial conducting objects will tend to short out the components of the electric field existing normally in the outer region of the waveguide and so the effect

is a compression of the mode into the inner area of the waveguide. This reduces the effective radiating aperture for this mode and tends to equate the beam-widths for the difference modes, which is a desirable feature. In the limiting case where the fins approximate an anisotropic surface, since the TM_{01} mode has only longitudinal surface currents on the waveguide walls, the fields will be the same as in ordinary waveguide of the reduced diameter and they will have identical distributions to the TE_{01} mode, resulting in the same radiation patterns.

4.2.2 Anisotropic Aperture Planes on Waveguide Radiators

The provision of a flange in the aperture plane of a waveguide radiator, consisting of a series of concentric quarter wave slots or chokes, can be assumed, to a first order of approximation, to appear as a short circuit to tangential electric field components due to the metallic walls separating the slots, and as an open circuit to radial components. For a first order answer, the TE_{01} mode in such a system can be treated as radiating from an aperture in an infinite, conducting ground plane whilst the TM_{01} mode can be assumed to be unaffected.

Using the equivalence theorem[52] radiation from

an aperture in an infinite ground plane is calculated as the radiation of equivalent magnetic currents

$$\underset{\sim}{M} = - \hat{\underset{\sim}{n}} \times \underset{\sim}{E}$$

adjacent to an infinite ground plane. The form of the radiation pattern for the TE_{01} is found by substituting E_θ from equation (2.6) into the radiation integral given in Appendix I and assuming the radiation contribution from H_ρ to be zero. Hence

$$E_\phi = j.ka\omega\mu. \frac{e^{-jkR}}{R}.\cos\theta \; \frac{J_o(\kappa_{01}a)\, J_o'(k a \sin\theta)}{1 - \left(\frac{k \sin\theta}{\kappa_{01}}\right)^2} \qquad (4.1)$$

This expression is identical to equation (2.8), giving normal TE_{01} radiation, except for the factor $\frac{1}{2}\left(\frac{\beta_{01}}{k} + \cos\theta\right)$ which is replaced by $\cos\theta$. For small waveguides, the ratio of phase constants β_{01}/k is small and the radiation pattern is not significantly changed, except that a true null occurs at $\theta = 90^\circ$. In large waveguides, β_{01}/k approaches unity and the difference is greater. However, as the aperture size increases the beamwidth decreases and the range of angles of interest also decreases and so over the main beam the term $\cos\theta$ remains essentially constant, and the two patterns are similar. Overall the effect in any wave-

guide produces a slight narrowing of the main beam and a faster drop-off of gain at wide angles. Figs. 4.1 and 4.2 give examples of the normal TE_{01} and TM_{01} radiation patterns together with the TE_{01} mode when used with a ground plane. These curves indicate only a slight improvement in the equality of the difference mode beam-widths.

It should be noted that equation (4.1) indicates equal radiation in the forward and backward directions. As this back radiation must exist as reflected energy returning along the waveguide, the addition of an aperture plane may result in a poor match at the aperture. This is true in the case of a small diameter radiator, but for large apertures the approximation is not good and must be taken as an indication only.

4.2.3 Corrugated Waveguide

Corrugated waveguide can be produced with either longitudinal or circumferential slots in the guide boundary. Provided the depth of the slots approaches a quarter wavelength and the slot pitch is small compared with a wavelength, the corrugated surface can be approximated by a continuous anisotropic surface with zero impedance parallel to the slots and a very high impedance normal to the slots. In practice longitudinal slots are

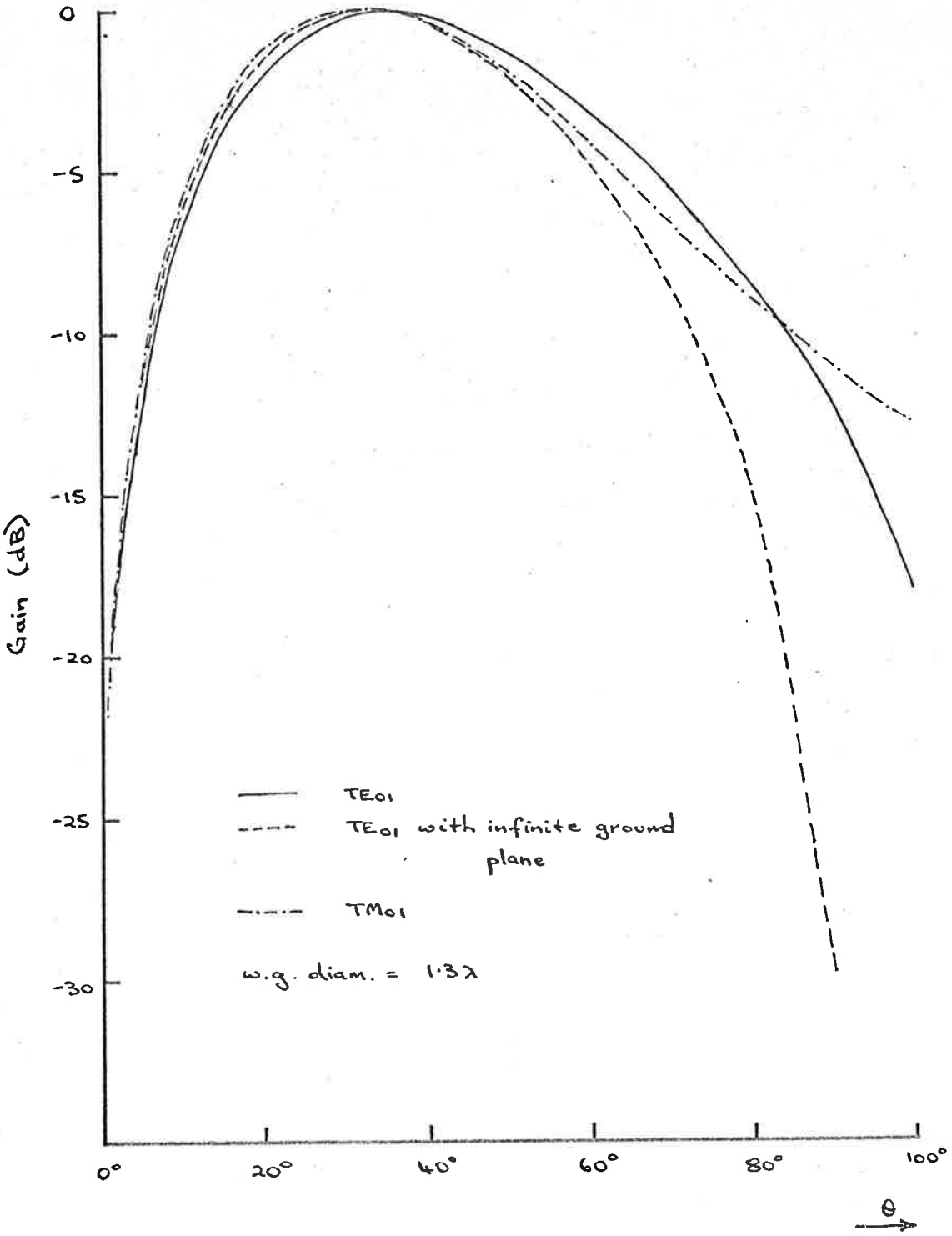

Fig. 4.1 Effect of ground plane on TE_{01} radiation.

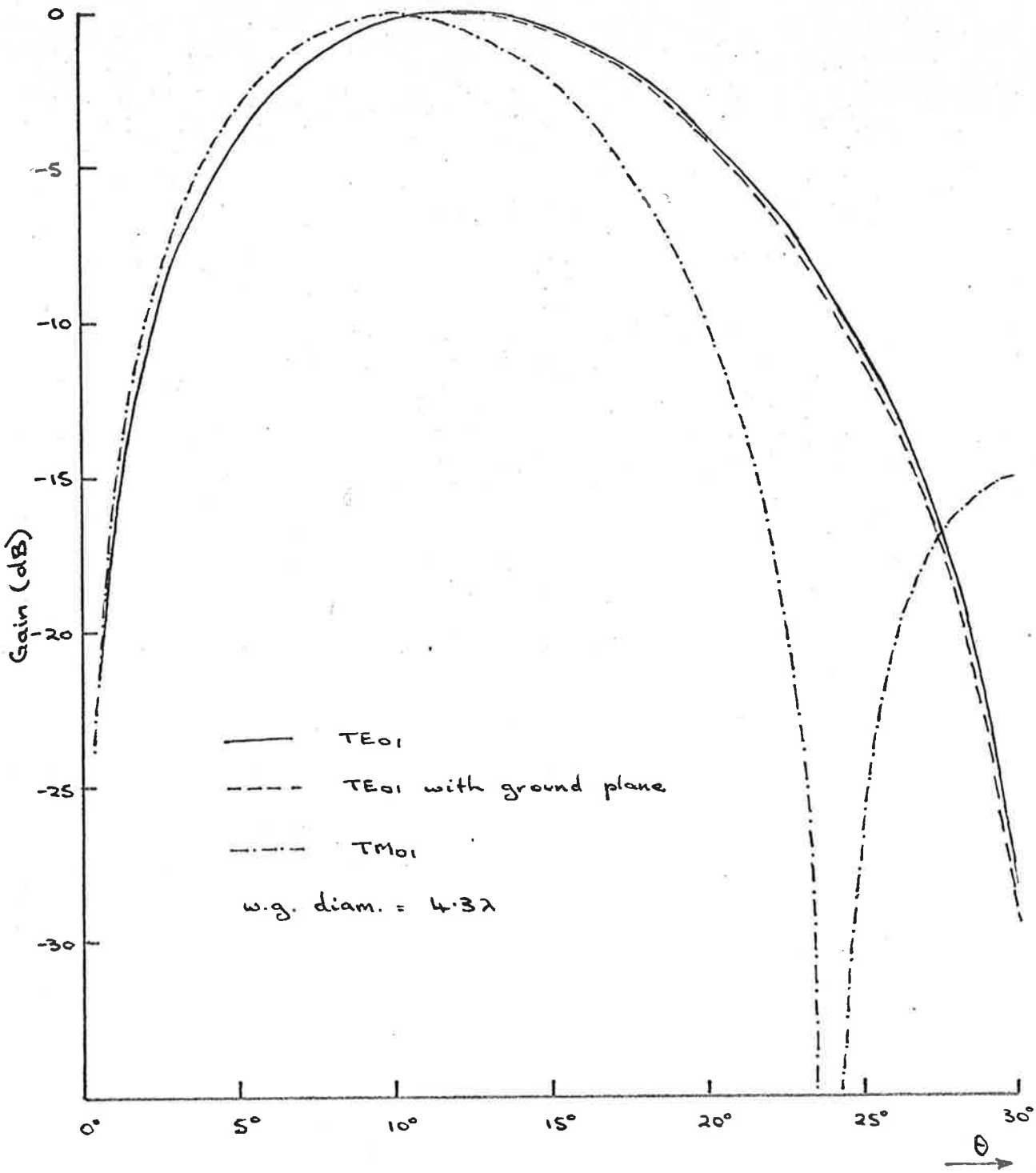

Fig. 4.2 Effect of ground plane on TE_{01} radiation.

not attractive for they have zero longitudinal impedance on the boundary which does not interrupt the surface current structure of any normal transverse magnetic modes and allows these modes to propagate freely.[29] However, circumferential slots, with an infinite longitudinal impedance, allow neither the normal transverse electric nor magnetic modes of greater than zero order to propagate, so simplifying the problem of mode control.

In the ideal case of corrugated waveguide with resonant circumferential slots, the boundary conditions at the walls of the waveguide require that

$$E_\theta = H_\theta = 0, \qquad (4.2)$$

since the surface impedances are

$$Z_\theta = 0 \quad \text{and} \quad Z_z = \infty .$$

For the TE_{01} mode which has only E_θ, H_ρ and H_z components the boundary conditions remain the same as in plain waveguide and the waveguide field components are given by equation 2.6. However, the TM_{01} mode, which has E_ρ, E_z and H_θ components, has its boundary condition changed from $E_z = 0$ to $H_\theta = 0$.

The general solution for a TM_{01} mode in cylindrical coordinates is (from equation 2.5)

$$E_z = \kappa'^2_{01}\, J_o(\kappa'_{01}\rho).\ e^{-\gamma'_{01} z}$$

$$E_\rho = -\gamma'_{01}\,\kappa'_{01}\, J'_o(\kappa'_{01}\rho).\ e^{-\gamma'_{01} z} = \frac{\gamma'_{01}}{j\omega\epsilon}.H_\theta$$

and the boundary condition requires that

$$J'_o(\kappa'_{01}\ a) = 0$$

where a = radius of waveguide. The radial variation for the TM_{01} mode is now seen to be identical with that for the TE_{01} mode.

Substituting these expressions into the radiation integral, given in Appendix I, the radiated field from the TM_{01} mode in corrugated guide becomes

$$E = \frac{jka\omega\mu}{\kappa'_{01}} \cdot \frac{e^{-jkR}}{R} \cdot \left(\frac{\epsilon}{\mu}\right)^{\frac{1}{2}} \frac{J_o(\kappa'_{01}a)\ J'_o(k\,a\sin\theta)}{1 - \left(\frac{k\sin\theta}{\kappa'_{01}}\right)^2} \qquad (4.3)$$

Comparing this expression with the equivalent for the TE_{01} mode (equation 2.8) shows that the theoretical TM_{01} radiation is now identical in form, save for a constant factor. Accordingly the two difference modes will now give identical performance in a tracking system.

The expressions for the waveguide field distribution of the dominant mode in corrugated guide can be

developed by taking a linear combination of the general first order solutions for transverse electric and magnetic modes in cylindrical coordinates and applying the boundary conditions of equation (4.2). Hence the first order hybrid mode has

$$E_z = - K_{11}^2 . Z_o . J_1(K_{11}\rho) . \cos\theta \, . e^{-j\beta_{11} z}$$

$$E_\rho = j\left[\beta_{11} K_{11} Z_o J_1'(K_{11}\rho) + \omega\mu \frac{J_1(K_{11}\rho)}{\rho} \right] . \cos\theta \, . e^{-j\beta_{11} z}$$

$$E_\theta = -j\left[\beta_{11} Z_o \frac{J_1(K_{11}\rho)}{\rho} + \omega\mu K_{11} J_1'(K_{11}\rho) \right] \sin\theta . e^{-j\beta_{11} z} \qquad (4.4)$$

$$H_z = - K_{11}^2 J_1(K_{11}\rho) . \sin\theta . e^{-j\beta_{11} z}$$

$$H_\rho = j\left[\omega\varepsilon . Z_o . \frac{J_1(K_{11}\rho)}{\rho} + \beta_{11} K_{11} J_1'(K_{11}\rho) \right] \sin\theta . e^{-j\beta_{11} z}$$

$$H = j\left[K_{11} \omega\varepsilon . Z_o . J_1'(K_{11}\rho) + \beta_{11} \frac{J_1(K_{11}\rho)}{\rho} \right] \cos\theta . e^{-j\beta_{11} z}$$

where $Z_o = (\frac{\mu}{\varepsilon})^{\frac{1}{2}}$ and the boundary conditions require

$$J_1'(K_{11}a) + \frac{\beta_{11}}{k} . \frac{J_1(K_{11}a)}{K_{11}a} = 0 \qquad (4.5)$$

These field components satisfy a sufficient condition, namely

$$E_\rho(\rho) = Z_o\, H_\rho(\rho)$$

and $$E_\theta(\rho) = -Z_o\, H_\theta(\rho).$$

for a symmetrical radiation pattern, which can be determined as

$$\left.\begin{matrix} E_\theta \\ E_\phi \end{matrix}\right\} = \omega\mu \cdot \frac{e^{-jkR}}{R} \cdot \begin{cases} I\cos\phi \\ I\sin\phi \end{cases} \qquad (4.6)$$

where

$$I = \left[\frac{\beta_{11}}{k} + \cos\theta\right].$$

$$\frac{K_{11}a\, J_1(K_{11}a)J_1'(ka\sin\theta) - ka\sin\theta\, J_1'(K_{11}a)J_1(ka\sin\theta)}{K_{11}\, k\left[1-\left(\frac{k\sin\theta}{K_{11}}\right)^2\right]}$$

$$+\left[1+\frac{\beta_{11}}{k}\cdot\cos\theta\right]\frac{J_1(K_{11}a)\, J_1(ka\sin\theta)}{k^2\sin\theta} \qquad (4.7)$$

and the boundary condition, equation 4.5, applies.

Theoretical plots of the radiation patterns for the dominant hybrid mode and the zero order circularly symmetric modes in circumferential corrugated guide are

given in figs. 4.3 and 4.4. These may be compared with the equivalent patterns for plain waveguide in figs. 2.4 and 2.7. The hybrid mode radiation corresponds closely to the H-plane pattern of the normal TE_{11} mode. Although the difference modes now have identical radiation patterns, there is no reduction in the high edge taper for these modes, assuming a reflector edge angle corresponding to a 10-12 dB taper in the sum mode. However, when the basic sum mode radiation is modified by the addition of higher modes corresponding to additional zeros of the boundary condition, equation (4.5), a larger waveguide aperture is required to contain the additional modes and the difference modes will have a narrower radiation characteristic. The change in beamwidth for the sum mode, in this situation, is small, but the shape of the pattern is modified to give a higher reflector aperture efficiency at the expense of the waveguide aperture efficiency. The overall effect is to produce a larger effective aperture for the difference modes with the possibility of achieving the ideal two to one ratio.

In theory, it is also possible to control the shape of the difference mode patterns by the addition of higher zero order modes - TE_{0n} and TM_{0n} modes- but this involves in the simplest case the production of a further two modes to be controlled in phase and

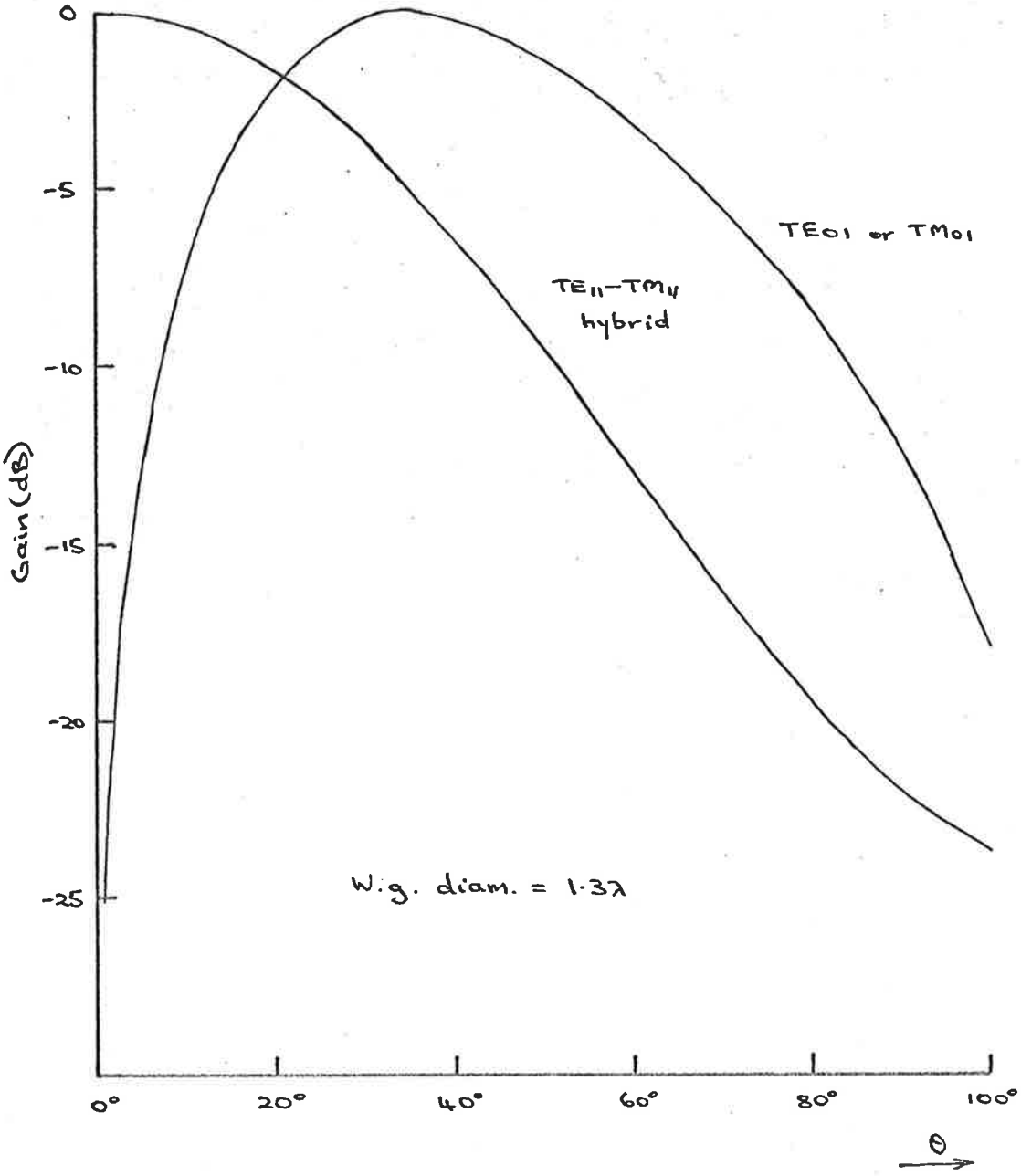

Fig. 4.3 Radiation from corrugated waveguide.

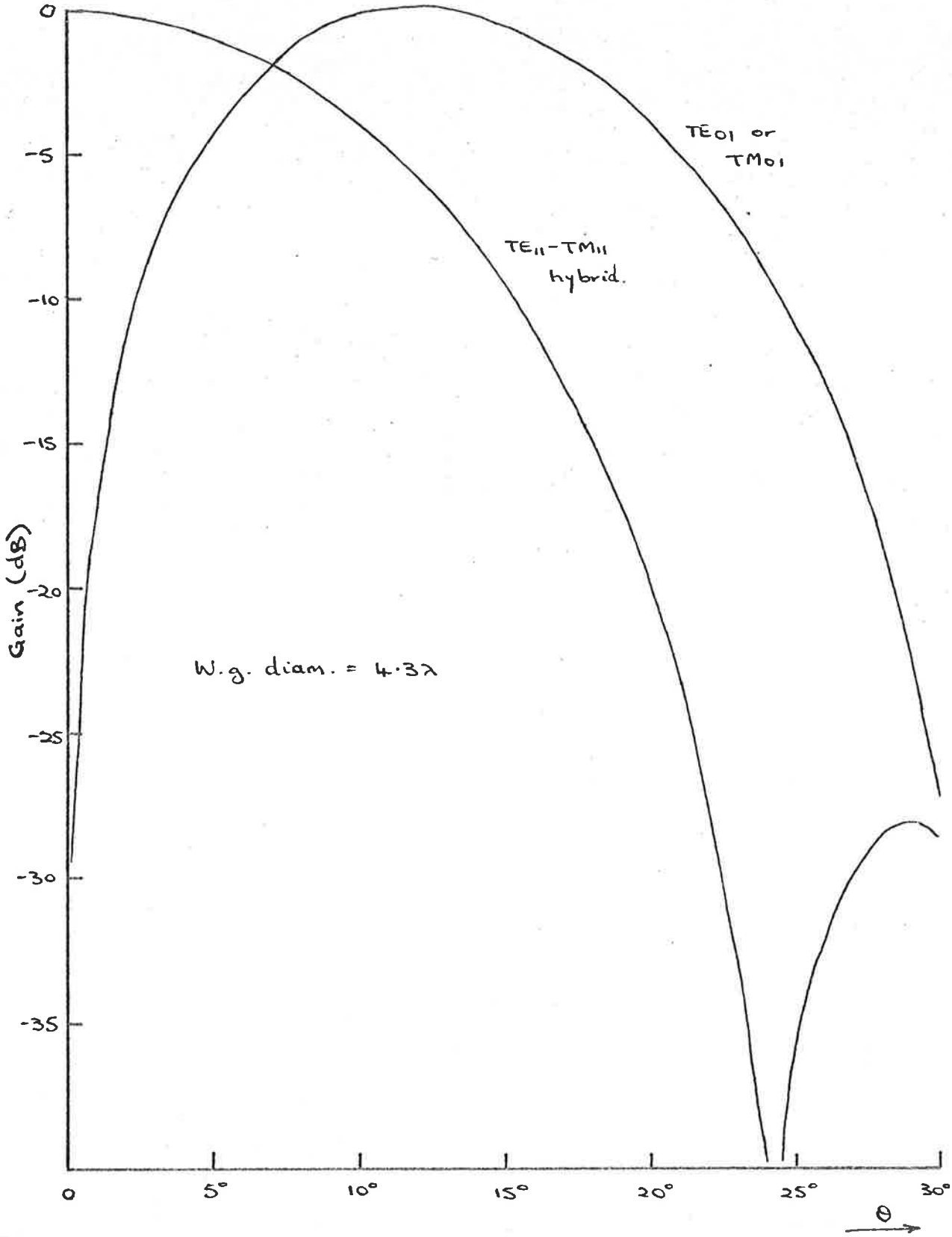

Fig. 4.4 Radiation from Corrugated Waveguide.

amplitude at the waveguide aperture. Where tracking can only be considered as a secondary role, such additional complexity is not justified.

4.2.4 Waveguides with Dielectric Linings

As can be deduced from the discussion of circularly symmetric modes in corrugated waveguide, the zero order transverse electric and magnetic modes in waveguide will have identical radial field variation within the guide and identical radiation patterns if the phase constants for the two modes can be made equal. It is shown in Appendix IV that this can be achieved by a uniaxially anisotropic dielectric lining in a waveguide, with a ratio of circumferential to longitudinal dielectric constants greater than one. This anisotropy is of the opposite form to that required for equal beamwidths from the dominant hybrid mode. Apart from the practical difficulty of manufacturing a dielectric with a specified anisotropy, this method of obtaining equal difference mode radiation patterns is undesirable in a high efficiency system because of its deleterious effect on the sum mode radiation pattern.

4.3 Experimental Results from Corrugated Waveguide

Some tests for the existence of the zero order

transverse magnetic mode, TM_{01}, and the radiation characteristics of both the TE_{01} and TM_{01} modes have been carried out with a section of corrugated waveguide, designed and manufactured at the Radio Physics Branch of the Commonwealth Industrial and Scientific Research Organization (C.S.I.R.O.). The facilities of this department were also used to carry out the tests.

The corrugated waveguide was fabricated from a series of annular aluminium rings with alternately small and large internal diameters so that, when bolted together, they formed a waveguide with circumferential slots. A sketch of the structure is given in fig. 4.5. A concentrically grooved flange used to preserve the boundary conditions in the aperture plane is shown in fig. 4.6.

Other equipment to be used was

General Radio Microwave Oscillator type 1360-A

Hewlett Packard Standing Wave Indicator

Scientific-Atlanta Series 1520 Automatic Rectangular Radiation Pattern Recorder

and assorted General Radio type 874 attenuator pads. The automatic radiation pattern recorder enables power patterns to be plotted directly, assuming linear crystal characteristics.

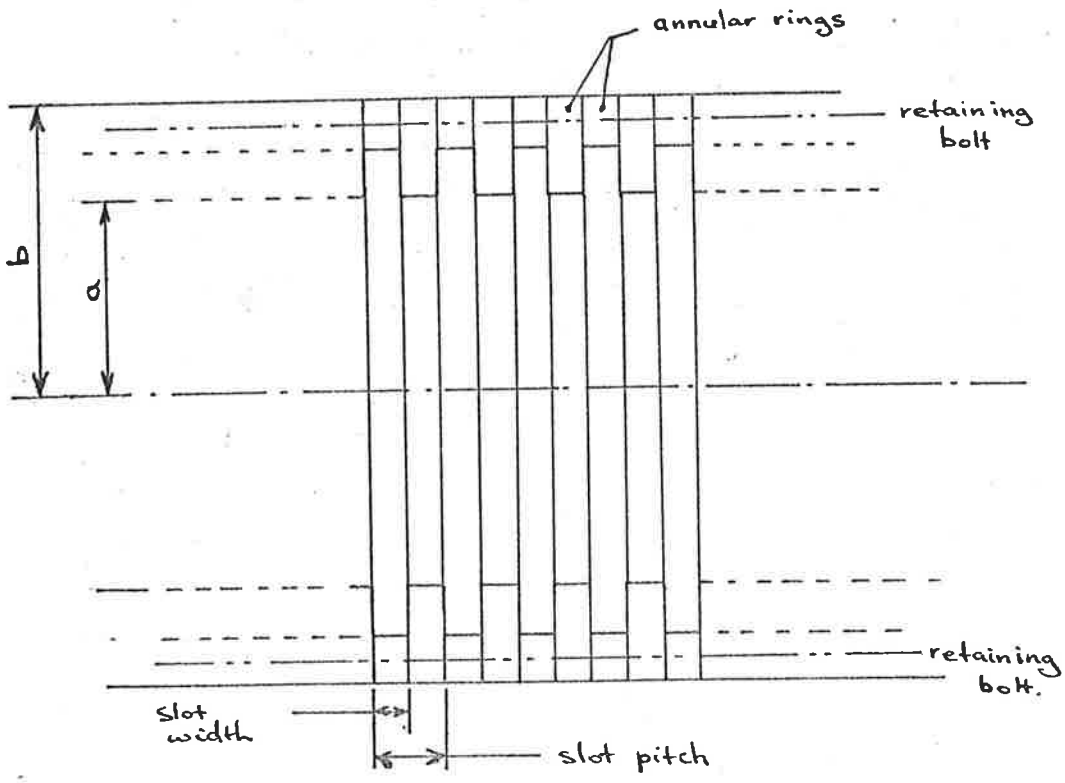

slot width = 0.5"

slot pitch = 0.25"

2b = 12.35"

2a = 10" or. 8.97"

Fig. 4.5 Corrugated Waveguide Construction.

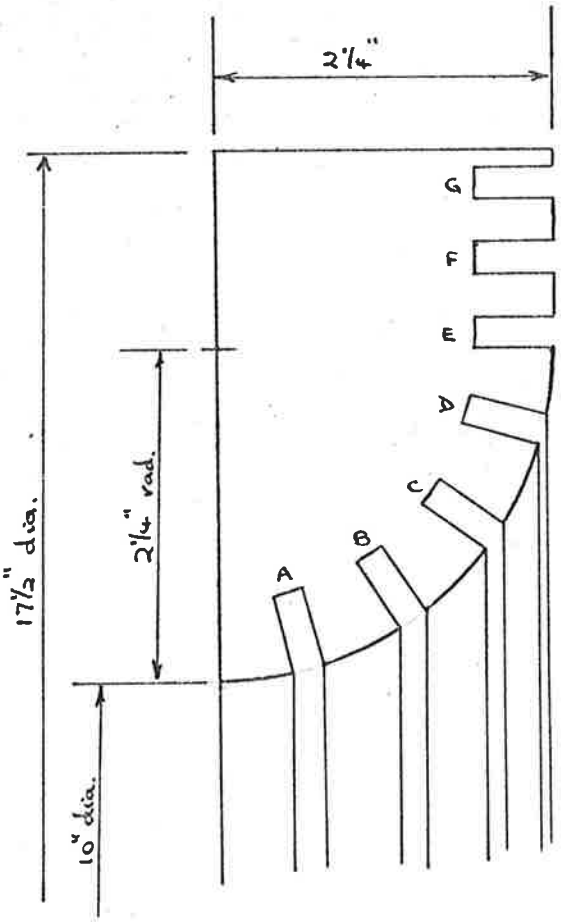

Slot details: all ¼" wide

depths:

A	1·17"
B	1·16"
C	1·14"
D	1·13"
E, F, G	1·12"

Fig. 4.6 Anisotropic flange for 10" i.d. corrugated waveguide (not to scale)

4.3.1 TM_{01} Mode in Corrugated Guide

The general solution for a zero order transverse magnetic mode in cylindrical coordinates is

$$E_z = \kappa'^2_{01} J_o(\kappa'_{01}\rho).e^{-j\beta'_{01}z}$$

$$E_\rho = -j\,\beta'_{01}\,\kappa'_{01}\,J'_o(\kappa'_{01}\rho).e^{-j\beta'_{01}z} \qquad (4.8)$$

$$H_\theta = -j\omega\epsilon\,\kappa'_{01}\,J'_o(\kappa'_{01}\rho).e^{-j\beta'_{01}z}$$

where

$$\beta'_{01} = [k^2 - (\kappa'_{01})^2]^{\frac{1}{2}}$$

In a general waveguide with an anisotropic boundary, the boundary conditions are satisfied by matching the wave impedance to the surface impedance at the boundary, $= a$. Thus

$$Z_z = -\frac{E_z}{H_\theta} \qquad (4.9)$$

$$= j\,\frac{\kappa'_{01}}{\omega\epsilon}\,\frac{J_o(\kappa'_{01}a)}{J'_o(\kappa'_{01}a)}$$

or

$$\frac{X_z}{Z_o} = \frac{\kappa'_{01}}{k}\cdot\frac{J_o(\kappa'_{01}a)}{J'_o(\kappa'_{01}a)} \qquad (4.10)$$

and $$Z_\theta = \frac{E_\theta}{H_z}$$

which is undefined for the TM_{01} mode.

In a circumferentially slotted waveguide, the surface impedances are approximately(53)

$$Z_\theta = 0$$

and

$$Z_z = jX_z = j.\delta. \frac{J_o(ka)\, N_o(kb) - N_o(ka)\, J_o(kb)}{J'_o(ka)\, N_o(kb) - N'_o(ka)\, J_o(kb)} \qquad (4.11)$$

where $$\delta = \frac{\text{slot width}}{\text{slot pitch}}$$

$$= 0.5 \text{ for waveguide used}$$

and a,b = radii measured to top and bottom of slots respectively (fig. 4.5),

and a radial TEM mode is assumed to exist in the slots. Matching equations (4.10) and (4.11) allows a solution for the radial variation constant κ'_{01} and hence

$$\beta'_{01} = [k^2 - \kappa'^2_{01}]^{\frac{1}{2}}$$

and $$\lambda_g = 2\pi/\beta'_{01}$$

Figs. 4.7 and 4.8 show the change of guide wavelength with frequency for two different corrugated waveguides,

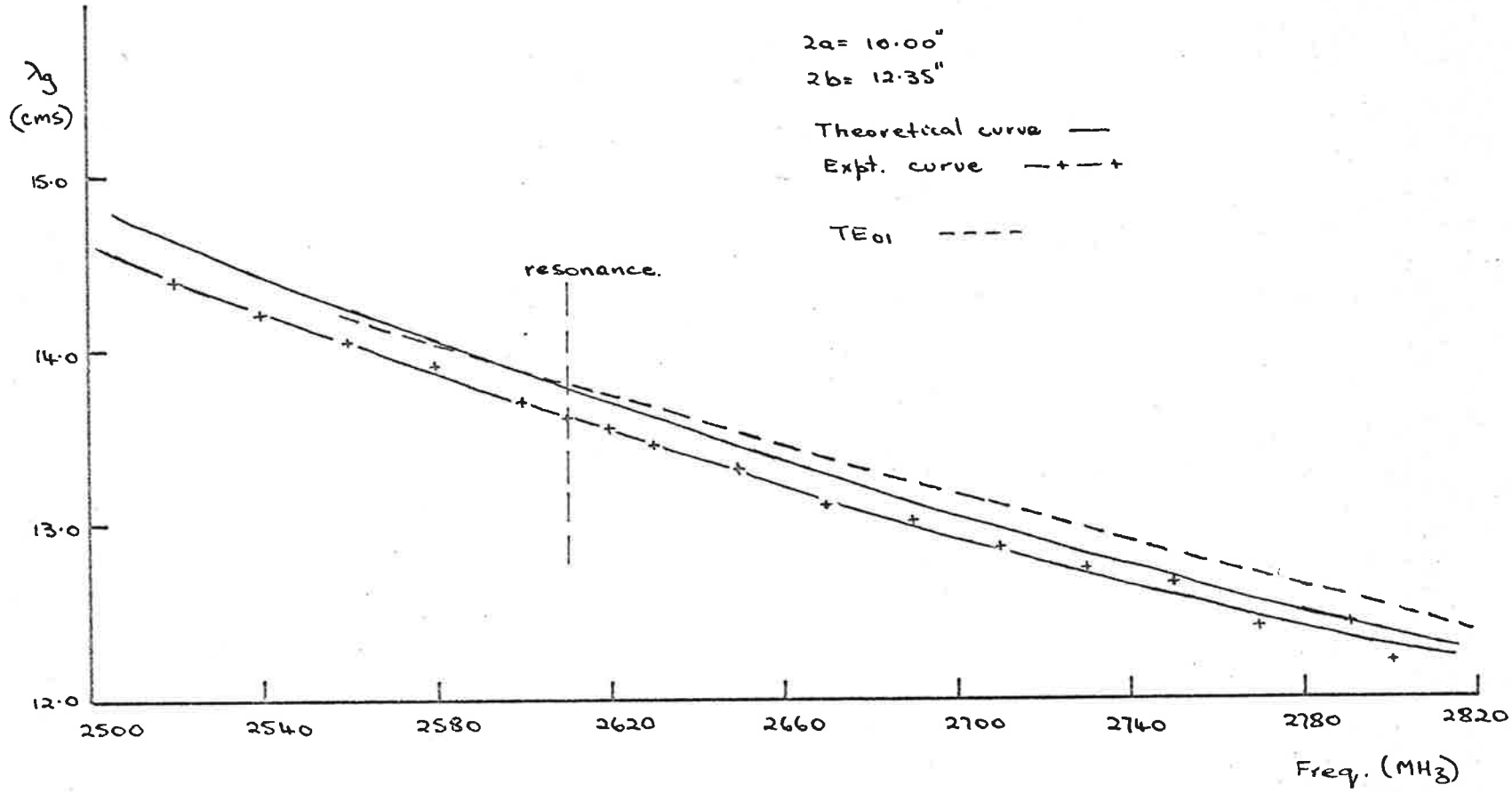

Fig. 4.7 TM01 mode in corrugated waveguide.

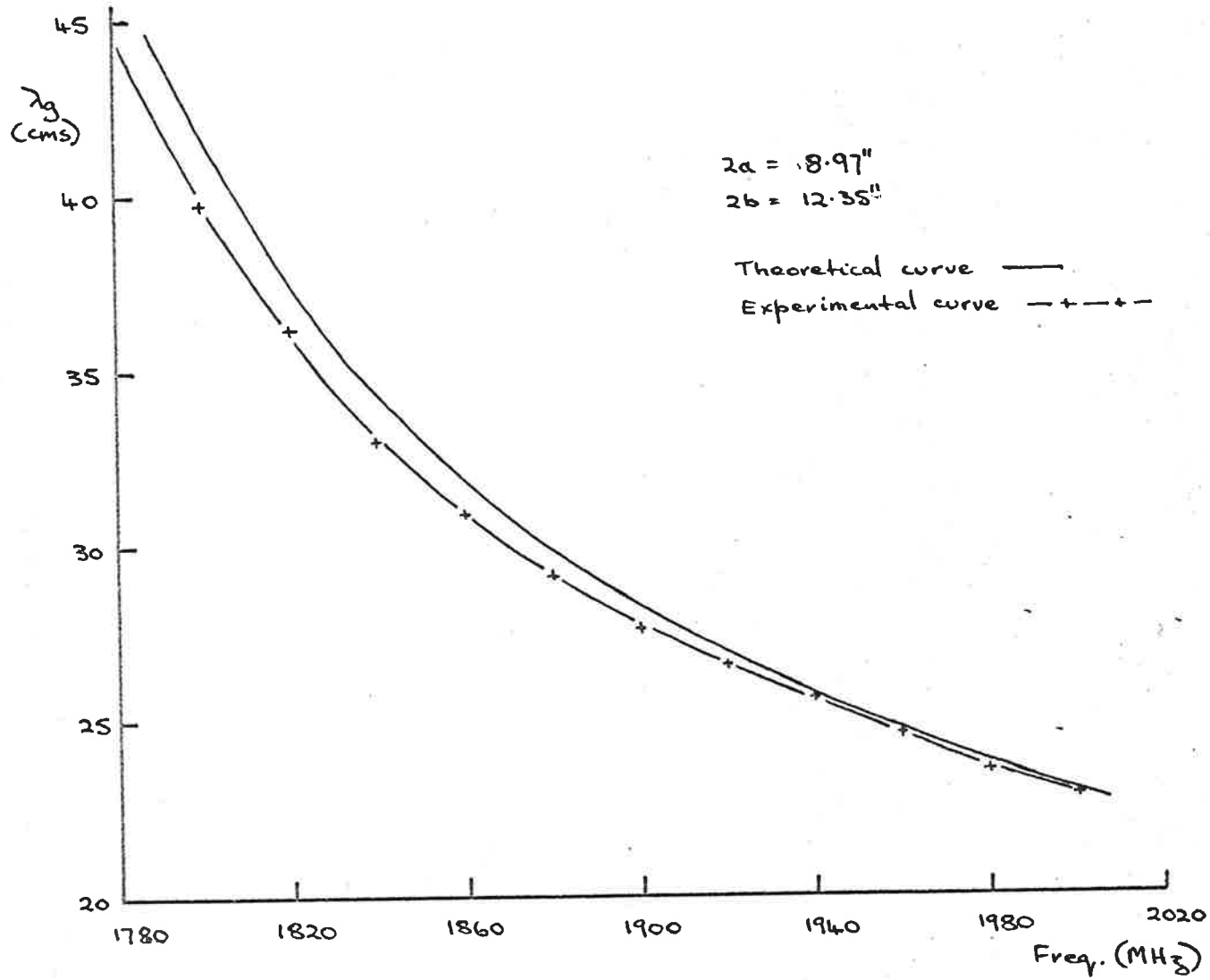

Fig. 4.8 TM01 mode in corrugated waveguide.

the dimensions of which are

$2b = 12.35"$ for both cases

and $2a = 8.97"$

and $2a = 10.00"$.

Equivalent experimental curves were obtained by using a section of the corrugated waveguide as a transmission cavity (fig. 4.9) and the guide wavelength was obtained by measuring the distance travelled by the short circuiting plunger between successive output peaks. As the length of waveguide available was only approximately one foot in length and the slot depth requires the frequency ranges shown to operate near resonance, only one half wavelength is obtainable is the smaller waveguide and two in the longer. This introduces an error because the end plates must be assumed perfect short circuits to determine the guide wavelength in the smaller internal dimension guide. This assumption was substantiated in the tests on the larger guide which gave the half guide wavelengths, when measured from the back plate and between maxima, within 1 m.m., the approximate measuring accuracy with the equipment.

A comparison of the predicted and measured guide wavelengths shows good agreement in both cases, with the error slightly increasing toward cut-off frequency. The

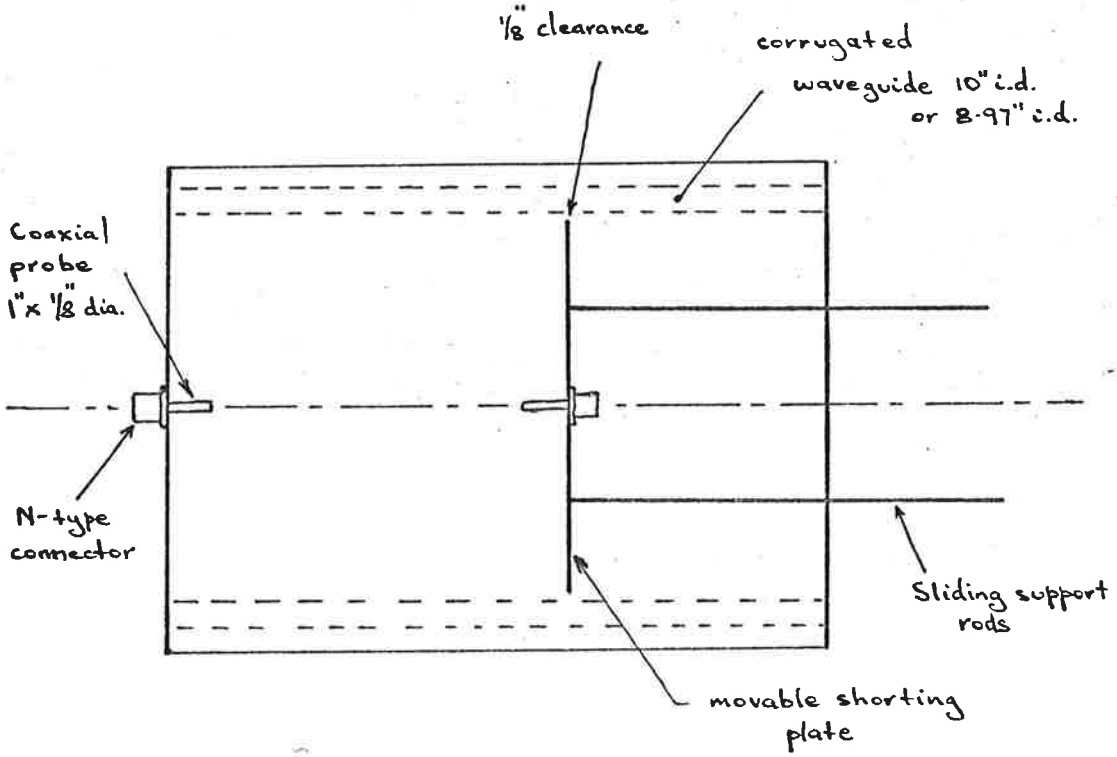

Fig. 4.9 Corrugated waveguide transmission cavity for TM_{01} mode.

maximum error in the smaller waveguide is 4.5% of the guide wavelength and in the larger guide the corresponding figure is 1.6%. These errors are sufficiently small to justify any approximations made and the technique outlined predicts the nature of the TM_{01} mode adequately.

4.3.2 Radiation by TE_{01} and TM_{01} modes in Corrugated Waveguide

The waveguide used to record radiation patterns of the circularly symmetric modes in corrugated guide was the larger of the two available and, choosing an operating frequency of 2600 Mc/s, the internal dimension of 10" corresponds to an aperture of 2.2 wavelengths. The operating frequency is sufficiently close to the resonant frequency of 2610 Mc/s that the radiation characteristics of both modes can be expected to be identical.

Details of the mode excitation techniques are given in figs. 4.10 and 4.11. In both the TE_{01} and TM_{01} cases the far from ideal step transition was used as an expedient method of achieving the excitation. This method is particularly poor for the TM_{01} mode which has a high electric field strength at the waveguide boundary. The abrupt change at the step will cause excitation of the TM_{02} mode in the corrugated guide and, as this mode

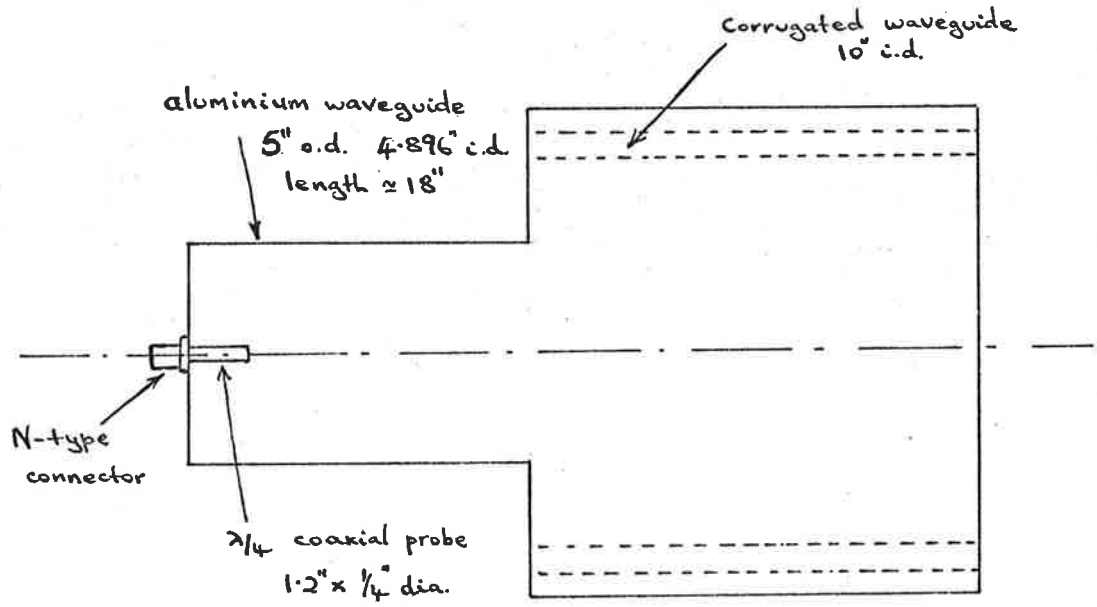

Fig. 4.10 TM01 feed with corrugated waveguide.

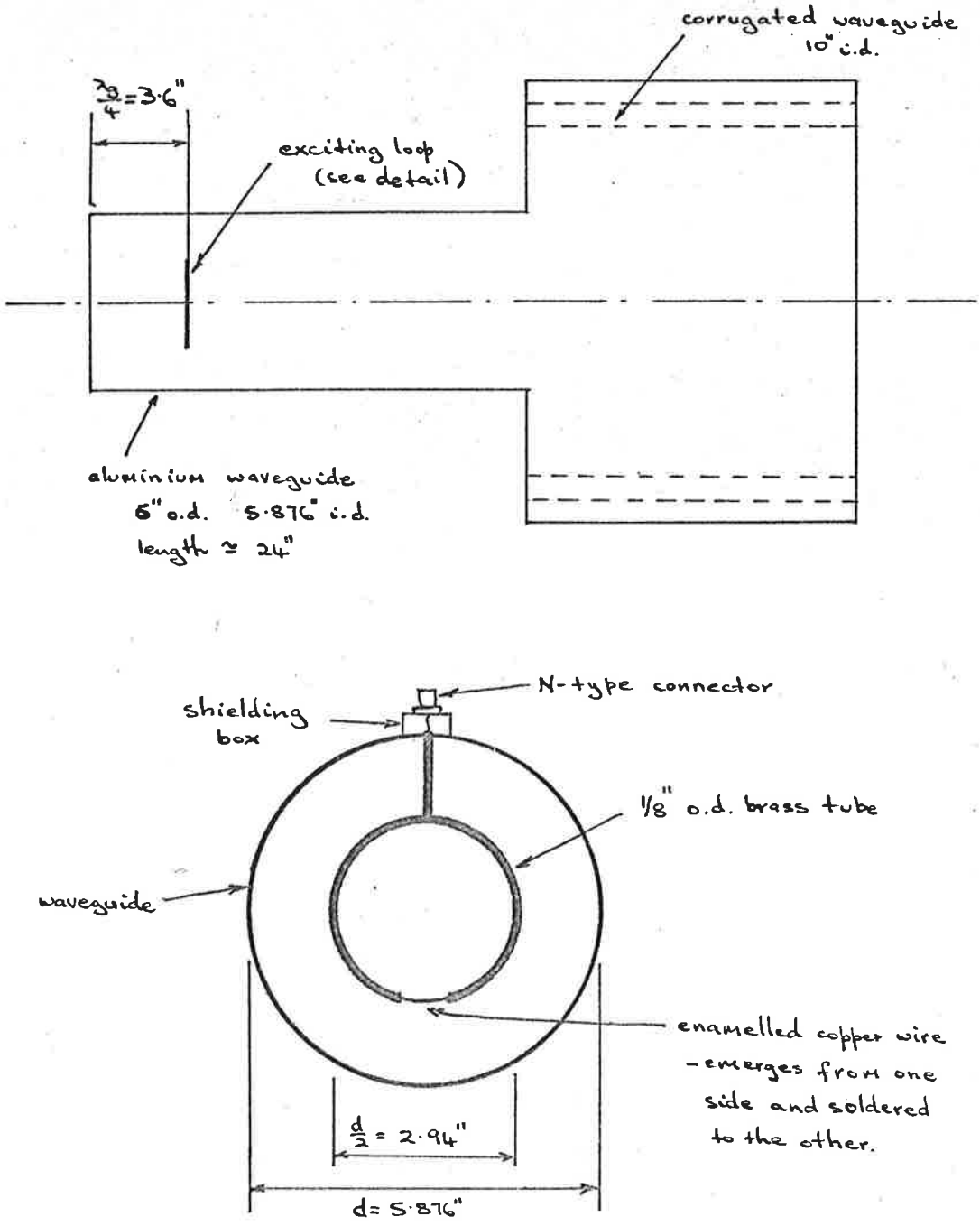

Fig. 4.11 TE01 feed with corrugated waveguide

has a cut-off frequency of 2630 Mc/s in this instance, it may propagate along the short distance to the aperture and modify the radiation pattern.

Excitation of the TM_{01} mode in a nominal 5" waveguide ensures that the next higher transverse magnetic mode (TM_{11}) is beyond cut-off (2900 Mc/s) and will not be excited. Similarly the TE_{01} mode is excited in a waveguide for which it is the highest propagating mode. The balanced loop configuration for the TE_{01} mode minimizes the possibility of excitation of other modes with radial electric field components by the support.

Fig. 4.12 gives the radiation patterns for the TE_{01} and TM_{01} modes from corrugated guide, together with the predicted pattern. The TM_{01} pattern shows a rippled nature and this is due to the presence of extra modes, predominantly the TM_{02} mode. This makes it difficult to assess the relative beamwidths of the TE_{01} and TM_{01} modes and only general comments can be made. The average angle off the axis for the first peak is the same in both cases; however, the 10 dB beamwidth is quite different in each case. Assuming the position of the first peak to be a more significant factor when other modes are present, the radiation

Fig. 4.12 Radiation Patterns.

10" i.d. corrugated waveguide
f = 2600 MHz.
without flange

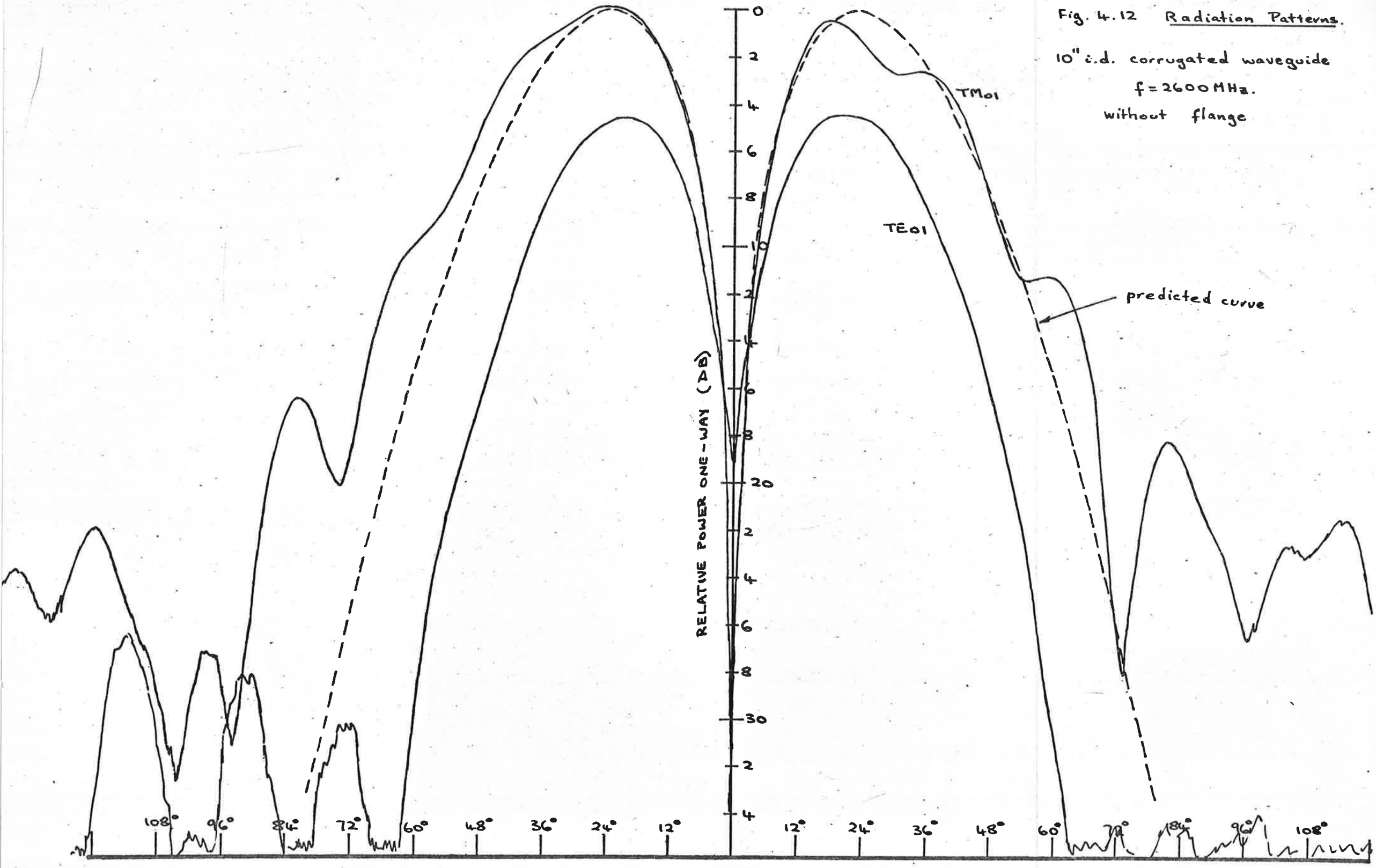

patterns can be assumed to be very similar at least up to this point.

An undesirable feature of the TM_{01} mode shown by these patterns is the high sidelobe level compared with the TE_{01} pattern. In practice, this would constitute high spillover and introduce susceptibility to noise. In this case it is difficult to assess what contribution to the sidelobes is made by the desired mode and what by the spurious modes.

Comparing the TE_{01} pattern with the predicted shape shows that the experimental result gives a slightly narrower beam. This may be caused by the effect of the small shorting flange at the aperture or by mismatch at the aperture.

Fig. 4.13 shows the same patterns repeated but with the addition of the corrugated flange at the aperture. The TE_{01} pattern remains essentially the same as before but with a slightly narrower beamwidth and a higher gain. These changes are to be expected, since, for this mode, the flange appears as a short circuit. Comparison of the changes in beamwidth with those to be expected from an infinite conducting aperture plane shows that the decrease in beamwidth is slightly greater than predited by this assumption of the effect of the

Fig. 4.13 Radiation Patterns

10" i.d. corrugated waveguide

f = 2600 MHz

with flange

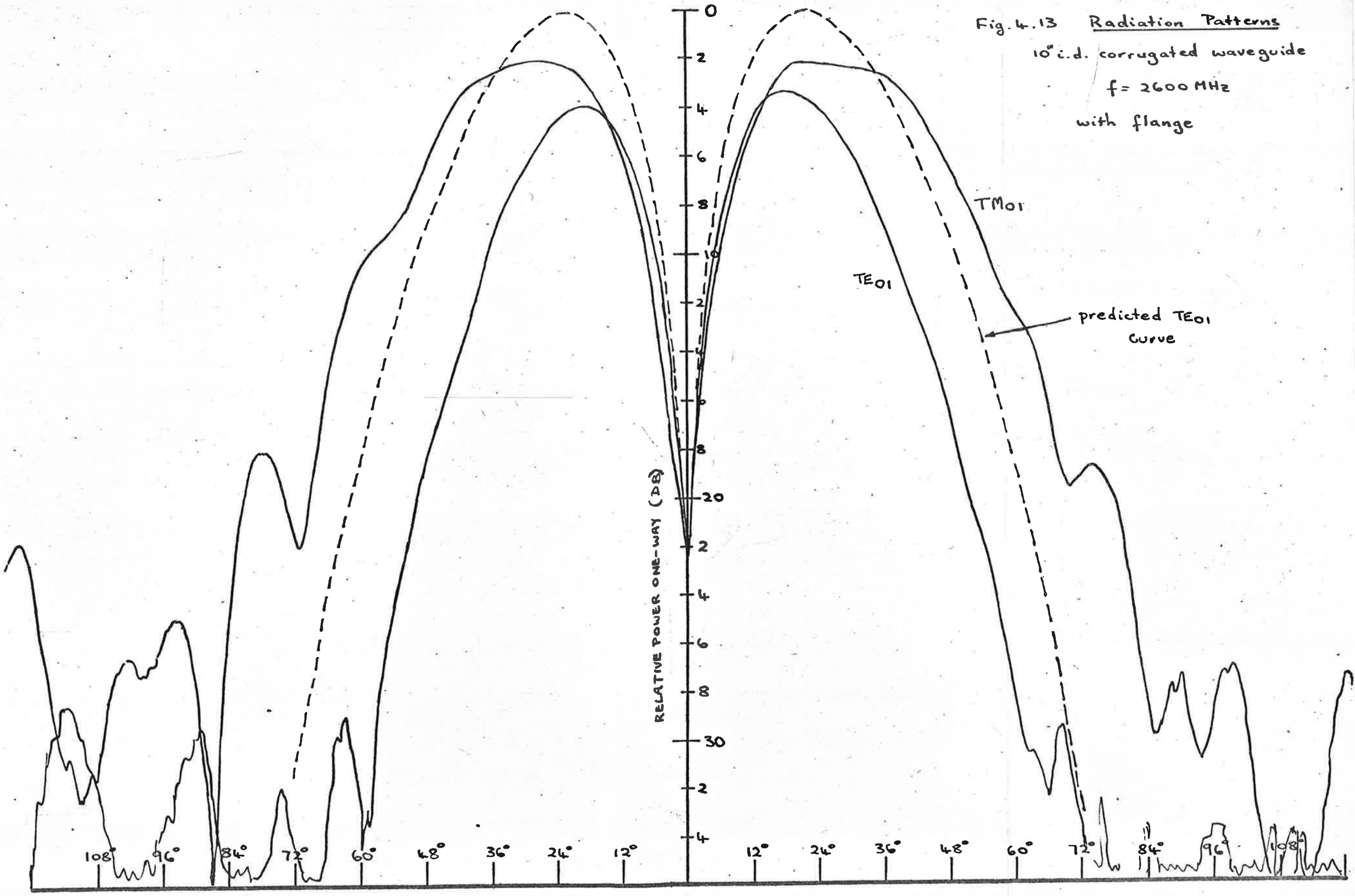

flange. This narrowing may also be due to the greater effective aperture produced by the curved section and to the possible better match achieved by this.

The TM_{01} mode characteristics appear to have broadened considerably. However, the still evident ripples suggest that the addition of the flange has produced a more effective radiating aperture for the TM_{02} mode. Fig. 4.14 gives plots of the relative voltage characteristics for TM_{01} and TM_{02} modes from equation (4.3) and indicates how a suitable combination can produce the radiation pattern obtained.

4.4 Conclusions

This Chapter has shown that, with the notable exception of thin dielectric linings in waveguides, all the techniques used to improve the efficiency of large reflector antennae by modification of the primary radiator improve the tracking mode characteristics. In all cases the changes to the feed systems improve the ratio of the effective apertures between the sum and difference modes and, where structural changes are made, there is also an improvement in the similarity between the two difference mode radiation characteristics.

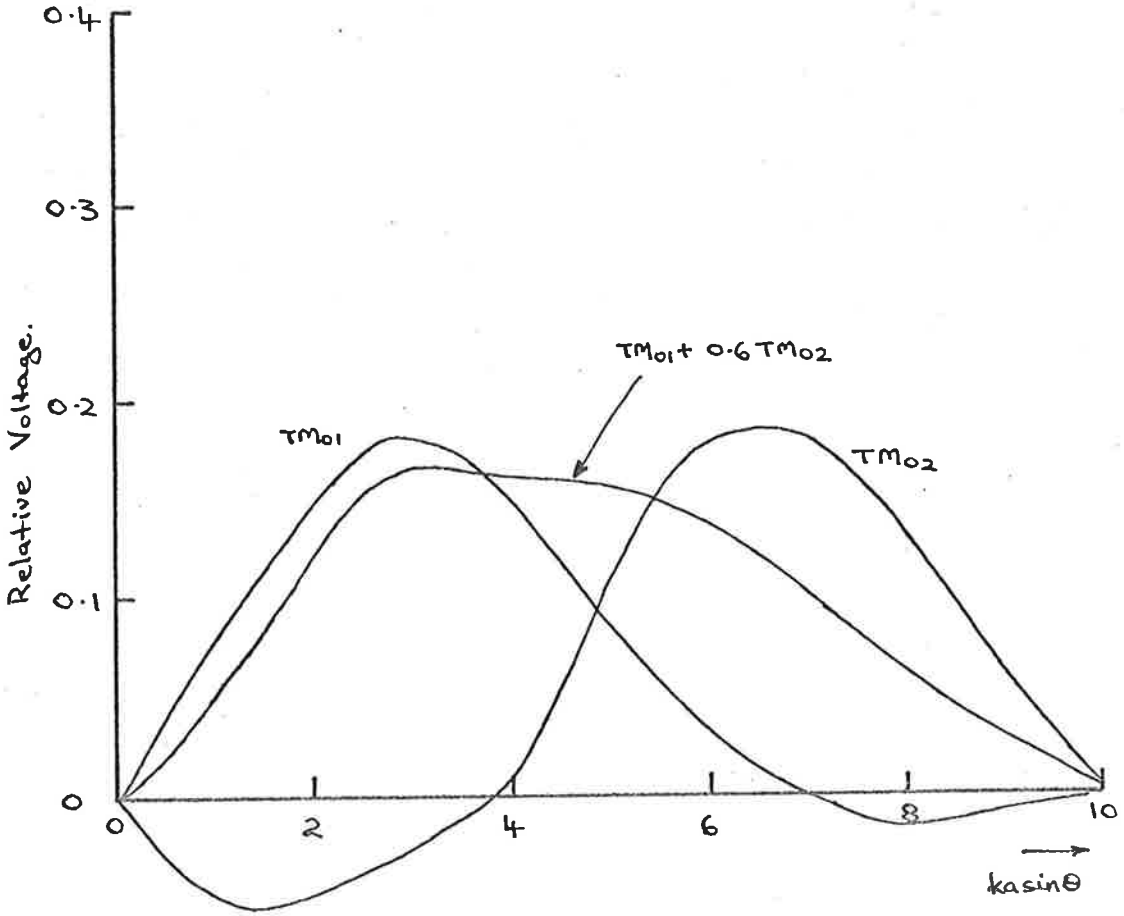

Fig. 4.14 TM_{01} and TM_{02} Radiation Characteristics.

CHAPTER V

A MODEL MULTIMODE FEED HORN

When discussing the multimode tracking system in the previous Chapters, particular emphasis has been placed upon the equality of the radiation patterns of the two difference modes, TE_{01} and TM_{01}. Ideally, these patterns should have identical amplitude and phase characteristics. Also, the relative phase between the sum mode, based on the TE_{11} mode in circular waveguide, and the difference modes is important in obtaining the azimuth angle for the tracking system. As the secondary radiation characteristics of large reflector antenna systems can be predicted from the primary radiation pattern with sufficient accuracy for practical purposes, at least over the first few sidelobes, only the feed assembly need be investigated practically. This is true, in general, although in a particular case the effect of surface tolerance and distortion errors must be included in the prediction.

Provided the main aperture is sufficiently large for the secondary beamwidth to be small enough for $\cos\theta \simeq 1$ and $\sin\theta \ll 1$, equality of the secondary gain functions for the difference modes is obtained if the primary gain functions are identical. The phase conditions require that all three modes have identical

phase fronts or, assuming that the wavefronts from the feed are truly spherical, the phase centres must be coincident. These restrictions are the ideal, but in the practical situation departures from these ideals must be accepted. The tolerances allowable in a given situation are largely dependent upon the system usage. A defocussing error of a quarter wavelength between the true focus and the actual feed phase centre causes a $\lambda/8$ phase taper in the main aperture of a reflector with $f/D \simeq 0.4$ and results in a drop of about 0.25 dB in gain, an increase in the first sidelobe level of 1-2 dB and a phase variation of some 15°-20° over the main lobe for a particular mode. This can be considered the maximum allowable misalignment in most cases, but may cause an excessive increase in sidelobe level in very low noise applications.

In a multimode tracking system, tolerances, such as those above, are quite acceptable for a servo driven steering system in the nominally focussed case. However, if the antenna is intentionally defocussed to achieve beambroadening, each of the modes is defocussed to a different degree, depending on the relative phase centres. The resulting amplitude differences between the difference modes will be small and acceptable in practice, but the phase differences will now be increased and will

increase more rapidly with feed displacement compared with the ideal case. So the maximum allowable defocussing displacement and consequent beamwidth increase is restricted by relative phase centre positions if stable tracking is to be maintained. Accordingly, tests on a multimode feed system must include determination of the phase centres.

5.1 Multimode Mode Tracking Feed Model

The design of a model tracking feed system was limited by the available test equipment and facilities. The equipment available was

Airborne Instruments Laboratory type 124 Power Oscillator 200-2500 MHz

Low power coaxial line oscillator 180-2000 MHz

Hewlett Packard Transfer Oscillator type 540B

Sanders V.S.W.R. Amplifier Mk.III

Philips D.C. Millivoltmeter type GM6020

and General Radio type 874 coaxial line components, including a slotted line, piston attenuators, voltage detectors, tubing stubs, line stretchers, attenuator pads, etc.

The circular waveguide available was standard copper, brass or aluminium piping with a maximum nominal diameter of 6" readily available and a short, 3 ft., length of 11"

i.d. tube fabricated from sheet steel and copper plated. By operating at a frequency of 1394 MHz ($\lambda = 8.47$ ins) a feed system with an aperture of 1.3λ was possible. This is approaching the minimum size suitable for use with the TE_{01} mode, which has a cut-off of 1310 MHz in 11" pipe, and is approximately the size required to focally excite a paraboloid reflector with a 60° edge angle.

The waveguide feed is designed to excite the three basic modes necessary for the multimode tracking technique. These are the TE_{11}, TE_{01} and TM_{01} modes in circular waveguide. No attempt has been made to improve the radiation characteristics of any of the modes, as would be desirable in a practical situation, especially for the dominant TE_{11} mode. The design is such that the three modes can be independently excited and the three exciters can be considered separately. Constructional details of the antenna are given in figs. 5.1 and 5.2.

(a) $\underline{TE_{11}}$ Exciter

In order to minimize cross-coupling problems, the dominant TE_{11} mode is excited in a waveguide capable of propagating only this mode. For the six inch diameter guide chosen, the cut-off frequencies for the TE_{11} and TM_{01} modes are 1154 MHz and 1510 MHz respectively.

Quarter Scale.

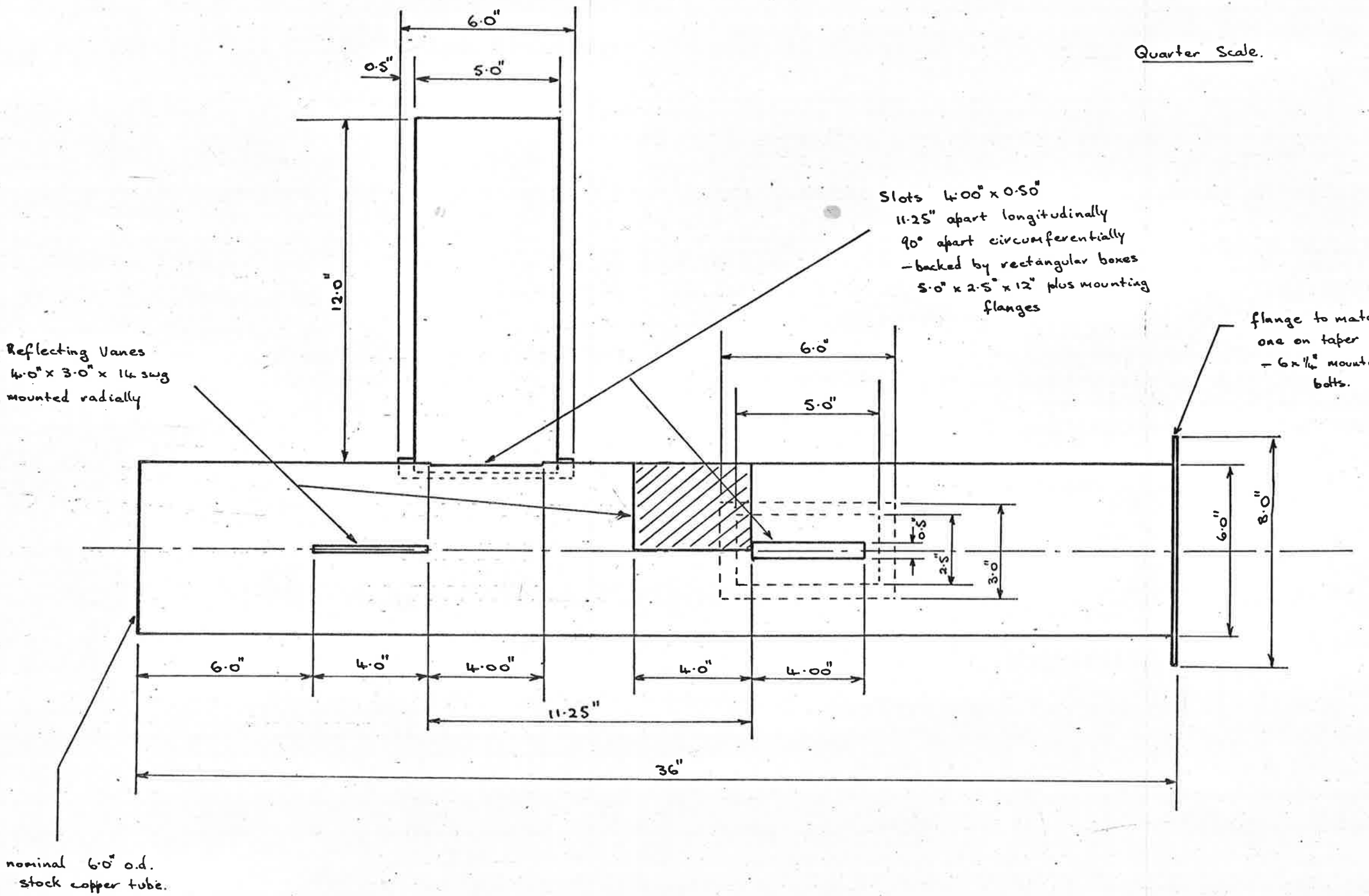

Fig. 5.1 TE_{11} Exciter

Assembly Drawing 1.

all tubing 14 swg.

Quarter Scale.

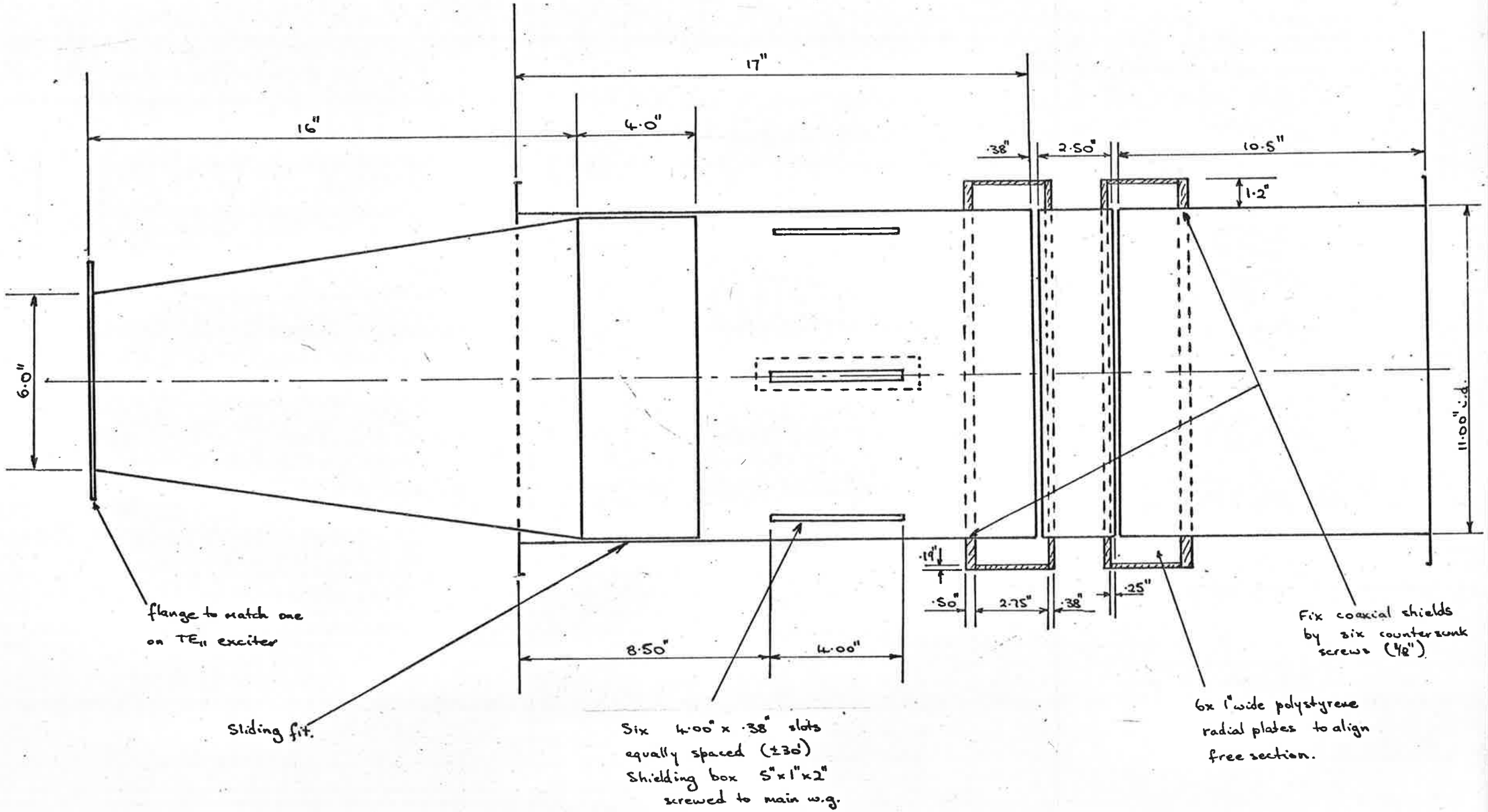

Fig. 5.2 Main Waveguide with TE_{01}, TM_{01} exciters

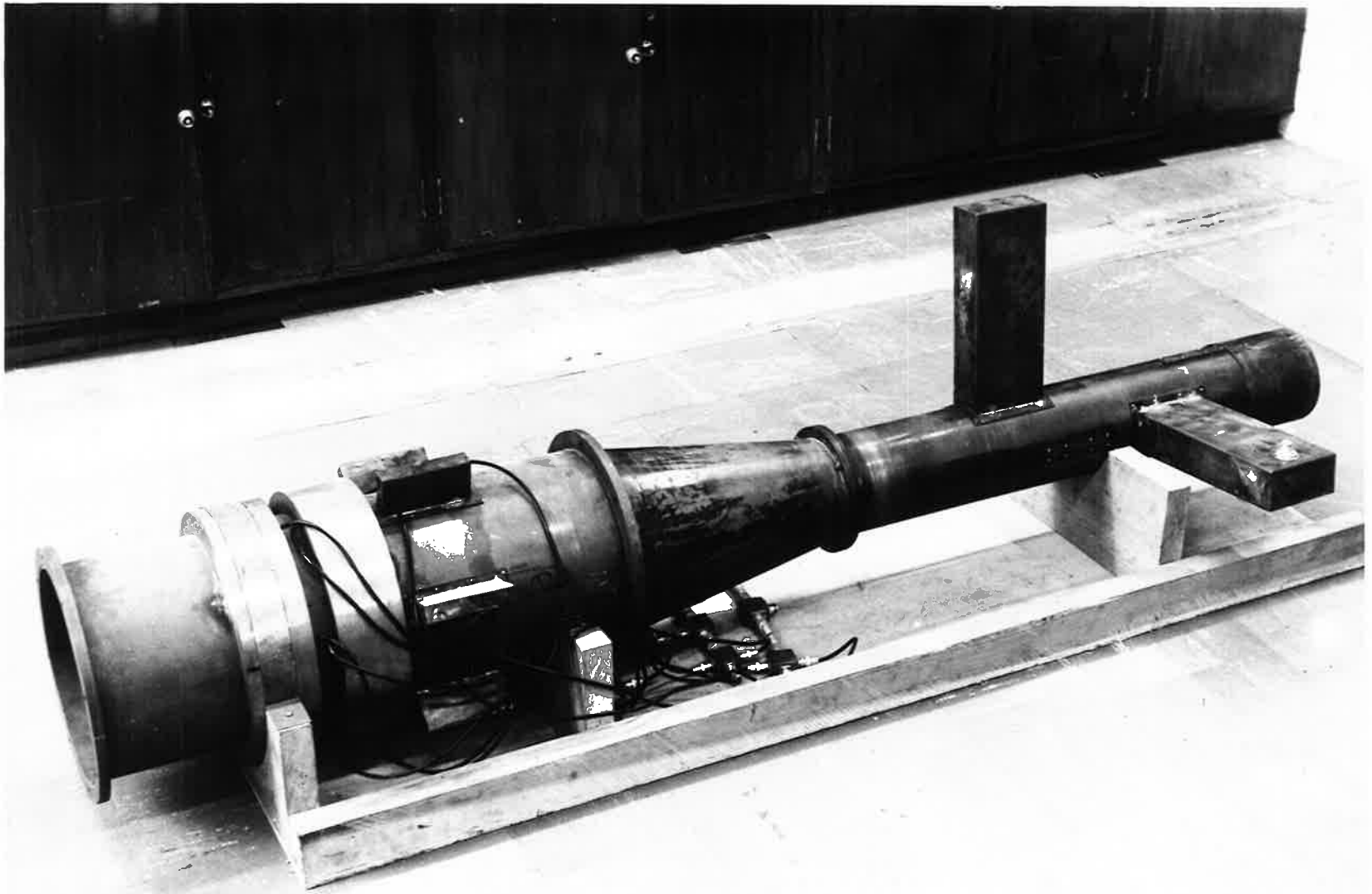

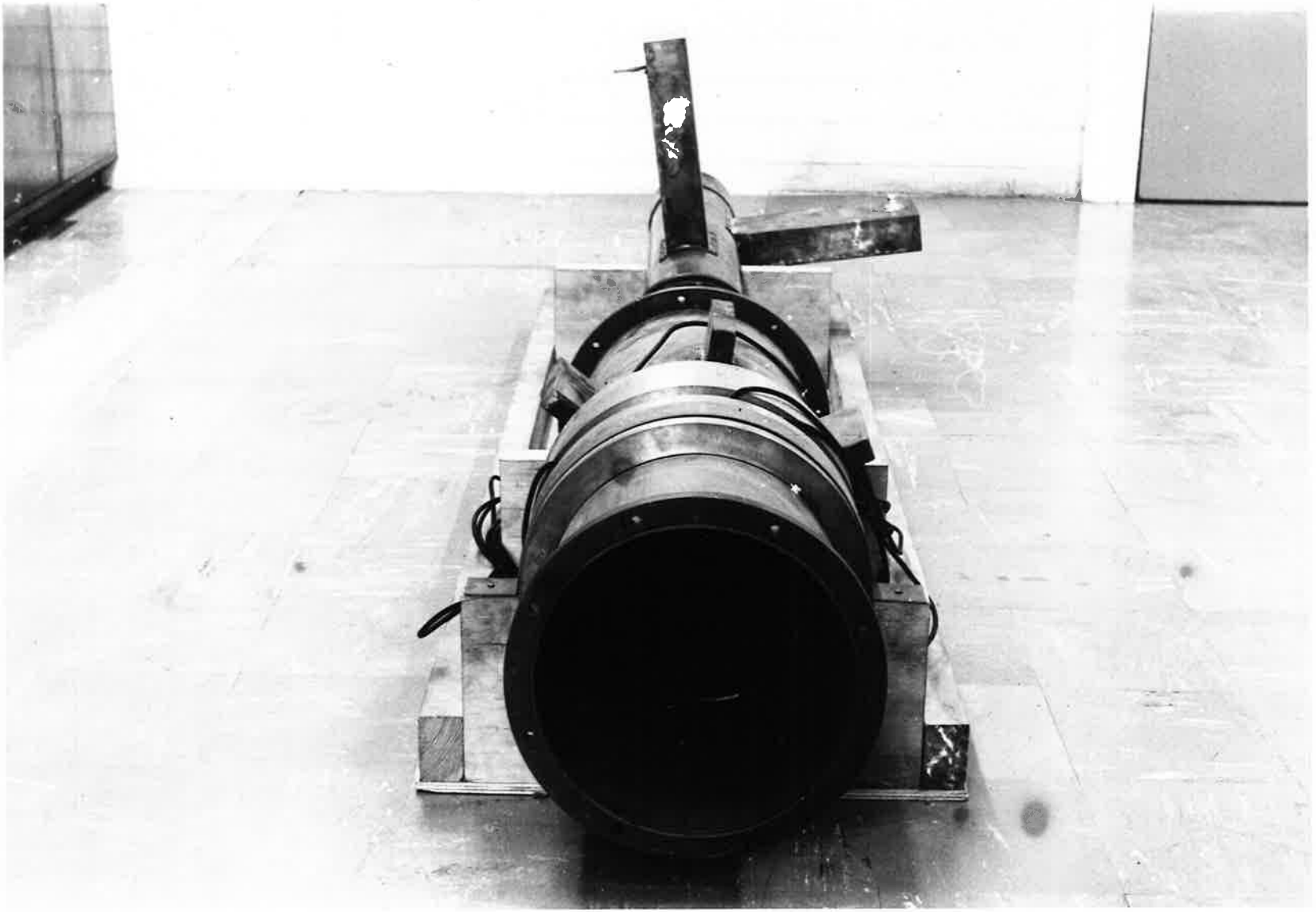

A tapered transition is used between the small and large waveguides.

The actual method of excitation of the dominant mode is similar to that used by Bell Telephone Laboratories for both the Echo and Telstar projects[54,55] and consists of a waveguide excited longitudinal slot in the cylindrical waveguide wall with a reflecting vane to produce propagation in the right direction. The rectangular waveguide feed is excited by a coaxial line through a transition as shown in fig. 5.3. The position and length of the probe is adjusted by trial and error to give a reasonable match.

Provision is made for the separate excitation of vertically and horizontally polarized waves. Circular polarization could be achieved by inserting a section prior to the taper, which gives a 90° phase shift to waves, polarized in the 45° plane midway between the exciter slots, relative to waves polarized in an orthogonal direction.

(b) TM_{01} Exciter

The TM_{01} mode is excited directly in the main waveguide. Because this mode has longitudinal wall currents, circumferential slots must be used to excite

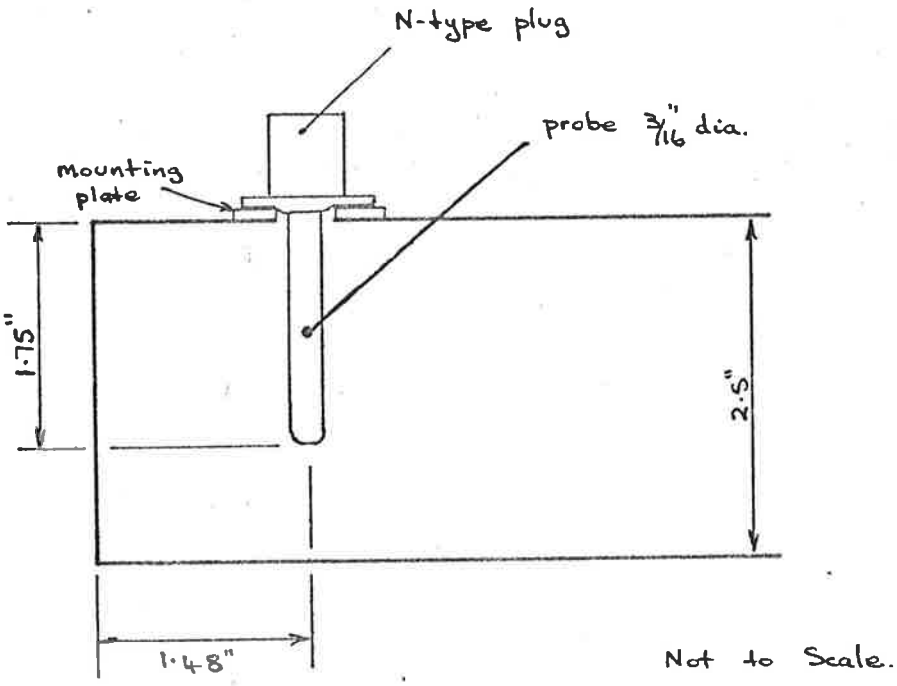

Fig. 5.3 Coaxial to Rectangular waveguide transition.

the mode. A minimum of four equally spaced slots is necessary to provide discrimination against the TE_{21} mode which may propagate in the waveguide. In the final design a continuous slot is fed by cable at six equally spaced points to approximate to a continuous distribution. The number of points chosen should provide discrimination against modes up to the fourth order. The slot is shielded against back radiation by a quarter wave coaxial stub on the outside of the waveguide, which also provides mechanical stability across the separate sections of waveguide.

The excitation of the TM_{01} mode is made independent of the other modes by feeding two slots, spaced $\lambda_g/4$ apart, 90° out of phase, so that only a forward propagating wave is produced. In the original design the width of the two slots was to be made adjustable to facilitate optimization of the exciter. However, mechanical stability problems made adjustment difficult and a fixed width of $3/8"$ was used for each slot.

The attachment of the cable inputs across the slots is detailed in fig. 5.4.

(c) $\underline{TE_{01}}$ Exciter

As the TE_{01} mode has only circumferential wall currents in the waveguide, this mode can be excited by

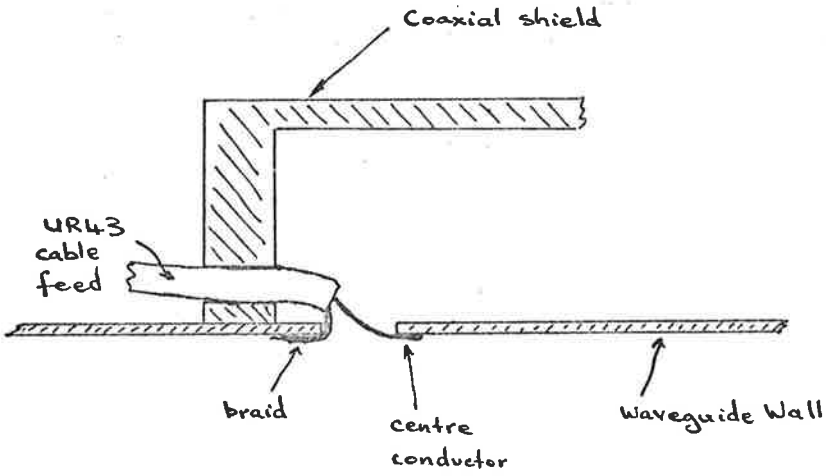

Fig. 5.4 Cable excitation of TM01 slot.

a series of half-wave slots equally spaced around the periphery of the guide. As for the TM_{01} case six slots are used to approximate a continuous distribution around the waveguide wall. The slots are cable fed in a manner similar to the TM_{01} mode, except that external attachment of the cable to the waveguide is possible in this case, and are backed by quarter wave shielding boxes.

The TE_{01} mode is tuned by the sliding tapered section between the main waveguide and the TE_{11} exciter waveguide. As the TE_{01} mode cuts-off at some point in the taper, the wave sees an infinite reactance and is wholly reflected. The position of the taper can be adjusted to give maximum forward propagation.

The power division necessary to feed the TM_{01} and TE_{01} exciters is achieved by combinations of two- and three-way power dividers, as shown in fig. 5.5. The power dividers used were simple resistive dividers, manufactured using carbon composition resistors and individually checked using a time domain reflectometer. Details of the dividers are given in figs. 5.6 and 5.7. The losses incurred by using resistive power dividers were accepted as a reasonable compromise for ease of manufacture and insensitivity to frequency. The losses

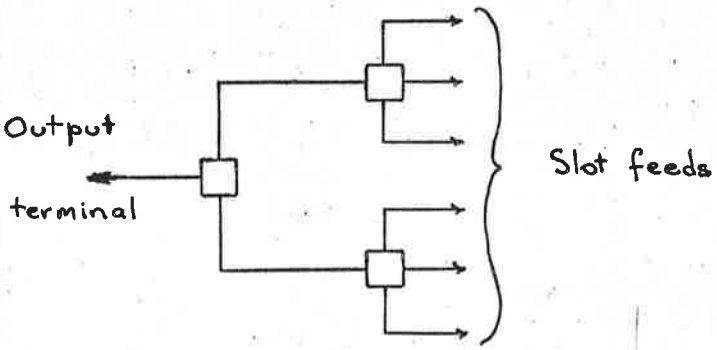

(a) TE_{01} Power Division.

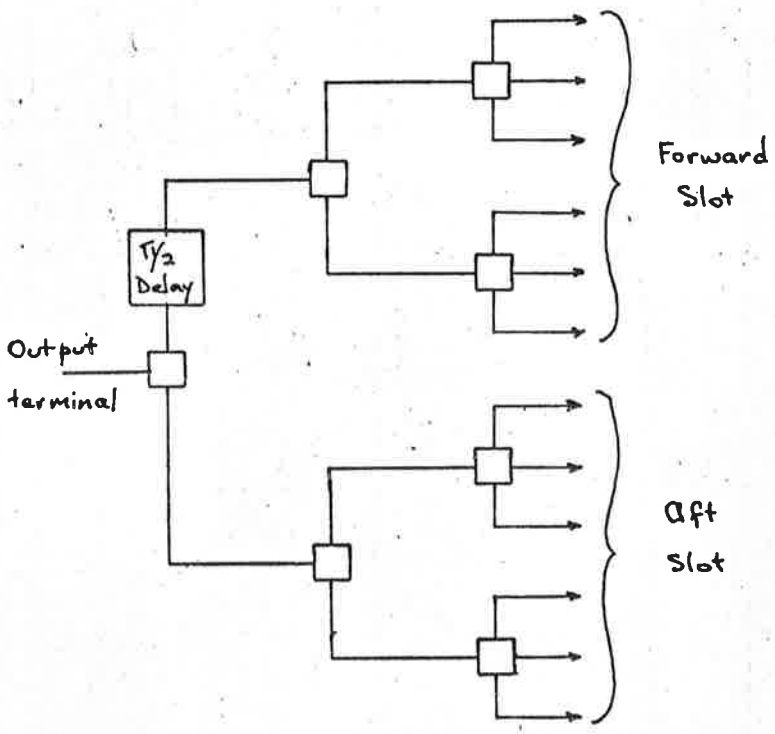

(b) TM_{01} Power Divider

Fig. 5.5 Power Divider Combinations.

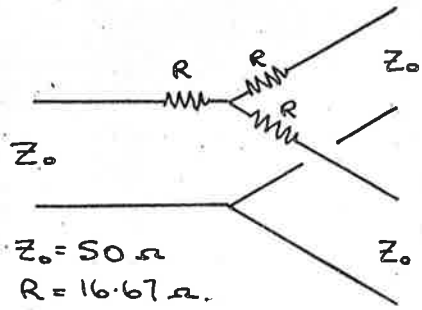

(a) Schematic diagram

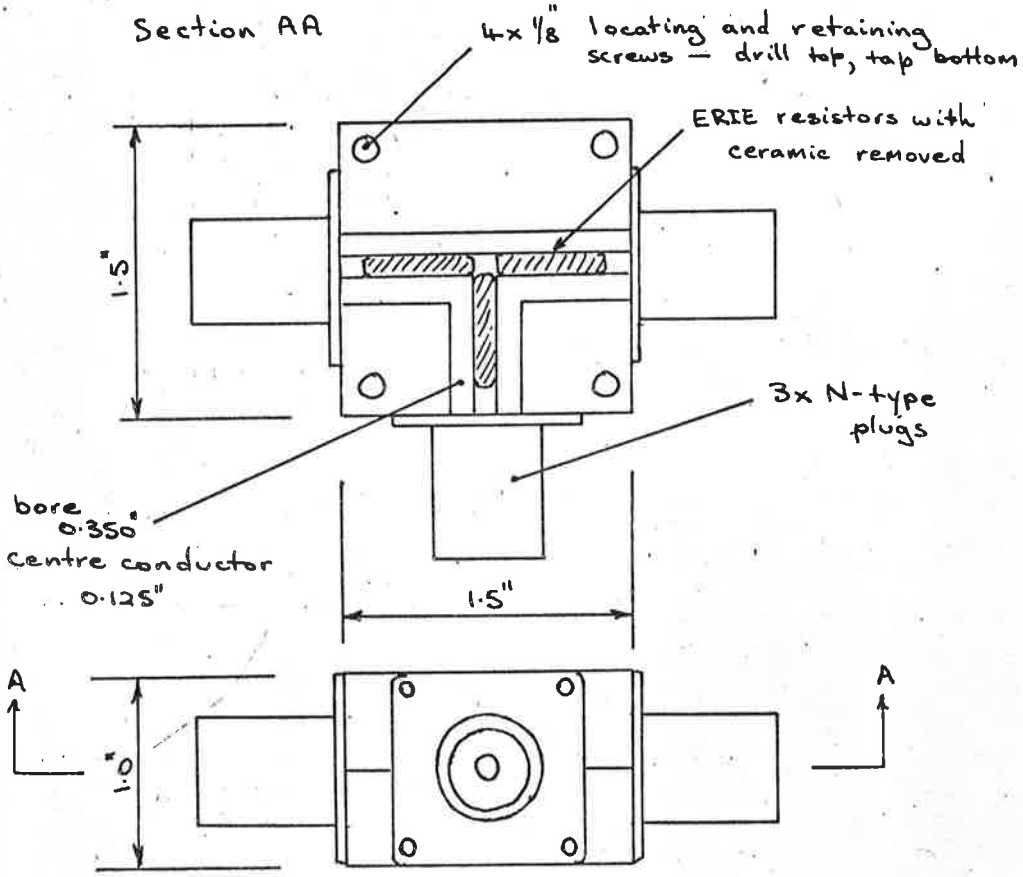

(b) Construction Details.

Fig. 5.6 Two-way Power Divider

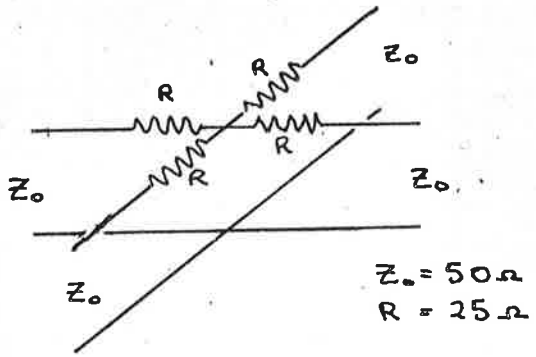

(a) 3-way power divider schematic.

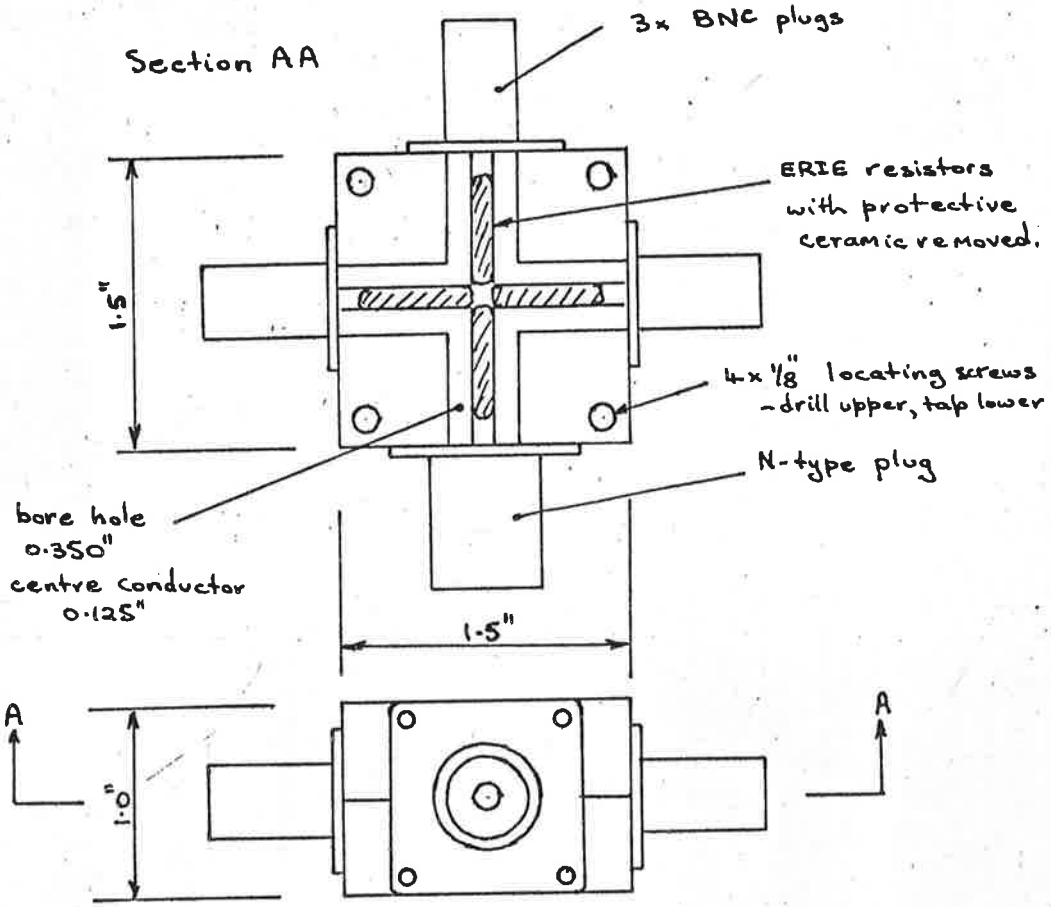

(b) Construction Details

Fig. 5.7 Three-way Power Divider

for each unit are

3 port device: 6 dB loss between any two terminals

4 port device: 9.6 dB " " " " "

The overall losses are thus

6 way divider: 7.8 dB

12 way divider: 10.8 dB.

5.2 Measuring Techniques

The measurements of the voltage standing wave ratios for the antenna inputs and the cross-coupling between the modes are straight forward and the circuits used are shown in figs. 5.8 and 5.9.

The site available for measuring the antenna radiation characteristics was a beach site to be used with a mobile laboratory. The turntable available was approximately 4'6" high and fixed the height of the test antenna, which was used as a receiver. In order to achieve adequate received signal strength, the transmission distance was required to be as short as possible. The final set up and a sketch of the site is given in fig. 5.10. The transmitting horn is a square aperture pyramidal horn, shown in fig. 5.11. The length of the test range is

$$1.65 \frac{(D+d)^2}{\lambda}$$

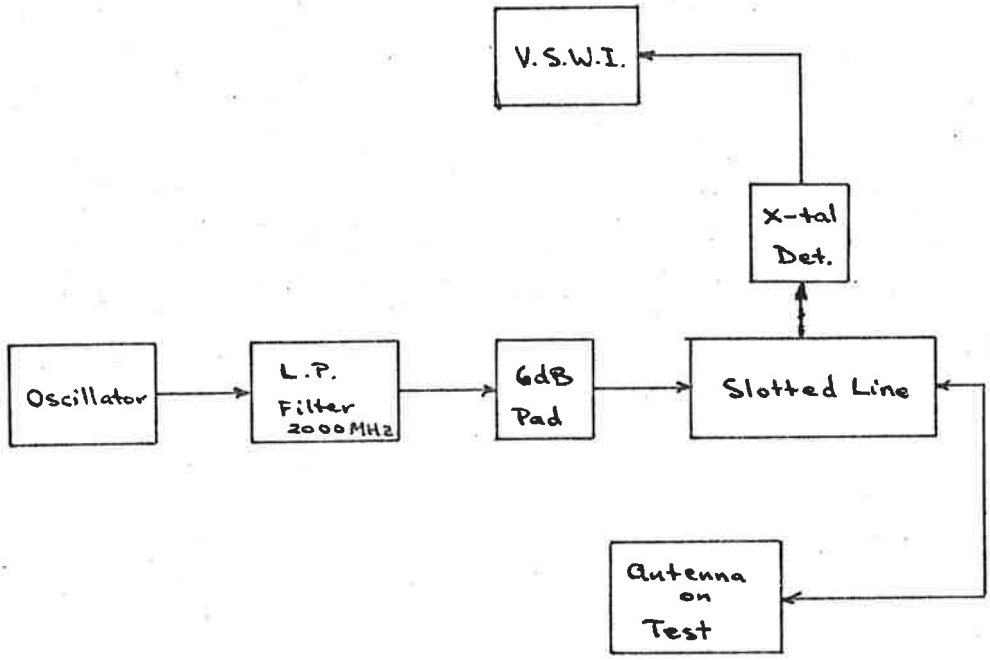

Fig. 5.8 Determination of V.S.W.R.

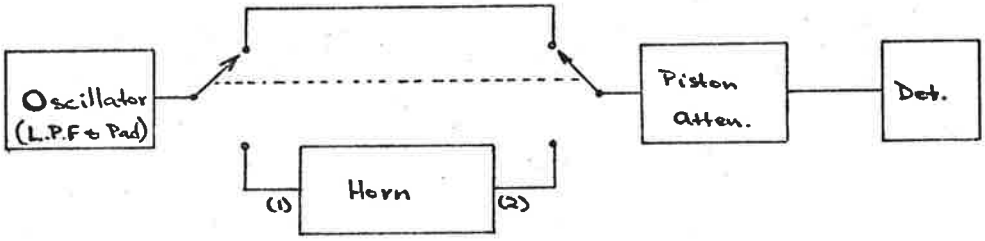

Cross-coupling = diff^{ce} in atten. readings to maintain constant level in detector

Fig. 5.9 Measurement of cross-coupling.

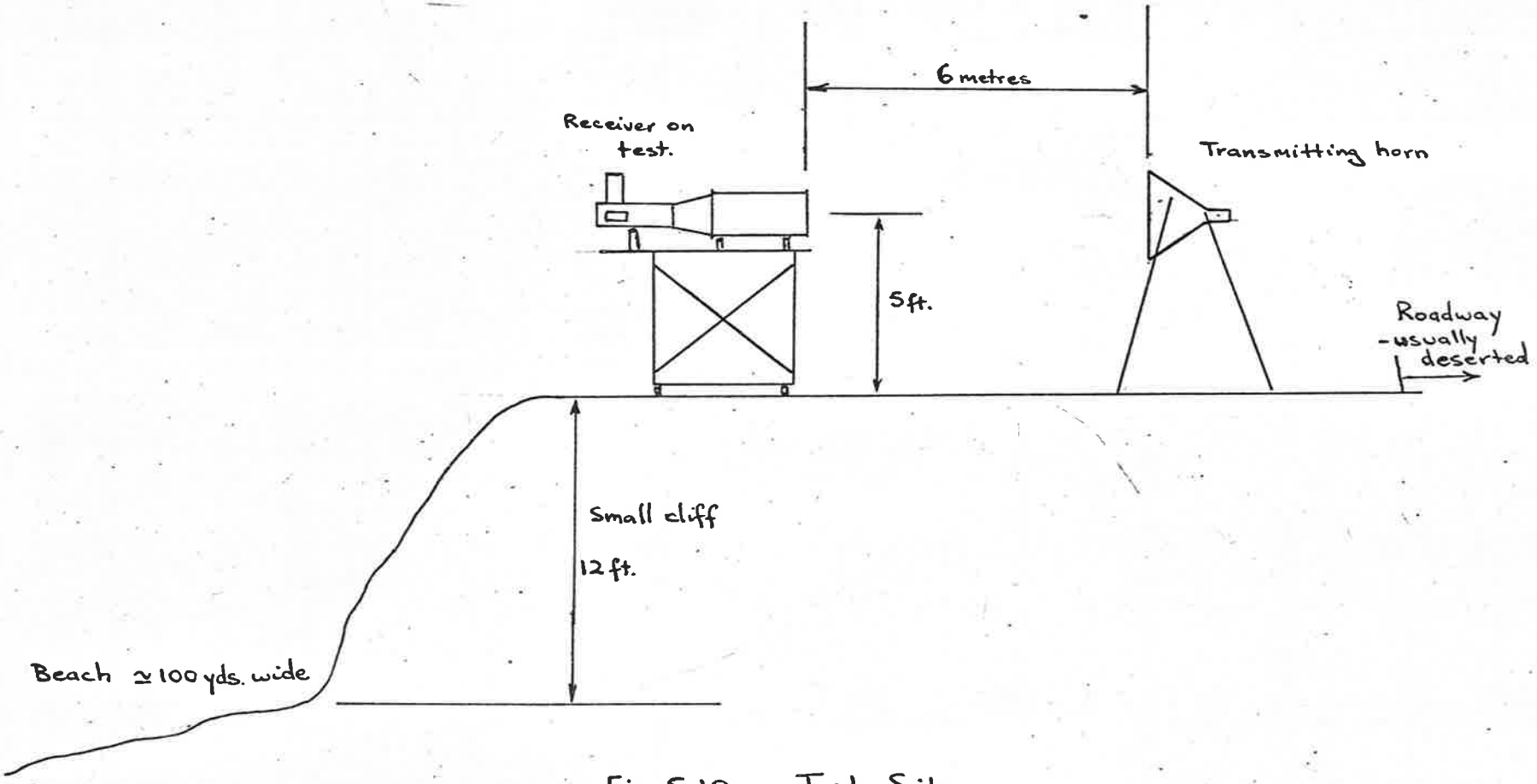

Fig. 5.10 Test Site.

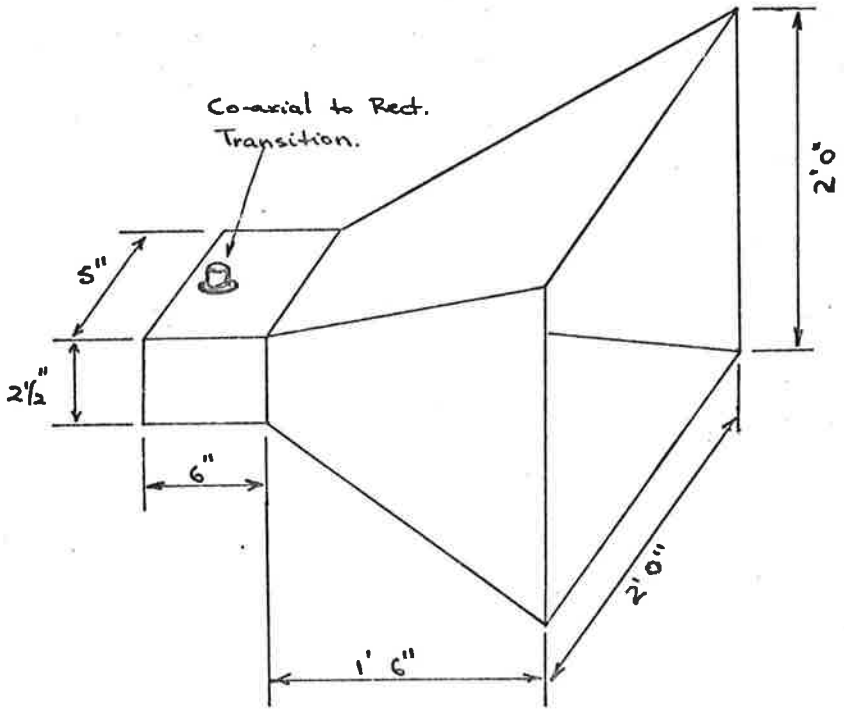

Fig. 5.11 Transmitting Horn used during radiation tests.

where D = aperture of transmitting horn = 2 ft.

and d = diameter of test antenna = 0.92 ft.

This is a satisfactory distance for maintaining small phase variations over the aperture. The ground reflection ray corresponds to a transmitting angle of 27^{o} which is approximately the position of the first null (30^{o}) of the transmitting horn. Although the test range is far from ideal, being neither a true ground reflection range nor a high level testing range, the results obtained do not indicate any anomalies due to the site.

The amplitude patterns for the TE_{11} mode were obtained directly in dB using a piston attenuator to maintain a constant power level in a crystal detector. The circuit used is shown in fig. 5.12. It was found that, with this circuit, the additional loss in the exciters for the TE_{01} and TM_{01} modes, together with the insertion loss in the piston attenuator, limited the range of measurement to only a few dB either side of the maxima for these modes. Consequently, the measuring technique was changed to that given in fig. 5.13. In this method the r.f. signal is detected directly by the crystal detector and the pattern recorded using a standing wave indicator with a modulation frequency attenuator. The crystal and standing wave indicator

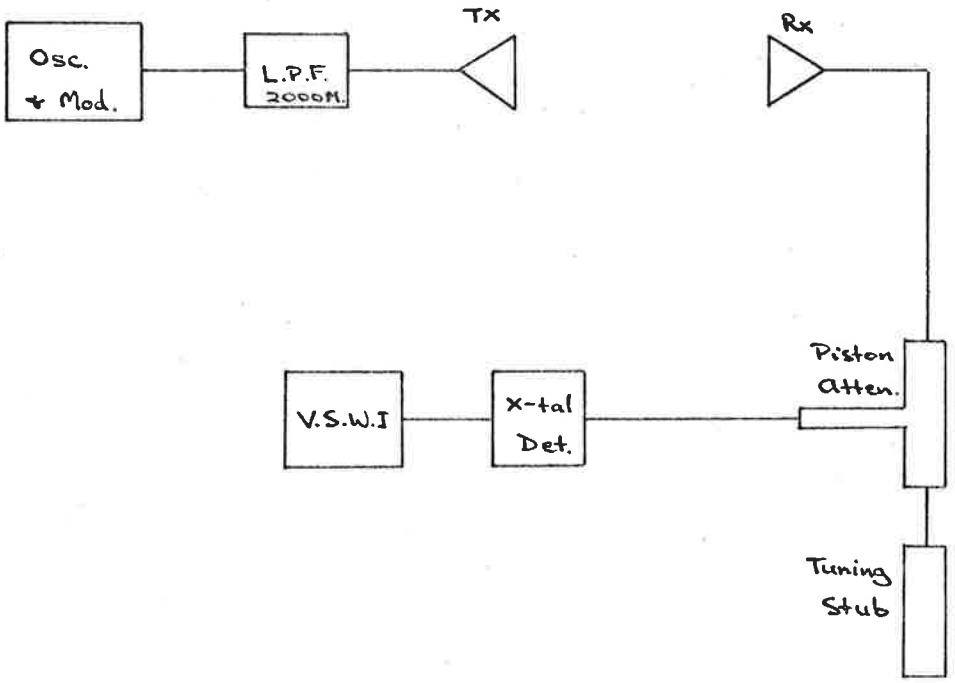

Fig. 5.12 Amplitude Pattern Measurement for TE_{11} Mode.

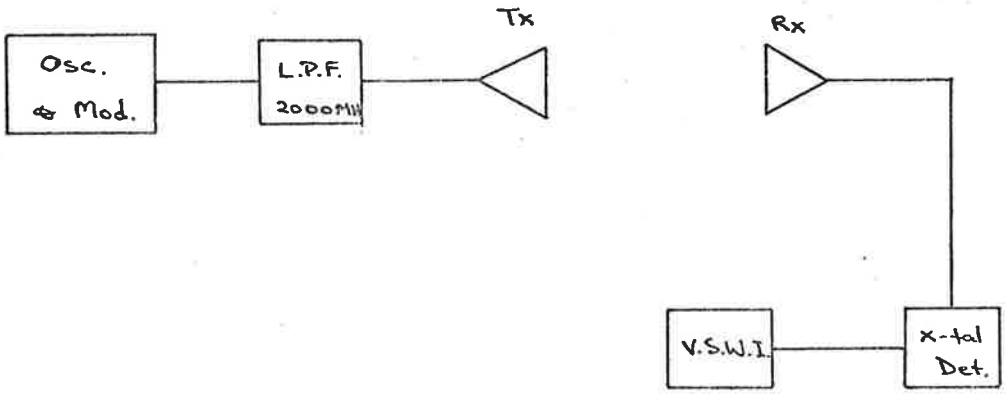

(a) Pattern recording circuit.

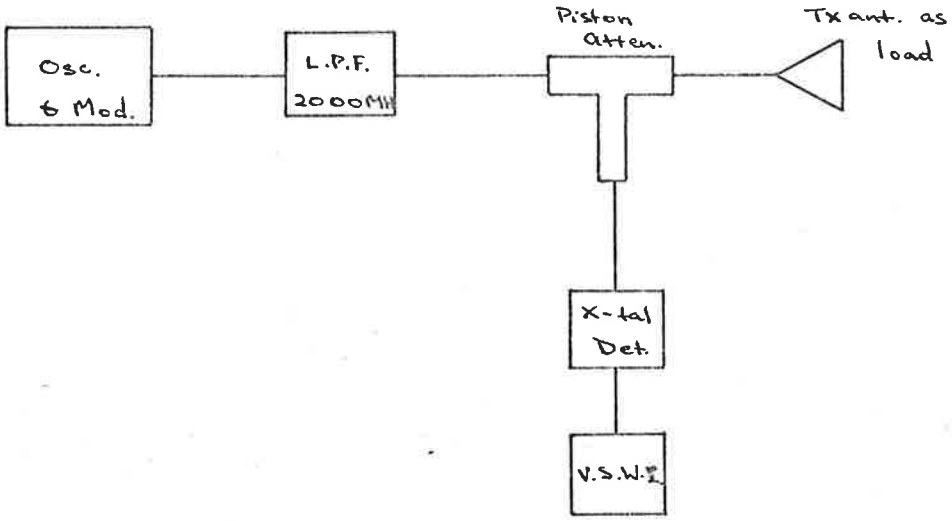

(b) Calibration of Crystal and Indicator

Fig. 5.13 Amplitude Pattern Measurement for TE_{01} and TM_{01} modes.

combination were calibrated directly against a piston attenuator (fig. 5.13(b)) after each pattern measurement.

The phase front measurements were carried out using the circuit of fig. 5.14. The relative phase change of the received signal was obtained by adjusting both the amplitude and phase of the reference signal, using the piston attenuator and line stretcher respectively, to obtain minimum reading for each angular position. The phase was simply recorded by measuring the extension of the line stretcher with a rule. The attenuator is necessary since a sharp null, necessary for an accurate phase reading, requires that the amplitudes of the received and reference signal be approximately equal. A piston attenuator is used because it provides a variable attenuation with negligible phase shift.

This technique of phase measurement, although somewhat slow, gives reasonably accurate results. An estimation of the measuring accuracy, considering the setting accuracy of the line stretcher, the frequency stability of the oscillator (within 1 Mc/s) monitored by the transfer oscillator and the differential path length (20λ) between the reference and test paths, gives an error of about $\pm 10^{\circ}$ at worst, and under good testing conditions approximately $\pm 5^{\circ}$. Good test

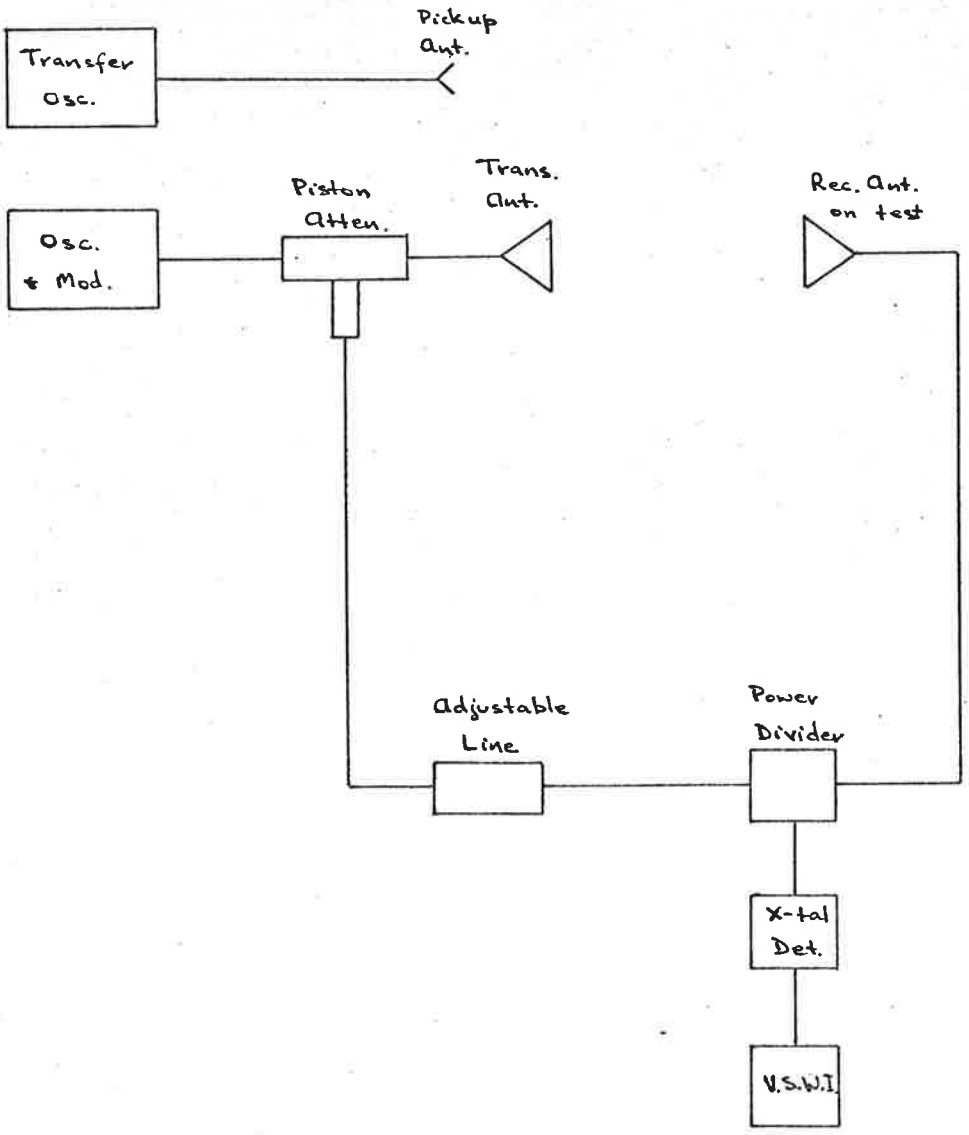

Fig. S.14 Phase front Measurement Technique.

conditions for phase measurements mainly require that there be little wind.

During all radiation characteristic measurements the transmitted power was monitored by the meter provided on the power oscillator.

5.3 Experimental Results

The voltage standing wave ratios measured at the feed points for the different modes over a frequency range, 1375 MHz and 1425 MHz, giving approximately 50 MHz range around the centre frequency, were as follows:

TE_{11} aft exciter	VSWR = 1.4 - 1.8
" forward "	VSWR = 1.4 - 2.2
TM_{01}	VSWR = 1.2 - 1.3
TE_{01}	VSWR = 1.3

These are all within practically acceptable limits, perhaps with the exception of the TE_{11} forward exciter. However, as a VSWR = 2 corresponds to only $\frac{1}{2}$ dB loss by reflection and as the main interest in the antenna is the radiation characteristic, this is an acceptable figure for testing purposes.

The pyramidal transmitting horn to be used for testing gave a constant VSWR of 1.15 over the same

frequency range.

In order that the radiation patterns of the various modes may be treated independently and compared directly, the cross-coupling between the modes must be low (Appendix II). This is also important in a tracking situation since the effect of cross-coupling between the modes is to modify the error signals so that misalignment of the antenna may occur. This limits the pointing accuracy of the antenna. This problem is unavoidable in the conventional four horn cluster tracking feed,[38] but with the multimode feed in circular waveguide it is possible to design exciters which produce low coupling between the modes. It is most important that the mutual coupling between the dominant or sum mode and the difference modes be very low because departures from the ideal for this case have a significant effect on the error signals near boresight. In practice, discrimination against the dominant mode by the two circularly symmetric modes can be achieved by using the different circumferential variations to provide cancellation of dominant mode signals in the exciter. Discrimination between the TE_{01} and TM_{01} modes, however, must rely on the exciting slots only responding to the desired mode. Since the wall currents for these two modes are orthogonal, in general, good discrimination can be achieved.

In the present case, the cross-couplings between modes are:

orthogonal TE_{11} feeds:		- 36 dB
TE_{01} - TM_{01}	:	< - 40 dB
TE_{11} aft - TE_{01}	:	≃ - 50 dB
- TM_{01}		< - 44 dB
TE_{11} forward - TE_{01}	:	- 47 dB
- TM_{01}		- 45 dB

These measurements were performed at a frequency of 1393 Mc/s using a low power coaxial line oscillator. Owing to the low power available together with the inherent losses in the measurement technique, measurements above 40 dB are not very accurate and are probably no better than $\pm$ 3 dB.

The isolation figures involving the TM_{01} and TE_{01} modes include about 10 dB of loss associated with the power dividers in the exciting circuit. However, accounting for this, it is estimated that the isolation between modes is better than 30 dB down, which can be considered adequate for the test antenna.

The radiation patterns for the three modes are given in figs. 5.15 and 5.16. These are typical patterns selected from the results obtained. It was found that the TE_{11} and TE_{01} modes gave consistent

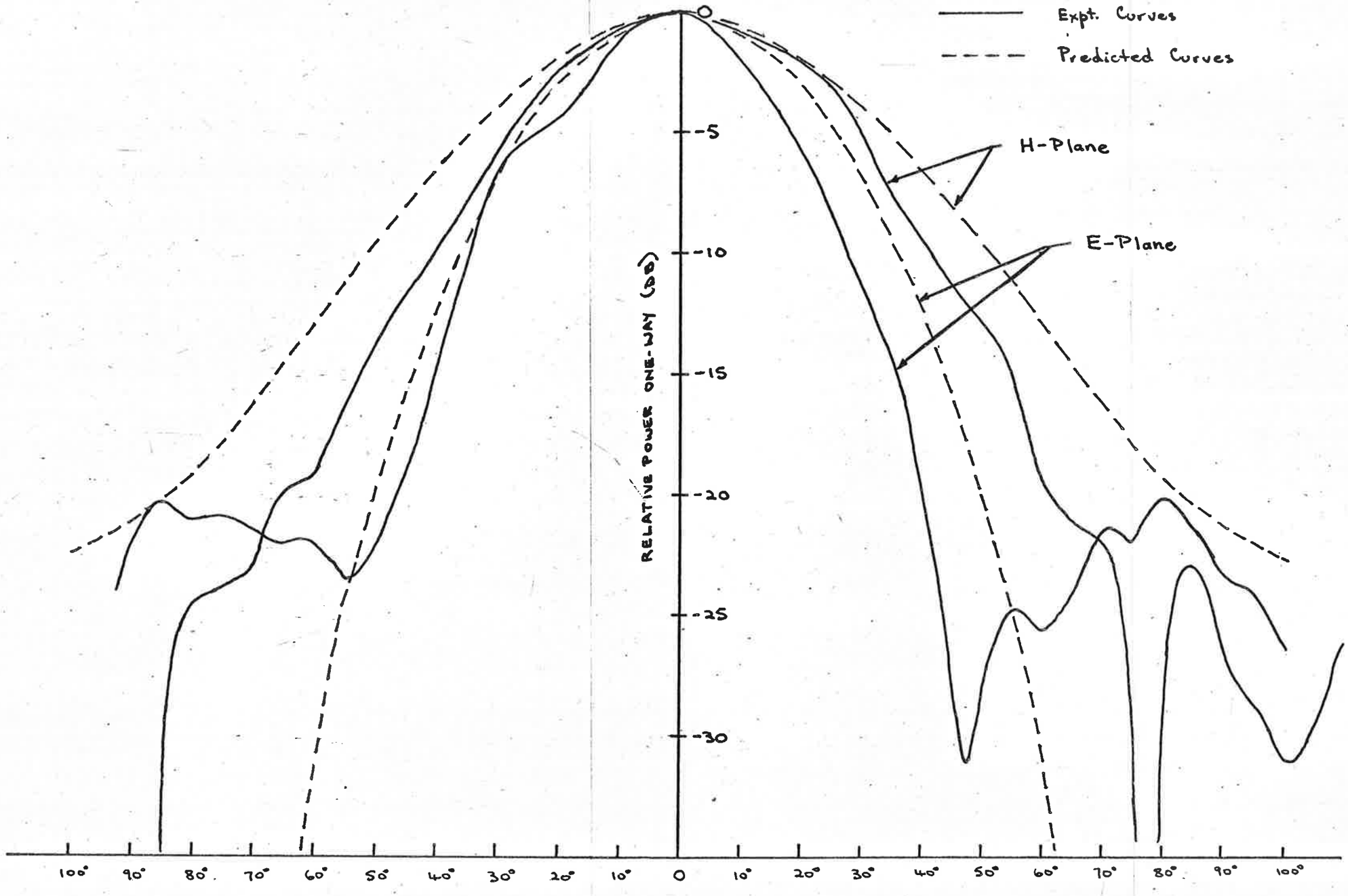

Fig. 5-15 TE_{11} Radiation Patterns.

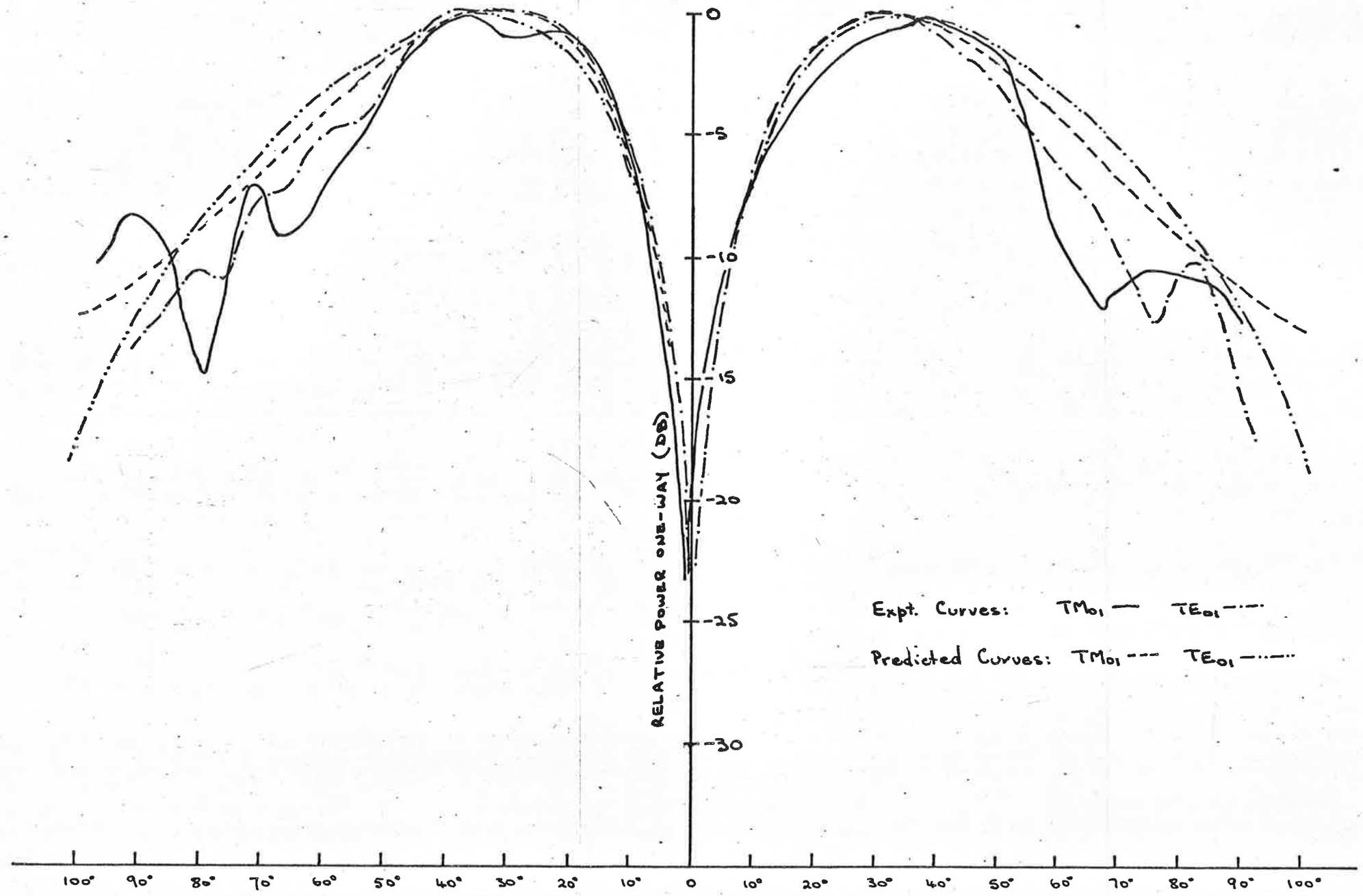

Fig. 5.16 Difference Mode Radiation Patterns.

results but that the TM_{01} mode was particularly sensitive to tuning. The final radiation patterns for the TM_{01} mode were obtained by exciting the slots and tuning for an optimum pattern with the sliding taper. This suggests that the spacing of the slots is not optimum. Owing to the long time involved in recording the patterns point by point, and as the test set up had to be completely erected and dismantled each day, an investigation into the effect of varying the relative phase of slot feeds as well as the tuning taper was not carried out because the interest at this stage was in the radiation characteristics rather than the exciting mechanism. Also, the proximity of the TM_{01} exciter to the aperture (about one guide wavelength) allows little distance for the mode to settle down.

The predicted radiation patterns are plotted together with the experimental curves for comparison. In all cases it is seen that the beamwidths obtained from the model are approximately 20% narrower than predicted. This indicates that there is considerable fringing of the waveguide fields at the aperture, causing the effective radiating area to increase. The TE_{01} mode, especially at higher angles, shows less discrepancy between the actual and predicted curves. This is expected since this mode has zero electric field

strength at the waveguide boundary and only circumferential wall currents, whereas the TE_{11} and TM_{01} both have longitudinal components. Other factors, which influence the shape of the radiation pattern and which are neglected in the theory, are mismatch at the aperture and the effect of the small shorting flange around the aperture.

The other feature of interest is the similarity between the radiation patterns for the TE_{01} and TM_{01} modes. These patterns are within 1 dB over the 10 dB H-plane beamwidth, which is the region of interest for a reflector antenna feed. The measuring error is of the order $\pm$ 0.5 dB and so the patterns are sufficiently similar to be used as difference modes in a tracking system.

The deep nulls on boresight in the symmetric mode cases indicate that the cross-coupling between the sum and difference modes is very low and better than the 40 dB measuring range possible below the sum mode peak gain.

The phase centre for the three modes were obtained by measuring the phase variation of the received signal against a reference (fig. 5.14) and by assuming that rays from the transmitting horn to the centre of rotation and phase centre are parallel. This

assumption is justified since the turntable allowed the receiving antenna to be mounted with its aperture a minimum of a half-wavelength in front of the pivot and a conservative estimate places the phase centre within a wavelength of the pivot. A one wavelength separation, together with the 30λ path length, will produce a maximum error of $\lambda/60$ in phase front and error of this order in the position of the phase centre. These errors are negligible.

The phase centres determined for the three modes are:

TE_{11}	H-plane	0.1λ in front of aperture
	E-plane	in aperture
TM_{01}		0.1λ in front of aperture
TE_{01}		0.1λ behind aperture.

The phase fronts are given in figs. 5.17-20.

The spread of the phase centres is seen to be 0.2 λ, which is small and allows a compromise focussing position for all three modes. Defocussing phase errors in the aperture for small displacements up to 0.1 in an antenna with $f/D \simeq 0.4$ will have an almost negligible effect on the gain and sidelobe structure of the secondary pattern, except for a filling of the nulls. In practice the focussing would be based on the dominant TE_{11} mode, producing a minimum phase error for this

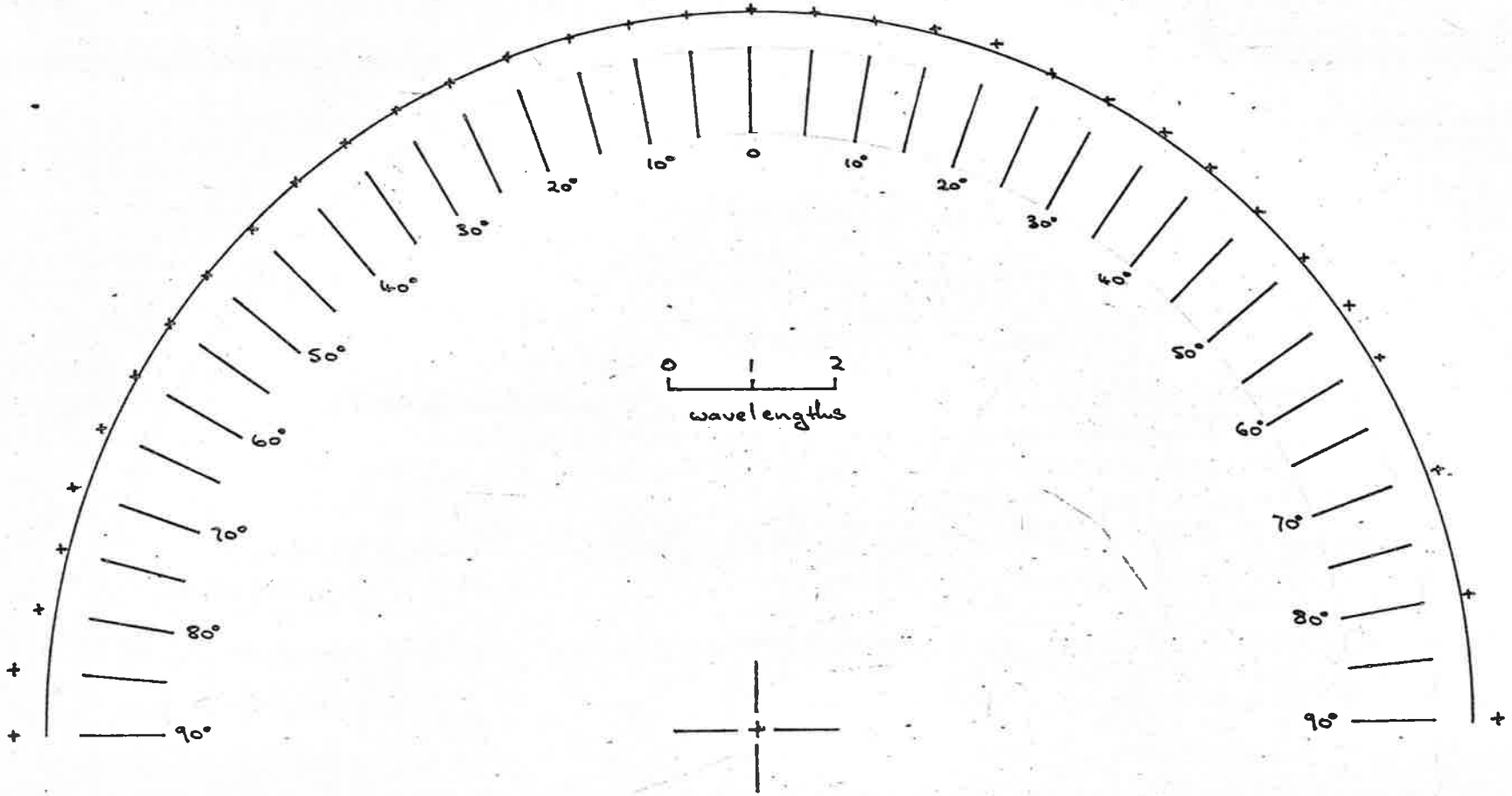

Fig. 5.17 TE_{11} H-Plane Phase Front

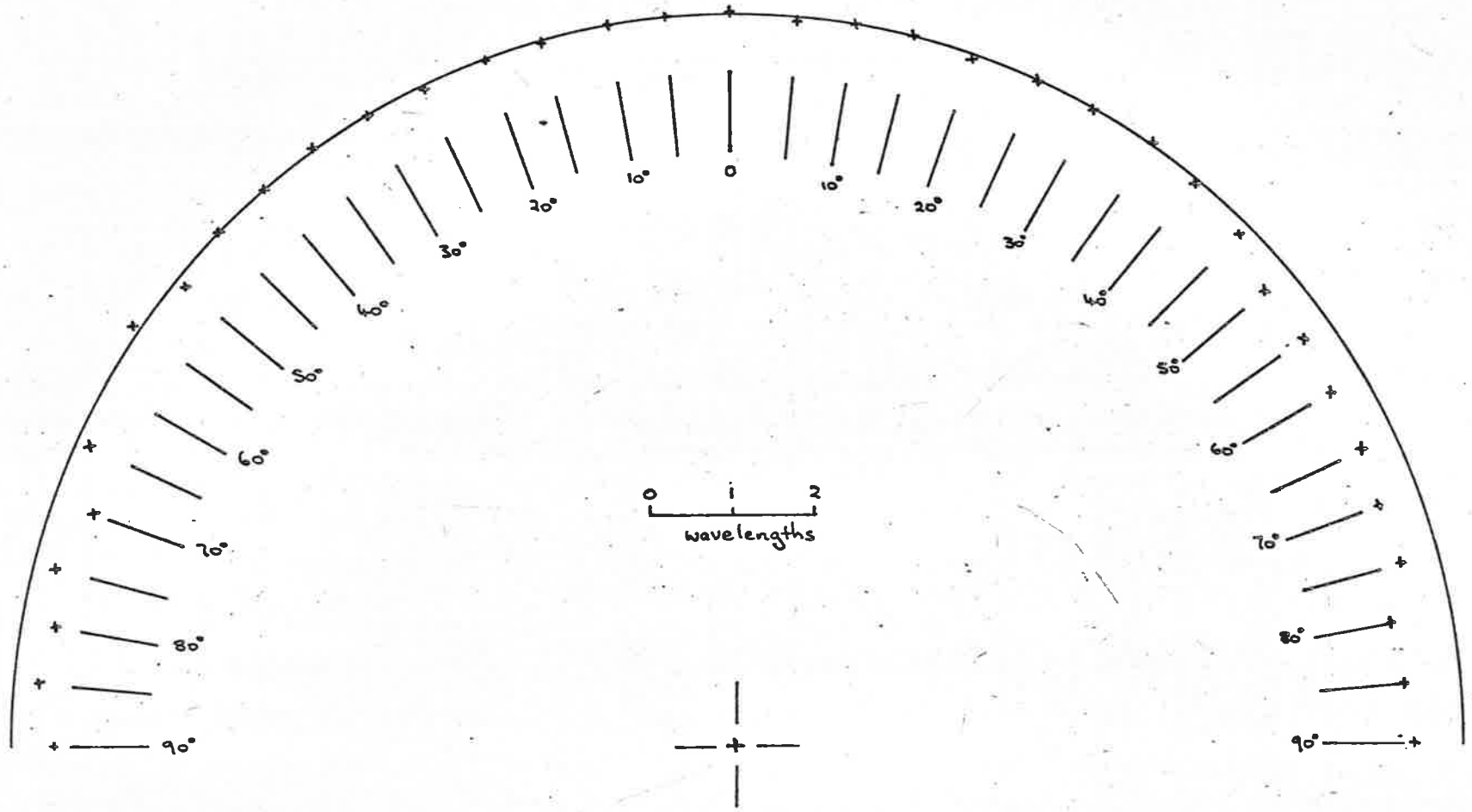

Fig. 5.18 TE_{11} E-Plane Phase Front

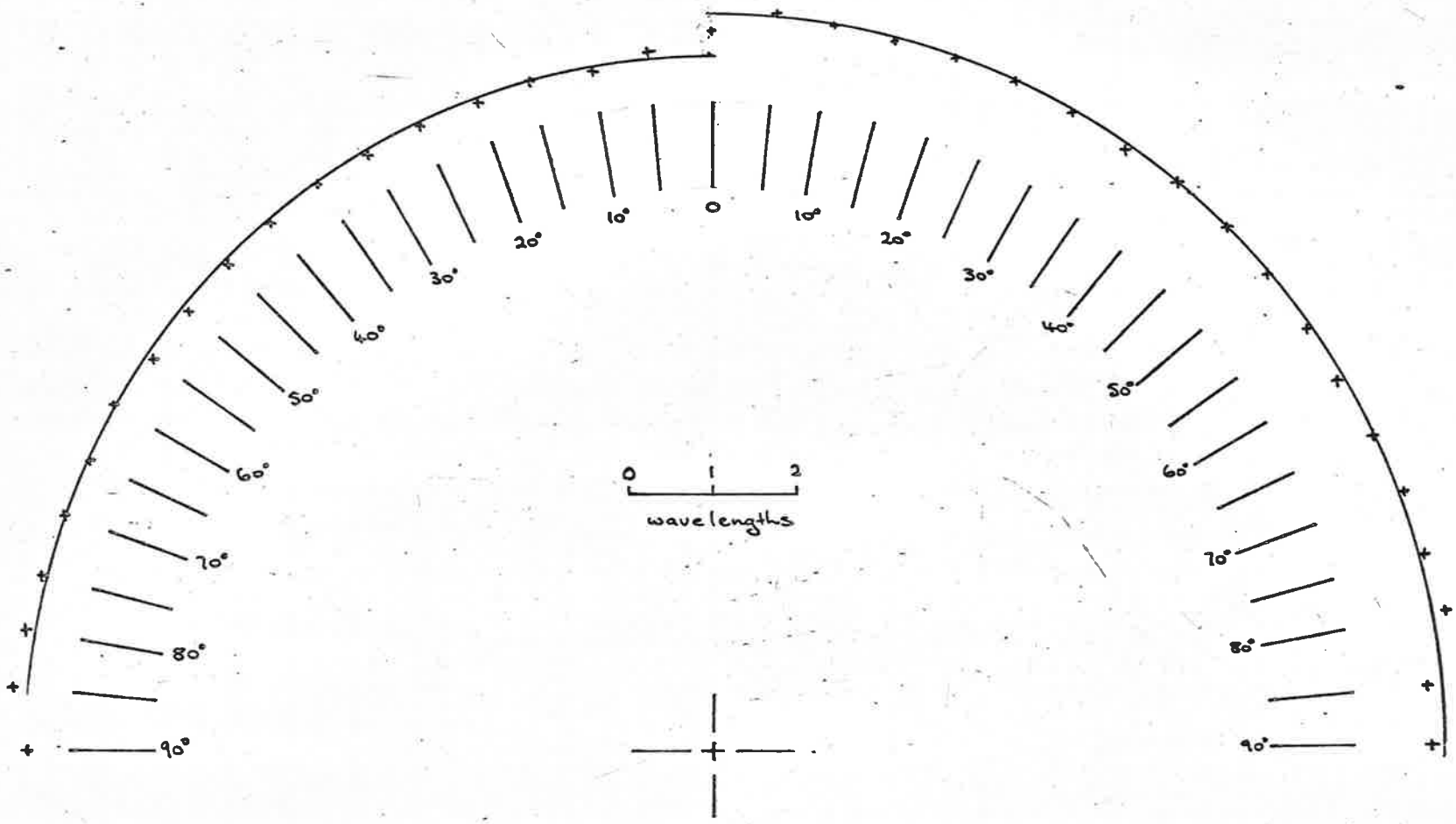

Fig. 5.19 TM_{01} Phase Front.

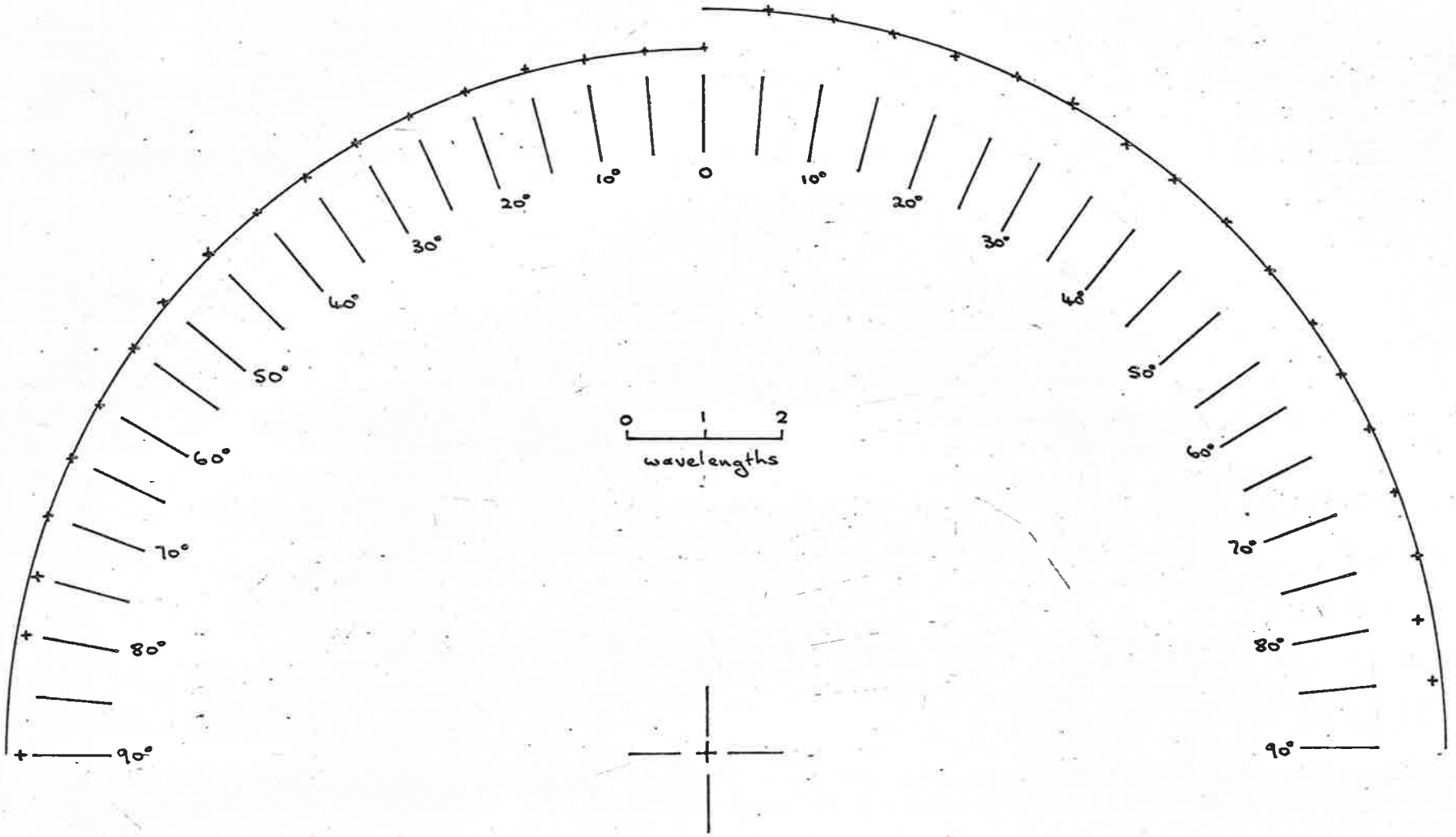

Fig. 5.20 TE01 Phase Centre.

mode and the TM_{01} mode. The increase in defocussing for the TE_{01} mode would be small and the change in secondary radiation insignificant.

The effect of the different phase centres for each of the modes will produce little discrepancy between the difference mode amplitude patterns, but will cause the phase errors to increase more rapidly with feed displacement. The phase errors may be separated into two parts. The first is an absolute error due to the different path lengths caused by the differing phase centres and will be approximately the same magnitude as the phase centre separation. This would be automatically compensated when aligning the system in the focussed case. The second and more important type of error is due to the differing variation in phase with elevation for the two modes with different degrees of defocussing. It is this error which will cause a reduction in the maximum feed displacement permissible.

Similarly the phase errors between the difference modes and the sum mode will be increased by the differential focussing and limit the extent of defocussing permissible.

It is difficult in general to estimate the maximum defocussing allowable in practice because other factors such as amplifier tolerances and reflector

surface tolerance must also be considered. However, with small differences, such as the 0.2λ in this case, the maximum allowable movement will remain at the order of 1.5 - 2.0λ and give beamwidth increases of approximately three times.

5.4 Conclusions

The multimode feed system for use with a focally excited reflector demonstrates that the provision of tracking facilities with such a system is feasible. This model shows that the difference mode radiation patterns are sufficiently alike to be regarded as the same in a practical servo system; that the phase centres of the three modes necessary in the ideal system, although not coincident, are sufficiently close together not to degrade significantly the performance of the antenna compared with the perfect case; and finally that the cross-coupling between the modes can be reduced to low levels with relatively unsophisticated techniques.

The model has several obvious disadvantages which preclude its use in a practical antenna system. The cable feed system is undesirable because of the losses associated with the cable introducing noise and the difficulty in obtaining a good match between the cable and the slots. The continuous annular slots used to

excite the TM_{01} mode produces high mutual coupling between the feed points. This slot and its coaxial shield may also affect other desirable modes in the waveguide. As the TE_{11} mode in coaxial shield is well above cut-off, the quarter wavelength section reflects an infinite impedance for this mode at the slot, causing a mismatch for the mode in the main waveguide. However as the TE_{11} mode in waveguide has predominantly circumferential wall currents, the effect is not great. More important is the effect of such a slot on any TM_{11} mode present. This mode has solely longitudinal currents and will excite the slot. In this case the corresponding mode in the coaxial waveguide is well below cut-off and will present a high reactance to the incident wave. The effect of this would be to prevent propagation of the TM_{11} mode to the aperture.

Most of these problems associated with the TM_{01} feed could be overcome by using the minimum four slots required for discrimination against the second order mode and by using dielectric loading to reduce the physical length of the slots to a less significant proportion of the waveguide periphery; for half wave slots take approximately one half the waveguide periphery. Such slots could then be waveguide excited.

The provision of power dividing networks to

excite the difference modes is unavoidable, although the number can be minimized. In a workable system, the power division must be lossless.

A diagrammatic representation of a modified feed system suitable for use in a low noise system is given in fig. 5.21. In this feed the dominant TE_{11} mode is again excited in a section of waveguide for which all other modes are cut off. Any convenient means of excitation can be used. This sketch shows a turnstile junction which allows right and left hand circular polarizations to be detected and is relatively compact. The waveguide is then expanded through a tapered transition to a size where only the TM_{01} and TE_{11} mode may propagate, all other modes being evanescent. To discriminate against the TE_{11} mode, two circumferential slots are required to excite the TM_{01} mode. This necessitates a single two way power divider, which may be a relatively simple waveguide Y-type.

The next transition converts the waveguide into one in which the TE_{01} mode may propagate and this mode is excited by four longitudinal slots to discriminate against the TE_{11}, TM_{11} and TE_{21} modes which may also propagate. Coupling to the TM_{01}, and also the TM_{11}, is minimized by the longitudinal slots which are not excited by the longitudinal wall currents of these modes.

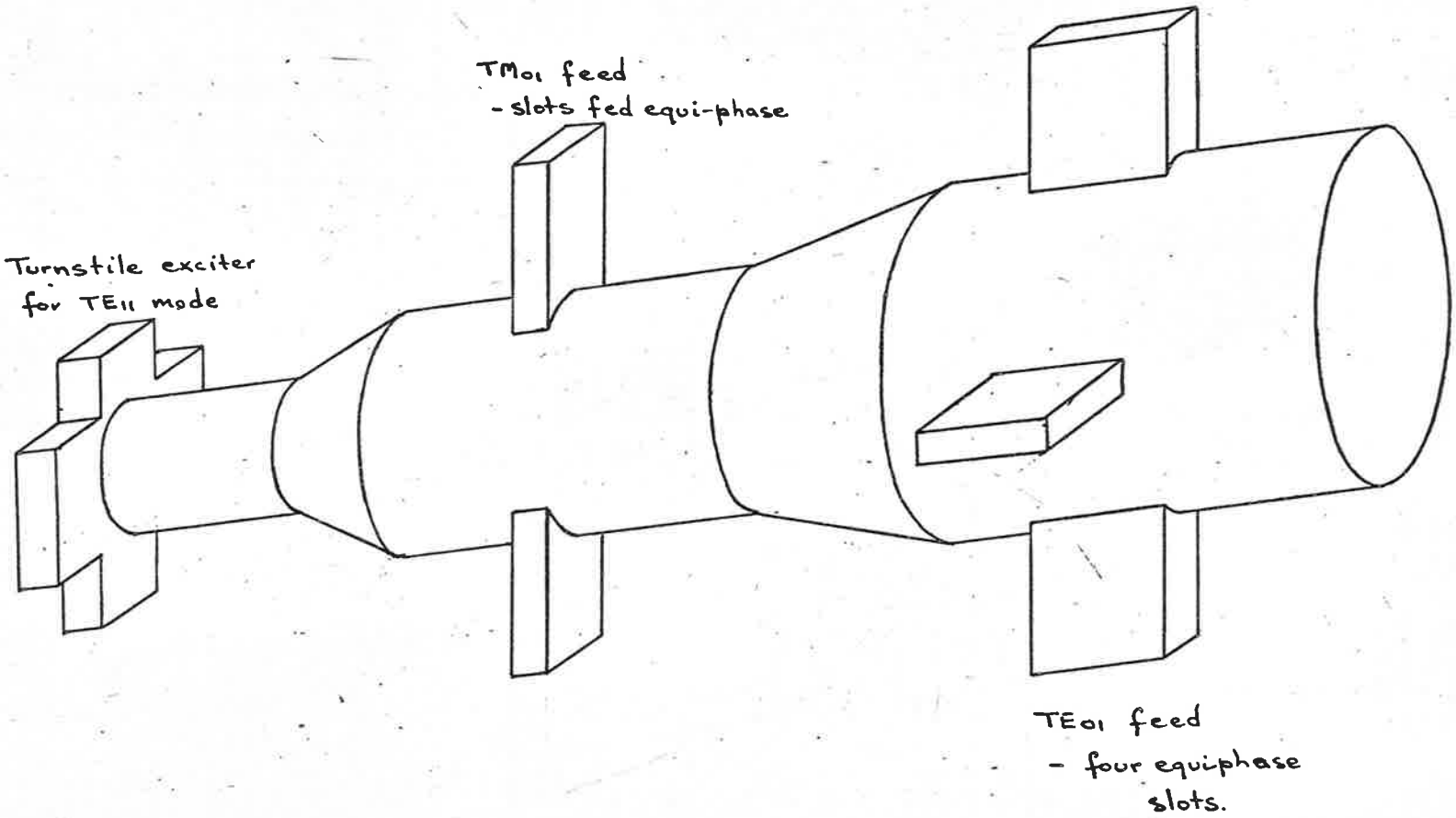

Fig. 5.21 Low Noise Tracking Feed.

Any mode conversion from the TE_{11} to the TM_{11} mode, desired to improve sum mode efficiency, can be achieved at this last transition since the TM_{02} mode is still evanescent and the TE_{21} is not excited from symmetry considerations. The TE_{01} exciter requires three two-way power dividers.

The position of the exciting slots must be made an integral number of half wavelengths from the cut off point in the preceding taper in order to achieve maximum foward propagation. This distance is necessary since the waveguide at cut off presents a high reactance to the incident wave which is reflected in phase. The determination of this position can be found experimentally, or, if the taper is slow, it may be estimated by first obtaining the approximate phase shift one way in the taper by integrating the phase constant with distance, i.e.:

$$\theta_{taper} = \int_{z_2}^{z_1} \beta \, dz$$

where $$\beta = [k^2 - (\frac{u}{a})^2]^{\frac{1}{2}}$$

with $$k = \frac{2\pi}{\lambda} ,$$

u derived from the boundary conditions

$$J_o'(u) = 0 \text{ for } TE_{01}$$

$$J_o(u) = 0 \text{ for } TM_{01}$$

and $a = a(z)$ is the radius of the waveguide at z.

z_1, z_2 are the limits of the taper given by the maximum dimension and the point at which the mode cuts off, i.e. $\beta = 0$. This technique allows reasonable accuracy because the rate of change of phase decreases to zero at cut-off.

Because of the large physical length of this type of feed horn, the multimode technique of providing tracking facilities is more suited to Cassegrain antennae than the focally excited antennae, except in the case of extremely large reflectors where the feed system is small compared with the reflector itself. The cassegrain system also has other advantages which include the greater flexibility in design for high efficiency and low noise illumination and also shorter transmission lines from the feed to the receiving equipment. It was shown in Chapter III that the cassegrain antenna was relatively insensitive to the feed horn focussing, and that, even though the larger primary feed aperture necessary to illuminate the sub-reflector introduces more uncertainty into the phase centre positions, the performance of the overall system will not be degraded by the focussing errors of the feed system. If a cassegrain system is to be defocussed, wave curvature

is achieved by moving the sub-reflector so that, over the few wavelengths of movement permissible, the additional phase errors caused by differential feed focussing will be negligible.

CHAPTER VI

CONCLUSIONS

The provision of tracking facilities in antenna installations designed for use in deep space research programs, is necessary to allow the flight path of the vehicle to be ascertained. Any corrections required can then be made. The inclusion of the tracking system in the feed system for the main reflector would allow more efficient use of the reflector, as well as increasing the tracking accuracy and range available, as compared with those provided by the current technique of using a subsiduary low gain tracking antenna to establish the path.

The application of the conventional four horn monopulse technique and its derivatives to high gain low noise reflector antennae is limited by the difficulty in achieving efficient aperture illumination in the sum mode, and by the additional loss associated with bridge circuitry used to process the received signals. In this thesis, a new method of obtaining tracking information has been presented. The technique uses the zero order modes in circular waveguides to generate directly the difference mode patterns of a tracking system. The direction of the target relative to the antenna boresight axis is obtained by comparing the phases of

the error mode signals with those derived from the usual dominant or sum mode. This system has the advantage of being completely compatible with any of the current techniques for improving the sum mode feed characteristics, and of allowing the tracking information to be obtained without jeopardizing the ultimate receiving capability of the antenna. Against this feature must be weighed the increased complexity of the signal processing circuits. However, the cost of a complex receiver is much less than the increase in cost necessary if the same performance is achieved by using a larger antenna and a less efficient feed system.

The multimode tracking feed system can be described as circular polarization oriented. The rather complex circuit required if tracking in a completely polarization diverse situation is necessary, can be considerably simplified where predominantly one type of circular polarization will be received. The simplified processor, which requires approximately half the number of components compared with the complete circuit, introduces no tracking error, but only results in the loss of information contained in the ignored circular polarization component.

The system is completely compatible with the techniques used to improve the aperture efficiency and

noise performance of large reflector antennae in receiving roles, or, in other words, the tracking performance is not degraded by the application of these techniques. In fact, in all usable methods, the tracking performance is improved by these techniques, because the boundary conditions near the feed horn aperture to provide symmetrical sum mode radiation also satisfy the conditions for identical radiation patterns for the transverse magnetic and transverse electric difference modes. The methods used for achieving high aperture efficiency also cause the aperture efficiency of the primary radiator to decrease, thus making the relative difference feed aperture greater compared with the sum mode. Ideally, for maximum difference slope and hence pointing accuracy, the difference mode aperture should be twice that of the sum mode. The multimode tracking feed has a pointing performance comparable with that achieved by the simple four horn cluster.

As an extension to the problem of providing tracking facilities on narrow beam antennae, the possibility of beam broadening by defocussing was considered with a view to decreasing acquisition times. It was found that the simplest methods of achieving increased beamwidth were defocussing by axial displacement of the feed in a focally excited paraboloid and by axial

displacement of the sub-reflector in a cassegrain system: two techniques which can be considered equivalent. The usable increases obtained were only moderate, being about three times in beamwidth corresponding to about an order increase in search element size and an equivalent reduction in acquisition time. The maximum attainable increase in beamwidth is limited by phase errors, introduced between the sum and difference modes, which must be considered in conjunction with the amplifier and servo drive system tolerances. Some form of phase compensation with feed displacement is necessary between the sum and difference modes.

In a practical system there are further limitations to the degree of defocussing permissible. In general, a practical feed system will not have coincident phase centres for all three modes, nor necessarily for the same mode in different planes, causing differential defocussing of the entire system. This further aggravates the phase conditions.

The reflector surface is never ideal and has errors which may be separated into manufacturing errors and errors caused by deflections in the antenna caused by gravitation, wind loading, thermal expansion, etc. In an article describing the Haystack Microwave Research Facility, Weiss[23] gives the manufacturing tolerances

of some large antennae. The best accuracy is achieved on the Haystack antenna, for which the ratio of diameter to r.m.s. surface tolerance is 72,000. Using a conservative figure of 10,000 for a 150λ diameter antenna gives an r.m.s. surface tolerance of 0.015λ. With surface errors of this order, phase errors of the order of a few hundredths of a wavelength could be expected and would not significantly effect the phase characteristics of the antenna radiation. More important, however, are the errors produced by antenna deflections in working positions. These are usually several times greater than the manufacturing tolerance, but are a specific property of an antenna installation and cannot be predicted. Provided that the surface phase errors do not become a significant part of a wavelength, perhaps one tenth, their effect on the phase characteristics can also be ignored.

Overall, beam broadening by defocussing is not particularly attractive because the gains in acquisition time are not great compared with the added complexity in the system. Its application is more suited to cassegrain antenna systems where only a passive sub-reflector need be moved. In systems where automatic focussing is required to ensure that the best fit paraboloid surface is always used, the basic feed control equipment is

necessary and the extension to a defocussing system is more easily achieved. Once again, the cassegrain system with sub-reflector position control is more attractive.

APPENDIX I

RADIATION INTEGRALS

General formulae for radiation by microwave current and field distributions have been developed by Silver.[56] This appendix gives particular forms suitable for the computation of radiation fields from plane apertures, paraboloidal reflectors and hyperboloidal reflectors.

A1.1 Radiation from Plane Aperture

The general integral for radiation from a plane aperture in the Fraunhofer region is[57]

$$\underset{\sim}{E}_s = -\frac{jk}{4\pi}\cdot\frac{e^{-jkR}}{R}\int_{S'}\hat{\underset{\sim}{R}}\times\left[\hat{\underset{\sim}{n}}\times\underset{\sim}{E}-\left(\frac{\mu}{\epsilon}\right)^{\frac{1}{2}}\hat{\underset{\sim}{R}}\times\left(\hat{\underset{\sim}{n}}\times\underset{\sim}{H}\right)\right]\,e^{jk\underset{\sim}{\rho}\cdot\hat{\underset{\sim}{R}}}\,dS' \qquad (A1.1)$$

where $\underset{\sim}{E}$, $\underset{\sim}{H}$ are the electric and magnetic field intensities in the aperture and the coordinates are defined in fig. A1.1.

For a circular aperture

$$dS' = \rho\, d\rho\, d\eta$$

and the fields may be written as

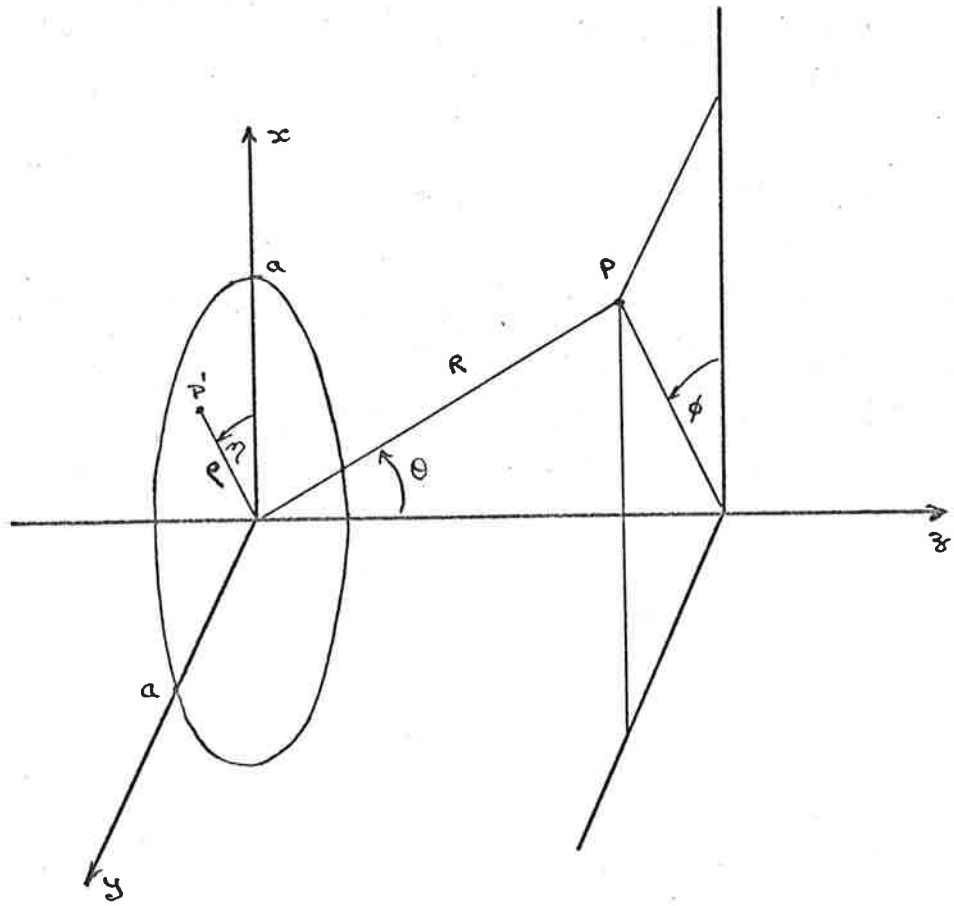

Fig. A1.1 Plane Aperture Co-ordinates

$$\underset{\sim}{E} = E_\rho \hat{\underset{\sim}{\rho}} + E_\eta \hat{\underset{\sim}{\eta}}$$

and $$\underset{\sim}{H} = H_\rho \hat{\underset{\sim}{\rho}} + H_\eta \hat{\underset{\sim}{\eta}}$$

Performing the scalar and vector products of equation (A1.1) gives the following expressions

$$\underset{\sim}{\rho} \cdot \hat{\underset{\sim}{R}} = \rho \sin\theta . \cos(\phi-\eta)$$

$$\hat{\underset{\sim}{R}} \times (\hat{\underset{\sim}{n}} \times \underset{\sim}{E}) = -\hat{\underset{\sim}{\theta}} [E_\rho \cos(\phi-\eta) + E_\eta \sin(\phi-\eta)]$$

$$+ \hat{\underset{\sim}{\phi}} [E_\rho \sin(\phi-\eta) - E_\eta \cos(\phi-\eta)] \cos\theta$$

and

$$-\hat{\underset{\sim}{R}} \times [\hat{\underset{\sim}{R}} \times (\hat{\underset{\sim}{n}} \times \underset{\sim}{H})] = \hat{\theta} [H_\rho \sin(\phi-\eta) - H_\eta \cos(\phi-\eta)] \cos\theta$$

$$+ \hat{\phi} [H_\rho \cos(\phi-\eta) + H_\eta \sin(\phi-\eta)]$$

Hence equation (A1.1) may be rewritten as

$$\left.\begin{matrix} E_\theta \\ E_\phi \end{matrix}\right\} = -\frac{jk}{4\pi} \cdot \frac{e^{-jkR}}{R} \left\{\begin{matrix} I_\theta \\ I_\phi \end{matrix}\right. \qquad \text{(A1.2)}$$

where

$$I_\theta = \int_0^{2\pi} \int_0^a \{-E_\rho \cos(\phi-\eta) - E_\eta \sin(\phi-\eta) + (\tfrac{\mu}{\epsilon})^{\frac{1}{2}} \cdot$$

$$[H_\rho \sin(\phi-\eta) - H_\eta \cos(\phi-\eta)] \cos\theta\}$$

$$\exp\{jk\rho \sin\theta \cos(\phi-\eta)\} \rho \, d\rho \, d\eta \qquad \text{(A1.3)}$$

and

$$I_\phi = \int_0^{2\pi}\int_0^a \{[\, E_\rho \sin(\phi-\eta) - E_\eta \cos(\phi-\eta)\,]\cos\theta + (\tfrac{\mu}{\epsilon})^{\frac{1}{2}}[\, H_\rho \cos(\phi-\eta) + H_\eta \sin(\phi-\eta)]\}\exp\{\ldots\}\,\rho\, d\rho\, d\eta \qquad (A1.4)$$

These expressions are most often used for the evaluation of radiation from a waveguide radiator.

The aperture fields for a waveguide radiator, propagating the m^{th} order mode, may be written

$$E_\rho = E_\rho(\rho).\cos m\,\eta$$
$$E_\eta = E_\eta(\rho).\sin m\,\eta$$
$$H_\rho = H_\rho(\rho).\sin m\,\eta$$
$$H_\eta = H_\eta(\rho).\cos m\,\eta$$

Substituting these expressions into equations (A1.3) and (A1.4) together with the relation

$$\exp\{\, jk\rho\sin\theta.\cos(\phi-\eta)\} = \sum_{n=-\infty}^{n=+\infty} j^n J_n(k_\rho \sin\theta)\cos n(\phi-\eta)$$

and integrating over the angle η,

$$I_\theta = -2\pi\, j^{m+1}\cos m\phi\int_0^a \{[-E_\rho - (\tfrac{\mu}{\epsilon})^{\frac{1}{2}} H_\eta\cos\theta]J_m'(k\rho\sin\theta) + [E_\eta - (\tfrac{\mu}{\epsilon})^{\frac{1}{2}} H_\rho\cos\theta]\frac{m\,J_m(k\rho\sin\theta)}{k\rho\sin\theta}\}\,\rho\, d\rho \qquad (A1.5)$$

and

$$I_\phi = -2\pi j^{m+1} \sin m\phi \int_0^a \{[E_\rho \cos\theta + (\tfrac{\mu}{\epsilon})^{\frac{1}{2}} H_\eta] \frac{m J_m(k\rho \sin\theta)}{k\rho \sin\theta}$$

$$- [E_\eta \cos\theta - (\tfrac{\mu}{\epsilon})^{\frac{1}{2}} H_\rho] J'_m(k\rho \sin\theta)\} \rho \, d\rho \quad (A1.6)$$

where the field terms are only dependent on ρ.

If the aperture field is rotated through one quadrant, so that

$$E_\rho = E_\rho(\rho).\sin m\eta \qquad H_\rho = H_\rho(\rho).\cos m\eta$$

$$E_\eta = E_\eta(\rho).\cos m\eta \qquad H_\eta = H_\eta(\rho).\sin m\eta,$$

the similar radiation expressions are

$$I_\theta = 2\pi j^{m+1} \sin m\phi \int_0^a \{[E_\rho + (\tfrac{\mu}{\epsilon})^{\frac{1}{2}} H_\eta \cos\theta] J'_m(u)$$

$$+ [E_\eta - (\tfrac{\mu}{\epsilon})^{\frac{1}{2}} H_\rho \cos\theta] \frac{m J_m(u)}{u} \rho \, d\rho \quad (A1.7)$$

and

$$I_\phi = 2\pi j^{m+1} \cos m\phi \int_0^a \{[E_\rho \cos\theta + (\tfrac{\mu}{\epsilon})^{\frac{1}{2}} H_\eta] \frac{m J_m(u)}{u}$$

$$+ [E_\eta \cos\theta - (\tfrac{\mu}{\epsilon})^{\frac{1}{2}} H_\rho] J'_m(u)\} \rho \, d\rho \quad (A1.8)$$

where $u = k\rho \sin\theta$.

From equations (A1.5) and (A1.6) or equations (A1.7) and (A1.8) it is easily deduced that symmetric radiation patterns require either

$$E_\rho(\rho) = \left(\frac{\mu}{\epsilon}\right)^{\frac{1}{2}} H_\rho(\rho)$$

$$\text{and} \quad E_\eta(\rho) = -\left(\frac{\mu}{\epsilon}\right)^{\frac{1}{2}} H_\eta(\rho) \qquad \text{(A1.9)}$$

or

$$E_\rho(\rho) = -\left(\frac{\mu}{\epsilon}\right)^{\frac{1}{2}} H_\rho(\rho)$$

$$\text{and} \quad E_\eta(\rho) = \left(\frac{\mu}{\epsilon}\right)^{\frac{1}{2}} H_\eta(\rho) \qquad \text{(A1.10)}$$

A1.2 Radiation from a Focussed Paraboloidal Reflector

The forward radiation from a large paraboloidal reflector can be treated in two ways: if the aperture field distribution is known and has a plane wave front, the radiation integrals developed above can be used, or, if the surface current distribution over the reflector is known, this can be used to determine the radiation pattern.

In the aperture integration technique, the expressions developed in the previous section can be further simplified since the aperture fields now satisfy the far field condition

$$\underset{\sim}{H} = \left(\frac{\epsilon}{\mu}\right)^{\frac{1}{2}} (\underset{\sim}{\hat{n}} \times \underset{\sim}{E})$$

where $\hat{\underset{\sim}{n}}$ = direction of propagation of the incident energy

= $\hat{\underset{\sim}{z}}$ for a plane aperture.

With this condition and for fields with symmetric radial distributions, the integral portions of equations (A1.5) to (A1.8) reduce to the familiar

$$(1 + \cos\theta) \int_0^a f(\rho).\ J_m(k\rho \sin\theta)\ \rho\ d\rho \qquad (A1.11)$$

where $f(\rho)$ = radial distribution function.

The aperture integration technique provides a convenient method of assessing the effect of changes in radial distribution on the radiation pattern. However, where only the primary feed radiation is specified, the aperture field must be approximated by the simple optical reflection law at the reflector surface, with inherent error except in the limit of zero wavelength. This limitation, together with the requirement that the wavefront in the aperture must be plane, makes the method unadaptable to situations where large phase errors may occur. In these cases, the radiation can be approximated by integrating over the surface currents induced on the reflector surface by the primary field.

Referring to fig. A1.2, the far zone scattered

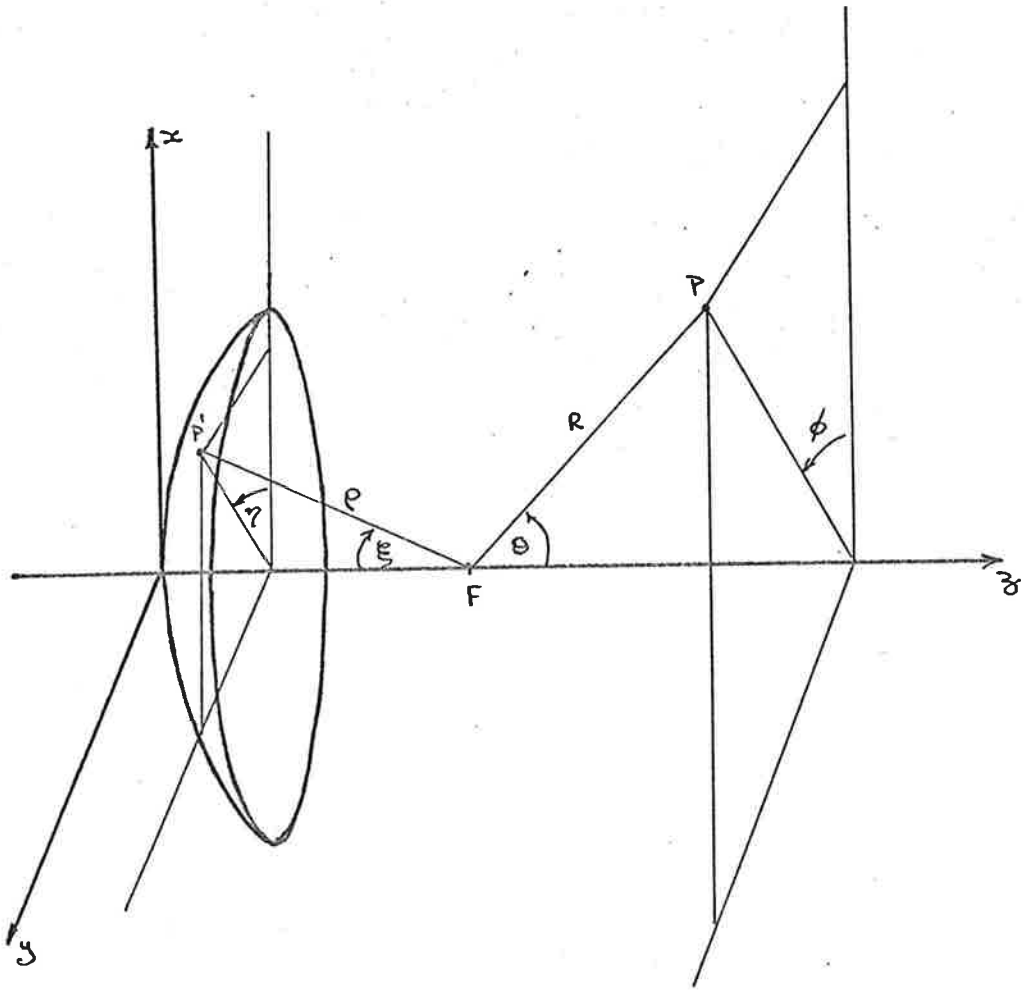

Fig. A1.2 Paraboloidal Reflector Co-ordinates.

field intensity of a current distribution on a reflector surface can be shown[44] to be

$$\underset{\sim}{E}_s = -\frac{j\omega\mu}{2\pi R}\cdot e^{-jkR}\int_s \{\hat{\underset{\sim}{n}}\times\hat{\underset{\sim}{H}}_i - [(\hat{\underset{\sim}{n}}\times\underset{\sim}{H}_i).\hat{\underset{\sim}{R}}]\,\hat{\underset{\sim}{R}}\}\; e^{jk\underset{\sim}{\rho}.\hat{\underset{\sim}{R}}}\,dS \qquad (A1.12)$$

where $\hat{\underset{\sim}{n}}$ = normal to the reflector surface

$\underset{\sim}{H}_i$ = incident magnetic field intensity

and $2(\hat{\underset{\sim}{n}}\times\underset{\sim}{H}_i)$ = surface current density.

Assuming the reflector to lie wholly in the far field of the primary feed

$$\underset{\sim}{H}_i = \left(\frac{\varepsilon}{\mu}\right)^{\frac{1}{2}}\hat{\rho}\times\underset{\sim}{E}_i$$

and equation (A1.12) becomes

$$\left.\begin{matrix}E_\theta\\ E_\phi\end{matrix}\right\} = -\frac{j\omega\mu}{2\pi R}\cdot e^{-jkR}\left(\frac{\varepsilon}{\mu}\right)^{\frac{1}{2}}\begin{cases}\hat{\underset{\sim}{\theta}}.\underset{\sim}{I}\\ \hat{\underset{\sim}{\phi}}.\underset{\sim}{I}\end{cases} \qquad (A1.13)$$

where

$$\underset{\sim}{I} = \int_s \hat{\underset{\sim}{n}}\times(\hat{\underset{\sim}{\rho}}\times\underset{\sim}{E}_i)\,\exp\{jk\underset{\sim}{\rho}.\hat{\underset{\sim}{R}}\}\,dS \qquad (A1.14)$$

The incident field may be written

$$\underset{\sim}{E}_i = (E_\xi\hat{\underset{\sim}{\xi}} + E_\eta\hat{\underset{\sim}{\eta}})\,e^{-jk\rho} \qquad (A1.15)$$

producing a new phase term

$$\exp\{-jk\rho[1 - \hat{\underset{\sim}{\rho}} \cdot \hat{\underset{\sim}{R}}]\}$$

Evaluating the vector triple product

$$[\hat{\underset{\sim}{n}} \times (\hat{\underset{\sim}{\rho}} \times \underset{\sim}{E}_1)]_\theta \rightarrow E_\xi[\cos\theta.\cos\xi/2.\cos(\phi-\eta) - \sin\theta.\sin\xi/2] + E_\eta[\cos\theta.\cos\xi/2\sin(\phi-\eta)]$$

and (A1.16)

$$[\hat{\underset{\sim}{n}} \times (\hat{\underset{\sim}{\rho}} \times \underset{\sim}{E}_1)]_\phi \rightarrow [E_\xi \sin(\eta-\phi) + E_\eta \cos(\eta-\phi)]\cos\xi/2$$

The phase term may be expanded as

$$\exp\{-jk\rho[1 + \cos\theta.\cos\xi - \sin\theta.\sin\xi.\cos(\phi-\eta)]\}$$

and the elemental surface element

$$dS = \rho^2 \sin\xi \sec\xi/2 \, d\xi \, d\eta$$

Equation (A1.14) may now be written as

$$I_\theta = \int_0^{2\pi}\int_0^{E}\{E_\xi[\cos\theta.\cos\xi/2\cos(\phi-\eta) - \sin\theta.\sin\xi/2] + E_\eta\cos\theta.\cos\xi/2\sin(\phi-\eta)\}\exp\{-jk\rho[1 + \cos\theta\cos\xi - \sin\theta\sin\xi\cos(\phi-\eta)]\}\rho^2\sin\xi\sec\xi/2 \, d\xi \, d\eta$$

(A1.17)

and

$$I_{\phi} = \int_0^{2\pi} \int_0^{E} \{-E_{\xi} \sin(\phi-\eta) + E_{\eta} \cos(\phi-\eta)\} \exp\{....\}$$

$$\rho^2 \sin\xi \, d\xi \, d\eta \qquad (A1.18)$$

In general the incident field components may be written in the form

$$E_{\xi} = f_1(\xi) \sin m\eta \qquad (A1.19)$$

and $$E_{\eta} = f_2(\xi) \cos m\eta$$

Substituting these expressions into equations (A1.17) and (A1.18) and using

$$\exp\{ j k\rho \sin\theta . \sin\xi . \cos(\phi-\eta)\} =$$

$$\sum_{n=-\infty}^{n=+\infty} j^n J_n(k\rho \sin\theta . \sin\xi) \cos n(\phi-\eta)$$

the integrals may be reduced to

$$I_{\theta} = -2\pi j^{m+1} \sin m\phi \int_0^{E} \{f_1 [\cos\theta . \cos\xi/2 . J'_m(w) - j \sin\theta . \sin\xi/2 \, J_m(w)] + f_2 \cos\theta . \cos\xi/2 \frac{m J_m(w)}{w}\}$$

$$\exp\{-jk\rho[1 + \cos\theta\cos\xi]\} \rho^2 \sin\xi \sec\xi/2 \, d\xi \qquad (A1.20)$$

and

$$I_\phi = -2\pi\, j^{m+1} \cos m\phi \int_0^E \{f_1 \frac{m\, J_m(w)}{w} + f_2\, J'_m(w)\} \exp\{\ldots\}$$

$$\rho^2 \sin\xi\, d\xi \qquad (A1.21)$$

where $w = k\rho \sin\xi \sin\theta$

The similar expressions obtained if

$$E_\xi = f_1(\xi) \cos m\eta$$

and $$E_\eta = f_2(\xi) \sin m\eta$$

are

$$I_\theta = -2\pi\, j^{m+1} \cos m\phi \int_0^E \{f_1 \; [\cos\theta . \cos\xi/2 . J'_m(w)$$

$$- j \sin\theta . \sin\xi/2\, J_m(w)] - f_2 \cos\theta . \cos\xi/2 \frac{m\, J_m(w)}{w}\}$$

$$\exp\{-jk\rho[1 + \cos\theta \cos\xi]\} \rho^2 \sin\xi \sec\xi/2\, d\xi \qquad (A1.22)$$

and

$$I_\phi = -2\pi\, j^{m+1} \sin m\phi \int_0^E \{-f_1 \frac{m\, J_m(w)}{w} + f_2\, J'_m(w)\}$$

$$\exp\{\ldots\} \rho^2 \sin\xi\, d\xi \qquad (A1.23)$$

In the limit of zero wavelength, for which

$$\cos\theta \to 1 \quad \text{and} \quad \sin\theta \to 0,$$

equations (A1.20) to (A1.23) reduce to the corresponding aperture integration expressions.

A1.3 Diffraction by an Hyperboloidal Reflector

As an hyperboloidal reflector produces a divergent wave, the aperture integration technique does not apply. However, there are still two methods available for estimating the reflected field: the geometric optics approximation and the current integration technique. The former of these methods provides a simple, but poor, approximation to the scattered field, whereas the latter gives a more reliable result at the expense of much more complexity.

A1.3.1 Geometric Optics Approximation

From Silver[58] the expression for the geometric optics approximation to the scattered field is

$$\underset{\sim}{E}_p = \frac{\nu}{p}\left\{(\hat{\underset{\sim}{n}}_h \cdot \underset{\sim}{E}_i)\hat{\underset{\sim}{n}}_h + \hat{\underset{\sim}{n}}_h \times (\hat{\underset{\sim}{n}}_h \times \underset{\sim}{E}_i)\right\} D^{\frac{1}{2}}\, e^{-jkp} \qquad (A1.24)$$

where $\hat{\underset{\sim}{n}}_h$ = normal to the hyperboloidal surface

$\underset{\sim}{E}_i$ = incident electric field intensity at the reflector surface

and D = ratio of scattered power per unit solid angle to the incident power per unit solid angle

$$= \frac{R_\xi R_\eta \cos i}{(4\nu^2 + R_\xi R_\eta)\cos i + 2\nu\,[R_\xi \sin^2\theta_1 + R_\eta \sin^2\theta_2]}$$

with R_ξ, R_η = the principal radii of curvature

i = angle between incident ray and normal to surface

and θ_1, θ_2 = angles between the incident ray and the principal axes ξ, η of the reflector.

From fig. (A1.3)

$$\hat{\underset{\sim}{n}}_h = \frac{1}{m(\alpha)}\,[(1 - e\cos\alpha)\,\hat{\underset{\sim}{\nu}} + e\sin\alpha\,\hat{\underset{\sim}{\alpha}}] \qquad (A1.25)$$

where $m(\alpha) = [\,(1 - e\cos\alpha)^2 + (e\sin\alpha)^2\,]^{\frac{1}{2}}$

The principal axes are defined by

$$\hat{\underset{\sim}{\xi}} = \frac{1}{m(\alpha)}\,[\,e\sin\alpha\,\hat{\underset{\sim}{\nu}} - (1 - e\cos\alpha)\,\hat{\underset{\sim}{\alpha}}]$$

and $$\hat{\underset{\sim}{\eta}} = \hat{\underset{\sim}{\beta}}$$

Hence the principal radii of curvature can be readily established as

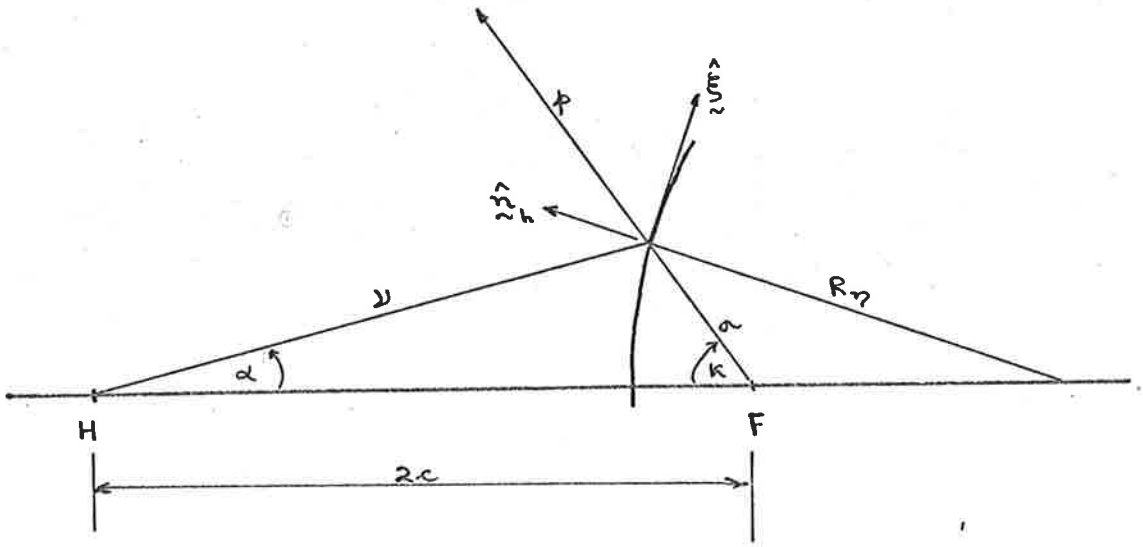

$\hat{\beta} = \hat{\eta}$ outwards from paper

Fig. A1.3 Hyperboloid Co-ordinates for Geometric Optics Approximation.

$$R_\eta = \nu\, m(\alpha)$$

and

$$R_\xi = \left| \frac{(\nu^2 + \nu'^2)^{3/2}}{\nu^2 + 2\nu'^2 - \nu\nu''} \right|$$

$$= \frac{\nu \cdot m^3(\alpha)}{(1 - e\cos\alpha)^2}$$

where $$\nu = \frac{-e.c\,(1 - \frac{1}{e^2})}{1 - e\cos\alpha}$$

Also $$\cos i = \hat{\underset{\sim}{\nu}} \cdot \hat{\underset{\sim}{n}}_h = -\frac{1 - e\cos\alpha}{m(\alpha)}$$

$$\sin\theta_1 = |\hat{\underset{\sim}{\nu}} \times \hat{\underset{\sim}{\xi}}| = -\frac{1 - e\cos\alpha}{m(\alpha)}$$

and $$\sin\theta_2 = |\hat{\underset{\sim}{\nu}} \times \hat{\underset{\sim}{\eta}}| = 1.$$

Hence $$D^{\frac{1}{2}} = \frac{m^2(\alpha)}{2(1 - e\cos\alpha) - m^2(\alpha)}$$

The polarization of the reflected field can be obtained from

$$\{(\hat{\underset{\sim}{n}}_h \cdot \underset{\sim}{E}_i)\hat{\underset{\sim}{n}}_h + \hat{\underset{\sim}{n}}_h \times (\hat{\underset{\sim}{n}}_h \times \underset{\sim}{E}_i)\} = -E_\alpha \hat{\underset{\sim}{\kappa}} - E_\beta \hat{\underset{\sim}{\beta}} \qquad (A1.25)$$

where $$\underset{\sim}{E}_i = E_\alpha \hat{\underset{\sim}{\alpha}} + E_\beta \hat{\underset{\sim}{\beta}}.$$

Accordingly, the magnitude of the reflected field is

$$E_p = E_i \frac{\nu}{\rho} D^{\frac{1}{2}} \qquad (A1.27)$$

Equation (A1.26) indicates that the reflected wave is spherical with an apparent source at F (fig. A1.3).

A1.3.2 Current Distribution Approximation

The development of the far zone scattered field by current integration over the surface of an hyperboloid reflector closely follows that of the paraboloid. Assuming the reflector to lie entirely in the far field of the primary radiator, equation (A1.12) can be written as

$$\left.\begin{matrix} E_\xi \\ E_\eta \end{matrix}\right\} = -\frac{j\omega\mu}{2\pi R} e^{-jkR} \left(\frac{\epsilon}{\mu}\right)^{\frac{1}{2}} \begin{Bmatrix} \hat{\xi} \cdot \underset{\sim}{I} \\ \hat{\eta} \cdot \underset{\sim}{I} \end{Bmatrix} \qquad (A1.28)$$

where

$$\underset{\sim}{I} = \int_s \hat{n}_h \times (\hat{\nu} \times \underset{\sim}{E}_i)\ e^{jk\underset{\sim}{\sigma}\cdot\hat{\rho}} dS \qquad (A1.29)$$

and the coordinates are given in fig. (A1.4).

Expressing the incident field by

$$\underset{\sim}{E}_i = (E_\alpha \hat{\alpha} + E_\beta \hat{\beta})\ e^{-jk\nu}$$

the new phase term becomes

$$\exp\{-jk[\nu - \underset{\sim}{\sigma}\cdot\hat{\rho}]\}$$

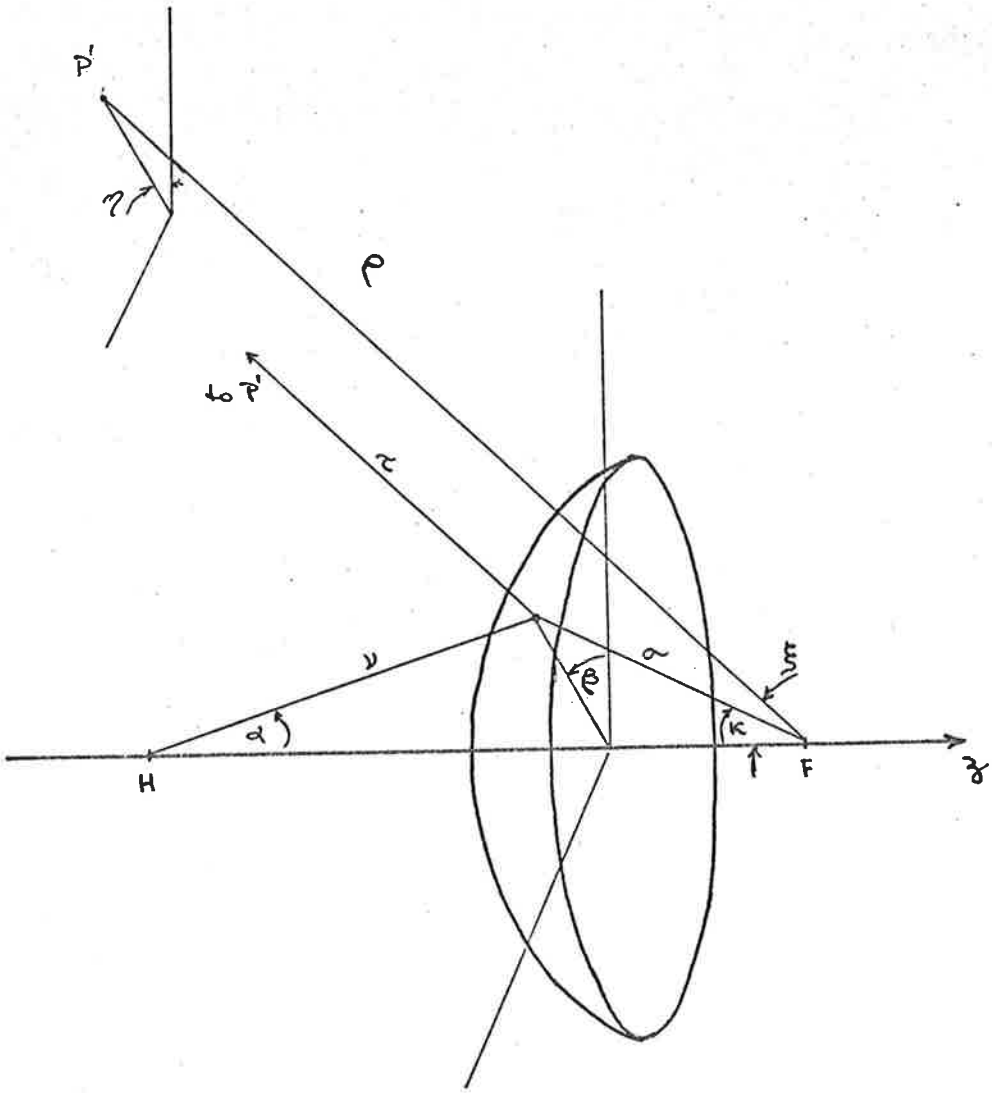

Fig. A1.4 Hyperboloid Co-ordinates.

Using equation (A1.25) the vector triple product can be expanded

$$[\hat{\underset{\sim}{n}}_h \times (\hat{\underset{\sim}{\nu}} \times \underset{\sim}{E}_i)]_\xi = \frac{1}{m(\alpha)} \{E_\alpha[\cos\xi(e - \cos\alpha)\cos(\eta-\beta) + \sin\xi\sin\alpha] - E_\beta \cos\xi(1 - e\cos\alpha)\sin(\eta-\beta)\}$$

and

$$[\hat{\underset{\sim}{n}}_h \times (\hat{\underset{\sim}{\nu}} \times \underset{\sim}{E}_i)]_\eta = \frac{1}{m(\alpha)} \{E_\alpha(\cos\alpha - e)\sin(\eta-\beta) - E_\beta(1 - e\cos\alpha)\cos(\eta-\beta)\}$$

The expanded phase term is

$$\exp\{-jk[\nu - \sigma(\cos\xi\cos\kappa + \sin\xi\sin\kappa\cos(\eta-\beta))]\}$$

and the elemental surface area is

$$dS = -\frac{\nu^2 \sin\alpha\, m(\alpha)}{1 - e\cos\alpha} \cdot d\alpha\, d\beta$$

$$= dS(\alpha) \cdot m(\alpha)\, d\alpha\, d\beta$$

with $$\nu = \frac{-ec(1-\frac{1}{e^2})}{1 - e\cos\alpha}$$

The integral, equation (A1.29), may now be written as

$$I_{\xi} = \int_0^{2\pi} \int_0^{A} \{ E_{\alpha}[\cos\xi(e - \cos\alpha)\cos(\eta-\beta) + \sin\xi \sin\alpha]$$

$$- E_{\beta} \cos\xi (1 - e\cos\alpha) \sin(\eta-\beta)\} \quad \exp\{....\}$$

$$dS(\alpha)\, d\alpha\, d\beta \qquad (A1.30)$$

and

$$I_{\eta} = \int_0^{2\pi} \int_0^{A} \{E_{\alpha} (\cos\alpha - e) \sin(\eta-\beta) - E_{\beta}(1 - e\cos\alpha)\cos(\eta-\beta)\}$$

$$\exp\{....\}\, dS(\alpha)\, d\alpha\, d\beta \qquad (A1.31)$$

Writing the incident field components in the form

$$E_{\alpha} = f_1(\alpha) \sin m\beta$$

and $$E_{\beta} = f_2(\alpha) \cos m\beta$$

and using the expression

$$\exp\{+ jk\sigma \sin\xi \sin\kappa \cos(\eta-\beta)\} =$$

$$\sum_{n=-\infty}^{n=\infty} j^n J_n(k\sigma \sin\xi \sin\kappa) \cos n(\eta-\beta)$$

equations (A1.29) and (A1.30) may be reduced to

$$I_\xi = -2\pi\, j^{m+1} \sin m\eta \int_0^A \{f_1 [\cos\xi(e-\cos\alpha)\, J_m'(u) + j \sin\xi \sin\alpha\, J_m(u)] - f_2 \cos\xi(1-e\cos\alpha)\frac{m\, J_m(u)}{u}\}$$

$$\exp\{-jk[\nu - \sigma\cos\xi\cos\kappa]\} dS(\beta)\, d\alpha \qquad (A1.32)$$

and

$$I_\eta = -2\pi\, j^{m+1} \cos m\eta \int_0^A \{f_1(e-\cos\alpha)\frac{m\, J_m(u)}{u} - f_2(1-e\cos\alpha)\, J_m'(u)\} \exp\{....\}\, dS(\alpha)\, d\alpha \qquad (A1.33)$$

where $u = k\sigma\sin\xi\sin\kappa$

$= k\nu\sin\xi\sin\alpha$

The similar expressions derived for

$$E_\alpha = f_1(\alpha)\cos m\beta$$

and $E_\beta = f_2(\alpha)\sin m\beta$

are

$$I_\xi = -2\pi\, j^{m+1} \cos m\eta \int_0^A \{f_1 [\cos\xi(e-\cos\alpha)\, J_m'(u) + j \sin\xi\sin\alpha\, J_m(u)] + f_2 \cos\xi(1-e\cos\alpha)\frac{m\, J_m(u)}{u}\}$$

$$\exp\{....\}\, dS(\alpha)\, d\alpha$$

and

$$I_\eta = -2\pi\, j^{m+1} \sin m\eta \int_0^A \{f_1(\cos\alpha - e)\, \frac{m\, J_m(u)}{u}$$

$$- f_2(1 - e\cos\alpha)\, J_m'(u)\} \exp\{....\}\, dS(\alpha)\, d\alpha$$

A1.3.3 Equivalent Paraboloid for a Cassegrain System

Hannan[6] has proposed an equivalent paraboloid to replace a dual reflector cassegrain system for calculation purposes. However, this must only be regarded as an approximation to the geometric optics approach and is thus less accurate.

Referring to fig. A1.5, the equivalent paraboloid is described by

$$\sigma = \frac{2\, f_e}{1 + \cos\alpha}$$

where $f_e = f\, \frac{e+1}{e-1}$

Hence the field distribution on the equivalent paraboloid can be represented as

$$E_e = \frac{E(\alpha,\beta)}{\sigma} \qquad (A1.34)$$

Expanding equation (A1.27) to give the true geometric optics amplitude distribution on the actual reflector gives

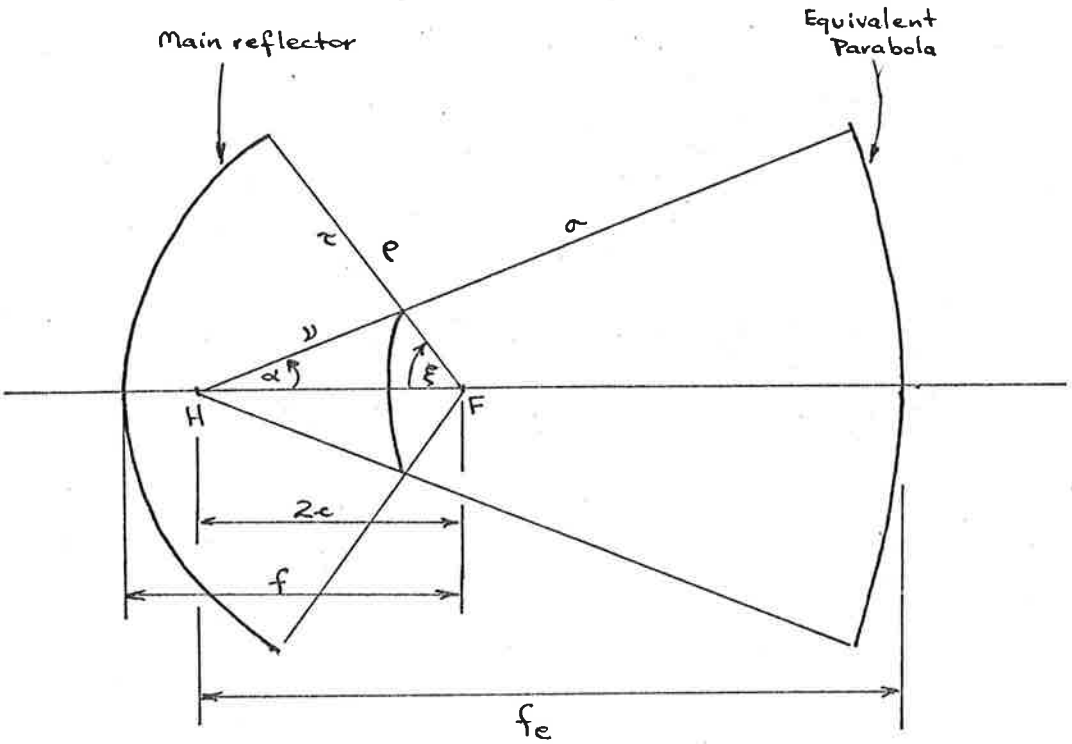

Fig. A1.5 Equivalent Parabola for a Cassegrain System.

$$E_a = \frac{E(\alpha,\beta)}{\sigma - \nu}$$

Comparison of this equation with equation (A1.34) shows that the equivalent paraboloid is only useful where the distance from the feed source to the sub-reflector is negligible compared with the distance to the equivalent paraboloid surface.

In the standard Cassegrain system used, the parameters were chosen to give the same aperture distribution as the feed gain function and these parameters are

paraboloid: $E = 60^\circ$ $(f/D = 0.433)$

$D/\lambda = 150$

hyperboloid: $c = 21.547$

$e = 1.591$

$A = 15^\circ$ $(D/\lambda = 20)$

With this system, the sub-reflector distance is approximately $1/8$ of the distance to the equivalent reflector and cannot be neglected.

APPENDIX II

INDEPENDENCE OF GAIN FUNCTIONS IN MULTIMODE RECEIVERS

Any antenna system consisting of a transmitter and receiver combination can be considered a linear network. The number of ports present is given by the number of modes detected in the main antenna plus one for the antenna located at some point in space.

Consider an antenna system with a two mode main antenna (Fig. A2.1(a)). By careful design of the exciter systems for each mode it is possible to reduce cross-coupling between the modes to a very low level. Thus in fig. A2.1(b) we can assumed no mutual coupling between ports (1) and (2).

From fig. A2.1(b)

A voltage v_1 in port (1) produces currents

$$i_{11} = y_{11} v_1$$

$$i_{31} = y_{13} v_1$$

and $i_{21} = 0$ (no mutual coupling)

and the current i_{31} in port (3) is independent of impedance z_2. A voltage v_3 in port (2) produces currents

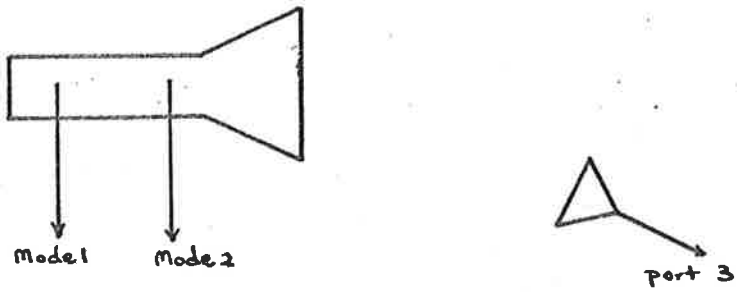

(a)

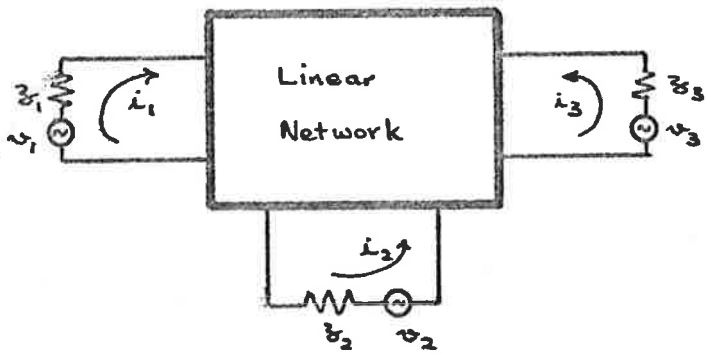

(b)

Fig. A2.1

$$i_{13} = y_{31}\, v_3$$

$$i_{23} = y_{32}\, v_3$$

and $$i_{33} = y_{33}\, v_3$$

By the reciprocity theorem,

$$y_{13} = y_{31}$$

i.e. $$\frac{i_{13}}{v_3} = \frac{i_{31}}{v_1}$$

and consequently the current in port (1) due to a driving voltage in port (3) is independent of the impedance z_2. A similar argument applies for ports (2) and (3) regarding the impedance z_1.

In the antenna situation this means that the relation between either of the modes in the main antenna and the distant antenna is independent of the second mode, whichever might be receiving or transmitting, provided that there is no mutual coupling between the two.

APPENDIX III

A COMPARISON OF FRESNEL AND FRAUNHOFER APPROXIMATIONS FOR SUB-REFLECTOR DIFFRACTION IN A CASSEGRAIN ANTENNA

In calculating the radiation from cassegrain antennae, the main reflector was assumed to lie entirely in the far field of the sub-reflector. In the example chosen, however, this was not strictly true, as is evident from the geometry of the system: the sub-reflector subtends an angle of 20° at the paraboloid vertex and the variations in distance from the vertex to points on the sub-reflector surface have a maximum of one wavelength. In order to assess the error introduced into the secondary radiation pattern by this assumption, the far-field approximation is compared with the Fresnel field approximation for the particular case of a focussed system.

From Silver, the near field solution for the scattered magnetic field intensity of a surface current distribution on a perfect conductor is

$$\underset{\sim}{H}_s = \frac{1}{2\pi} \int_s (\hat{\underset{\sim}{n}}_h \times \underset{\sim}{H}_i) \times \underset{\sim}{\nabla}\psi \; dS \qquad (A3.1)$$

where

$$\psi = \frac{e^{-jk\tau}}{\tau}$$

and $\underset{\sim}{H}_i$ = incident magnetic field at the reflector surface.

The coordinate system for a complete cassegrain system is given in fig. A3.1.

As the sub-reflector lies entirely in the far field of the primary radiator

$$\underset{\sim}{H}_i = \left(\frac{\epsilon}{\mu}\right)^{\frac{1}{2}} \hat{\underset{\sim}{\nu}} \times \underset{\sim}{E}_i$$

Also $$\underset{\sim}{\nabla}\psi = \left(jk + \frac{1}{\tau}\right) \frac{e^{-jk\tau}}{\tau} \hat{\underset{\sim}{\tau}}$$

Consequently,

$$\underset{\sim}{H}_s = \frac{j\omega\epsilon}{2\pi} \int_a \{[\hat{\underset{\sim}{n}}_h \times (\hat{\underset{\sim}{\nu}} \times \underset{\sim}{E}_i)] \times \hat{\underset{\sim}{\tau}}\}\left(1 - j\frac{1}{k\tau}\right).\frac{e^{-jk\tau}}{\tau} dS \qquad (A3.2)$$

where $$dS = -\frac{\nu^2 \sin\alpha\, m(\alpha)}{1 - e\cos\alpha} d\alpha\, d\beta$$

$$= -\frac{e\, c\, (1 - \frac{1}{e^2})}{1 - e\cos\alpha}$$

$$\tau = [\rho^2 + \sigma^2 - 2\rho\sigma(\cos\xi\cos\kappa + \sin\xi\sin\kappa\cos(\eta-\beta)]^{\frac{1}{2}}$$

For the example chosen, with parameters:

paraboloid: $D/\lambda = 150$ $f/D = 0.433$

hyperboloid: $c = 21.547$ $e = 1.591$

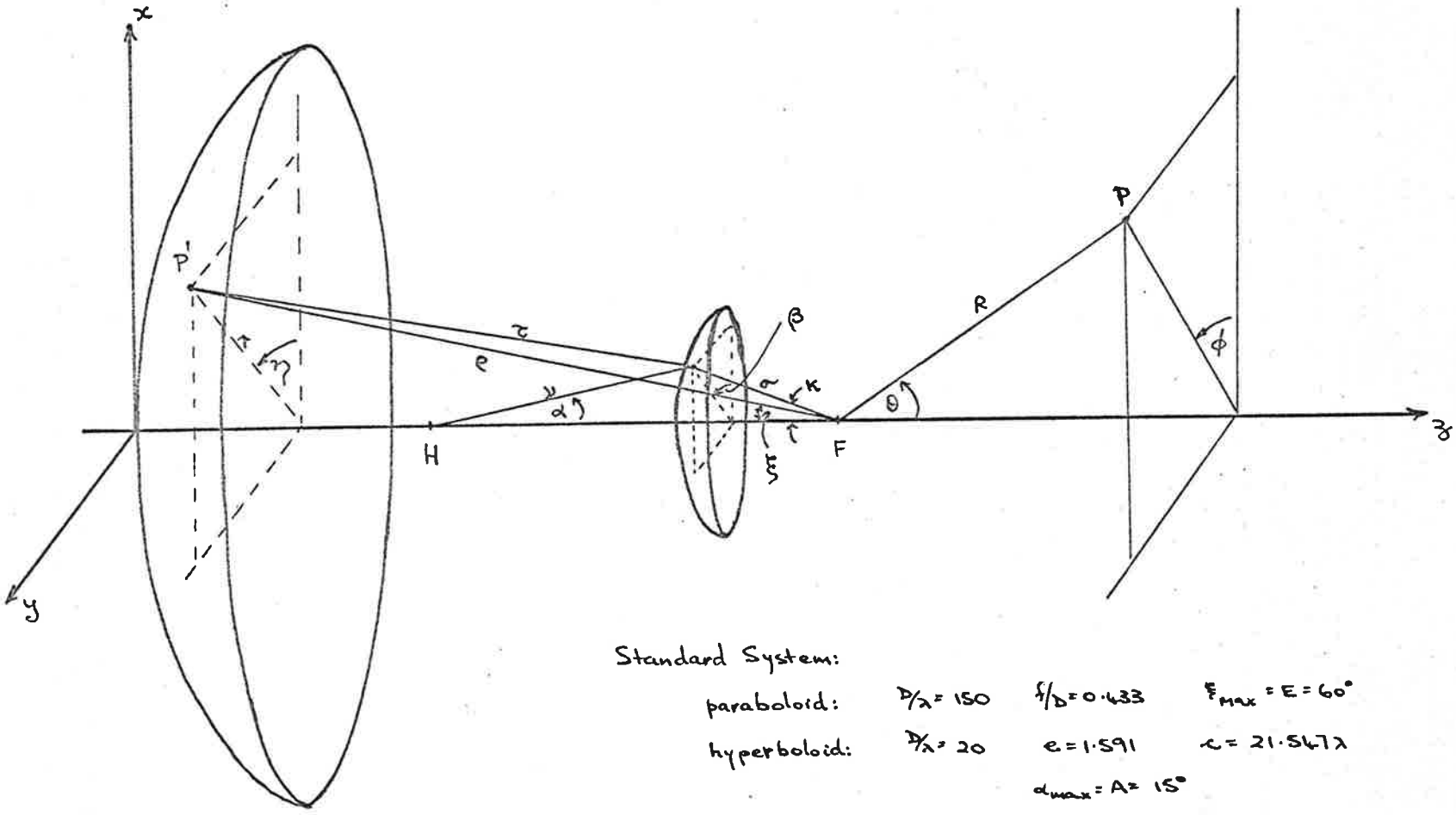

Standard System:

paraboloid:	$D/\lambda = 150$	$f/D = 0.633$	$\xi_{max} = E = 60°$
hyperboloid:	$D/\lambda = 20$	$e = 1.591$	$c = 21.547\lambda$
		$\alpha_{max} = A = 15°$	

Fig. A3.1 Cassegrain System Geometry.

$$k\tau > 300$$

and $(1 - \frac{1}{k\tau}) \simeq 1$

The incident electric field may be written as

$$\underset{\sim}{E}_i = (E_\alpha \, \underset{\sim}{\hat{\alpha}} + E_\beta \, \underset{\sim}{\hat{\beta}}) \frac{e^{-jk\nu}}{\nu}$$

The vector product is most conveniently evaluated by using the identity

$$[\underset{\sim}{\hat{n}}_h \times (\underset{\sim}{\hat{\nu}} \times \underset{\sim}{E}_i)] \times \underset{\sim}{\hat{\tau}} = (\underset{\sim}{\hat{\tau}} \cdot \underset{\sim}{\hat{n}}_h)(\underset{\sim}{\hat{\nu}} \times \underset{\sim}{E}_i) - [\underset{\sim}{\hat{\tau}} \cdot (\underset{\sim}{\hat{\nu}} \times \underset{\sim}{E}_i)] \underset{\sim}{\hat{n}}_h$$

The components of this expression are

$$\underset{\sim}{\hat{\tau}} \cdot \underset{\sim}{\hat{n}}_h = \frac{1}{\tau \, m(\alpha)} \{\rho[\sin\alpha \sin\xi \cos(\eta-\beta) - \cos\xi(\cos\alpha - e)] + ep + 2c(\cos\alpha - e)\} \quad (A3.3)$$

$$\underset{\sim}{\hat{\tau}} \cdot (\underset{\sim}{\hat{\nu}} \times \underset{\sim}{E}_i) = \frac{1}{\tau} \{E_\alpha \rho \sin\xi \sin(\eta-\beta) + E_\beta [-\rho(\sin\alpha\cos\xi + \sin\xi\cos\alpha\cos(\eta-\beta)) + 2c\sin\alpha]\} \quad (A3.4)$$

$$\hat{\underset{\sim}{\nu}} \times \underset{\sim}{E}_1 = \hat{\underset{\sim}{\rho}}: \quad E_\alpha \sin\xi \sin(\eta-\beta) - E_\beta \left[\sin\xi \cos\alpha \cos(\eta-\beta) + \cos\xi \sin\alpha\right]$$

$$\hat{\underset{\sim}{\xi}}: \quad E_\alpha \cos\xi \sin(\eta-\beta) - E_\beta \left[\cos\xi \cos\alpha \cos(\eta-\beta) - \sin\xi \sin\alpha\right]$$

$$\hat{\underset{\sim}{\eta}}: \quad E_\alpha \cos(\eta-\beta) + E_\beta \cos\alpha \sin(\eta-\beta) \qquad \text{(A3.5)}$$

$$\hat{\underset{\sim}{n}}_h = \frac{1}{m(\alpha)} \{\hat{\underset{\sim}{\rho}}: \quad \sin\xi \sin\alpha \cos(\eta-\beta) + \cos\xi(e - \cos\alpha)$$

$$\hat{\underset{\sim}{\xi}}: \quad \cos\xi \sin\alpha \cos(\eta-\beta) + \sin\xi(\cos\alpha - e)$$

$$\hat{\underset{\sim}{\eta}}: \quad -\sin\alpha \sin(\eta-\beta)\} \qquad \text{(A3.6)}$$

By making the substitutions

$$E_\alpha = f_1 \sin\beta$$

and $$E_\beta = f_1 \cos\beta$$

and inspecting the form of the resulting integral, the scattered magnetic field is seen to have the form

E-plane $\eta = \pi/2$ $\quad$ H_η component only

H-plane $\eta = 0$ $\quad$ H_ρ, H_ξ components only.

Hence, the Fresnel field may be approximated by

$$\underset{\sim}{H}_s = (H_\rho \hat{\underset{\sim}{\rho}} + H_\xi \hat{\underset{\sim}{\xi}})\cos\eta + H_\eta \sin\eta \hat{\underset{\sim}{\eta}} \qquad (A3.7)$$

Equation (A3.7) neglects any higher order variations with the angle η, that may be introduced by the phase term. However, as the radiation pattern from the sub-reflector is approximately symmetrical, little error is introduced.

The secondary radiation from the paraboloidal reflector may now be derived from the results of Appendix I.

$$\left.\begin{matrix} E_\theta \\ E_\phi \end{matrix}\right\} = -\frac{j\omega\mu}{2\pi R} \cdot e^{-jkR} \left\{ \begin{matrix} \hat{\underset{\sim}{\theta}} \cdot \underset{\sim}{I} \\ \hat{\underset{\sim}{\phi}} \cdot \underset{\sim}{I} \end{matrix} \right. \qquad (A3.8)$$

where $$\underset{\sim}{I} = \int_s \hat{\underset{\sim}{n}} \times \underset{\sim}{H}_s \exp\{jk\underset{\sim}{\rho} \cdot \underset{\sim}{R}\} \, dS \qquad (A3.9)$$

Expanding the integral (A3.9) gives

$$I_\theta = 2\pi j \sin\phi \int_0^E - H_\eta[\cos\theta \cos\xi/2 \, J_1'(w)$$

$$- j \sin\theta \sin\xi/2 \, J_1(w)] + (H_\rho \sin\xi/2 + H_\xi \cos\xi/2) \cos\theta$$

$$\frac{J_1(w)}{w}\} \exp\{-jk\rho \cos\xi \cos\theta\} \rho^2 \sin\xi \sec\xi/2 \, d\xi$$

and

$$I_\phi = 2\pi j \cos\phi \int_0^E \{ - H_\eta \cos \xi/2 \frac{J_1(w)}{w}$$

$$+ (H_\rho \sin \xi/2 + H_\xi \cos \xi/2) J_1'(w)\} \exp \{....\}$$

$$\rho^2 \sin\xi \sec \xi/2 \, d\xi$$

where $w = k\rho \sin\xi \sin\theta$.

In fig. A3.2 the scattered field from the hyperboloid is shown on the paraboloid surface for both the Fresnel approximation and the far field approximation. The results for the Fresnel case are presented as an "equivalent" electric field for direct comparison with the far field results. The equivalent electric field is derived from the magnetic field components by

$$E = (\frac{\mu}{\epsilon})^{\frac{1}{2}}.H \qquad \text{where } (\frac{\mu}{\epsilon})^{\frac{1}{2}} = \text{characteristic impedance of air.}$$

The phase curves for the H_ξ and H_η components are reduced to an equivalent spherical surface for ease of plotting. Consequently, both the gain and phase curves can be treated as the aperture distributions of the main reflector for a qualitative assessment. Only the E-plane characteristics are plotted for the far field

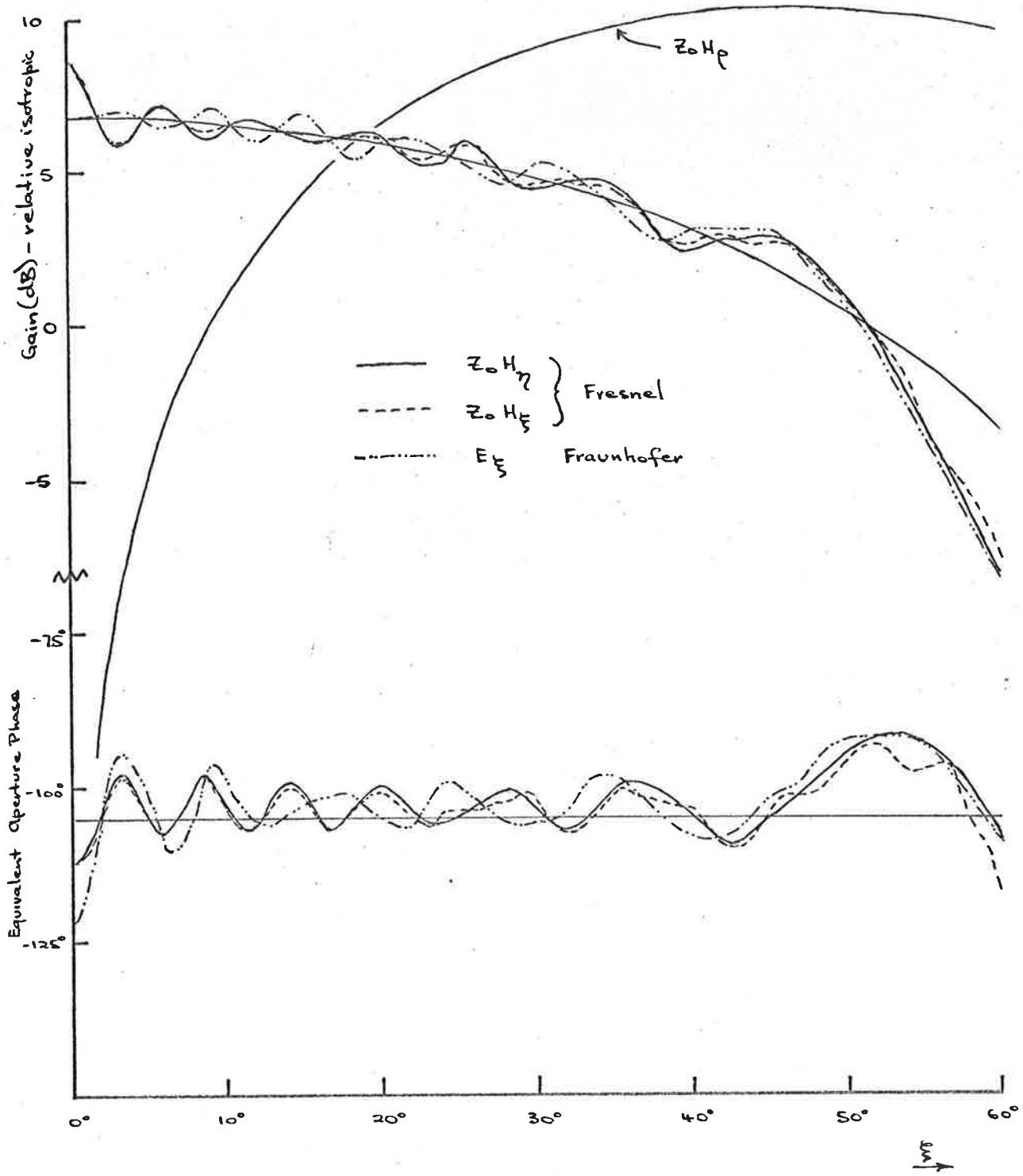

Fig. A3.2 Paraboloid Surface Field Intensities and Equivalent Aperture Phase Distributions for Fresnel and Fraunhofer Approximations.

case as the E- and H-plane characteristics are almost identical. The far field E-plane characteristic, E_ξ, is equivalent to the H_η pattern in the Fresnel case.

Ignoring the H_ρ component in the Fresnel field, the diagram shows that the Fresnel field produces an almost symmetric illumination function. Comparing this with the far field curves shows that the two approximations give similar results, producing interference ripples in the gain and phase curves of approximately the same magnitudes. Although the ripples do not correspond exactly, the small size of the variations (peak to peak amplitudes of about 1 dB and 10°), and large number of cycles over the main aperture (fourteen in the Fresnel case and twelve in the other), will produce small differences in the secondary radiation patterns calculated from the two distributions.

Although there is a large longitudinal magnetic field component in the Fresnel field, its phase is constant over the main reflector surface and corresponds to an aperture field with a very large phase taper, equivalent to a path length variation of 20λ from the centre to the edge of the aperture. Accordingly, the contribution of this component in the far field of the secondary pattern will be negligible at least over the first few sidelobes.

Fig. A3.3 gives the H-plane far field patterns for the main reflector using the far field and Fresnel approximations to the illumination function. The Fresnel patterns are plotted for the cases when the longitudinal component, H_ρ, is included, and for when it is ignored and assumed to contribute nothing in the far field. Of the two curves, the latter is a better indication of the actual far field radiation pattern, since the numerical integration process used only produces accurate results when the equivalent aperture phase taper is small. Any attempt to increase the integration accuracy would result in a prohibitive time for the calculation of the Fresnel field of the sub-reflector.

A comparison of the results of the full far field case and the Fresnel field case where the H_ρ contribution is assumed negligible, in fig. A3.3 and in the tabulated results in tables A3.2 and A3.3, shows that the gain and phase characteristics are almost identical over the main lobe and first three side lobes and can be assumed the same for practical purposes. Consequently, the far field approach to the cassegrain feed system provides a sufficiently accurate approximation to the gain functions.

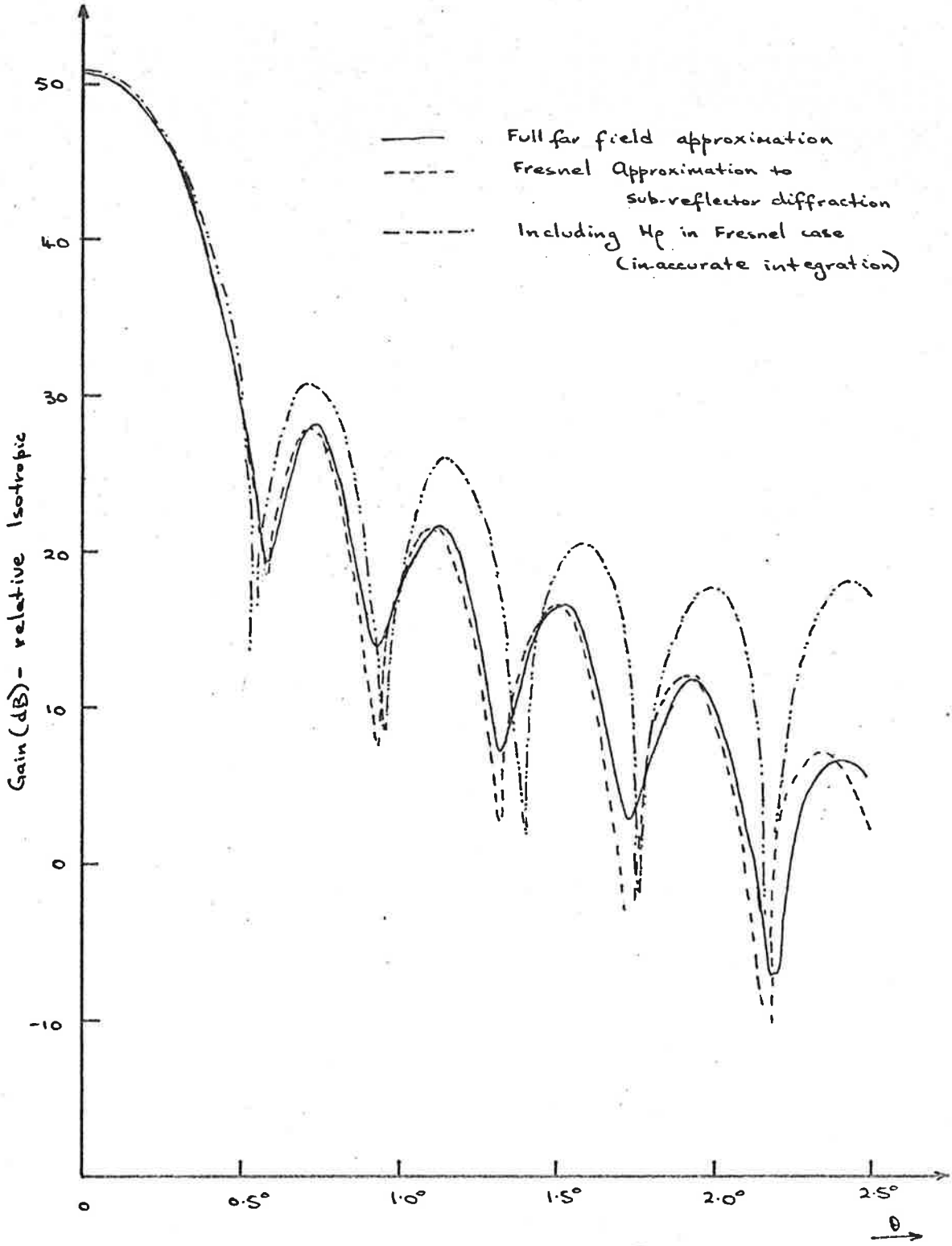

Fig. A3.3 Secondary Radiation from Cassegrain System.

10DB-TAPER

	E-PLANE		H-PLANE	
THETA	GAIN(dB)	PHASE	GAIN(dB)	PHASE
0.0	5.0856E+01	-86.48	5.0856E+01	-86.48
0.1	5.0295E+01	-86.56	5.0302E+01	-86.25
0.2	4.8549E+01	-86.83	4.8570E+01	-85.54
0.3	4.5388E+01	-87.42	4.5396E+01	-84.23
0.4	4.0202E+01	-88.79	4.0039E+01	-81.86
0.5	3.0778E+01	-93.58	2.9326E+01	-74.58
0.6	1.8495E+01	116.50	2.4601E+01	86.64
0.7	2.7326E+01	96.84	3.0583E+01	96.64
0.8	2.5667E+01	90.77	2.8995E+01	100.87
0.9	1.6881E+01	70.80	2.0548E+01	107.08
1.0	1.5840E+01	-54.25	1.7480E+01	-82.47
1.1	2.0542E+01	-72.85	2.5038E+01	-75.61
1.2	1.8523E+01	-81.97	2.5072E+01	-73.42
1.3	9.3619E+00	-115.30	2.0080E+01	-75.54
1.4	1.2300E+01	136.45	5.7110E+00	-171.24
1.5	1.5909E+01	121.17	1.8651E+01	130.78
1.6	1.3624E+01	113.98	2.0383E+01	126.97
1.7	3.1536E+00	82.97	1.6845E+01	119.08
1.8	8.1241E+00	-34.00	8.9932E+00	53.32
1.9	1.2100E+01	-42.15	1.5855E+01	-5.01
2.0	1.0430E+01	-41.56	1.7754E+01	-9.11
2.1	1.8342E+00	-38.52	1.4267E+01	-4.88
2.2	-6.8080E-01	148.87	-1.2779E+01	83.54
2.3	6.7397E+00	156.49	1.4103E+01	-175.31
2.4	7.0637E+00	167.81	1.7858E+01	-162.99
2.5	3.5763E+00	-176.38	1.7332E+01	-146.23

Table A3.1 Fresnel Field Secondary Radiation

(including longitudinal component, but with low integration accuracy)

10DB-TAPER

	E-PLANE		H-PLANE	
THETA	GAIN(dB)	PHASE	GAIN(dB)	PHASE
0.0	5.0776E+01	-84.82	5.0776E+01	-84.82
0.1	5.0203E+01	-84.91	5.0201E+01	-84.85
0.2	4.8419E+01	-85.23	4.8410E+01	-84.95
0.3	4.5180E+01	-85.95	4.5159E+01	-85.22
0.4	3.9825E+01	-87.62	3.9778E+01	-85.93
0.5	2.9837E+01	-94.02	2.9670E+01	-88.94
0.6	2.0665E+01	115.98	2.0225E+01	105.89
0.7	2.7598E+01	99.17	2.7481E+01	97.51
0.8	2.5324E+01	92.63	2.5124E+01	93.85
0.9	1.4865E+01	65.61	1.3662E+01	74.23
1.0	1.7802E+01	-59.29	1.7431E+01	-64.24
1.1	2.1489E+01	-72.89	2.1233E+01	-74.83
1.2	1.8957E+01	-81.67	1.8523E+01	-80.09
1.3	8.8901E+00	-121.22	6.3640E+00	-113.03
1.4	1.3706E+01	133.25	1.3185E+01	124.76
1.5	1.6933E+01	119.77	1.6496E+01	117.02
1.6	1.4525E+01	111.77	1.3818E+01	113.52
1.7	4.7597E+00	77.08	1.3184E+00	88.87
1.8	8.9693E+00	-30.64	8.2776E+00	-43.15
1.9	1.2651E+01	-42.03	1.1994E+01	-46.22
2.0	1.0785E+01	-44.90	9.8216E+00	-42.90
2.1	1.8399E+00	-55.72	-4.7750E-01	-33.42
2.2	1.5368E+00	168.47	9.2979E-01	143.14
2.3	7.5801E+00	163.86	6.6214E+00	156.96
2.4	7.3685E+00	171.23	6.2840E+00	173.75
2.5	2.8766E+00	-176.48	2.4668E+00	-161.14

Table A3.2 Fresnel Field Secondary Radiation

(neglecting longitudinal component)

MAIN FIELD 10DB-TAPER FEED

	E-PLANE		H-PLANE	
THETA	GAIN(DB)	PHASE	GAIN(DB)	PHASE
0.0	5.0744E+01	-84.65	5.0744E+01	-84.65
0.1	5.0173E+01	-84.72	5.0173E+01	-84.71
0.2	4.8395E+01	-84.95	4.8395E+01	-84.91
0.3	4.5169E+01	-85.48	4.5169E+01	-85.38
0.4	3.9839E+01	-86.79	3.9837E+01	-86.57
0.5	2.9916E+01	-91.95	2.9904E+01	-91.34
0.6	2.0211E+01	114.08	2.0153E+01	113.05
0.7	2.7542E+01	99.35	2.7536E+01	99.29
0.8	2.5387E+01	94.00	2.5377E+01	94.34
0.9	1.5058E+01	71.77	1.4944E+01	73.15
1.0	1.7243E+01	-59.38	1.7193E+01	-60.15
1.1	2.1313E+01	-71.69	2.1301E+01	-71.72
1.2	1.8995E+01	-78.40	1.8976E+01	-77.89
1.3	8.8103E+00	-108.07	8.5866E+00	-106.24
1.4	1.2621E+01	133.91	1.2556E+01	132.94
1.5	1.6465E+01	122.43	1.6453E+01	122.37
1.6	1.4415E+01	118.19	1.4403E+01	118.81
1.7	4.7200E+00	101.07	4.5498E+00	103.61
1.8	6.4928E+00	-30.82	6.4187E+00	-32.42
1.9	1.1485E+01	-37.49	1.1493E+01	-37.69
2.0	1.0350E+01	-33.62	1.0377E+01	-33.06
2.1	3.5656E+00	-23.79	3.6336E+00	-21.79
2.2	-6.9776E+00	143.50	-6.6087E+00	138.16
2.3	4.5822E+00	171.08	4.6683E+00	170.28
2.4	6.5613E+00	-170.16	6.6503E+00	-170.22
2.5	5.4884E+00	-151.91	5.5723E+00	-151.38

Table A3.3 Secondary Radiation, using far field approximation to illumination function.

APPENDIX IV

DIELECTRIC LINED WAVEGUIDE

A4.1 Introduction

Thin linings of either dielectric or magnetic materials in a waveguide modify the boundary conditions, so altering the propagation constants of the waveguide modes, and, in the case of modes of orders greater than zero, providing cross-coupling between equivalent transverse magnetic and transverse electric modes. In the context of high efficiency tracking feeds, linings are interesting because they may allow the equating of the tracking mode radiation patterns and the production of a symmetrical linearly polarized radiation pattern. The former condition requires that the TE_{01} and TM_{01} modes in the lined waveguide have identical propagation constants, and the latter requires that the waveguide fields satisfy the conditions derived in Appendix I, namely

$$E_\rho(\rho) = \pm \left(\frac{\mu}{\epsilon}\right)^{\frac{1}{2}} H_\rho(\rho)$$

$$E_\phi(\rho) = \mp \left(\frac{\mu}{\epsilon}\right)^{\frac{1}{2}} H_\phi(\rho)$$

The sign is chosen so that a non-zero central gain is produced. As the radiation conditions above can only be satisfied in the inner region and not within the

lining itself, the waveguide lining must be kept sufficiently thin for the contribution to the radiated field from the field within the lining to be negligible.

Because a practical antenna system must be capable of receiving any signal polarization, the waveguide lining used must not be polarization sensitive. This restricts the lining to anisotropic linings with inductive capacity tensors of the form

$$\underset{\sim}{\alpha} = \begin{bmatrix} \alpha_1 & 0 & 0 \\ 0 & \alpha_2 & 0 \\ 0 & 0 & \alpha_3 \end{bmatrix}$$

Gyromedia which have non-zero terms on other than the leading diagonal cause Faraday rotation of linearly polarized signals and different propagation constants for right and left hand circularly polarized signals, making it impossible to satisfy the radiation symmetry conditions for all polarizations. In this Appendix only uniaxially anisotropic media will be considered so that

$$\alpha_1 = \alpha_2$$

A4.2 Characteristic Equation and Field Components

Referring to fig. A4.1, the inner region is assumed to be uniform and homogeneous and to have

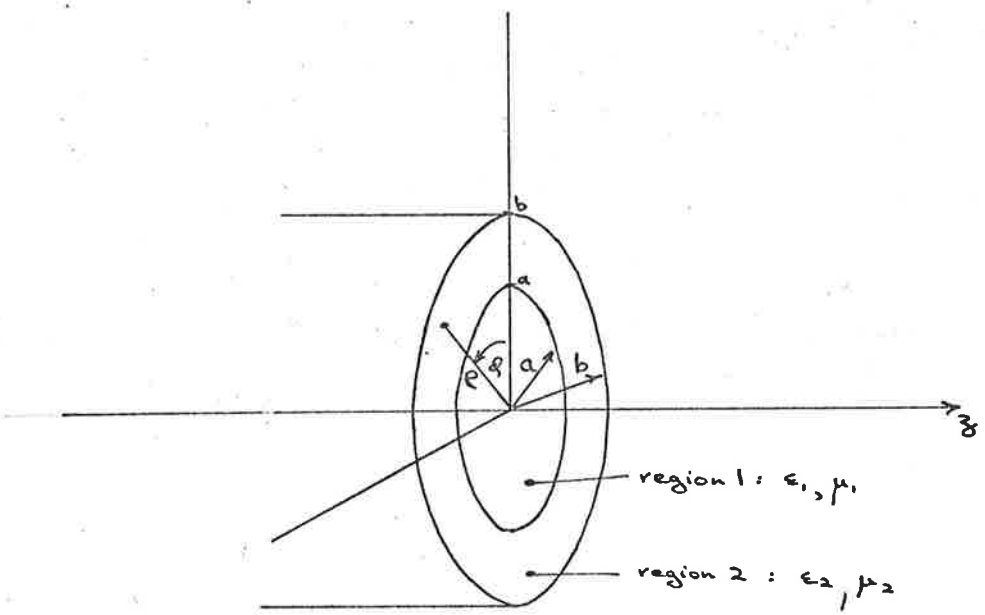

Fig. A4.1 Circular Waveguide with Lining

electric and magnetic inductive capacities ϵ_1 and μ_1 respectively. The outer region is uniaxially anisotropic and, in general, has inductive capacities

$$\underset{\sim}{\epsilon}_2 = \begin{bmatrix} \epsilon_2 & 0 & 0 \\ 0 & \epsilon_{2t} & 0 \\ 0 & 0 & \epsilon_{2z} \end{bmatrix} \quad \text{and} \quad \underset{\sim}{\mu}_2 = \begin{bmatrix} \mu_{2t} & 0 & 0 \\ 0 & \mu_{2t} & 0 \\ 0 & 0 & \mu_{2z} \end{bmatrix}$$

The boundary at $\rho = b$ is assumed to be perfectly conducting.

Following Harrington,[59] wave functions for the transverse electric and transverse magnetic components of a waveguide field may be chosen to satisfy the boundary conditions

$$E_\phi = E_z = 0 \quad \text{at } \rho = b$$

The wave functions are

region 1:

$$\psi_{m1} = A\, Jn(k_{\rho 1}\rho) \cos n\phi \; e^{-jk_z z}$$

$$\psi_{e1} = B\, Jn(k_{\rho 1}\rho) \sin n\phi \; e^{-jk_z z} \qquad (A4.1)$$

where $k_{\rho 1}^2 = k_1^2 - k_z^2 \quad (k_z < k_1)$

and $k_1^2 = \omega^2 \mu_1 \epsilon_1$

k_1 = free space propagation constant for region 1

k_z = waveguide propagation constant for given mode.

region 2:

$$\psi_{m2} = C\,[\,Jn(k_{\rho 3}\rho)Nn(k_{\rho 3}b) - Nn(k_{\rho 3}\rho)Jn(k_{\rho 3}b)]\;\cos n\phi\,.\,e^{-jk_z z} \qquad (A4.2)$$

$$\psi_{e2} = D\,[Jn(k_{\rho 4}\rho)Nn'(k_{\rho 4}b) - Nn(k_{\rho 4}\rho)Jn'(k_{\rho 4}b)]\;\sin n\phi\,.\,e^{-jk_z z}$$

where $$k^2_{\rho 3} = \frac{\epsilon_{2z}}{\epsilon_{2t}}\,k^2_2$$

$$k^2_{\rho 4} = \frac{\mu_{2z}}{\mu_{2t}}\,k^2_2$$

$$k^2_{\rho 2} = k^2_2 - k^2_z$$

and $$k^2_2 = \omega^2\,\mu_{2t}\,\epsilon_{2t}$$

$$= \frac{\mu_{2t}}{\mu_1}\,.\,\frac{\epsilon_{2t}}{\epsilon_1}\,.\,k^2_1$$

Jn = Bessel function of the first kind, order n.

and Nn = Bessel function of the second kind, order n.

The field components are derived from the wave functions from the following formulae:

	TM	TE
H_z:	-	$\frac{1}{j\omega\mu} k_\rho^2 \psi_e$
E_z:	$\frac{1}{j\omega\epsilon} \cdot k_\rho \psi_m$	-
H_ρ:	$\frac{1}{\rho} \frac{\partial \psi_m}{\partial \phi}$	$\frac{1}{j\omega\mu} \frac{\partial^2 \psi_e}{\partial \rho \partial z}$
E_ρ:	$\frac{1}{j\omega\epsilon} \frac{\partial^2 \psi_m}{\partial \rho \partial z}$	$-\frac{1}{\rho} \frac{\partial \psi_e}{\partial \phi}$
H_ϕ:	$-\frac{\partial \psi_m}{\partial \rho}$	$\frac{1}{j\omega\mu} \cdot \frac{1}{\rho} \cdot \frac{\partial^2 \psi_e}{\partial \phi \partial z}$
E_ϕ:	$\frac{1}{j\omega\epsilon} \cdot \frac{1}{\rho} \cdot \frac{\partial^2 \psi_m}{\partial \phi \partial z}$	$\frac{\partial \psi_e}{\partial \rho}$

where $\epsilon = \epsilon_{1,2t}$, $\mu = \mu_{1,2t}$ and $k_\rho = k_{\rho 1,2}$.

Continuous tangential components of the electric and magnetic fields at the boundary between regions 1 and 2 ($\rho = a$) require that

$$\text{(a)}\quad H_{z)1} = H_{z)2} \qquad \text{(b)}\quad E_{z)1} = E_{z)2}$$

$$\text{(c)}\quad H_{\phi)1} = H_{\phi)2} \qquad \text{(d)}\quad E_{\phi)1} = E_{\phi)2} \qquad \text{(A4.3)}$$

Defining

$$Un(\rho) = Jn(k_{\rho 3}\rho)\ Nn(k_{\rho 3}b) - Nn(k_{\rho 3}\rho)\ Jn(k_{\rho 3}b)$$

$$Vn(\rho) = Jn'(k_{\rho 4}\rho)\ Nn'(k_{\rho 4}b) - Nn'(k_{\rho 4}\rho)\ Jn'(k_{\rho 4}b)$$

$$Wn(\rho) = Jn(k_{\rho 4}\rho)\ Nn'(k_{\rho 4}b) - Nn(k_{\rho 4}\rho)\ Jn'(k_{\rho 4}b)$$

$$Zn(\rho) = Jn'(k_{\rho 3}\rho)\ Nn(k_{\rho 3}h) - Nn'(k_{\rho 3}\rho)\ Jn(k_{\rho 3}b)$$

at $\rho = a$ the conditions (A4.3) require

$$\text{(a)}\quad B.\ \frac{k_{\rho 1}^2}{\mu_1}.Jn(k_{\rho 1}a) = D\ \frac{k_{\rho 4}^2}{\mu_{2z}}.Wn(a)$$

$$\text{(b)}\quad A.\ \frac{k_{\rho 1}^2}{\epsilon_1}.Jn(k_{\rho 1}a) = C\ \frac{k_{\rho 3}^2}{\epsilon_{2z}}.\ Un(a)$$

$$\text{(c)}\quad A.\ k_{\rho 1}Jn'(k_{\rho 1}a) + B\ \frac{n\ k_z}{\mu_1 a}.Jn(k_{\rho 1}a) = \qquad \text{(A4.4)}$$

$$C\ k_{\rho 3}\ Zn(a) + D\ \frac{n\ k_z}{\omega\mu_{2t}a}\ Wn(a)$$

$$\text{(d)}\quad A.\ \frac{n\ k_z}{\omega\epsilon_1 a}\ Jn(k_{\rho 1}a) + B.k_{\rho 1}Jn'(k_{\rho 1}a) =$$

$$C\ \frac{n\ k_z}{\omega\epsilon_{2t}a}.Un(a) + D\ k_{\rho 4}\ Vn(a)$$

On dividing throughout by A in the above relations, it is seen that there are four equations in three unknowns, B/A, C/A and D/A. A non-trivial solution requires that the determinant of the coefficients in equation (A4.4) is zero. Evaluating this determinant gives the characteristic equation for the system

$$k_{\rho 1}^2 \, k_{\rho 2}^2 \left[k_{\rho 1} \frac{(\epsilon_t \epsilon_z)_2^{\frac{1}{2}}}{\epsilon_1} \cdot \frac{Zn}{Un} - k_{\rho 2} \frac{Jn}{Jn} \right]_{\rho=a}$$

$$\left[k_{\rho 1} \frac{(\mu_t \mu_z)_2^{\frac{1}{2}}}{\mu_1} \cdot \frac{Vn}{Wn} - k_{\rho 2} \frac{Jn}{Jn} \right]_{\rho=a}$$

$$- \frac{n^2 k_z^2 \, k_1^2}{a^2} \left[1 - \frac{\mu_{2t}}{\mu_1} \cdot \frac{\epsilon_{2t}}{\epsilon_1} \right]^2 = 0 \qquad (A4.5)$$

where $k_z < k_1$.

This characteristic equation may be solved for the propagation constant k_z and this value may then be used to determine the amplitude ratios from the simultaneous linear equations (A4.4). Since this equation is even in the mode order, n, there is no Faraday rotation or, in other words, the same propagation constant applies for right and left circularly polarized components.

The development of the characteristic equation assumed that the waveguide phase constant was always less than the free space constant for the inner medium. However, if the permittivity or permeability of the outer region is made sufficiently large, or if the outer region is allowed to almost completely fill the guide, a wave can propagate with a phase constant greater than the free space value for the inner region. (If the inner region is assumed to be air, the situation where the phase constant may exceed the free space value for the outer region requires the relative permeability or permittivity in the outer region to be less than unity. For practical purposes, this case can be ignored).

The characteristic equation for the case where $k_z > k_1$ can be derived by replacing the wave functions (A4.1) by

$$\psi_{m1} = A\, In(k_{\rho 1}\rho)\, \cos n\phi .\, e^{-jk_z z}$$
$$\psi_{e1} = B\, In(k_{\rho 1}\rho)\, \sin n\phi .\, e^{-jk_z z} \qquad (A4.6)$$

and carrying out a similar procedure to that above, or the equation may be obtained directly from equation (A4.5) by the substitutions

$$Jn(jx) \rightarrow j^n\, In(x)$$
$$Jn'(jx) \rightarrow j^{n-1}\, In'(x)$$

where In = modified Bessel function of the first kind, order n.

Hence

$$k_{\rho 1}^2 \, k_{\rho 2}^2 \left[k_{\rho 1} \frac{(\epsilon_t \epsilon_z)_2^{\frac{1}{2}}}{\epsilon_1} \frac{Zn}{Un} + k_{\rho 2} \frac{In'}{In} \right]_{\rho=a}$$

$$\left[k_{\rho 1} \frac{(\mu_t \mu_z)_2^{\frac{1}{2}}}{\mu_1} \frac{Vn}{Wn} + k_{\rho 2} \frac{In'}{In} \right]_{\rho=a}$$

$$- \frac{n^2 k_z^2 k_1^2}{a^2} \left[\frac{\mu_{2t}}{\mu_1} \frac{\epsilon_{2t}}{\epsilon_1} - 1 \right]^2 = 0 \qquad (A4.7)$$

where $k_z > k_1$ and $k_{\rho 1}^2 = k_z^2 - k_1^2$.

The modes of interest are those for which n=0 and n=1. The zero order modes correspond to the difference modes in a tracking antenna and the first order modes correspond to the sum or reference modes. Substituting these values into the characteristic equations and deriving the transverse field components, we find

<u>n=0</u>:

TM_{01} mode:

characteristic equation

$$k_z < k_1 \quad \left[k_{\rho 1} \frac{(\epsilon_t \epsilon_z)_2^{\frac{1}{2}}}{\epsilon_1} \cdot \frac{Z_o}{U_o} - k_{\rho 2} \frac{J_o'}{J_o} \right]_{\rho=a} = 0$$

$$k_z > k_1 \left[k_{\rho 1} \frac{(\epsilon_t \epsilon_z)_2^{\frac{1}{2}}}{\epsilon_1} \cdot \frac{Z_o}{U_o} + k_{\rho 2} \frac{I_o}{I_o} \right]_{\rho = a} = 0$$

field components:

inner region:

$$E_\rho = \frac{-k_z k_{\rho 1}}{\omega \epsilon_1} \cdot B_o'(k_{\rho 1} \rho)$$

$$H_\phi = -k_{\rho 1} B_o'(k_{\rho 1} \rho) \qquad (A4.8)$$

where $B_o = \begin{cases} J_o & k_z < k_1 \\ I_o & k_z > k_1 \end{cases}$

outer region:

$$E_\rho = - \frac{C}{A} \cdot \frac{k_z k_{\rho 3}}{\omega \epsilon_{2t}} \cdot Z_o(\rho)$$

$$H_\phi = - \frac{C}{A} \cdot k_{\rho 3} Z_o(\rho)$$

TE_{01} mode:

characteristic equation:

$$k_z < k_1 \left[k_{\rho 1} \frac{(\mu_t \mu_z)_2^{\frac{1}{2}}}{\mu_1} \frac{V_o}{W_o} - k_{\rho 2} \frac{J_o}{J_o} \right]_{\rho = a} = 0$$

$$k_z > k_1 \left[k_{\rho 1} \frac{(\mu_t \mu_z)_2^{\frac{1}{2}}}{\mu_1} \frac{V_o}{W_o} + k_{\rho 2} \frac{I_o}{I_o} \right]_{\rho = a} = 0$$

field components:

inner region:

$$E_\phi = \frac{B}{A} k_{\rho 1} B_o'(k_{\rho 1} \rho)$$

$$H_\rho = - \frac{B}{A} \cdot \frac{k_z k_{\rho 1}}{\mu_1} B_o'(k_{\rho 1} \rho) \qquad (A4.9)$$

$$\text{where } B_o = \begin{cases} J_o & k_z < k_1 \\ I_o & k_z > k_1 \end{cases}$$

$$\text{outer region:} \quad E = \frac{D}{A} k_{\rho 4} V_o(\rho)$$

$$H = -\frac{D}{A} \frac{k_z k_{\rho 4}}{\mu_{2t}} V_o(\rho)$$

From Appendix I, the radiation integrals for zero order modes are

$$TM_{01}: \quad I_\theta = \int_o^a [E_\rho - (\tfrac{\mu}{\epsilon})^{\frac{1}{2}} \cos\theta . H_\eta] J_1(k\rho \sin\theta) \rho d\rho$$

and

$$TE_{01}: \quad I_\phi = \int_o^a [-E_\eta \cos\theta + (\tfrac{\mu}{\epsilon})^{\frac{1}{2}} H_\rho] J_1(k\rho \sin\theta) \rho d\rho$$

Substituting equations (A4.8) and (A4.9) into these integrals and noting that

$$k_1^2 = \omega^2 \mu_1 \epsilon_1$$

it is seen that the radiation patterns for the TM_{01} and TE_{01} patterns will have identical shapes if

$$k_z)_{TM_{01}} = k_z)_{TE_{01}}$$

n=1:

characteristic equation:

$$k_z < k_1 \quad k_{\rho 1}^2 \; k_{\rho 2}^2 \left[k_{\rho 1} \cdot \frac{(\epsilon_t \epsilon_z)_2^{\frac{1}{2}}}{\epsilon_1} \cdot \frac{Z_1}{U_1} - k_{\rho 2} \frac{J_1'}{J_1} \right]_{\rho = a}$$

$$\left[k_{\rho 1} \frac{(\mu_t \mu_z)_2^{\frac{1}{2}}}{\mu_1} \frac{V_1}{W_1} - k_{\rho 2} \frac{J_1'}{J_1} \right]_{\rho = a}$$

$$- \frac{k_z^2 \, k_1^2}{a^2} \left[1 - \frac{\epsilon_{2t}}{\epsilon_1} \frac{\mu_{2t}}{\mu_1} \right]^2 = 0$$

$$k_z > k_1 \quad k_{\rho 1}^2 \; k_{\rho 2}^2 \left[k_{\rho 1} \frac{(\epsilon_t \epsilon_z)_2^{\frac{1}{2}}}{\epsilon_1} \frac{Z_1}{U_1} + k_{\rho 2} \frac{I_1'}{I_1} \right]_{\rho = a}$$

$$\left[k_{\rho 1} \frac{(\mu_t \mu_z)_2^{\frac{1}{2}}}{\mu_1} \frac{V_1}{W_1} + k_{\rho 2} \frac{I_1'}{I_1} \right]_{\rho = a}$$

$$- \frac{k_z^2 \, k_1^2}{a^2} \left[1 - \frac{\epsilon_{2t}}{\epsilon_1} \frac{\mu_{2t}}{\mu_1} \right]^2 = 0$$

field components:

inner region:

$$E_\rho = - \left[\frac{k_z k_1}{\omega \epsilon_1} B_1' + \frac{B}{A} \frac{B_1}{\rho} \right] \cos \phi$$

$$E_\phi = \left[\frac{k_z}{\omega \epsilon_1} \frac{B_1}{\rho} + \frac{B}{A} k_{\rho 1} B_1' \right] \sin \phi$$

$$H_\rho = - \left[\frac{B_1}{\rho} + \frac{B}{A} \frac{k_z k_{\rho 1}}{\omega \mu_1} B_1' \right] \sin \phi \qquad (A4.10)$$

$$H_\phi = - \left[k_{\rho 1} B_1' + \frac{B}{A} \frac{k_z}{\omega \mu_1} \frac{B_1}{\rho} \right] \cos \phi$$

where $B_1 = \begin{cases} J_1 & k_z < k_1 \\ I_1 & k_z > k_1 \end{cases}$

outer region:

$$E_\rho = -\left[\frac{C}{A}\frac{k_z\, k_{\rho 3}}{\omega\epsilon_{2t}} Z_1 + \frac{D}{A}\frac{1}{\rho} W_1\right]\cos\phi$$

$$E_\phi = \left[\frac{C}{A}\frac{k_z}{\rho\omega\epsilon_{2t}} U_1 + \frac{D}{A} k_{\rho 4} V_1\right]\sin\phi$$

$$H_\rho = -\left[\frac{C}{A}\frac{1}{\rho} U_1 + \frac{D}{A}\frac{k_z\, k_{\rho 4}}{\omega\mu_{2t}} V_1\right]\sin\phi$$

$$H_\phi = -\left[\frac{C}{A} k_{\rho 3} Z_1 + \frac{D}{A}\frac{k_z}{\rho\omega\mu_{2t}} W_1\right]\cos\phi$$

On comparing the field components for the inner region, equation (A4.10), with the field components for the first order hybrid mode in corrugated waveguide (equation (4.4)), it can be seen that a symmetric radiation pattern from this region requires that

$$E_\rho(\rho) = Z_o\, H_\rho(\rho)$$

$$E_\phi(\rho) = -Z_o\, H_\phi(\rho)$$

where $Z_o = \left(\frac{\mu_1}{\epsilon_1}\right)^{\frac{1}{2}}$.

Hence, the required amplitude condition is

$$\frac{B}{A} = Z_o.$$

4.3 Effect of Dielectric Linings

In assessing the effect of linings in waveguide only dielectrics have been considered, because in practice they allow a greater range of values of inductive capacity, and with modern plastics are amenable to fabrication of linings. Accordingly, in the above equations,

$$\mu_1 = \mu_{2t} = \mu_{2z} = \mu.$$

The particular results presented are calculated for a waveguide of 1.3λ internal diameter. The curves given are typical for any waveguide size.

4.3.1 Zero Order Modes:

It has been shown that for identical radiation patterns the two zero order modes must have equal phase constants. The two modes, TE_{01} and TM_{01}, can exist independently in the lined waveguide and it can be shown that for an isotropic lining the TM_{01} will always have a higher phase constant than the TE_{01} mode. Consequently, anisotrophic dielectrics are necessary if the phase constants are to be equated.

A study of the characteristic equations for the two modes shows that the phase constant for the TM_{01} mode is dependent on both ϵ_{2z} and ϵ_{2t} and the TE_{01} mode only on ϵ_{2t}. This is to be expected from the nature

of the waveguide fields.

Fig. A4.2 shows the variation of the TM_{01} phase constant plotted against the ratio $\sigma = {}^{a}/_{b}$ where (b-a) = lining thickness, with the anisotropy, $({}^{\epsilon_z}/_{\epsilon_t})_2$, as a parameter. The curves show that for an air inner dielectric, which demands ${}^{\epsilon_z}/_{\epsilon_t} > \frac{2}{3}$, it is impossible to achieve equal phase constants. The curves corresponding to ${}^{\epsilon_z}/_{\epsilon_t} < \frac{2}{3}$ can produce the desired condition, but require a dielectric rod in the middle of the guide so that $\epsilon_z \geq \epsilon_1$. However, a waveguide completely filled with dielectric is impractical in a high efficiency system due to the losses incurred. Alternatively this case can be treated by fixing the axial dielectric constant and by varying the transverse value.

The effect of maintaining a constant longitudinal dielectric constant in the lining and of varying the circumferential value is shown in fig. A4.3. In this case, it is seen that the phase constants can be equated. However, in order to achieve this, with a thin lining, a high degree of anisotropy is required and the slope of the TE_{01} phase constant curve near the cross-over point is extremely steep, making the field structure very sensitive to lining thickness.

For a given lining thickness, increases in the dielectric constant of the outer medium will allow the

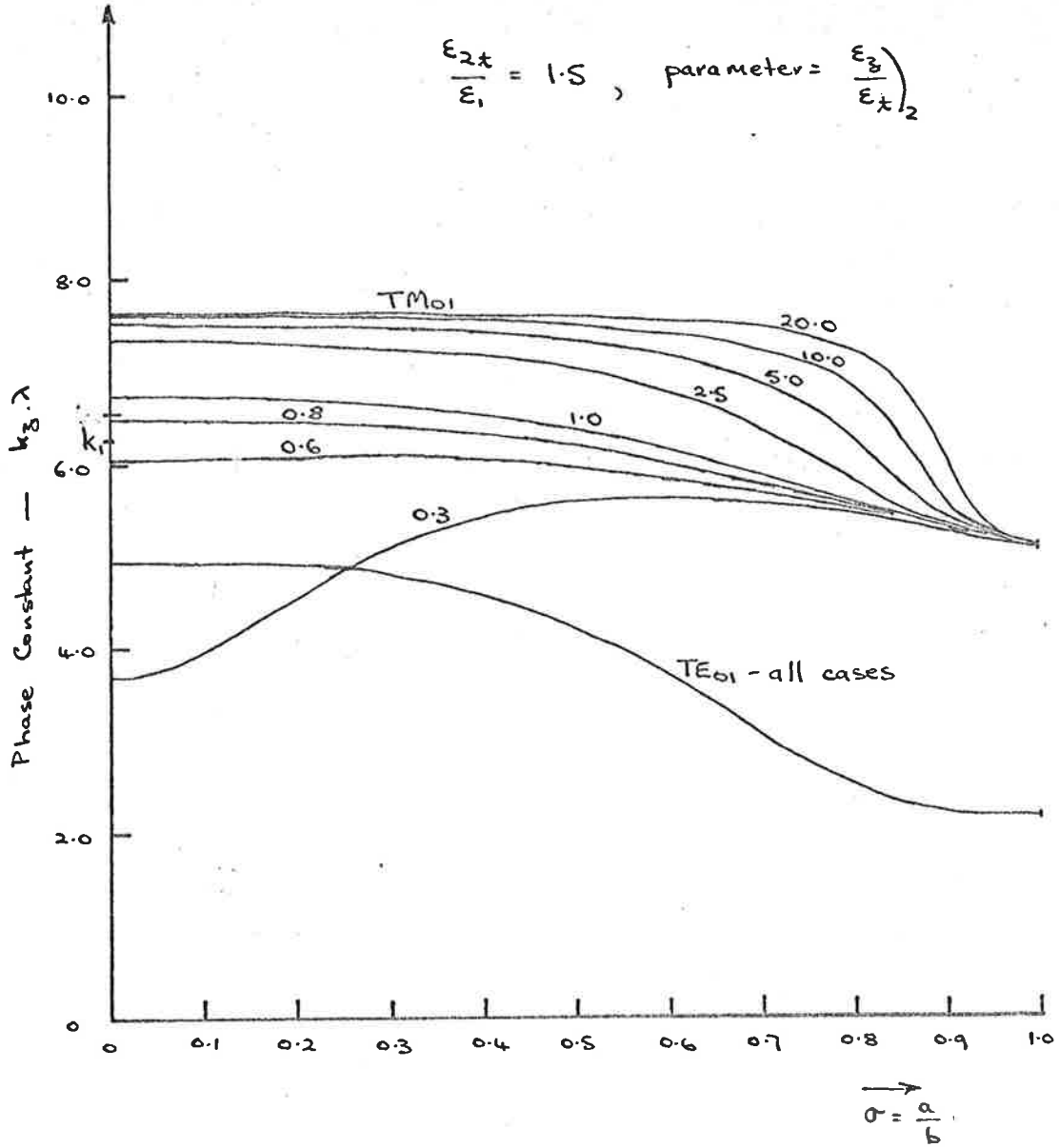

Fig. A4.2 Zero order modes with dielectric lining

$\left(\frac{\varepsilon_{2t}}{\varepsilon_1} = 1.5\right)$

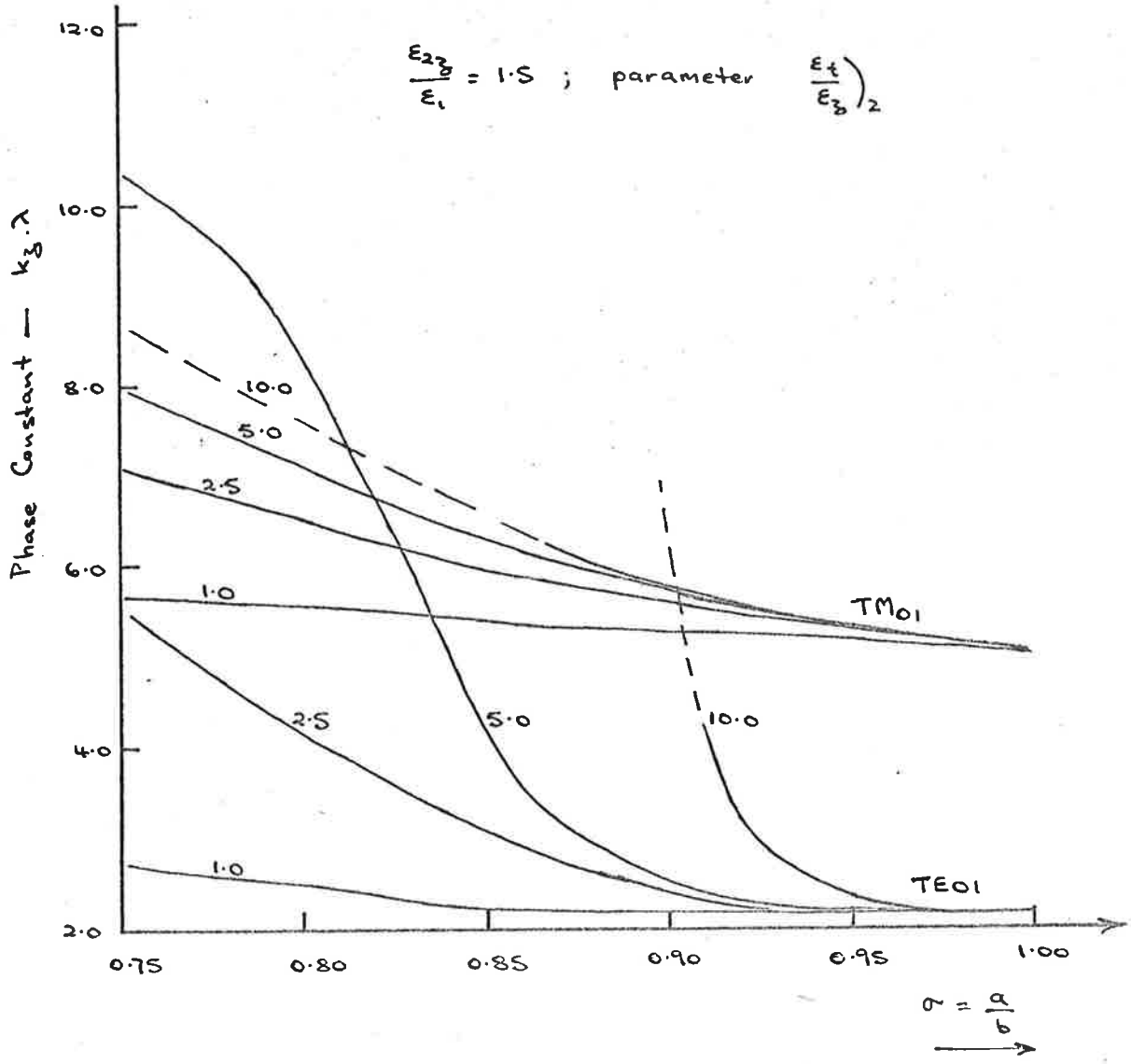

Fig. A4.3 Zero order modes with a dielectric lining

$\left(\frac{\varepsilon_{z_3}}{\varepsilon_1} = 1.5\right)$

phase constants to be equated with less anisotropy and with a lower rate of change of phase constant between the two modes, although the absolute phase constant will still change rapidly with lining thickness.

A4.3.2 First Order Modes:

For first order modes the phase constant is no longer of interest and the ratio of the amplitudes of the transverse electric and transverse magnetic modes in the centre region becomes important. (This assumes that the phase constant does not approach too close to the free space value for the inner region, at which point the characteristic equation becomes identically zero and the fields in the waveguide become zero, i.e. no mode propagates for this phase constant).

A preliminary investigation showed that the hybrid mode which reduced to the TM_{11} mode in the empty waveguide, "quasi-TM_{11}", was the mode of interest and produced cross-couplings with thin linings so that $B/A \rightarrow Z_o$.

Fig. A4.4 gives the change in cross-coupling B/A with an homogeneous dielectric lining. This curve shows that even very high ratios of dielectric constant between the outer and inner regions does not achieve the required result.

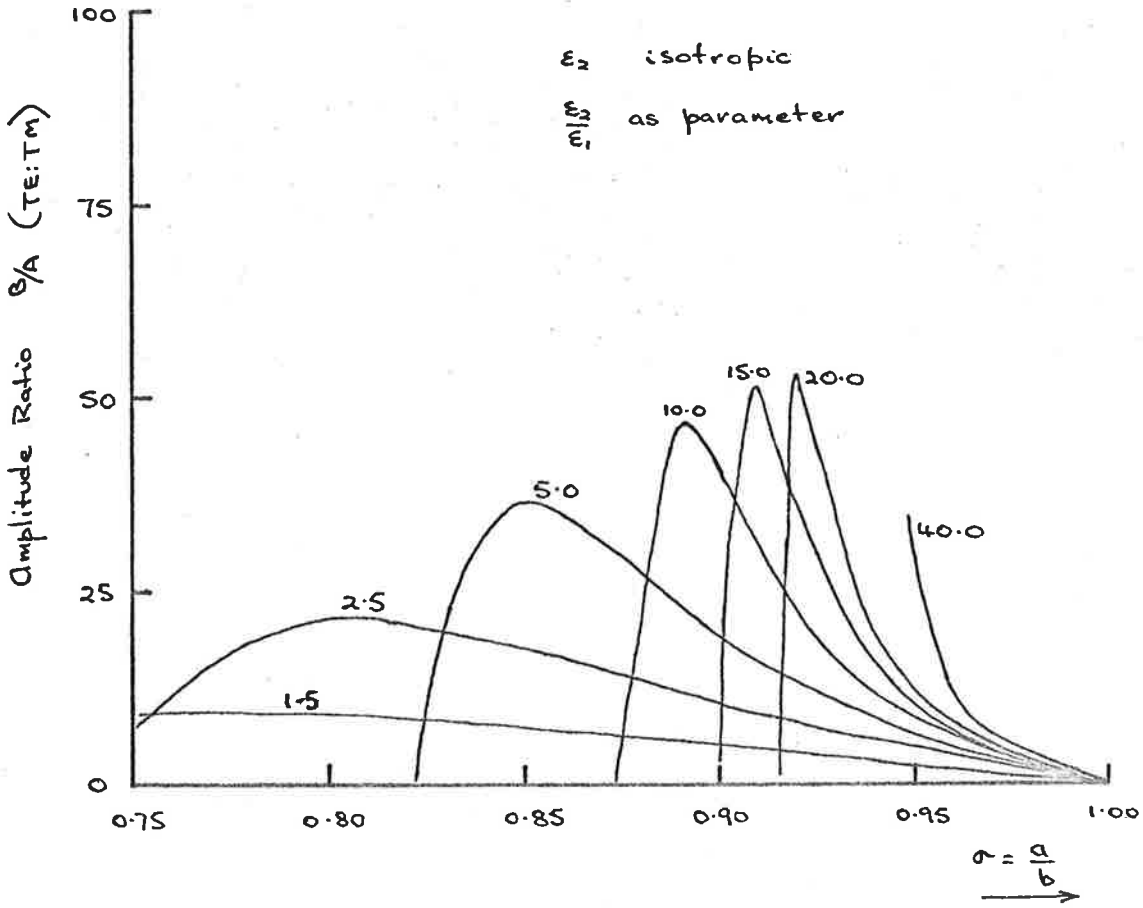

Fig. A4.4 Homogeneous Dielectric Lining in Circular Waveguide.

Figs. A4.5 and A4.6 give curves for anisotropic linings with two different constant values of circumferential dielectric constant, where the longitudinal value is varied. From these diagrams it can be seen that the desired ratio $B/A = Z_o \simeq 377$ can be achieved either by a relatively low circumferential constant and a high anisotropy or by a high base dielectric constant and low anisotropy. Generally, for higher values of the outer region relative to the centre, a thinner lining is required. Fig. A4.6 shows that by careful choice of the lining parameters, the amplitude ratio can be obtained at a stationary point of the curve, giving low sensitivity to lining thickness.

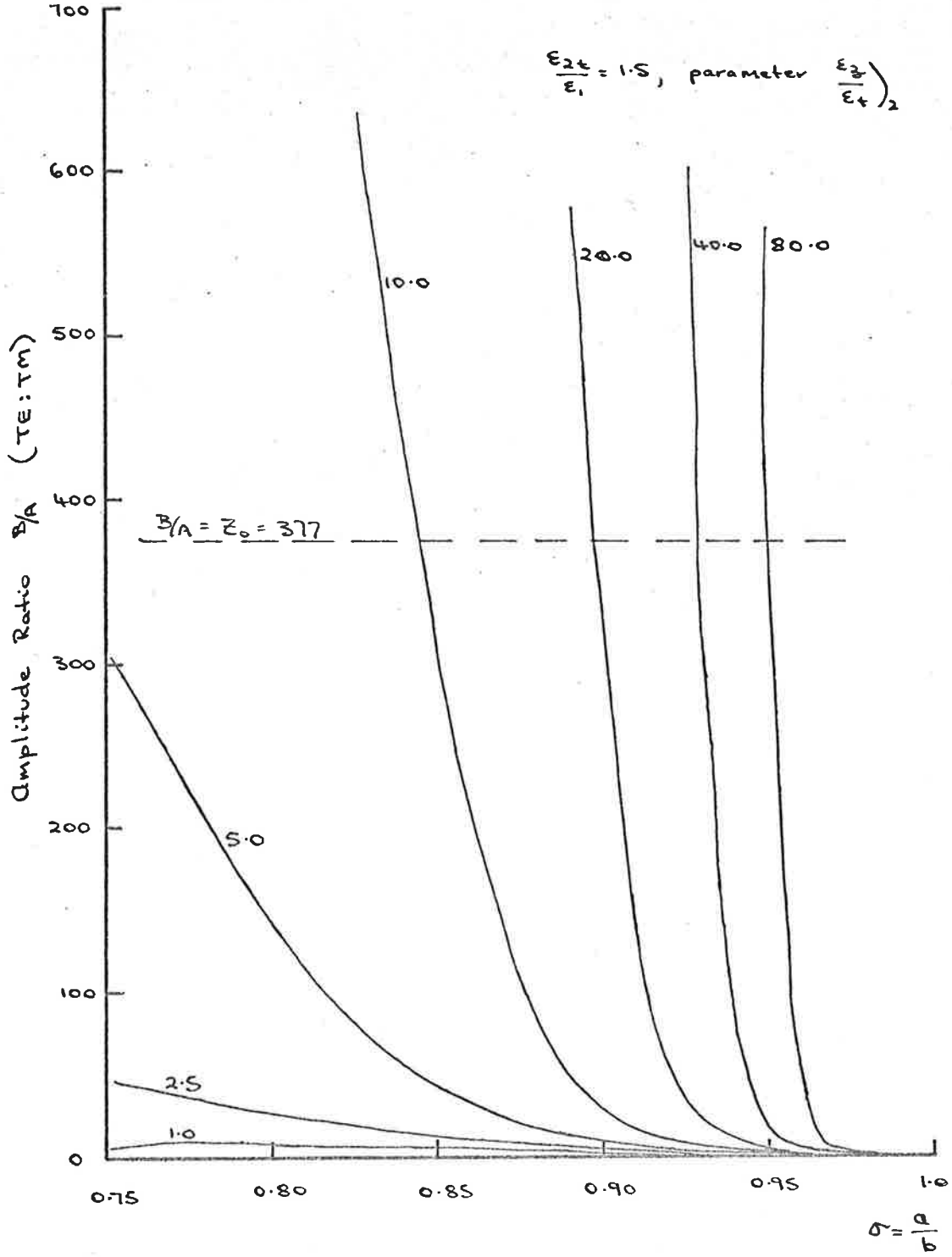

Fig. A4.5 Quasi-TM_{11} Mode in Dielectric Lined Waveguide

$\left(\frac{\varepsilon_{2t}}{\varepsilon_1} = 1.5\right)$

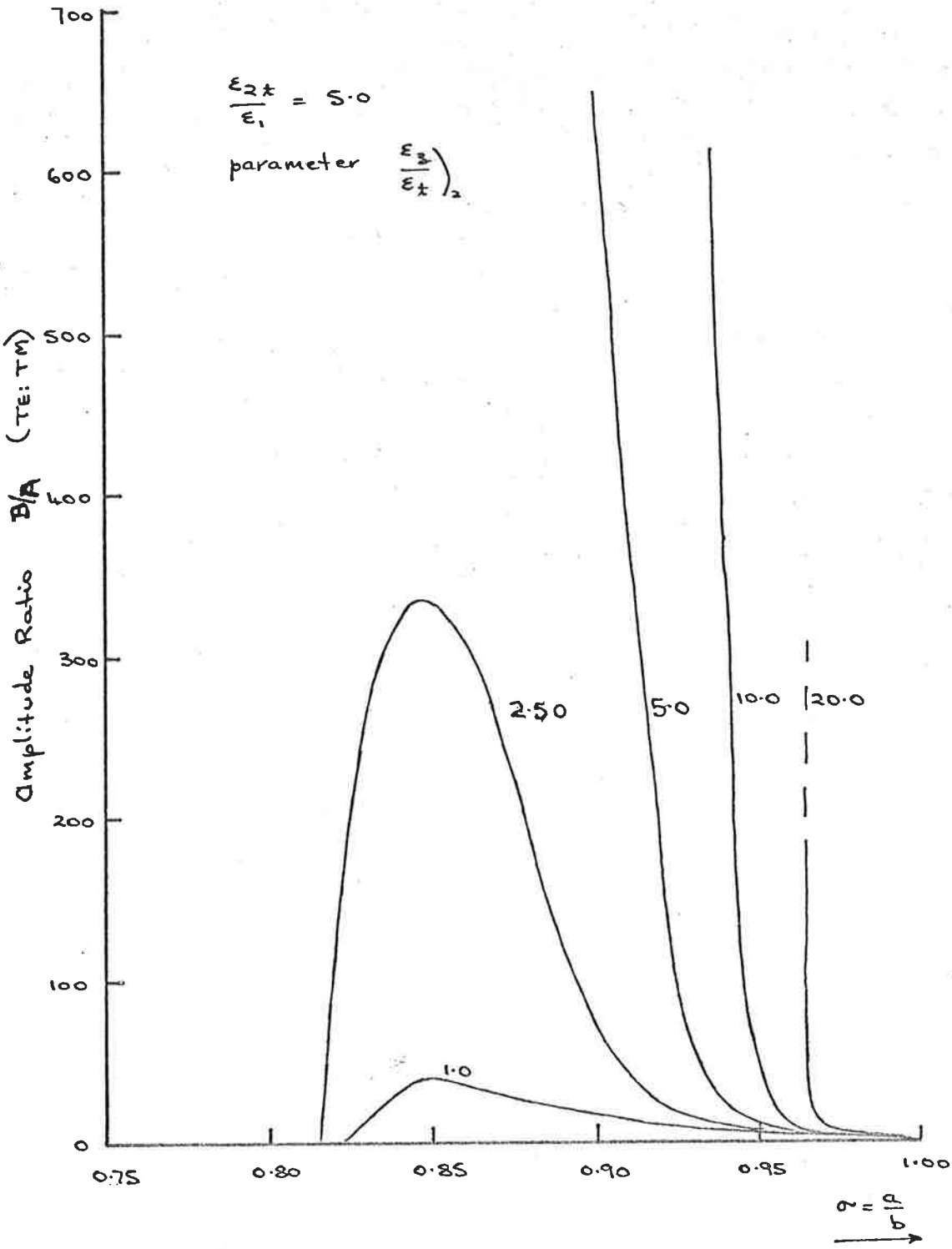

Fig. A4.6 Quasi-TM_{11} Mode in Dielectric Lined Waveguide

$\left(\frac{\varepsilon_{2t}}{\varepsilon_1} = 5.0\right)$

REFERENCES

(1) D. C. Hogg and W.W. Mumford:
"The effective noise temperature of the sky"
Microwave J. v.3, no.3, Mar. 1960, pp. 80-84.

(2) P.D. Potter:
"Design of Antennas for Space Communications"
J.P.L. Report.

(3) G.E. Mueller:
"A pragmatic approach to space communication"
Proc. IRE, v.48, no.4, Apr. 1960, pp. 557-560.

(4) C.J. Sletten:
"User views about recent antenna research results"
Microwave J. v.10, no.13, Dec. 1967, pp. 20-28, 58-64.

(5) H.H. Reed:
"Communication satellite ground station antennas"
Microwave J. v.10, no.7, June 1967, pp. 63-69.

(6) P.W. Hannan:
"Microwave antennas derived from the Cassegrain telescope"
IRE Trans. v.AP-9, no.2, Mar. 1961, pp.140-153.

(7) P.D. Potter:
"The application of the Cassegrainian principle to ground antennas for space communications"
IRE Trans. v.SET-8, no.2, June 1962, pp.154-158.

(8) P.D. Potter:
"Aperture illumination and gain of cassegrain systems"
IEEE Trans. v.AP-11, no.3, May 1963, pp.373-375.

(9) P.D. Potter:
"Application of spherical wave theory to Cassegrainian-fed paraboloids"
IEEE Trans. v.AP-15, no.6, Nov. 1967, pp.727-736.

(10) W.V.T. Rusch:
"Scattering from a hyperboloidal reflector in a Cassegrain feed system"
IEEE Trans. v.AP-11, no.4, July 1963, pp.414-421.

(11) P.D. Potter:
"A new horn antenna with suppressed sidelobes and equal beamwidths"
Microwave J. v.6, no.6, June 1963, pp.71-78.

(12) S. Silver, ed.:
"Microwave Antenna Theory and Design"
M.I.T. R.L. Series, New York, McGraw-Hill, 1949. pp.338-340, 344.

(13) R.N. Page:
"Monopulse Radar"
IRE Conv.Rec. pt.I, 1955, pp.132-134.

(14) C.Cohen and C.M. Steinmetz:
"Amplitude and phase sensing monopulse system parameters"
Microwave J. v.2, no.10, Oct. 1959, pp.27-33
and no.11, Nov. 1959, pp.33-38.

(15) W. Hansz and R.A. Zachory:
"Phase amplitude monopulse system"
IRE Trans. v.MIL-6, no.2, Apr. 1962, p.140.

(16) L. Peters and F.C. Weimer:
"Tracking radars for complex targets"
Proc. IEE v.110, no.12, Dec. 1963, pp.2149-2162.

(17) P.W. Hannan:
"Optimum feeds for all three modes of a monopulse antenna: Pt. I"
IRE Trans. v.AP-9, no.5, Sept. 1961, pp.444-453.

(18) ibid.
Pt. II: pp. 454-460.

(19) K.T. Keeping:
"The design and construction of a multimode circularly polarized tracking feed for high power application in a cassegrain reflector system"
IEEE Int.Conv., New York, Mar. 1965.

(20) L.J. Ricardi and L. Niro:
"Design of a twelve horn monopulse feed"
IRE Int.Conv. Rec. Pt. I. 1959, pp. 49-56.

(21) P.W. Hannan and P.A. Loth:
"A monopulse antenna having independent optimization of the sum and difference modes"
IRE Int.Conv.Rec. pt.I, 1961, pp. 57-60.

(22) S.W. Drabowitch:
"Multimode Antennas"
Microwave J. v. 9, no. 1, Jan.1966, pp.41-51.

(23) H.G. Weiss:
"The Haystack Microwave Research Facility"
IEEE Spectrum v.2, no.2, Feb. 1965, pp.50-69.

(24) P.A. Jensen:
"A low noise multimode cassegrain monopulse feed with polarization diversity"
IEEE NEREM Rec. 1963, pp.94-95.

(25) P.Foldes and S. Komlos:
"A new multimode monopulse feed"
IEEE NEREM Rec. 1963, pp.100-101.

(26) V.V. Galindo and C.Y. Pon:
"Control and optimization of a multimode square feed for sum and difference patterns"
IEEE NEREM Rec. 1963, pp.96-97.

(27) D.N. Cooper:
"A new circularly polarized monopulse feed system"
Proc. IEEE v.53, no.9, Sept.1965, pp. 1252-1254.

(28) S. Silver, ed.:
"Microwave antenna theory and design"
op.cit. p.218.

(29) H.C. Minnet and B.MacA. Thomas:
"A method of synthesising radiation patterns with axial symmetry"
IEEE Trans. v.AP-14, no.5, Sept.1966, pp. 654-656.

(30) H. Geyer:
"Circular horn radiator with annular wave chokes"
Frequenz v.20, no.1, Jan.1966, pp.22-28.

(31) J.J. Epis:
"Compensated electromagnetic horns"
Microwave J. v.4, no.5, May 1961, pp.84-89.

(32) Nixon and D. Schuster:
"Beam shaping for paraboloid feeds"
Electronics, v.34, no.32, Aug. 11 1961,
Cover and p. 141.

(33) S.Silver, ed.:
"Microwave antenna theory and design"
op.cit. pp. 233-234.

(34) ibid.
pp. 337-338.

(35) ibid.
pp. 177-179.

(36) ibic.
p. 341.

(37) J.A. Stratton:
"Electromagnetic Theory"
McGraw-Hill, New York, 1941, pp. 542-543.

(38) G.M. Pelchat:
"Relationships between squinted sum and difference radiation patterns of amplitude monopulse antennas with mutual coupling between feeds"
IEEE Trans. v.AP-15, no.4, July 1967,
pp.519-526.

(39) S. Silver, ed.:
"Microwave antenna theory and design"
op.cit. pp. 421-422.

(40) ibid.
p. 195.

(41) ibid,
pp. 188-191, 430-431.

(42) ibid.
chapt. 5, pp. 144-151.

(43) ibid.
p. 162.

(44) ibid.
p. 149.

(45) ibid.
p. 192-192.

(46) H. Jasik, ed.:
"Antenna Engineering Handbook"
McGraw-Hill, New York, 1961.

(47) J.S. Cook, E.M. Elam and H. Zucker:
"The open cassegrain antenna. Pt. I Electromagnetic Design and Analysis"
B.S.T.J. v. 44, Sept. 1965, pp. 1255-1300.

(48) E.R. Nageberg and J.Schefer:
"Mode conversion in circular waveguides"
B.S.T.J. v.44, Sept. 1965, pp. 1321-1338.

(49) C. Yeh:
"Excitation of higher order modes by a step discontinuity of a circular waveguide"
J.P.L. Tech. Rept. no.32-496, Feb. 1, 1964.

(50) P.D. Potter and A.C. Ludwig:
"Beamshaping by use of higher order modes in conical horns"
IEEE NEREM Rec. Nov. 1963, pp.92-93.

(51) G.F. Koch:
"Paraboloid antennas with low-noise temperature"
NTZ Communications Journal, v.5, no.3, 1966, pp. 125-131; as quoted by C.J. Sletten:
"User views about recent antenna research results"
Microwave J. v.10, no.13, Dec. 1967, pp. 28E, 58.

(52) R.F. Harrington:
"Time-harmonic electromagnetic fields"
McGraw-Hill New York 1961. pp.106-113.

(53) H.C. Minnet and B. Thomas:
C.S.I.R.O. internal report; also private discussion with Dr. B. Thomas.

(54) "Echo Project" B.S.T.J. v.40, no.4, July 1961.

(55) Telstar Project, B.S.T.J. v.42, no.5, Sept. 1963.

(56) S. Silver, ed.:
"Microwave antenna theory and design"
op.cit. Ch. 1-5.

(57) ibid.
p.161.

(58) ibid.
pp. 138-143.

(59) R.F. Harrington:
"Time-harmonic electromagnetic fields"
op.cit. pp. 219-223.

BIBLIOGRAPHY

TRACKING RADAR

M. D. Aasen:
"Methods for predicting interference effects in tracking radars"
IEEE Int.Conv.Rec. v.12, pt.7, 1964, p.27.

R. C. Baker:
"A circularly polarized feed for an automatic tracking telemetry antenna"
IRE Nat.Conv.Rec. v.7, pt.5, 1959, p. 143.
Also: IRE Trans. v. SET-5, no.3, Sept. 1959, pp. 103-110.

W. L. Barrow and C. Schulman:
"Multiunit electromagnetic horns"
Proc. IRE v.20, no.3, Mar. 1940, p. 130.

D. K. Barton:
"Accuracy of a monopulse radar"
IRE Proc 3rd Nat.Mil.Elec.Conv. June 30, 1959, pp. 179-186.

W. D. Boyer:
"A diplex, doppler phase comparison radar"
IEEE v. ANE-10, no.1, Mar. 1963, p. 27.

C. E. Bockner:
"Angular jitter in conventional conical scanning, automatic tracking radar systems"
Proc. IRE v. 39, no. 1, Jan. 1951, pp. 51-55.

H. T. Budenbom:
"Monopulse automatic tracking and the thermal bound"
IRE Nat.Conv. on Mil.Elec. June 1957.

W. Cohen and C.M. Steinmetz:
"Amplitude and phase sensing monopulse system parameters"
Microwave J. v.2, no.10, Oct. 1959, pp. 27-3
and no.11, Nov. 1959, pp. 33-38.
Discussion: F.J. Gardiner, v. 3, no.1, Jan. 1960, pp. 18-20.

J. R. Copeland:
"Radar target classification by polarization properties"
Proc. IRE v.48, no.7, July 1960, p. 1290.

F. S. Coxe:
"Operational characteristics of the TLM-18 automatic tracking telemetry antenna"
IRE Trans. v.SET-5, no.2, June 1959, pp. 87-91.

J. B. Damonte and D.J. Stoddard:
"An analysis of conical scan antennas for tracking"
IRE Nat. Conv.Rec. pt.I, 1956, pp.39-47.

R. H. Delano:
"A theory of target glint or angular scintillation in radar tracking"
Proc. IRE, v. 41, no.12, Dec. 1953, pp.1778-1784.

R. H. Delano:
"The effect of AGC on tracking noise"
Proc. IRE v. 44, no.6, June 1956, pp.801-810.

J. A. Develet:
"Thermal noise errors in simultaneous lobing and conical scan angle tracking systems"
IRE Trans. v. SET-7, no.2, June 1961, pp. 42-51.

J. H. Dunn and D. D. Howard:
"Precision tracking with monopulse radar"
Electronics v. 33, no.17, Apr. 22 1960, pp. 51-56.

P. Foldes and S. Komlos:
"A new multimode monopulse feed"
IEEE NEREM Rec.1963, pp. 100-101.

H. T. Friis and W. D. Lewis:
"Radar Antennas"
B.S.T.J. v. 26, 1947, pp. 219-317.

V. V. Galindo and C.Y. Pon:
"Control and optimization of a multimode square feed for sum and difference patterns"
IEEE NEREM Rec. 1963 pp. 96-97.

A. F. Gangi:
"The active adaptive antenna array system"
IEEE Trans. v.AP-11, no.4, July 1963, pp.405-414.

P. W. Hannan:
"Maximum gain in monopulse difference mode"
IRE Trans. v.AP-9, no.3, Apr. 1961, p. 314.

P. W. Hannan:
"Optimum feeds for all three modes of a monopulse antenna"
IRE Trans. v.9, no.5, Sept. 1961,
pt I pp. 444-453
pt II pp. 454-460.

P. W. Hannan and P. A. Loth:
"A monopulse antenna having independent optimization of the sum and difference modes"
IRE Internat.Conv.Rec. pt.I, 1961, pp. 57-60.

R. C. Hansen:
"Microwave Scanning Antennas - Vol. I. Apertures"
Academic Press. 1964.

W. Hansz and R. A. Zachory:
"Phase amplitude monopulse system"
IRE Trans. v.MIL-6, no.2, Apr. 1962, p.140.

H. Jasik, A. D. Bresler and A. Kampinsky:
"A wide band conical scan antenna feed system"
Microwave J. v.4, 1961, p.97.

P. A. Jensen:
"A low-noise multimode cassegrain monopulse feed with polarization diversity"
IEEE NEREM Rec. 1963, pp.94-95.

K. J. Keeping:
"The design and construction of a multimode circularly polarized tracking feed for high power application in a cassegrain reflector system"
IEEE Internat.Conv. Mar. 1965.

S. Kazel and J. N. Faraone:
"Improvement in tracking accuracy of pulse radar by coherent techniques"
IRE Trans. v. MIL-5, no.4, Oct.1961, pp.286-293.

K. C. Kelly and F. J. Goebels:
"Annular slot monopulse antennas"
IRE Internat. Conv.Rec. v.10, pt.I, 1962,
pp.71-80.

K. C. Kelly and G. J. Goebels:
"Annular slot monopulse antenna arrays"
IEEE Trans. v.AP-12, no.4, July 1964, p.391.

G. M. Kirkpatrick:
"Aperture illumination for radar angle-of-arrival measurements"
IRE Trans. v.PGAE-9, Dec.1953, p.20.

S. G. Komlos, P.Foldes and K. Jasinki:
"Feed systems for clockwise and counter clockwise circular polarization"
IRE Trans. v.AP-9, no.6, Nov.1961, p.577.

M.Korff, C. M. Brindley and M. H. Lowe:
"Multiple target data handling with a monopulse radar"
IRE Trans. v. MIL-6, no.4, Oct.1962, pp.359-367.

C. S. Lerch:
"Phased array radars for satellite tracking"
IRE Internat. Conv.Rec. v.10, pt.5, 1962, p.50.

K. W. Linnes, W.D. Merrick and R. Stevens:
"Ground antenna for space communication system"
IRE Trans v. SET-6, no.1, Mar. 1960, pp. 45-55.

J. G. McCann and R. J. Stegen:
"A high performance conically scanning X-band antenna of novel design"
IRE Trans. v. AP-4, no.4, Oct.1956, pp. 628-632.

R. Manasse:
"Maximum angular accuracy of tracking a radio star by lobe comparison"
IRE Trans. v.AP-8, no.1, Jan.1960, pp.50-57.
Also N.George: "Comment on 'Maximum angular accuracy of tracking a radio star by lobe comparison'" IRE Trans. v.AP-8, no.6, Nov.1960, p.632.

R. W. Martin and L. Schartzman:
"A monopulse cassegrainian antenna"
IRE Internat.Conv.Rec. v.8, pt I, 1960, pp.96-102.

W. H. Nester:
"Study of tracking accuracy in monopulse phased arrays"
IRE Trans. v.AP-10, no.3, May 1962, pp. 237-246.

F. C. Ogg:
"Steerable array radars"
IRE Trans. v.MIL-5, no.2, Apr. 1961, pp.80-93.

M. R. O'Sullivan:
"Tracking systems employing delay lock discriminators"
IRE Trans. v.SET-8, no.1, Mar.1962, pp.1-8.

R. N. Page:
"Monopulse Radar"
IRE Conv.Rec. pt.I, 1955, pp.132-134.

G. M. Pelchat:
"The effects of receiver and antenna noise on the performance of a conical scan tracking system"
Microwave J. v.8, no.2, Feb. 1965.

G. M. Pelchat:
"Relationships between squinted sum and difference radiation patterns of amplitude monopulse antennas with mutual coupling between feeds"
IEEE Trans. v.AP-15, no.4, July 1967, pp.519-526.

L. Peters and F. C. Weimer:
"Concerning the assumption of random distribution of scatterers as a model of an aircraft for tracking radars"
IRE Trans. v.AP-9, no.1, Jan.1961, pp. 110-111.

L. Peters and F. C. Weimer:
"Tracking radars for complex targets"
IEEE Proc. v.110, no.12, Dec.1963, pp.2149-2162.

E. J. Powers:
"Utilization of Lambda functions in the analysis and synthesis of monopulse antenna difference patterns"
IEEE Trans. v.AP-15, no.6, Nov. 1967, pp.771-777.

O. R. Price and R. F. Hyneman:
"Distribution functions for monopulse antenna difference patterns"
IRE Trans. v.AP-8, no.6, Nov. 1960, pp.567-577.

H. B. Querido:
"Amplitude comparison error of a signal received by two circularly polarized antennas due to off-axis ellipticity"
IRE Trans. v.AP-9, no.2, Mar.1961, p.222.

J. F. Ramsay, J.P. Thompson and W. D. White:
"Polarization tracking of antennas"
IRE Internat. Conv.Rec. pt.I, 1962, pp. 13-42.

H. W. Redlien:
"Monopulse difference chart"
IEEE Internat Conv.Rec. v.11, pt.1, 1963, pp. 129-131.

L. J. Ricardi and L. Niro:
"Design of a twelve horn monopulse feed"
IRE Internat.Conv.Rec. pt.I, 1959, pp.49-56.

G. Ross and L. Schartzman:
"Continuous beam steering and null tracking with a fixed multiple beam antenna array system"
IEEE Trans. v.AP-12, no.5, Sept.1964, pp.541-551.

W. L. Rubin and S. K. Kamen:
"SCAMP - A single channel monopulse radar signal processing technique"
IRE Trans. v. MIL-6, no.2, Apr.1962, p.146.
Also Microwave J. v.8, no.1, Jan.1965.

S. Sharenson:
"Angle estimation accuracy with monopulse radar in search mode"
IRE Trans. v. ANE-9, no.3, Sept.1962, pp.175-179.

J. P. Shelton:
"Improved feed design for amplitude monopulse radar antennas"
IRE Nat.Conv.Rec. v.7, pt.I, 1959, pp.93-102.

J. R. Sklar and F. C. Schweppe:
"On the angular resolution of multiple targets"
Proc.IEEE v.52, no.9, Sept.1964, pp.1044-1045.

M. I. Skolnik:
"Introduction to Radar Systems"
McGraw-Hill, New York, 1962.

P. H. Smith:
"Null tracking doppler-navigation radar"
IEEE Trans. v.ANE-10, no.1, Mar.1963, p.50.

H. W. Somme:
"An improved simultaneous phase comparison guidance radar"
IRE Trans. v.ANE-3, no.2, June 1956, pp.67-70.

R. J. Stegen:
"The null depth of a monopulse tracking antenna"
IEEE Trans. v.AP-12, no.5, Sept. 1964, p. 645.

D. Thunquist:
"Circle diagram applied to monopulse"
IRE Trans. v.CS-10, no.3, Sept. 1962, pp. 246-257.

G. de Vito:
"A new type of monopulse vemier obtained by the excitation of both H_{11} and E_{01} modes in a circular waveguide"
IRE Trans. v.AP-10, no.6, Nov. 1962, p. 781.

H. A. Wheeler:
"Antenna beam patterns which retain their shape with defocussing"
IRE Trans. v.AP-10, no.5, Sept.1962, pp. 573-580.

W. D. White and L. K. De Size:
"Scanning characteristics of two reflector antenna systems"
IRE Internat. Conv.Rec. v.10, pt.I, 1962, pp.44-70.

Special issues:

"Advanced Radar Techniques"
IRE Trans. v. MIL-5, no.2, Apr. 1961.

"Signal Processing Radar"
IRE Trans. v. MIL-6, no.2, Apr. 1962.

Cooper, D. N. (1965). A new circularly polarized monopulse feed system. *Proceedings of the IEEE*, *53*(9), 1252-1254.